NUMERICAL ALGORITHMS FOR FRACTIONAL PARTIAL DIFFERENTIAL EQUATIONS WITH TIME-DEPENDENT BOUNDARY CONDITIONS

by

Toheeb Ayinde Biala

A Dissertation

Presented to the Faculty of the Computational Science Program

Middle Tennessee State University

March 2021

In Partial Fulfillment

of the Requirements for the Degree

Doctor of Philosophy in Computational Science

Dissertation Committee:

Dr. Abdul Khaliq, Chair
Department of Mathematical Sciences

Dr. Zachariah Sinkala
Department of Mathematical Sciences

Dr. Tibor Koritsanszky
Department of Chemistry

Dedicated to

my beloved parents (Iya ni wura, Baba ni jigi), who strived so hard to ensure I have the best education;

my loving wife (Ìfẹ́ mí), whose love and support during the program is unfathomable;

my wonderful son (Mahfouz) and our "Oun bọ lọ́nàá" (Bilal), whose presence motivates me to work harder.

ACKNOWLEDGMENTS

I express my sincere gratitude to everyone who has contributed to the successful completion of my Ph.D. program. I am deeply indebted to my supervisor, Dr. Abdul Khaliq, for his guidance, advice, encouragement, and suggestions that are invaluable towards completing the program. I am grateful and would like to thank him for introducing me to the fascinating fractional calculus field. He is my "envelope pusher," and I would like to specifically mention that this dissertation would not have been possible without him. I am also grateful to the Computational Science Program Director, Dr. John Wallin, for admitting me into the program, providing some of the best facilities to the students, and providing financial assistance to attend conferences, workshops, and seminars. Most significantly, I appreciate him for approving my assistantship for the entire duration of the program. I am sincerely thankful to my dissertation committee members, Drs. Zachariah Sinkala and Tibor Koritsanzky, and Dr. Yuri Melnikov, for carefully reading my manuscript, pointing out corrections, and making insightful suggestions. I am grateful for their knowledgeable assistance and recommendations in making the dissertation better. I am also grateful to the Department of Mathematics and Statistics Chair at Austin Peay State University, Dr. Samuel N. Jator, for his advice and suggestions towards completing the program. I want to thank Drs. Khaled Furati and Jianfei Huang for their collaborations and contributions towards the program. I acknowledge the help and support of the faculty and students of the Departments of Computer Science and Mathematical Sciences at MTSU and my fellow graduate students in the Computational Science Ph.D. program.

Finally, my deepest gratitude goes to my loving family, who supported me throughout the program. My sincere gratitude goes to my Mum and siblings for their prayers and support. My acknowledgment is not complete without the help of my loving wife and sweet sons for their inspiration and encouragement, to my in-laws for their prayers, to Dr. Samuel Iyiola, my friends, too numerous to mention, for their constant motivations.

DECLARATION

I declare that this dissertation has not been submitted to any other university for any degree. The results presented in this dissertation are based on the following work at Middle Tennessee state university (MTSU):
Published/ Submitted Papers:

- A. Q. M. Khaliq, T. A. Biala, S. S. Alzahrani, K. M. Furati, Linearly implicit predictor-corrector methods for space-fractional reaction-diffusion equations with non-smooth initial data, *Computer & Mathematics with Applications*, 75 (8) (2018) 2629 – 2657.

- T. A. Biala and A. Q. M. Khaliq, Parallel algorithms for nonlinear time-space fractional parabolic PDEs, *Journal of Computational Physics*, 375 (2018) 135 – 154.

- T. A. Biala and A. Q. M Khaliq, Predictor-corrector schemes with Gaussian quadrature for nonlinear space-fractional PDEs with time-dependent Robin boundary conditions, *Applied Numerical Mathematics*, 160 (2021) 1 – 12.

- T. A. Biala, Second-order predictor-corrector schemes for nonlinear distributed-order space-fractional differential equations with non-smooth initial data, *International Journal of Computer Mathematics,* 96 (6) (2019) 1861 – 1878.

- T. A. Biala and A. Q. M. Khaliq, A fractional-order compartmental model for predicting the spread of the COVID-19 pandemic. *Communications in Nonlinear Science and Numerical Simulation*, 98 (2021) 105764

- T. A. Biala, Y. O Afolabi and A. Q. M. Khaliq, How Efficient is Contact Tracing in Mitigating the Spread of COVID-19? A Mathematical Modeling Approach. *Submitted to Applied Mathematical Modelling. (under 2nd Review)*

ABSTRACT

This dissertation focuses on developing and analyzing numerical schemes for fractional partial differential equations (PDEs). The development is important because several models involving fractional derivatives exhibit non-locality and memory dependencies, making them difficult to solve. Moreover, many of such models do not have analytical solutions due to the non-linearity involved in their formulation.

In the first part of the study, we develop numerical schemes for space-fractional reaction-diffusion equations with time-dependent boundary conditions. The methods are based on using the matrix transfer technique (MTT) for spatial discretization, and rational approximations to the matrix exponential function are used in time. In particular, predictor-corrector schemes based on $(1,1)$- and $(0,2)$-Padé, and a real distinct pole approximation to the exponential function are developed. We observe that the solutions produced by the $(1,1)$-Padé scheme incur oscillatory behavior for some time steps. These oscillations are due to high-frequency components present in the solution and diminish as the order of the space-fractional derivative decreases (slow diffusion). A priori reliability constraint is proposed to avoid these unwanted oscillations. Furthermore, the constraints are generalized for all (m,m)-Padé approximants, $m \in \mathbb{Z}^+$, to the matrix exponential functions.

In the second part of the study, a novel numerical scheme for time-space fractional PDEs is developed. The developed scheme is similar to the Crank-Nicholson scheme for integer-order PDEs and is shown to be of order $1+\alpha$ in time, where α is the order of the time derivative described in the Caputo sense. We implement the algorithms in parallel using the shared memory systems (OpenMP) and the distributed memory systems (MPI). We discuss the merits and demerits of each of the parallel versions of the algorithms. Error and stability analysis of the scheme is also discussed. Unlike the Crank-Nicholson scheme for integer-order PDEs, the derived scheme has a lower order $(1+\alpha)$. This lower order is due to the singular kernel (as a result of the Caputo derivative) involved in the scheme's formulation. We used the time-graded mesh to improve the scheme's accuracy from $1+\alpha$ to two.

The last part of the study focuses on applying fractional derivatives and, in particular, the derived schemes to a scientific domain. We propose a time-fractional compartmental model comprising the susceptible, exposed, infected, hospitalized, recovered, and dead population for the COVID-19 epidemic. The properties and dynamics of the proposed model are discussed. We run several model simulations and estimate parameters using the Center for Systems and Science Engineering data at John Hopkins University for some selected states in the US. Furthermore, the efficacy of contact tracing (CT) is investigated by linking the disease model dynamics with actions of contact tracers such as monitoring and tracking. CT's impact on the reproduction number $\mathcal{R}_0$ of COVID-19 is described. In particular, the importance and relevance of the model parameters such as the number of reported cases, effectiveness of tracking and monitoring policy, and the transmission rates to CT are discussed.

TABLE OF CONTENTS

List of Tables

List of Figures

CHAPTER 1

Introduction and Preliminaries

1.1 Background of the Study

Fractional partial differential equations (PDEs) are equations involving non-integer partial derivatives. The fractional calculus concept is as old as the traditional or classical calculus, which Leibniz independently proposed and Newton [121], [130]. It began with the inquisitiveness of L'Hópital when he and Leibniz had correspondence where they discussed the meaning and interpretation of fractional derivatives of order one-half (non-integer order). The first definition of a fractional derivative may be attributed to Fourier [109], [121], who suggested an integral representation for the derivative. The first application of the fractional calculus was carried out by Abel in 1826 [1], [109], [121], who solved the integral equation associated with the tautochrone problem. This integral is later generalized as Abel's integral. The tautochrone problem deals with determining the curve for which the time taken by an object sliding without friction in uniform gravity to its lowest point is independent of its starting point on the curve. A few years later, the various formula for defining the fractional derivatives and integrals were formulated. Liouville [109], [121] in 1832 suggested a first formula based on differentiating the exponential function. A second definition that he formulated involves the gamma function. He applied both definitions to problems in potential theory. One of the main downsides of these definitions is that they are restricted to certain classes of functions. Years later, the Riemann-Liouville integral operator, which Liouville [102] and Riemann [139] proposed independently came to the limelight. Grünwald [63] and Letnikov [95] independently defined the fractional derivatives as a limit to a convergent series. Other notable works in this field appeared in the 18th century. Weyl [169] introduced a derivative similar to the Riemann-Liouville integral except that the limits and kernel are different. Riesz [140] proved the mean value theorem for fractional integrals. Caputo [29] proposed a new definition of the fractional derivative. This definition is more appropriate for problems involving fractional differential equations because of incorporating the initial conditions in the definition. Other notable researchers in this field's development include Bernoulli, Euler, Lagrange, Laplace, and Heaviside. Most of the widely used definitions of fractional derivatives and theorems in fractional calculus today are due to the researchers above' early works. Oldham published the first monograph on the subject and Spanner [130] in 1974. The first conference on the subject, which Ross [142] organized, took place at the University of New Haven in 1974. Several books on the analysis of fractional calculus have since then appeared in the literature, among which are the classical books of Podlubny [133], Kilbas *et al.* [87], Diethelm [80], Samko *et al.* [147], Pozrikidis [135], among others.

Several models of physical and biological processes are better described using fractional PDEs than the corresponding integer-order PDEs. They serve as a generalization of the integer-order PDEs and give some degree of freedom in varying the rate of change of these physical and biological processes. Such models include the modeling of memory-dependent phenomena (Caputo and Mainardi [27], Di Giuseppe *et al.* [41], Baleanu *et al.* [12], Podlubny [133]), mechanical properties of materials (Caputo and Mainardi [28]), anomalous diffusion in porous media (Fomin *et al.* [55], Metzler and Klafter [120]), groundwater flow problems (Cloot and Bootha [36], Iaffaldano *et al.* [71], Atangana *et al.* [9]), control theory (Podlubny [132], Baleanu *et al.* [11]), waves in viscoelasticity (Mainardi [113]), dynamics of particles (Tarasov [163]), nuclear reactor physics (Ray [137]), wave propagation in mechanics (Atanackovic [8]), finance and economics (Machado and Mata [111], Fallagoul *et al.* [53], Mainardi *et al.* [114]), biological and biochemical evolution (Bruce [168], Magin [112]). Due to the complexities (such as nonlocality, nonlinearity, memory dependencies) involved in the formulation of many of the models described above, their analytical solutions do not exist. Thus, the need for numerical approximations for the solution of such models. This need has led to a vast increase in the development of fast, robust, and reliable numerical schemes over the last few decades. Such numerical methods are based on finite difference approximations, finite volume, or finite element discretizations of the fractional operators. The space-fractional derivatives in a fractional PDE are discretized using the matrix transfer technique, the Grünwald-Letnikov approximations, fractional-centered approximations, Krylov methods, Fourier spectral methods, L1-L2 approximations, among others. For the discretization of time-fractional derivative, methods such as fractional linear multistep methods, the Grünwald-Letnikov approximations, L1-L2 approximations, among others, are used.

In this dissertation, we consider two classes of fractional PDEs, namely the space-fractional PDEs (fractional space-derivative and integer-order time derivative) and the time-space fractional PDEs (fractional time and space derivatives). We adopt the matrix transfer technique for spatial discretization, which easily generalizes the centered-difference approximation for integer-order PDEs. For space-fractional PDEs, we develop rational approximations to the exponential function for time stepping. For the time-space fractional PDEs, we develop novel numerical schemes based on the integral representation of the systems of ordinary differential equations obtained from the spatial discretization.

1.2 Aim and Objectives

This dissertation's main goal is the development and theoretical analysis of novel numerical methods for fractional PDEs and their applications. The objectives include:

(i) the development of numerical schemes for space-fractional PDEs with general boundary conditions;

(ii) the development of numerical methods for time-space fractional PDEs with general boundary conditions;

(iii) the theoretical analysis of the derived numerical schemes;

(iv) the fast implementation of the schemes using shared and distributed memory systems;

(v) the application of the schemes on a fractional-order compartmental model for predicting the dynamics of COVID-19;

(vi) studying and quantifying the efficacy of contact tracing in mitigating the spread of the COVID-19 epidemic.

1.3 Significance of the Study

The significance of the study lies in:

(i) the importance and applicability of fractional PDEs to a compartmental model for COVID-19;

(ii) fast implementation of numerical schemes; and

(iii) improving mathematical and computational research, and contributing to the body of knowledge.

1.4 Research Methodology

In this dissertation, we study the numerical integration of the nonlinear fractional PDE

$$ {}_cD^{\alpha}_{0,t}u = -\kappa(-\Delta)^{\frac{\beta}{2}}u(x,t) + f(u), \quad \text{in } \ \Omega \times (0,T] \tag{1.1} $$

coupled with a suitable initial and boundary conditions, where κ is the diffusivity, Ω is bounded in $\mathbb{R}$, ${}_cD^{\alpha}_{0,t}$ is the Caputo derivative (with respect to t) of order $0 < \alpha \leq 1$, $(-\Delta)^{\frac{\beta}{2}}$ is the fractional Laplacian of order $1 < \beta \leq 2$ and $f(u)$ is a nonlinear function of u. The definitions of the Caputo derivative and the fractional Laplacian are given in the next chapter. The fractional PDE (1.1) is discretized using the matrix transfer technique to obtain the systems of ordinary differential equations

$$ {}_cD^{\alpha}_{0,t}\mathbf{u} = -A^{\frac{\beta}{2}}\mathbf{u} + \mathbf{f}(\mathbf{u}) + \mathbf{g}(t) \tag{1.2} $$

where $\mathbf{g}(t)$ constitutes the effects at the boundaries of the problem, $\mathbf{u}$ and $\mathbf{f}(\mathbf{u})$ are the node values of u and $f(u)$, respectively. We develop schemes based on whether α

is an integer or not. For $\alpha = 1$, the exact solution of (1.2) is equivalent to the integral equation

$$\mathbf{u}(t_{k+1}) = e^{-\tau A^{\frac{\beta}{2}}}\mathbf{u}(t_k) + \tau \int_0^1 e^{-\tau A^{\frac{\beta}{2}}(1-s)}\,\mathbf{f}(\mathbf{u}(t_k + s\tau))\,ds + \tau \int_0^1 e^{-\tau A^{\frac{\beta}{2}}(1-s)}\,\mathbf{g}(t_k + s\tau)\,ds, \tag{1.3}$$

where t_k are the node points in the t-stencil. We approximate each of the terms in (1.3) using different rational approximations to the exponential function and, linear and constant approximations to the nonlinear function. If $\alpha \neq 1$, then eqn. (1.2) is equivalent to the Volterra integral equation

$$\mathbf{u}(t) - \mathbf{u}_0 = \frac{1}{\Gamma(\alpha)} \int_0^t (t-s)^{\alpha-1} \left(-A^{\frac{\beta}{2}}\mathbf{u}(s) + \mathbf{f}(\mathbf{u}(s)) + \mathbf{g}(s) \right) ds. \tag{1.4}$$

Numerical schemes are developed using approximations to the integral equation. In particular, constant and linear approximations to the nonlinear function are used.

The compartmental model described in this dissertation is a modification of the SEIR (Suscpetible-Exposed-Infected-Recovered) model. We modify the model by incorporating

(i) two compartments for the infected individuals: symptomatic and asymptomatic compartments;

(ii) hospitalized and dead compartments that denote the number of individuals that are hospitalized and dead, respectively;

(iii) the effect of time-fractional derivative on the model.

(iv) the effect of contact tracing in mitigating the spread of COVID-19.

CHAPTER 2

Fractional Calculus

2.1 Fractional Integral and Derivatives

We give some definitions of the fractional integrals and derivatives used in this dissertation. The gamma function is one of the most widely used functions in fractional calculus. It generalizes the factorial function and allows the independent variable to take values in $\mathbb{R}$ or even in $\mathbb{C}$.

Definition 2.1.1. *The gamma function $\Gamma(x)$ is defined by the integral [133]*

$$\Gamma(x) = \int_0^\infty e^{-t} t^{x-1}\, dt$$

which converges in the right half of the complex plane.

We define $L^1[a,b]$, where $-\infty \le a < x < b \le \infty$, to be the space consisting of all real-valued integrable functions on [a, b]. Furthermore, we define the space

$$W^{n,1}[a,b] = \left\{ f \in L^1[a,b] : \frac{d^n f}{dx^n} \in L^1[a,b] \right\}$$

which is the space of differentiable functions in $L^1[a,b]$. The Riemann-Liouville fractional integral and derivative forms the basis for most of the widely defined fractional derivatives.

Definition 2.1.2. *Let $f \in L^1[a,b]$, then the left- and right-sided Riemann-Liouville integrals of the function $f(x)$ are defined, respectively, as*

$$I^\alpha_{U^+} f(x) = \frac{1}{\Gamma(\alpha)} \int_a^x (x-\xi)^{\alpha-1} f(\xi)\, d\xi$$

and

$$I^\alpha_{b^-} f(x) = \frac{1}{\Gamma(\alpha)} \int_x^b (\xi - x)^{\alpha-1} f(\xi)\, d\xi.$$

Definition 2.1.3. *Let $f \in L^1[a,b]$, and $I^{n-\alpha}_{U^+}, I^{n-\alpha}_{b^-} \in W^{n,1}[a,b]$, $n = \lceil \alpha \rceil$, then the left- and right-sided Riemann-Liouville derivatives of the function $f(x)$ are defined, respectively, as*

$${}_{RL}D^\alpha_{a^+} f(x) = I^{n-\alpha}_{U^+} f(x) = \frac{1}{\Gamma(n-\alpha)} \frac{d^n}{dx^n} \int_a^x (x-\xi)^{n-\alpha-1} f(\xi)\, d\xi$$

and

$$ {}_{RL}D^{\alpha}_{b^-} f(x) = I^{n-\alpha}_{b^-} f(x) = \frac{(-1)^n}{\Gamma(n-\alpha)} \frac{d^n}{dx^n} \int_x^b (\xi - x)^{n-\alpha-1} f(\xi)\, d\xi, $$

where $\lceil \cdot \rceil$ *is the ceiling function.*

Another widely used fractional derivative is the Caputo derivative which was proposed by Michelle Caputo in 1967 and it is equivalent to the Riemann-Liouville derivative if the integer-order derivatives of the function at the given point are zeros. Let

$$ C^n[a,b] = \left\{ f : [a,b] \to \mathbb{R} : \frac{d^{n-1} f}{dx^{n-1}} \in C[a,b] \right\} $$

be the space of real-valued continuous functions $f(x)$ which have continuous derivatives up to order $n-1$ on $[a,b]$ such that $f^{n-1}(x)$ is absolutely continuous.

Definition 2.1.4. *Let* $f \in C^n[a,b]$*, then the left- and right-sided Caputo fractional derivative of order* α *is defined, respectively, as*

$$ {}_{c}D^{\alpha}_{a,x} f(x) = I^{n-\alpha}_{U^+} D^n f = \frac{1}{\Gamma(n-\alpha)} \int_a^x (x - \xi)^{n-\alpha-1} f^n(\xi)\, d\xi $$

and

$$ {}_{c}D^{\alpha}_{x,b} f(x) = I^{n-\alpha}_{b^-} D^n f = \frac{(-1)^n}{\Gamma(n-\alpha)} \int_x^b (\xi - x)^{n-\alpha-1} f^n(\xi)\, d\xi, $$

where $D^n f = \dfrac{d^n f}{dx^n}$.

Another definition of the fractional derivative was introduced by Grünwald and Letnikov which is taken as a limit of the sum of a convergent series.

Definition 2.1.5. *The Grünwald Letnikov left- and right-sided derivative of order* α *is defined as*

$$ {}_{GL}D^{\alpha}_{a,x} = \lim_{h \to 0} \frac{1}{h^{\alpha}} \sum_{k=0}^{\lfloor n \rfloor} (-1)^k \frac{\Gamma(\alpha+1) f(x - kh)}{\Gamma(k+1)\Gamma(\alpha - k + 1)}, \quad nh = x - a $$

and

$$ {}_{GL}D^{\alpha}_{x,b} = \lim_{h \to 0} \frac{1}{h^{\alpha}} \sum_{k=0}^{\lfloor n \rfloor} (-1)^k \frac{\Gamma(\alpha+1) f(x + kh)}{\Gamma(k+1)\Gamma(\alpha - k + 1)}, \quad nh = b - x. $$

Definition 2.1.6. *The Riesz fractional derivative of the function* $f(x)$ *of order* $n-1 < \alpha \leq n,\ n \geq 1$ *is defined as*

$$ \frac{\partial^{\alpha}}{\partial |x|^{\alpha}} f(x) = -\frac{1}{2\cos\left(\frac{\alpha\pi}{2}\right)} \frac{1}{\Gamma(n-\alpha)} \frac{d^n}{dx^n} \left\{ \int_{-\infty}^x (x - \xi)^{n-\alpha-1} f(\xi) d\xi + \int_x^{\infty} (\xi - x)^{n-\alpha-1} f(\xi) d\xi \right\}. $$

This definition shows that the Riesz derivative is a multiplicative sum of the left-sided and right-sided Riemann Liouville derivative.

There are several definitions of the fractional Laplacian in the literature, we give the definition of a few of them here.

1. **Singular Integral Representation**

   Definition 2.1.7. *[103], [135] The fractional Laplacian of a function $f(x)$ of order $\frac{\beta}{2}$, defined over the entire x-axis, is defined as*

   $$(-\Delta)^{\frac{\beta}{2}} f(x) = C(d,\beta)\, p.v. \int_{\mathbb{R}^d} \frac{f(x)-f(y)}{|x-y|^{d+\beta}}, \tag{2.5}$$

   where $C(d,\beta) = \dfrac{2^\beta \Gamma\left(\frac{\beta}{2}+\frac{d}{2}\right)}{\pi^{\frac{d}{2}} \left|\Gamma(-\frac{\beta}{2})\right|}$ *and p.v. denotes the principal value integral.*

   The term $f(x)-f(y)$ in (2.5) varnishes at the singularity of the integral and provides a regularization which together with averaging of positive and negative parts allows the principal value to exist, e.g., for smooth f with sufficient decay [103]. This definition shows the representation via the singular integral in real space $\mathbb{R}^d$.

2. **Fourier Definition**

   Definition 2.1.8. *[103], [147] The fractional Laplacian of a function $f(x)$ of order $\frac{\beta}{2}$, defined over the entire x-axis, is defined as*

   $$(-\Delta)^{\frac{\beta}{2}} f(x) = \frac{1}{(2\pi)^d} \int_{\mathbb{R}^d} |\xi|^\beta \, (f, e^{-i\xi\cdot x}) e^{i\xi\cdot x}\, d\xi = \mathcal{F}^{-1}\left\{ |\xi|^\beta \, \mathcal{F}\{u\}(\xi) \right\}(x),$$

   where $\mathcal{F}$ and $\mathcal{F}^{-1}$ are the Fourier and inverse Fourier transforms, respectively.

   This definition shows that Fractional Laplacian is a Fourier multiplier operator with symbol $|\xi|^\beta$. There is a relation between the Riesz derivative and the fractional Laplacian defined via the Fourier transform representation which is given in the following lemma.

   Lemma 2.1.1. *[177] For a function $f(x)$ defined on the entire real axis, the following inequality holds*

   $$-(-\Delta)^{\frac{\beta}{2}} = -\frac{1}{2cos(\frac{\beta\pi}{2})} \left[{}_{RL}D^{\beta}_{-\infty^+} + {}_{RL}D^{\beta}_{\infty^-} \right] = -\frac{\partial^\beta}{\partial|x|^\beta} f(x),$$

   where ${}_{RL}D^{\beta}_{-\infty^+}$ and ${}_{RL}D^{\beta}_{\infty^-}$ are the left- and right-sided Riemann-Liouville derivatives, respectively.

Yang *et al.* [177] also showed that this lemma also holds in a finite interval provided we assume that $f(x) = 0$ at the boundary points and beyond. This gives a major drawback for this definition as it is suitable only, in numerical discretizations, for problems with zero boundary conditions.

3. **Spectral Representation**

Definition 2.1.9. *[73] Suppose the Laplacian $(-\Delta)$ has a complete set of orthonormal eigenfunctions φ_n corresponding to the eigenvalues λ_n on a bounded region $\mathcal{D}$, i.e., $(-\Delta)\varphi_n = \lambda_n\varphi_n$ on $\mathcal{D}$; $\mathcal{B}(\varphi) = 0$ on ∂D, where $\mathcal{B}(\varphi)$ is one of the standard three homogeneous boundary conditions. Let*

$$\mathcal{F}_\eta = \left\{ f = \sum_{n=1}^{\infty} d_n\varphi_n,\ d_n = \langle f, \varphi_n \rangle \;\middle|\; \sum_{n=1}^{\infty} |d_n||\lambda|_n^{\frac{\eta}{2}} < \infty, \quad \eta = max(\beta, 0) \right\}.$$

Then for any $f \in \mathcal{F}_\eta$, the fractional Laplacian is defined as

$$(-\Delta)^{\frac{\beta}{2}} f = \sum_{n=1}^{\infty} d_n \lambda_n^{\frac{\eta}{2}} \varphi_n.$$

In this dissertation, we shall make use of the last definition of the fractional Laplacian because of its use for general boundary conditions.

2.2 Literature Review

This subsection shall review some numerical methods proposed for the numerical integration of space-fractional PDEs and time-space fractional PDEs.

For the space-fractional PDEs, several numerical methods based on the different definitions of the space derivatives have been proposed. Meerschaert and Tadjeran *et al.* [118], [119], [161], Sousa and Li [157], [158], and Shen *et al.* [151] developed numerical methods based on the Grünwald-Letnikov and the shifted Grünwald-Letnikov formula to the space-fractional derivatives. Liu *et al.* [104] obtained solutions of the fractional-in-space Fokker-Planck equations and the space-time fractional diffusion equations. Ortigueira [131], on the other hand, presented fractional centered approximations to the space-fractional derivative. His approach was followed by Çelik and Duman [30], and Khaliq *et al.* [83] to solve the space-fractional diffusion equations and the space-fractional Schrödinger equations, respectively. Ilic *et al.* [73] presented the Matrix Transfer Technique (MTT) for the numerical solution of fractional differential equations. Ding and Zhang [49] developed fourth-order methods based on the MTT. Yang *et al.* [178] also followed the MTT approach, who proposed a novel numerical technique for solving the time-space fractional diffusion equations based on approximating the matrix function vector product by the preconditioned Lanczos

method or the M-Lanczos method. Recently, Aceto and Novati [2] proposed a rational approximation to the dense matrix formed by the MTT by approximating its integral representation with the Gauss Jacobi quadrature rule. Chen *et al.* [33] solved the space-fractional telegraph equation using diagonal Padé approximants up to order 6. Li and Chen [99] gave a comprehensive survey of numerical methods for fractional partial differential equations. The class of exponential time differencing schemes was originally proposed by Cox and Mathews [39] for integer-order PDEs. This class of schemes was later modified and applied to space-fractional PDEs. In particular, we review the works of Khaliq, Bruce, Voss, and their collaborators. Khaliq [85] proposed a real distinct approximation to the exponential function and show that the scheme has close to maximal order for integer-order PDEs. This scheme was later modified to space-fractional PDEs [7], [76], [77]. Different Padé approximations to the exponential function were also proposed and later modified for space-fractional PDEs with efficient implementation techniques[15], [16], [83], [88].

Several numerical methods have also been proposed for solving time-space fractional equations based on different definitions of the space and time derivative. Mustapha [125] proposed an implicit finite-difference time-stepping method with finite-element space-discretization for sub-diffusion equations. Mustapha *et al.* [124] developed a discontinuous Galerkin method for time-fractional equations. Shen *et al.* [151] proposed finite difference approximation scheme for space-time fractional advection-diffusion equations. Xu and Hesthaven [174], [175] developed numerical schemes based on discontinuous Galerkin methods and spectral penalty methods, respectively, for fractional PDEs. Biala and Jator [17] developed a class of block implicit Adams methods for fractional differential equations. Deng [40] proposed finite element methods for space and time fractional Fokker-Planck equation. Diethelm [45], [80] and Diethelm *et al.* [46]–[48] discussed extensively numerical schemes for fractional differential equations and their error analysis. Diethelm [79] developed parallel algorithms for fractional differential equations. Li *et al.* [96] used Galerkin finite element in space and finite difference scheme in time for the numerical approximation of nonlinear fractional differential equations with sub- and super-diffusion. Zeng *et al.* [185], [186] proposed finite difference/element scheme to solve time-fractional equations. Zheng *et al.* [190] proposed a novel spectral method for the time-fractional Fokker-Planck equation. Zayernouri and Karniadakis [182], [183] developed a scheme that uses a Petrov-Galerkin in time and discontinuous Galerkin in space (PG-DG) method for fractional PDEs. They extended the PG-DG scheme to the DG-DG scheme in which spatial discretization is carried out using the discontinuous domain spectral/hp element method. They also introduced new fractional polynomials called polyfractonomials (used as basis functions) for spatial and temporal discretizations in an earlier paper[181]. Zayernouri and Matzavinos [184] developed fractional Adams type methods with applications to the fractional Keller-Segel chemotaxis system. Hu *et al.* [69] presented a finite difference scheme for multidimensional Caputo-type parabolic equation with fractional Laplacian. Li *et al.* [99] presented a space-time fractional phase-

field model and developed a lossless fast numerical method for the model's numerical simulation. Garrappa [141] discussed some theoretical and computational aspects of a trapezoidal method for fractional differential equations. Garrappa and Popolizio [61], and Garrappa [60] proposed a generalized exponential time differencing scheme that generalizes the aforementioned exponential scheme for time-stepping. Arshad *et al.* [5] developed a trapezoidal scheme for time-space fractional diffusion equations with Riesz derivatives. Iyiola *et al.* [76] developed a real distinct pole approximation to the generalized Mittag Lefler function and applied the approximation to an ultra-slow diffusion model. Xu *et al.* [176] proposed a parareal-in-time integration of time-fractional differential equations. Wu and Zhou [172], [173] developed parareal algorithms for fractional diffusion equations and time-fractional differential equations, respectively.

CHAPTER 3

Numerical Methods for Space-Fractional PDEs

3.1 Introduction

In this chapter, we discuss a class of schemes for space-fractional PDEs ($\alpha = 1$ in (1.1)) with time-dependent boundary conditions. This implies that we develop schemes for the class of PDEs

$$\frac{\partial u}{\partial t} = -\kappa\,(-\Delta)^{\frac{\beta}{2}}\,u + f(u),\ \text{in}\ \Omega \times (0,T],\quad 1 < \beta \leq 2, \tag{3.6}$$

with time-dependent boundary conditions and prescribed initial conditions where κ is the diffusion coefficient, Ω is bounded in $\mathbb{R}^d$ and d is the dimension of the problem. This is achieved via a combination of the MTT for spatial discretization and rational approximations to the exponential function for time-stepping. In particular, we develop the $[0,1]$-, $[1,1]$- and $[0,2]$-Padé approximations and a real distinct pole approximation to the exponential function. All simulations in this chapter were written in Matlab on an Intel(R) Core(TM) i7-4870HQ CPU running at 2.50GHz.

3.2 Spatial Discretization

The MTT was introduced by Ilić *et al.* in [72], [73] and is used for spatial discretization of the space-fractional derivative in (3.6). The choice of the MTT is based on the ease of extension to different types boundary problems and to higher dimensional problems. The basic idea of the MTT is to approximate the fractional Laplacian $(-\Delta)^{\frac{\beta}{2}}$ by the discrete matrix representation $A^{\frac{\beta}{2}}$, where A is a symmetric positive (semi) definite matrix obtained from the discrete representation of the standard Laplace operator subject to the boundary conditions imposed on (3.6).

Definition 3.2.1. *Suppose the Laplacian $(-\Delta)$ has a complete set of orthonormal eigenfunctions ϕ_n, $\phi_{n,m}$, or $\phi_{n,m,l}$ corresponding to the eigenvalues λ_n, $\lambda_{n,m}$, or $\lambda_{n,m,l}$, respectively, on a bounded region Ω, i.e., for $n, m, l = 0, 1, 2, \cdots$*

$$\begin{aligned}
(-\Delta)\phi_n &= \lambda_n \phi_n, && d = 1,\\
(-\Delta)\phi_{n,m} &= \lambda_{n,m}\phi_{n,m}, && d = 2,\\
(-\Delta)\phi_{n,m,l} &= \lambda_{n,m,l}\phi_{n,m,l}, && d = 3,
\end{aligned}$$

in Ω*;* $\mathcal{B}(\phi) = 0$ *on* $\partial\Omega$*, where* $\mathcal{B}(\phi)$ *is the homogeneous Dirichlet boundary conditions. Let*

$$f_1 = \sum_{n=0}^{\infty} c_n \phi_n \quad \textit{such that} \quad \sum_{n=0}^{\infty} |c_n|^2 |\lambda_n|^\beta < \infty, \qquad d = 1,$$

$$f_2 = \sum_{n=0}^{\infty}\sum_{m=0}^{\infty} c_{n,m} \phi_{n,m} \quad \textit{such that} \quad \sum_{n=0}^{\infty}\sum_{m=0}^{\infty} |c_{n,m}|^2 |\lambda_{n,m}|^\beta < \infty, \qquad d = 2,$$

$$f_3 = \sum_{n=0}^{\infty}\sum_{m=0}^{\infty}\sum_{l=0}^{\infty} c_{n,m,l} \phi_{n,m,l} \quad \textit{such that} \quad \sum_{n=0}^{\infty}\sum_{m=0}^{\infty}\sum_{l=0}^{\infty} |c_{n,m,l}|^2 |\lambda_{n,m,l}|^\beta < \infty, \qquad d = 3,$$

then $(-\Delta)^{\frac{\beta}{2}}$ *is defined by*

$$(-\Delta)^{\frac{\beta}{2}} f_1 = \sum_{n=0}^{\infty} c_n \lambda_n^{\frac{\beta}{2}} \phi_n, \qquad d = 1,$$

$$(-\Delta)^{\frac{\beta}{2}} f_2 = \sum_{n=0}^{\infty}\sum_{m=0}^{\infty} c_{n,m} \lambda_{n,m}^{\frac{\beta}{2}} \phi_{n,m}, \qquad d = 2,$$

$$(-\Delta)^{\frac{\beta}{2}} f_3 = \sum_{n=0}^{\infty}\sum_{m=0}^{\infty}\sum_{l=0}^{\infty} c_{n,m,l} \lambda_{n,m,l}^{\frac{\beta}{2}} \phi_{n,m,l}, \qquad d = 3.$$

Remark 3.2.1. *For homogeneous Dirichlet boundary conditions with* $\Omega = (a,b)^d$*,* $d = 1, 2, 3$*, and* $\mathbf{x} \in \Omega$*, then*

$$\lambda_{\eta_1,\cdots,\eta_d} = \sum_{n=\eta_1}^{\eta_d} \left(\frac{(n+1)\pi}{b-a} \right)^2,$$

and

$$\phi_{\eta_1,\cdots,\eta_d} = \left(\sqrt{\frac{2}{b-a}} \right)^d \prod_{n=\eta_1}^{\eta_d} \sin\left(\frac{(n+1)\pi(x_n - a)}{b-a} \right), \quad \eta_i = 0, 1, 2, \cdots.$$

Now, discretizing the fractional Laplacian $(-\Delta)^{\frac{\beta}{2}}$ with a uniform mesh of stepsize h in each spatial direction and using the MTT, we obtain

$$(-\Delta)^{\frac{\beta}{2}} u \approx \frac{A^{\frac{\beta}{2}}}{h^\beta} u,$$

where $h^{-2}A$ is the approximate matrix representation of the standard Laplace operator obtained using a finite difference approximation and $h^{-\beta}A^{\frac{\beta}{2}}$ is the approximate matrix representation of the fractional Laplacian. The matrix $h^{-\beta}A^{\frac{\beta}{2}}$ need not be formed explicitly but is constructed from the eigenvalues and eigenvectors of the matrix representation of the standard Laplacian. In particular, $h^{-\beta}A^{\frac{\beta}{2}} = H\Lambda^{\frac{\beta}{2}}H^{-1}$ where Λ and H are the eigenvalues and eigenvectors of the matrix $h^{-2}A$.

3.2.1 Spatial Discretization for One Dimensional Problems

In this subsection, we consider the spatial discretization of (3.6) in one dimension, that is $d = 1$. With homogeneous Dirichlet boundary conditions, the eigenvalues and eigenvectors of A are given as $\Lambda = \text{diag}(\lambda_1, \lambda_2, \cdots, \lambda_{N-1})$ and $H = (P_1, P_2, \cdots, P_{N-1})$, respectively, where

$$\lambda_i = 4 \sin\left(\frac{i\pi}{2N}\right), \quad i = 1, 2, \cdots, N-1$$

and

$$P_i = \left(\sin\left(\frac{1i\pi}{N}\right), \sin\left(\frac{2i\pi}{N}\right), \cdots, \sin\left(\frac{(N-1)i\pi}{N}\right)\right), \quad i = 1, 2, \cdots, N-1.$$

Consequently, the MTT transforms (3.6) into a system of nonlinear differential equations,

$$\begin{aligned} \frac{d\mathbf{u}}{dt} &= -\frac{\kappa}{h^\beta} A^{\frac{\beta}{2}} \mathbf{u} + \mathbf{f}(\mathbf{u}) + \mathbf{g}(t), \\ \mathbf{u}(0) &= \mathbf{u}_0, \end{aligned} \tag{3.7}$$

where $\mathbf{g}(t)$ constitutes the effects at the boundaries of the problem, $\mathbf{u}_0$ is the initial data and, $\mathbf{u}$ and $\mathbf{f}(\mathbf{u})$ denote the vectors of the node values of u and f, respectively. For simplicity and clarity, we demonstrate the idea by considering (3.6) in one dimension with the non-homogeneous mixed time-dependent boundary conditions and initial condition given by

$$\begin{aligned} \eta_1 u(0,t) + u_x(0,t) &= h_1(t), \quad t \in (0,T], \\ \eta_2 u(L,t) + u_x(L,t) &= h_2(t), \quad t \in (0,T], \\ u(x,0) &= u_0(x), \qquad x \in (0,L), \end{aligned} \tag{3.8}$$

where η_1 and η_2 are constants. At first, we consider the integer-order ($\beta = 2$) equivalent of (3.6) subject to (3.8). Given a positive integer N, with $h = L/N$ the spatial step size, we define the spatial grid points $x_n = nh$, $n = 0(1)N$ and let $u_n = u(x_n, t)$ and $f_n = f(u_n)$. Using second-order central difference approximations, we obtain

$$\begin{aligned} \frac{du_0}{dt} &= -\frac{\kappa}{h^2}(-u_{-1} + 2u_0 - u_1) + f_0, \\ \frac{du_n}{dt} &= -\frac{\kappa}{h^2}(-u_{n-1} + 2u_n - u_{n+1}) + f_n, \quad 1 \le n \le N-1, \\ \frac{du_N}{dt} &= -\frac{\kappa}{h^2}(-u_{N-1} + 2u_N - u_{N+1}) + f_N. \end{aligned} \tag{3.9}$$

The fictitious values are fixed using (3.8) as follows:

$$u_{-1} = u_1 + 2h\eta_1 u_0 - 2hh_1(t),$$

$$u_{N+1} = u_{N-1} - 2h\eta_2 u_N + 2hh_2(t)$$

so that (3.9) is rewritten as

$$\begin{aligned}
\frac{du_0}{dt} &= -\frac{\kappa}{h^2}\left((2-2h\eta_1)u_0 - 2u_1\right) + f_0 - \frac{2\kappa}{h}h_1(t),\\
\frac{du_n}{dt} &= -\frac{\kappa}{h^2}(-u_{n-1} + 2u_i - u_{n+1}) + f_n, \quad 1 \le n \le N-1,\\
\frac{du_N}{dt} &= -\frac{\kappa}{h^2}\left(-2u_{N-1} + (2+2h\eta_2)u_0\right) + f_N + \frac{2\kappa}{h}h_2(t),
\end{aligned} \tag{3.10}$$

which gives a semi-discrete approximation of the integer-order equivalent of (3.6) subject to (3.8). In matrix form, we can rewrite (3.10) as

$$\frac{d\mathbf{u}}{dt} = -\kappa\left(\frac{1}{h^2}A\mathbf{u} + \frac{2}{h}\mathbf{e}_0 h_1(t) - \frac{2}{h}\mathbf{e}_N h_2(t)\right) + \mathbf{f}(\mathbf{u}), \tag{3.11}$$

where $\mathbf{e}_0$ and $\mathbf{e}_N$ are standard basis vectors in $\mathbb{R}^{N+1}$, and A is the tridiagonal $(N+1)\times(N+1)$ given by

$$A = \begin{pmatrix}
2-2h\eta_1 & -2 & & & \\
-1 & 2 & -1 & & \\
 & \ddots & \ddots & \ddots & \\
 & & -1 & 2 & -1\\
 & & & -2 & 2+2h\eta_2
\end{pmatrix}.$$

Now, we observe that (3.6) could be written as

$$\frac{\partial u}{\partial t} = -\kappa\left(-\Delta\right)^{\frac{\beta}{2}-1}\left(-\Delta\right)u + f(u).$$

Let $m(-\Delta) = h^{-2}A$ be the matrix representation of the standard Laplace operator where homogeneous boundary conditions is imposed. If the function u does not satisfy homogeneous boundary conditions, the modified matrix representation $m((-\Delta)u) = \frac{1}{h^2}Au - \frac{2}{h}\mathbf{e}_0 h_1(t) + \frac{2}{h}\mathbf{e}_N h_2(t)$ is used. Assuming that the fractional Laplacian satisfies $m((-\Delta)^{\frac{\beta}{2}-1}) = \left(\frac{1}{h^2}A\right)^{\frac{\beta}{2}-1}$, then eqn. (3.6) with (3.8) have the spatial discretization

$$\frac{d\mathbf{u}}{dt} = -\kappa\left(\frac{1}{h^2}A\right)^{\frac{\beta}{2}-1}\left(\frac{1}{h^2}A\mathbf{u} + \frac{2}{h}\mathbf{e}_0 h_1(t) - \frac{2}{h}\mathbf{e}_N h_2(t)\right) + \mathbf{f}(\mathbf{u}), \tag{3.12}$$

which may be written as

$$\frac{d\mathbf{u}}{dt} = -\frac{\kappa}{h^{\beta}} A^{\frac{\beta}{2}} \mathbf{u} + \mathbf{f}(\mathbf{u}) + \mathbf{g}(t), \tag{3.13}$$

where,

$$\mathbf{g}(t) = -\frac{2\kappa}{h^{\beta-1}} A^{\frac{\beta}{2}-1} \left(\mathbf{e}_0 h_1(t) - \mathbf{e}_N h_2(t) \right),$$

is a contribution of the boundaries to the solution.

3.2.2 Spatial Discretization for Higher Dimensional Problems

Semi-discrete approximations for higher dimensional problems can be done in a similar manner to the one-dimensional problem. For instance, consider a 2D problem with $(x,\ y) = [0, L]^2$ subject to the non-homogeneous mixed time-dependent boundary conditions

$$\begin{aligned}
\eta_1 u(0, y, t) + u_x(0, y, t) &= h_1(y, t), \quad t \in (0, T], \quad y \in [0, L], \\
\eta_2 u(L, y, t) + u_x(L, y, t) &= h_2(y, t), \quad t \in (0, T], \quad y \in [0, L], \\
\eta_3 u(x, 0, t) + u_y(x, 0, t) &= h_3(x, t), \quad t \in (0, T], \quad x \in [0, L], \\
\eta_3 u(x, L, t) + u_y(x, L, t) &= h_4(x, t), \quad t \in (0, T], \quad x \in [0, L].
\end{aligned} \tag{3.14}$$

Let N be the number of grid points in the x and y directions with $h = L/N$, the spatial stepsize and $x_n = y_n = nh,\ n(1)N$. We also define $u_{i,j} = u(x_i, y_j, t)$, $f_{i,j} = f(u_{i,j})$ and $U_{i,j},\ i, j = -1, (N+1)$ to be fictitious values, then by using second order finite difference approximations, we obtain

$$
\begin{aligned}
\frac{du_{0,0}}{dt} &= -\frac{\kappa}{h^2}\left(-u_{0,1} - U_{0,-1} + 4u_{0,0} - U_{-1,0} - u_{1,0}\right) + f_{0,0},\\
\frac{du_{0,j}}{dt} &= -\frac{\kappa}{h^2}\left(-u_{0,j+1} - u_{0,j-1} + 4u_{0,j} - U_{-1,j} - u_{1,j}\right) + f_{0,j}, \quad j = 1(1)(N-1),\\
\frac{du_{i,0}}{dt} &= -\frac{\kappa}{h^2}\left(-u_{i,1} - U_{0,-1} + 4u_{i,0} - u_{i-1,0} - u_{i+1,0}\right) + f_{i,0}, \quad i = 1(1)(N-1),\\
\frac{du_{0,N}}{dt} &= -\frac{\kappa}{h^2}\left(-U_{0,N+1} - u_{0,N-1} + 4u_{0,N} - U_{-1,N} - u_{1,N}\right) + f_{0,N},\\
\frac{du_{N,0}}{dt} &= -\frac{\kappa}{h^2}\left(-u_{N,1} - U_{N,-1} + 4u_{N,0} - u_{N-1,0} - U_{N+1,0}\right) + f_{N,0},\\
\frac{du_{i,j}}{dt} &= -\frac{\kappa}{h^2}\left(-u_{i,j+1} - u_{i,j-1} + 4u_{i,j} - u_{i-1,j} - u_{i+1,j}\right) + f_{i,j}, \quad i,j = 1(1)(N-1),\\
\frac{du_{N,j}}{dt} &= -\frac{\kappa}{h^2}\left(-u_{N,j+1} - u_{N,j-1} + 4u_{N,j} - u_{N-1,j} - U_{N+1,j}\right) + f_{N,0}, \quad j = 1(1)(N-1),\\
\frac{du_{i,N}}{dt} &= -\frac{\kappa}{h^2}\left(-U_{i,N+1} - u_{i,N-1} + 4u_{i,N} - u_{i-1,N} - u_{i+1,N}\right) + f_{i,N}, \quad i = 1(1)(N-1),\\
\frac{du_{N,N}}{dt} &= -\frac{\kappa}{h^2}\left(-U_{N,N+1} - u_{N,N-1} + 4u_{N,N} - u_{N-1,N} - U_{N+1,N}\right) + f_{N,N}.
\end{aligned}
\tag{3.15}
$$

The fictitious values are fixed using (3.14) as follows:

$$U_{-1,j} = u_{1,j} + 2h\eta_1 u_{0,j} - 2h\, h_1(jh,t),$$

$$U_{N+1,j} = u_{N-1,j} - 2h\eta_2 u_{N,j} + 2h\, h_2(jh,t),$$

$$U_{i,-1} = u_{i,1} + 2h\eta_3 u_{i,0} - 2h\, h_3(ih,t),$$

$$U_{i,N+1} = u_{i,N-1} - 2h\eta_4 u_{i,N} + 2h\, h_4(ih,t),$$

$$i,\ j = 0(1)N.$$

so that (3.15) is written in matrix form as

$$\frac{d\mathbf{u}}{dt} = -\frac{\kappa}{h^2}A\mathbf{u} + \mathbf{f}(\mathbf{u}) + \mathbf{G}(t),$$

where

$$A = \begin{pmatrix} B_0 & C_0 & 0 & \cdots & 0 \\ C_1 & B_1 & C_1 & \cdots & 0 \\ \vdots & \ddots & \ddots & \ddots & 0 \\ 0 & \cdots & C_{N-1} & B_{N-1} & C_{N-1} \\ 0 & 0 & \cdots & C_N & B_N \end{pmatrix},$$

$$B_0 = \begin{pmatrix} 4-2h\eta_1-2h\eta_3 & -2 & & & \\ -1 & 4-2h\eta_1 & -1 & & \\ & \ddots & \ddots & \ddots & \\ & & -1 & 4-2h\eta_1 & -1 \\ & & & -2 & 4-2h\eta_1+2\eta_4 \end{pmatrix},$$

$$B_i = \begin{pmatrix} 4-2h\eta_3 & -2 & & & \\ -1 & 4 & -1 & & \\ & \ddots & \ddots & \ddots & \\ & & -1 & 4 & -1 \\ & & & -2 & 4+2h\eta_4 \end{pmatrix}, \quad i = 1(1)(N-1),$$

$$B_N = \begin{pmatrix} 4+2h\eta_2-2h\eta_3 & -2 & & & \\ -1 & 4+2h\eta_2 & -1 & & \\ & \ddots & \ddots & \ddots & \\ & & -1 & 4+2h\eta_2 & -1 \\ & & & -2 & 4+2h\eta_2+2h\eta_4 \end{pmatrix},$$

$C_0 = C_N = -2I$ and $C_i = -I,\ i = 1(1)(N-1)$ where I is the identity matrix. The vector $\mathbf{G}(t)$ is given as

$$\mathbf{G}(t) = \frac{2\kappa}{h} \begin{bmatrix} \mathbf{g}_0(t) \\ \mathbf{g}_1(t) \\ \vdots \\ \mathbf{g}_N(t) \end{bmatrix},$$

where

$$\mathbf{g}_0(t) = \left[-h_1(0,t) - h_3(0,t),\ -h_1(h,t),\ -h_1(2h,t), \cdots,\ -h_1((N-1)h,t),\ -h_1(Nh,t) + h_4(0,t)\right]^T,$$

$$\mathbf{g}_i(t) = \left[-h_3(ih,t), 0, \cdots, 0, h_4(ih,t)\right],\ i = 1(1)(N-1),$$

$$\mathbf{g}_N(t) = \left[h_2(0,t) - h_3(Nh,t),\ h_2(h,t),\ h_2(2h,t), \cdots,\ h_2((N-1)h,t),\ h_2(Nh,t) + h_4(Nh,t)\right]^T.$$

Thus, by the MTT, eqn. (3.6) with (3.14) results into the system of integer-order differential equations

$$\frac{d\mathbf{u}}{dt} = -\frac{\kappa}{h^{\beta}} A^{\frac{\beta}{2}} \mathbf{u} + \mathbf{f}(\mathbf{u}) + \mathbf{G}(t), \tag{3.16}$$

where $G(t)$ is now given as

$$\mathbf{G}(t) = -\frac{2\kappa}{h^{\beta-1}} A^{\frac{\beta}{2}-1} \begin{bmatrix} \mathbf{g}_0(t) \\ \mathbf{g}_1(t) \\ \vdots \\ \mathbf{g}_N(t) \end{bmatrix}.$$

A similar idea can be used for the non-homogeneous Dirichlet time–dependent boundary conditions

$$\begin{aligned} u(0, y, t) &= h_1(y, t), \qquad u(L, y, t) = h_2(x, t), \\ u(x, 0, t) &= h_3(x, t), \qquad u(x, L, t) = h_4(x, t), \end{aligned}$$

which has the semi-discrete approximation (3.16) with $A = \text{tridiag}(-I, B, I)$, where $B = \text{tridiag}(-1, 4, -1)$, and

$$\mathbf{G}(t) = \frac{\kappa}{h^{\beta}} A^{\frac{\beta}{2}-1} \begin{bmatrix} \mathbf{g}_1(t) \\ \vdots \\ \mathbf{g}_{N-1}(t) \end{bmatrix},$$

where

$$\mathbf{g}_1(t) = \left[h_1(h, t) + h_3(h, t),\ h_1(2h, t), \cdots,\ h_1((N-2)h, t),\ h_1((N-1)h, t) + h_4(h, t)\right]^T,$$

$$\mathbf{g}_i(t) = \left[h_3(ih, t), 0, \cdots, 0, h_4(ih, t)\right],\ i = 2(1)(N-2),$$

$$\begin{aligned} \mathbf{g}_{N-1}(t) = [&h_2(h, t) + h_3((N-1)h, t),\ h_2(2h, t), \cdots,\ h_2((N-2)h, t), \\ &h_2((N-1)h, t) + h_4((N-1)h, t)]^T. \end{aligned}$$

Remark 3.2.2. *Under certain assumptions on a projection and an interpolating operator defined in a Banach space, Simpson [153, pp. 26–27] showed that the matrix representation of the fractional Laplacian $A^{\frac{\beta}{2}}$ has the same order of convergence as the matrix representation of the standard Laplacian.*

3.3 Time Discretization

In this subsection, we discuss the time-stepping schemes for the numerical solution of the semi-discretized problem (3.13) or (3.16). For simplicity of notation, we will replace the matrix $\frac{\kappa}{h^\beta}A^{\frac{\beta}{2}}$ by $A^{\frac{\beta}{2}}$ with the intention that the $\frac{\kappa}{h^\beta}$ is already included in $A^{\frac{\beta}{2}}$. Let $t_k = k\tau,\ k = 0, \cdots, M$, where $\tau = T/M$ is the time step size and $\mathbf{u}(t_k) := \mathbf{u}_k$, then by the Duhamel principle, the exact solution of (3.13) can be written as

$$\mathbf{u}(t_{k+1}) = e^{-\tau A^{\frac{\beta}{2}}}\mathbf{u}(t_k) + \tau\int_0^1 e^{-\tau A^{\frac{\beta}{2}}(1-s)}\,\mathbf{f}(\mathbf{u}(t_k+s\tau))\,ds + \tau\int_0^1 e^{-\tau A^{\frac{\beta}{2}}(1-s)}\,\mathbf{g}(t_k+s\tau)\,ds. \tag{3.17}$$

The regularity of the initial and boundary data has to be carefully considered in order to develop stable numerical schemes with robust convergence properties. Having said this, we pursue the class of schemes which has the following form:

$$\mathbf{u}_{k+1} = R(\tau A^{\frac{\beta}{2}})\mathbf{u}_k + \tau\sum_{i=1}^{r} P_i(\tau A^{\frac{\beta}{2}})\,\mathbf{f}(\mathbf{u}_{k+i-1}) + \tau\sum_{j=1}^{m} Q_j(\tau A^{\frac{\beta}{2}})\,\mathbf{g}(t_k+\xi_j\tau), \tag{3.18}$$

where $R(z)$, $\{P_i(z)\}_{i=1}^{r}$, $\{Q_j(z)\}_{j=1}^{s}$ are rational functions bounded on the spectrum of $\tau A^{\frac{\beta}{2}}$ uniformly in τ, $\{\xi_j\}_{j=1}^{s}$ are Gaussian quadrature points in the interval $[0,1]$. The following proposition, which is a slight modification of the one proposed in [164, p. L8.1], describes the accuracy and equivalency of some relations which we shall use in the sequel.

Proposition 3.3.1. *The time discretization scheme (3.18) is accurate of order q if and only if*

$$R(z) = e^{-z} + O(z^{q+1}), \quad z \to 0, \tag{3.19}$$

and, for $0 \le l \le q$,

$$\sum_{i=1}^{m}\xi_i^l Q_i(z) = \frac{l!}{(-z)^{l+1}}\left(e^{-z} + \sum_{j=0}^{l}\frac{(-z)^j}{j!}\right) + O(z^{q-l}), \quad as \quad z \to 0, \tag{3.20}$$

or equivalently

$$\sum_{i=1}^{m}\xi_i^l Q_i(z) = \int_0^1 s^l e^{-z(1-s)}\,ds + O(z^{q-l}), \quad as \quad z \to 0, \tag{3.21}$$

and, for $1 \le k \le q$,

$$P_k(z) = \frac{(k-1)!}{(-z)^k}\left(e^{-z} + \sum_{j=0}^{k-1}\frac{(-z)^j}{j!}\right) + O(z^{q-k+1}), \quad as \quad z \to 0, \tag{3.22}$$

or equivalently

$$P_k(z) = \int_0^1 s^{(k-1)} e^{-z(1-s)}\, ds + O(z^{q-k+1}), \quad as \;\; z \to 0. \tag{3.23}$$

Proof. The exact solution of (3.13) is given as (3.17) using the variation of constant formula. If $f = g = 0$, then

$$\mathbf{u}(t_{k+1}) = e^{-\tau A^{\frac{\beta}{2}}} \mathbf{u}(t_k) = R(\tau A^{\frac{\beta}{2}}) \mathbf{u}(t_k) + O(\tau^{q+1}), \quad \text{as} \;\; \tau \to 0$$

which implies that

$$R(\tau A^{\frac{\beta}{2}}) = e^{-\tau A^{\frac{\beta}{2}}} + O(\tau^{q+1}), \quad \text{as} \;\; \tau \to 0.$$

This shows eqn. (3.19) of the proposition. We also observe from eqns. (3.17) and (3.18) that

$$\int_0^1 e^{-\tau A^{\frac{\beta}{2}}(1-s)} \mathbf{g}(t_k + s\tau)\, ds = \sum_{j=1}^{m} Q_j(\tau A^{\frac{\beta}{2}}) \mathbf{g}(t_k + \xi_j \tau) + O(\tau^{q+1}), \quad \text{as} \;\; \tau \to 0.$$

Expanding the terms $\mathbf{g}(t_k + s\tau)$ and $\mathbf{g}(t_k + \xi_j \tau)$ about t_k, we obtain

$$\int_0^1 s^l\, e^{-\tau A^{\frac{\beta}{2}}(1-s)}\, ds = \sum_{j=1}^{m} \xi_j^l\, Q_j(\tau A^{\frac{\beta}{2}}) + O(\tau^{q-l}), \quad \text{as} \;\; \tau \to 0$$

which gives the result in eqn. (3.20). It is easy to infer, using integration by parts and mathematical induction, that

$$\begin{aligned} \frac{1}{l!} \int_0^1 s^l e^{-z(1-s)}\, ds &= \frac{1}{(-z)^{l+1}} \sum_{j=l+1}^{\infty} \frac{(-z)^j}{j!} \\ &= \frac{1}{(-z)^{l+1}} \left(e^{-z} - \sum_{j=0}^{l} \frac{(-z)^j}{j!} \right) \end{aligned}$$

which proves the result in eqn. (3.21). For eqn. (3.22) and (3.23), we note that $\mathbf{f}(\mathbf{u})$ in (1.3) is approximated by a linear combination of the powers of $s\tau$, for example the constant function $\phi(s) = \mathbf{f}(\mathbf{u}_k)$ and the linear function

$$\phi(s) = \mathbf{f}(\mathbf{u}_k) + (t - t_k) \frac{\mathbf{f}(\mathbf{u}_{k+1}) - \mathbf{f}(\mathbf{u}_k)}{\tau}, \qquad t = s\tau$$

are different approximations to $\mathbf{f}(\mathbf{u})$. Thus

$$P_k(z)\, \mathbf{f}(\mathbf{u}(t_k + j\tau)) = \int_0^1 \phi(s)\, e^{-z(1-s)}\, ds, \quad j = 0, 1,$$

from which we obtain

$$P_k(z) = \int_0^1 s^{(k-1)} e^{-z(1-s)}\, ds + O(z^{q-k+1}), \quad \text{as} \quad z \to 0$$

and the results follows. □

It is computationally efficient to have $R(z)$, $\{P_i(z)\}_{i=1}^r$, $\{Q_j(z)\}_{j=1}^m$ share the same poles [86]. Thus, by considering a form similar to [86], [164], that is,

$$R(z) = \frac{\mathcal{N}(z)}{\mathcal{D}(z)}, \quad P_i(z) = \frac{\mathcal{N}_i(z)}{\mathcal{D}(z)}, \qquad Q_j(z) = \frac{\mathcal{M}_j(z)}{\mathcal{D}(z)},$$

where $\mathcal{N}(z)$, $\mathcal{N}_i(z)$, $\mathcal{M}_j(z)$, $\mathcal{D}(z)$, $(i = 1, \cdots, r, \quad j = 1, \cdots, m)$ are polynomials, we obtain the class of schemes

$$\mathcal{D}(\tau A^{\frac{\beta}{2}})\mathbf{u}_{k+1} = \mathcal{N}(\tau A^{\frac{\beta}{2}})\mathbf{u}_k + \tau \sum_{i=1}^{r} \mathcal{N}_i(\tau A^{\frac{\beta}{2}})\mathbf{f}(\mathbf{u}_{k+i-1}) + \tau \sum_{j=1}^{m} \mathcal{M}_j(\tau A^{\frac{\beta}{2}})\mathbf{g}(t_k + \xi_j \tau). \tag{3.24}$$

In what follows, we shall use different rational approximations to the exponential function to approximate the first quantity on the right hand side of (3.18), constant or linear approximations to the nonlinear function $\mathbf{f}(\mathbf{u})$ to approximate the second quantity and eqn. (3.20) in proposition (3.3.1) to approximate the last quantity.

3.3.1 First Order Accurate Method

3.3.1.1 (0, 1)-Padé approximation with Gaussian Quadrature (R01-G Scheme)

The simplest approximation to (3.17) is to approximate $\mathbf{f}(\mathbf{u})$ by the constant vector $\mathbf{f}(\mathbf{u}_k)$ and use the one-point Gaussian quadrature rule. This corresponds to $r = m = 1$ in (3.18) and we obtain the scheme

$$\mathbf{u}_{k+1} \approx \mathbf{v}_{k+1} = R(\tau A^{\frac{\beta}{2}})\mathbf{v}_k + \tau P_1(\tau A^{\frac{\beta}{2}})\mathbf{f}(\mathbf{v}_k) + \tau\, Q_1(\tau A^{\frac{\beta}{2}})\mathbf{g}(t_k + \xi_1 \tau), \tag{3.25}$$

where $P_1(z) = -\dfrac{1}{z}(e^{-z} - 1)$, $Q_1(z) = (1 + z)^{-1}$ and $\xi_1 = \dfrac{1}{2}$.

Approximating the exponential functions in (3.25) by the (0,1)-Padé approximation yields the scheme (3.24) with $\mathcal{D}(z) = (1 + z)$, $\mathcal{N}(z) = \mathcal{N}_1(z) = \mathcal{M}_1(z) = 1$ as

$$\left(I + \tau A^{\frac{\beta}{2}}\right)\mathbf{v}_{k+1} = \mathbf{v}_k + \tau\left(\mathbf{f}(\mathbf{v}_k) + \mathbf{g}(t_k + \xi_1 \tau)\right) \tag{3.26}$$

which we shall call the R01-G scheme.

3.3.2 Second Order Accurate Methods

Suppose $\mathbf{f}(\mathbf{u})$ in eqn. (3.17) is approximated by the linear function

$$\mathbf{f}(\mathbf{u}) \approx \mathbf{f}(\mathbf{u}_k) + (t - t_k)\frac{\mathbf{f}(\mathbf{u}^*_{k+1}) - \mathbf{f}(\mathbf{u}_k)}{\tau}, \quad t \in [t_k,\ t_{k+1}],$$

with the two-point Gaussian quadrature rule (these corresponds to $r = m = 2$ in eqn. (3.18), we obtain the scheme

$$\begin{aligned}\mathbf{u}_{k+1} \approx \mathbf{v}_{k+1} &= R(\tau A^{\frac{\beta}{2}})\mathbf{v}_k + \tau(P_1(\tau A^{\frac{\beta}{2}})\mathbf{f}(\mathbf{v}_k) + P_2(\tau A^{\frac{\beta}{2}})\mathbf{f}(\mathbf{v}^*_{k+1})) + \tau\sum_{i=1}^{2} Q_i(\tau A^{\frac{\beta}{2}})\mathbf{g}(t_k + \xi_i\tau) \\ &= R(\tau A^{\frac{\beta}{2}})\mathbf{v}_k + \tau\varphi(\tau A^{\frac{\beta}{2}})\mathbf{f}(\mathbf{v}_k) + \tau P_2(\tau A^{\frac{\beta}{2}})(\mathbf{f}(\mathbf{v}^*_{k+1}) - \mathbf{f}(\mathbf{v}_k)) + \tau\sum_{i=1}^{2} Q_i(\tau A^{\frac{\beta}{2}})\mathbf{g}(t_k + \xi_i\tau),\end{aligned}$$

where $\varphi(z) = -\frac{1}{z}(e^{-z}-1)$, $P_2(z) = \frac{1}{z^2}(e^{-z}-1+z)$, $P_1(z) = \varphi(z) - P_2(z)$. Therefore, we have the predictor-corrector scheme

$$\begin{aligned}\mathbf{v}^*_{k+1} &= R(\tau A^{\frac{\beta}{2}})\mathbf{v}_k + \tau\,\varphi(\tau A^{\frac{\beta}{2}})\mathbf{f}(\mathbf{v}_k) + \tau\sum_{j=1}^{2} Q_j(\tau A^{\frac{\beta}{2}})\,\mathbf{g}(t_k + \xi_j\tau)) \\ \mathbf{v}_{k+1} &= \mathbf{v}^*_{k+1} + \tau P_2(\tau A^{\frac{\beta}{2}})(\mathbf{f}(\mathbf{v}^*_{k+1}) - \mathbf{f}(\mathbf{v}_k)),\end{aligned} \tag{3.27}$$

where

$$\xi_1 = \frac{3-\sqrt{3}}{6} \quad \text{and} \quad \xi_2 = \frac{3+\sqrt{3}}{6}$$

are the Gaussian quadrature points of order 2. We shall report three schemes based on different rational approximations to the exponential function in (3.27).

3.3.2.1 (1, 1)-Padé approximation with Gaussian Quadrature (R11-G)

At first, we obtain $Q_j(z)$, $j = 1, 2$ by using proposition (3.3.1) and letting $R(z) = R_{1,1}(z)$ be the (1,1)-Padé approximation to the exponential function, then

$$\begin{aligned}Q_1(z) + Q_2(z) &= -\frac{1}{z}\left(\frac{2-z}{2+z} - 1\right), \\ \xi_1\,Q_1(z) + \xi_2\,Q_2(z) &= \frac{1}{z^2}\left(\frac{2-z}{2+z} - 1 + z\right),\end{aligned}$$

from which we obtain $Q_1(z) = Q_2(z) = (2+z)^{-1}$. Thus, using the (1,1)-Padé approximation for approximating the exponential functions in (3.27) we obtain (3.24)

with $\mathcal{D}(z) = (2+z),\ \mathcal{N}(z) = (2-z),\ \mathcal{N}_1(z) = \mathcal{N}_2(z) = \mathcal{M}_1(z) = \mathcal{M}_2(z) = 1$ which gives

$$\left(2I + \tau A^{\frac{\beta}{2}}\right)\mathbf{v}_{k+1} = \left(2I - \tau A^{\frac{\beta}{2}}\right)\mathbf{v}_k + \tau\left(\mathbf{f}(\mathbf{v}_k) + \mathbf{f}(\mathbf{v}_{k+1}) + \mathbf{g}(t_k + \xi_1\tau) + \mathbf{g}(t_k + \xi_2\tau)\right)$$

$$\mathbf{v}_{k+1} = \left(2I + \tau A^{\frac{\beta}{2}}\right)^{-1}\left[\left(2I - \tau A^{\frac{\beta}{2}}\right)\mathbf{v}_k + \tau\left(2\mathbf{f}(\mathbf{v}_k) + \mathbf{g}(t_k + \xi_1\tau) + \mathbf{g}(t_k + \xi_2\tau)\right)\right]$$

$$+ \tau\left(2I + \tau A^{\frac{\beta}{2}}\right)^{-1}\left(\mathbf{f}(\mathbf{v}_{k+1}) - \mathbf{f}(\mathbf{v}_k)\right).$$

Thus, we obtain the predictor-corrector (R11-G) scheme given as

$$\mathbf{v}^*_{k+1} = \left(4\left(2I + \tau A^{\frac{\beta}{2}}\right)^{-1} - I\right)\mathbf{v}_k + \tau\left(2I + \tau A^{\frac{\beta}{2}}\right)^{-1}\left(2\mathbf{f}(\mathbf{v}_k) + \mathbf{g}(t_k + \xi_1\tau) + \mathbf{g}(t_k + \xi_2\tau)\right)$$

$$\mathbf{v}_{k+1} = \mathbf{v}^*_{k+1} + \tau\left(2I + \tau A^{\frac{\beta}{2}}\right)^{-1}\left(\mathbf{f}(\mathbf{v}^*_{k+1}) - \mathbf{f}(\mathbf{v}_k)\right). \tag{3.28}$$

3.3.2.2 (0, 2)-Padé approximation with Gaussian Quadrature (R02-G)

Let $R(z)$ and all exponential functions in (3.27) be replaced by the $R_{0,2}(z)$ rational approximation, then $Q_1(z)$ and $Q_2(z)$ are obtained by solving the system

$$Q_1(z) + Q_2(z) = -\frac{1}{z}\left(\frac{2}{2 + 2z + z^2} - 1\right),$$

$$\xi_1\, Q_1(z) + \xi_2\, Q_2(z) = \frac{1}{z^2}\left(\frac{2}{2 + 2z + z^2} - 1 + z\right),$$

to obtain

$$Q_1(z) = -\frac{1}{2}\left(\frac{-2 + (\sqrt{3} - 1)z}{2 + 2z + z^2}\right), \qquad Q_2(z) = \frac{1}{2}\left(\frac{2 + (\sqrt{3} + 1)z}{2 + 2z + z^2}\right).$$

Thus, after some algebraic simplification, the scheme (3.24) is obtained with $\mathcal{D}(z) = (2 + 2z + 2z^2),\ \mathcal{N}(z) = 2,\ \mathcal{N}_1(z) = 1,\ \mathcal{N}_2(z) = 1 + z,\ \mathcal{M}_1(z) = -\frac{1}{2}(-2 + (\sqrt{3} -$

$1)z),\ \mathcal{M}_2(z) = \frac{1}{2}(2 + (\sqrt{3}+1)z)$ which gives

$$\begin{aligned}
\left(2I + 2\tau A^{\frac{\beta}{2}} + \tau^2 A^{\beta}\right)\mathbf{v}_{k+1} &= 2\mathbf{v}_k + \tau\left[\mathbf{f}(\mathbf{v}_k) + (I + \tau A^{\frac{\beta}{2}})\mathbf{f}(\mathbf{v}_{k+1})\right. \\
&\quad -\frac{1}{2}\left((-2I + (\sqrt{3}-1)\tau A^{\frac{\beta}{2}})\mathbf{g}(t_k + \xi_1\tau)\right. \\
&\quad \left.\left.-(2I + (\sqrt{3}+1)\tau A^{\frac{\beta}{2}})\mathbf{g}(t_k + \xi_2\tau)\right)\right], \\
\mathbf{v}_{k+1} &= \left(2I + 2\tau A^{\frac{\beta}{2}} + \tau^2 A^{\beta}\right)^{-1}\left[2\mathbf{v}_k + \tau(2I + \tau A^{\frac{\beta}{2}})\mathbf{f}(\mathbf{v}_k)\right. \\
&\quad -\frac{\tau}{2}\left((-2I + (\sqrt{3}-1)\tau A^{\frac{\beta}{2}})\mathbf{g}(t_k + \xi_1\tau)\right. \\
&\quad \left.\left.-(2I + (\sqrt{3}+1)\tau A^{\frac{\beta}{2}})\mathbf{g}(t_k + \xi_2\tau)\right)\right] \\
&\quad + \tau\left(2I + 2\tau A^{\frac{\beta}{2}} + \tau^2 A^{\beta}\right)^{-1}\left(I + \tau A^{\frac{\beta}{2}}\right)(\mathbf{f}(\mathbf{v}_{k+1}) - \mathbf{f}(\mathbf{v}_k)).
\end{aligned}$$

Thus, we obtain the predictor-corrector (R02-G) scheme given as

$$\begin{aligned}
\left(2I + 2\tau A^{\frac{\beta}{2}} + \tau^2 A^{\beta}\right)\mathbf{v}^*_{k+1} &= \left[2\mathbf{v}_k + \tau(2I + \tau A^{\frac{\beta}{2}})\mathbf{f}(\mathbf{v}_k) - \frac{\tau}{2}\left((-2I + (\sqrt{3}-1)\tau A^{\frac{\beta}{2}})\mathbf{g}(t_k + \xi_1\tau)\right.\right. \\
&\quad \left.\left.-(2I + (\sqrt{3}+1)\tau A^{\frac{\beta}{2}})\mathbf{g}(t_k + \xi_2\tau)\right)\right], \\
\mathbf{v}_{k+1} &= \mathbf{v}^*_{k+1} + \tau\left(2I + 2\tau A^{\frac{\beta}{2}} + \tau^2 A^{\beta}\right)^{-1}\left(2I + \tau A^{\frac{\beta}{2}}\right)\left(\mathbf{f}(\mathbf{v}^*_{k+1}) - \mathbf{f}(\mathbf{v}_k)\right).
\end{aligned} \tag{3.29}$$

The terms $\tau^2 A^{\beta} = \left(\tau A^{\frac{\beta}{2}}\right)^2$ in the R02-G scheme corresponds to the power of a matrix which poses a computational challenge. Numerical instability may arise from schemes involving higher order polynomials and such schemes may be subject to cancellation errors. To avoid this, we use the partial fraction technique, see ([59],

[85]) to obtain

$$R_{0,2}(z) = 2Re\left(\frac{\omega}{z-c}\right),$$
$$\varphi(z) = 2Re\left(\frac{\omega_1}{z-c}\right),$$
$$Q_1(z) = 2Re\left(\frac{\omega_2}{z-c}\right),$$
$$Q_2(z) = 2Re\left(\frac{\omega_3}{z-c}\right),$$
$$P_2(z) = 2Re\left(\frac{\omega_4}{z-c}\right),$$

where $Re(z)$ denotes the real part of z, $c = -1+i$, $\omega = -i$, $\omega_1 = \frac{1}{2} - \frac{1}{2}i$, $\omega_2 = \frac{-(\sqrt{3}-1)}{4} - \frac{(\sqrt{3}+1)}{4}i$, $\omega_3 = \frac{(\sqrt{3}+1)}{4} + \frac{(\sqrt{3}-1)}{4}i$, $\omega_4 = \frac{1}{2}$.

Thus, we may rewrite the R02-G scheme in a more efficient way as

$$\begin{aligned}
\left(\tau A^{\frac{\beta}{2}} - cI\right)\mathbf{w}^*_{k+1} &= \omega\mathbf{v}_k + \tau\left(\omega_1\mathbf{f}(\mathbf{v}_k) + \omega_2\mathbf{g}(t_k+\xi_1\tau) + \omega_3\mathbf{g}(t_k+\xi_2\tau)\right), \\
\mathbf{v}^*_{k+1} &= 2Re(\mathbf{w}^*_{k+1}), \\
\mathbf{v}_{k+1} &= \mathbf{v}^*_{k+1} + \tau\omega_4\left(\tau A^{\frac{\beta}{2}} - cI\right)^{-1}\left(\mathbf{f}(\mathbf{v}^*_{k+1}) - \mathbf{f}(v_k)\right).
\end{aligned} \tag{3.30}$$

3.3.2.3 Real Distinct Pole approximation with Gaussian Quadrature (RDP-G Scheme)

In this subsection, we consider a real distinct pole rational approximation (RDP) to the exponential function first discussed in [167] and later followed by [7], [75]. It has been shown that the approximation

$$R_{RDP}(z) = \frac{12-5z}{(3+z)(4+z)}$$

is nearly optimal in error constant with second-order convergence. Replacing the exponential functions in (3.27) by the RDP, we solve the system

$$Q_1(z) + Q_2(z) = -\frac{1}{z}\left(\frac{12-5z}{12+7z+z^2} - 1\right),$$
$$\xi_1\, Q_1(z) + \xi_2\, Q_2(z) = \frac{1}{z^2}\left(\frac{12-5z}{12+7z+z^2} - 1 + z\right)$$

to obtain

$$Q_1(z) = \frac{6 + \frac{1}{2}(1-\sqrt{3})z}{12 + 7z + z^2}, \quad Q_2(z) = \frac{6 + \frac{1}{2}(1+\sqrt{3})z}{12 + 7z + z^2}.$$

With some simplification, the scheme (3.24) is obtained with $\mathcal{D}(z) = (12 + 7z + 2z^2)$, $\mathcal{N}(z) = 12 - 5z$, $\mathcal{N}_1(z) = 6$, $\mathcal{N}_2(z) = 6 + z$, $\mathcal{M}_1(z) = 6 + \frac{1}{2}(1-\sqrt{3})z$, $\mathcal{M}_2(z) = 6 + \frac{1}{2}(1+\sqrt{3})z$ which gives

$$\begin{aligned}
\left(12I + 7\tau A^{\frac{\beta}{2}} + 2\tau^2 A^{\beta}\right)\mathbf{v}_{k+1} &= (12I - 5\tau A^{\frac{\beta}{2}})\mathbf{v}_k + \tau\left[6\mathbf{f}(\mathbf{v}_k) + \left(6I + \tau A^{\frac{\beta}{2}}\right)\mathbf{f}(\mathbf{v}_{k+1})\right. \\
&\quad + \left(6I + \frac{1}{2}(1-\sqrt{3})\tau A^{\frac{\beta}{2}}\right)\mathbf{g}(t_k + \xi_1\tau) \\
&\quad \left. + \left(6I + \frac{1}{2}(1+\sqrt{3})\tau A^{\frac{\beta}{2}}\right)\mathbf{g}(t_k + \xi_2\tau)\right], \\
\mathbf{v}_{k+1} &= \left(12I + 7\tau A^{\frac{\beta}{2}} + 2\tau^2 A^{\beta}\right)^{-1}\left[(12I - 5\tau A^{\frac{\beta}{2}})\mathbf{v}_k + \tau\left(12I + \tau A^{\frac{\beta}{2}}\right)\mathbf{f}(\mathbf{v}_k)\right. \\
&\quad + \tau\left(6I + \frac{1}{2}(1-\sqrt{3})\tau A^{\frac{\beta}{2}}\right)\mathbf{g}(t_k + \xi_1\tau) \\
&\quad \left. + \tau\left(6I + \frac{1}{2}(1+\sqrt{3})\tau A^{\frac{\beta}{2}}\right)\mathbf{g}(t_k + \xi_2\tau)\right] \\
&\quad + \tau\left(12I + 7\tau A^{\frac{\beta}{2}} + 2\tau^2 A^{\beta}\right)^{-1}\left(6I + \tau A^{\frac{\beta}{2}}\right)\left(\mathbf{f}(\mathbf{v}_{k+1}) - \mathbf{f}(\mathbf{v}_k)\right)
\end{aligned}$$

Thus, we obtain the predictor-corrector (RDP-G) scheme given as

$$\begin{aligned}
\left(12I + 7\tau A^{\frac{\beta}{2}} + 2\tau^2 A^{\beta}\right)\mathbf{v}^*_{k+1} &= \left[(12I - 5\tau A^{\frac{\beta}{2}})\mathbf{v}_k + \tau\left(12I + \tau A^{\frac{\beta}{2}}\right)\mathbf{f}(\mathbf{v}_k)\right. \\
&\quad + \tau\left(6I + \frac{1}{2}(1-\sqrt{3})\tau A^{\frac{\beta}{2}}\right)\mathbf{g}(t_k + \xi_1\tau) \\
&\quad \left. + \tau\left(6I + \frac{1}{2}(1+\sqrt{3})\tau A^{\frac{\beta}{2}}\right)\mathbf{g}(t_k + \xi_2\tau)\right] \\
\mathbf{v}_{k+1} &= \mathbf{v}^*_{k+1} + \tau\left(12I + 7\tau A^{\frac{\beta}{2}} + 2\tau^2 A^{\beta}\right)^{-1}\left(6I + \tau A^{\frac{\beta}{2}}\right)\left(\mathbf{f}(\mathbf{v}^*_{k+1}) - \mathbf{f}(\mathbf{v}_k)\right)
\end{aligned} \tag{3.31}$$

Similarly, a partial fraction decomposition technique results in

$$R_{RDP}(z) = \sum_{i=1}^{2} \left(\frac{\omega_i}{z - c_i} \right),$$
$$\varphi(z) = \sum_{i=1}^{2} \left(\frac{\omega_{1i}}{z - c_i} \right),$$
$$Q_1(z) = \sum_{i=1}^{2} \left(\frac{\omega_{2i}}{z - c_i} \right),$$
$$Q_2(z) = \sum_{i=1}^{2} \left(\frac{\omega_{3i}}{z - c_i} \right),$$
$$P_2(z) = \sum_{i=1}^{2} \left(\frac{\omega_{4i}}{z - c_i} \right),$$

where

$$c_1 = -3, \quad c_2 = -4, \quad \omega_1 = 27, \quad \omega_2 = -32$$
$$\omega_{11} = 9, \quad \omega_{12} = -8, \quad \omega_{21} = \frac{9 + 3\sqrt{3}}{2}, \quad \omega_{22} = -4 - 2\sqrt{3},$$
$$\omega_{31} = \frac{9 - 3\sqrt{3}}{2}, \quad \omega_{32} = -4 + 2\sqrt{3}, \quad \omega_{41} = 3, \quad \omega_{42} = -2.$$

Thus, we may rewrite the RDP-G scheme in more efficient way as

$$\begin{aligned}
\left(\tau A^{\frac{\beta}{2}} - c_1 I\right) \mathbf{a}^*_{k+1} &= \omega_1 \mathbf{v}_k + \tau \left(\omega_{11} \mathbf{f}(\mathbf{v}_k) + \omega_{21} \mathbf{g}(t_k + \xi_1 \tau) + \omega_{31} \mathbf{g}(t_k + \xi_2 \tau)\right), \\
\left(\tau A^{\frac{\beta}{2}} - c_2 I\right) \mathbf{b}^*_{k+1} &= \omega_2 \mathbf{v}_k + \tau \left(\omega_{12} \mathbf{f}(\mathbf{v}_k) + \omega_{22} \mathbf{g}(t_k + \xi_1 \tau) + \omega_{32} \mathbf{g}(t_k + \xi_2 \tau)\right), \\
\mathbf{v}^*_{k+1} &= \mathbf{a}^*_{k+1} + \mathbf{b}^*_{k+1}, \\
\mathbf{a}_{k+1} &= \left(\tau A^{\frac{\beta}{2}} - c_1 I\right)^{-1} \omega_{41} \left(\mathbf{f}(\mathbf{v}^*_{k+1}) - \mathbf{f}(\mathbf{v}_k)\right), \\
\mathbf{b}_{k+1} &= \left(\tau A^{\frac{\beta}{2}} - c_2 I\right)^{-1} \omega_{42} \left(\mathbf{f}(\mathbf{v}^*_{k+1}) - \mathbf{f}(\mathbf{v}_k)\right), \\
\mathbf{v}_{k+1} &= \mathbf{v}^*_{k+1} + \tau(\mathbf{a}_{k+1} + \mathbf{b}_{k+1}).
\end{aligned} \tag{3.32}$$

3.4 Efficient Implementation of the Schemes

The scheme developed in the previous section can be efficiently implemented by performing an LU decomposition (or efficiently precomputing the inverse) of the right

hand matrices, followed by a matrix-vector multiplications. We give the algorithms for the schemes below.

Algorithm 1 R11-G Scheme

1: Efficiently precompute the inverse of the matrix $\left(2I + \tau A^{\frac{\beta}{2}}\right)$, i.e., $B = \left(2I + \tau A^{\frac{\beta}{2}}\right)^{-1}$.

2: **for** $k = 1, \cdots, m.$ **do**

3: Obtain the solution vector $\mathbf{y}$ by the matrix-vector multiplication:

4: $$\mathbf{y} = B\left(4\mathbf{v}_k + \tau\left(2\mathbf{f}(\mathbf{v}_k) + \mathbf{g}(t_k + \xi_1\tau) + \mathbf{g}(t_k + \xi_2\tau)\right)\right).$$

5: Compute the predictor as $\mathbf{v}^*_{k+1}$ from $\mathbf{v}^*_{k+1} = \mathbf{y} - \mathbf{v}_k$.

6: Perform another matrix-vector multiplication to obtain $\mathbf{w}$:

7: $$\mathbf{w} = B\left(\tau\left[\mathbf{f}(\mathbf{v}^*_{k+1}) - \mathbf{f}(\mathbf{v}_k)\right]\right).$$

8: Compute the corrected solution as $\mathbf{v}_{k+1} = \mathbf{v}^*_{k+1} + \mathbf{w}$

9: **end for**

Algorithm 2 R02-G Scheme

1: Efficiently precompute the inverse or the LU decomposition of the matrix $(\tau A^{\frac{\beta}{2}} - cI)$, i.e, $B = (\tau A^{\frac{\beta}{2}} - cI)^{-1}$

2: **for** $k = 1, \cdots, (M-1)$, **do**

3: Obtain the solution vector $\mathbf{y}$ by the matrix-vector multiplication:

4: $$\mathbf{y} = B\left(\omega \mathbf{v}_k + \tau(\omega_1 \mathbf{f}(\mathbf{v}_k) + \omega_2 \mathbf{g}(t_k + \xi_1 \tau) + \omega_3 \mathbf{g}(t_k + \xi_2 \tau))\right).$$

5: Compute the predictor as $\mathbf{v}^*_{k+1} = 2\mathcal{R}e(y)$

6: Perform another matrix-vector multiplication to obtain $\mathbf{w}$:

7: $$\mathbf{w} = B\left(\omega_4 \tau \left[\mathbf{f}(\mathbf{v}^*_{k+1}) - \mathbf{f}(\mathbf{v}_k)\right]\right).$$

8: Compute the corrected solution as $\mathbf{v}_{k+1} = \mathbf{v}^*_{k+1} + 2\mathcal{R}e(\mathbf{w})$.

9: **end for**

Algorithm 3 RDP-G Scheme

1: Efficiently precompute the inverse or the LU decomposition of the matrices $(\tau A^{\frac{\beta}{2}} - c_1 I)$ and $(\tau A^{\frac{\beta}{2}} - c_2 I)$, i.e, $B1 = (\tau A^{\frac{\beta}{2}} - c_1 I)^{-1}$ and $B2 = (\tau A^{\frac{\beta}{2}} - c_2 I)^{-1}$

2: **for** $k = 1, \cdots, (M-1)$, **do**

3: Obtain the solution vectors:

4: $$\mathbf{w}1 = B1\left(\omega_1 \mathbf{v}_k + \tau(\omega_{11}\mathbf{f}(\mathbf{v}_k) + \omega_{21}\mathbf{g}(t_k + \xi_1\tau) + \omega_{31}\mathbf{g}(t_k + \xi_2\tau))\right).$$

5: $$\mathbf{w}2 = B2\left(\omega_2 \mathbf{v}_k + \tau(\omega_{12}\mathbf{f}(\mathbf{v}_k) + \omega_{22}\mathbf{g}(t_k + \xi_1\tau) + \omega_{32}\mathbf{g}(t_k + \xi_2\tau))\right).$$

6: Compute the predictor as $\mathbf{v}^*_{k+1} = \mathbf{w}1 + \mathbf{w}2$

7: Perform another matrix-vector multiplication to obtain:

8: $$\mathbf{w}1 = B1\left(\tau\omega_{41}(\mathbf{f}(\mathbf{v}^*_{k+1}) - \mathbf{f}(\mathbf{v}_k))\right).$$

9: $$\mathbf{w}2 = B2\left(\tau\omega_{42}(\mathbf{f}(\mathbf{v}^*_{k+1}) - \mathbf{f}(\mathbf{v}_k))\right).$$

10: Compute the corrected solution as $\mathbf{v}_{k+1} = \mathbf{v}^*_{k+1} + \mathbf{w}1 + \mathbf{w}2$.

11: **end for**

3.4.1 Computational complexity of the algorithms

The matrix $A^{\frac{\beta}{2}}$ is fully dense which implies that the computation of the exponential term in (3.17) is costly [39]. Algorithm 1 and 2 reduce the computational efforts by precomputing the the inverse of the matrices $\left(2I + \tau A^{\frac{\beta}{2}}\right)$ and $\left(\tau A^{\frac{\beta}{2}} - cI\right)$, respectively (once and outside of the loop), and then performing two matrix-vector multiplications at each step. For algorithm 3, the precomputation of the inverses $\left(\tau A^{\frac{\beta}{2}} - c_1 I\right)^{-1}$ and $\left(\tau A^{\frac{\beta}{2}} - c_2 I\right)^{-1}$ is performed, followed by four matrix-vector multiplications at each step. The matrix-vector multiplications require only $O(n^2)$ operations. The algorithms are performed quite efficiently by precomputing the inverses once and storing them. This makes the methods highly efficient and suitable for solving large systems of fractional-in-space multidimensional PDEs as is demonstrated in Numerical Examples Section. Another approach for algorithms 1, 2 and 3 is to

compute the LU decomposition of $\left(2I + \tau A^{\frac{\beta}{2}}\right)$, $\left(\tau A^{\frac{\beta}{2}} - cI\right)$ and, $\left(\tau A^{\frac{\beta}{2}} - c_1 I\right)$ and $\left(\tau A^{\frac{\beta}{2}} - c_2 I\right)$ respectively (once and outside of the loop), and then perform a forward and backward substitution at each step. However, this approach is much more costly since it requires four $O(n^2)$ operations (algorithms 1 and 2) and eight $O(n^2)$ (algorithm 3) at each step for the forward and backward substitution. Lastly, the explicit treatment of the reaction term ensures that we do not need to solve a nonlinear system at each step.

3.5 Convergence and Stability Analysis

In this subsection, we provide error estimates and discuss the stability of the schemes derived in the previous section.

3.5.1 Convergence Analysis

For simplicity, we shall simply write A for $A^{\frac{\beta}{2}}$ and consider the abstract initial value problem

$$\begin{aligned} \mathbf{u}' + A\mathbf{u} &= \mathbf{f}(\mathbf{u}) + \mathbf{g}(t), \quad t > 0 \\ \mathbf{u}(0) &= \mathbf{0} \end{aligned} \tag{3.33}$$

in a Hilbert space $\mathcal{H}$, where A is linear, self-adjoint, positive (semi-) definite on $\dot{H}^s = \mathcal{D}(A^{s/2})$ a subspace in L_2 with the corresponding norm

$$|v|_s = (A^s v,\, v)^{1/2} = ||A^{s/2} v||,$$

where $||\cdot|| = ||\cdot||_{L_2}$. We assume that the nonlinear function $\mathbf{f}(\mathbf{u})$ is Lipschitz continuous i.e. there exists a constant L such that for $\mathbf{u},\ \mathbf{v} \in \mathcal{D}(A^q)$, $||\mathbf{f}(\mathbf{u}) - \mathbf{f}(\mathbf{v})|| \leq L||\mathbf{u} - \mathbf{v}||$. This implies that $||\mathbf{f}(\mathbf{u})|| \leq L||\mathbf{u}|| + ||\mathbf{f}(\mathbf{0})||$. We shall use the notation $\mathbf{g}^{(k)}$ to denote $(d/dt)^k \mathbf{g}(t)$ in the sequel.

At first, we give an error estimate in the L_2 space norm for the time-stepping scheme (3.26) in the case that the initial data $\mathbf{v}$ is smooth, that is, $\mathbf{v} \in \mathcal{D}(A^q)$ for some $q \geq 1$.

Theorem 3.5.1. *Assume that the time discretization (3.26) is accurate of order one and that $|R(z)| < 1$ for $z > 0$. Then, if $\mathbf{g}(t) \in \dot{H}^2$, when $t \geq 0$ and $\mathbf{f}(\mathbf{u})$ is Lipschitz continuous with respect to $\mathbf{u}$, then for the solution of (3.26) and (3.33), the error estimate*

$$||\mathbf{e}_k|| \leq C\tau \left(\int_0^{t_k} \phi_1 \, ds + t_k \phi_2 \right),$$

holds uniformly for $0 \le t_k \le T$, *where* $\phi_1 = |\mathbf{u}|_2 + |\mathbf{g}|_2 + |\mathbf{f}(0)|_2 + ||\mathbf{g}^{(1)}|| + ||\mathbf{f}'||\,||\mathbf{u}'||$ *and* $\phi_2 = ||\mathbf{f}|| + \sup_{s\le t_k} |\mathbf{g}(s)|_2 + 1$.

Proof. A recursive application of the time-stepping scheme (3.26) to (3.33) gives

$$\mathbf{v}_k = \tau \sum_{j=0}^{k-1} R^{k-j-1}(\tau A)\left(P_1(\tau A)\mathbf{f}(\mathbf{v}_j) + Q_1(\tau A)\mathbf{g}(t_j + \xi_1\tau)\right).$$

The solution of (3.33) may be written, by setting $E(t) = e^{-\tau A}$, as

$$\begin{aligned}\mathbf{u}(t_k) &= \int_0^{t_k} E(t-s)\left(\mathbf{f}(\mathbf{u}(s)) + \mathbf{g}(s)\right) ds \\ &= \tau \sum_{j=0}^{k-1} E(t_{k-j-1})\, I_\tau(\mathbf{f}(\mathbf{u}(t_j)) + \mathbf{g}(t_j)),\end{aligned}$$

where

$$I_\tau \mathbf{g}(t) = \int_0^1 E(\tau(1-s))\mathbf{g}(t + s\tau)\, ds.$$

Using the error notation $\mathbf{e}_j = \mathbf{v}_j - \mathbf{u}(t_j)$, $P_\tau \mathbf{f}(\mathbf{v}_j) = P_1(\tau A)\mathbf{f}(\mathbf{v}_j)$ and $Q_\tau \mathbf{g}(t_j) = Q_1(\tau A)\mathbf{g}(t_k + \xi_1\tau)$, we have

$$\begin{aligned}\mathbf{e}_k &= \tau \sum_{j=0}^{k-1} \left\{R^{k-j-1}(\tau A)P_\tau \mathbf{f}(\mathbf{v}_j) - E(t_{k-j-1})I_\tau \mathbf{f}(\mathbf{u}(t_j)) + R^{k-j-1}(\tau A)Q_\tau \mathbf{g}(t_j) - E(t_{k-j-1})I_\tau \mathbf{g}(t_j)\right\} \\ &= \tau \sum_{j=0}^{k-1} \left[R^{k-j-1}(\tau A)P_\tau(\mathbf{f}(\mathbf{v}_j) - \mathbf{f}(\mathbf{u}(t_j))) + \left(R^{k-j-1}(\tau A)P_\tau - E(t_{k-j-1})I_\tau\right)\mathbf{f}(\mathbf{u}(t_j))\right] \\ &\quad + \tau \sum_{j=0}^{k-1} \left[\left(R^{k-j-1}(\tau A) - E(t_{k-j-1})\right) I_\tau \mathbf{g}(t_j) + R^{k-j-1}(\tau A)(Q_\tau - I_\tau)\mathbf{g}(t_j)\right] \\ &= \tau \sum_{j=0}^{k-1} \left(R^{k-j-1}(\tau A) - E(t_{k-j-1})\right) I_\tau(\mathbf{f}(\mathbf{u}(t_j)) + \mathbf{g}(t_j)) \\ &\quad + \tau \sum_{j=0}^{k-1} R^{k-j-1}(\tau A)(P_\tau - I_\tau)\,\mathbf{f}(\mathbf{u}(t_j)) + \tau \sum_{j=0}^{k-1} R^{k-j-1}(\tau A)P_\tau(\mathbf{f}(\mathbf{v}_j) - \mathbf{f}(\mathbf{u}(t_j))) \\ &\quad + \tau \sum_{j=0}^{k-1} R^{k-j-1}(\tau A)(Q_\tau - I_\tau)\,\mathbf{g}(t_j) \\ &= \mathbf{e}_k^1 + \mathbf{e}_k^2 + \mathbf{e}_k^3 + \mathbf{e}_k^4.\end{aligned}$$

Using eqn. (3.19) ($q = 1$) of proposition (3.3.1), the Lipschitz continuity of $\mathbf{f}(\mathbf{u})$ and observing that $E(\tau(1-s))$ commutes with $R^k(\tau A) - E(t_k)$, we obtain

$$\begin{aligned}
||\mathbf{e}_k^1|| &\leq \tau \sum_{j=0}^{k-1} \int_0^1 \left|\left|(R^{k-j-1}(\tau A) - E(t_{k-j-1}))(\mathbf{f}(\mathbf{u}(t_j)) + \mathbf{g}(t_j))\right|\right| \, ds \\
&\leq C\tau^2 \sum_{j=0}^{k+1} \int_0^1 \left|\mathbf{f}(\mathbf{u}(t_j + s\tau)) + \mathbf{g}(t_j + s\tau)\right|_2 \, ds \\
&\leq C\tau \int_0^{t_k} \left(|\mathbf{u}|_2 + |\mathbf{g}|_2 + |\mathbf{f}(0)|_2\right) \, ds.
\end{aligned}$$

To estimate e_k^2, we write

$$\begin{aligned}
I_\tau \mathbf{f}(\mathbf{u}(t_j)) &= \int_0^1 E(\tau(1-s))\mathbf{f}(\mathbf{u}(t_j + s\tau)) \, ds \\
&= \int_0^1 E(\tau(1-s))\mathbf{f}(\mathbf{u}(t_j)) \, ds + H_{1,1}\, \mathbf{f}(\mathbf{u}(t_j)),
\end{aligned}$$

where

$$H_{1,1}\, \mathbf{f}(\mathbf{u}(t_j)) = \int_0^1 E(\tau(1-s)) \left(\int_{t_j}^{t_j + s\tau} \mathbf{f}'(\mathbf{u}(w))\mathbf{u}'(w) \, dw \right) \, ds.$$

Therefore,

$$(P_\tau - I_\tau)\mathbf{f}(\mathbf{u}(t_j)) = h_1(\tau A)\mathbf{f}(\mathbf{u}(t_j)) + H_{1,1}\, \mathbf{f}(\mathbf{u}(t_j)),$$

where $h_1(z) = P_1(z) - \int_0^1 e^{-z(1-s)} \, ds$. From eqn. (3.23) of proposition (3.3.1), we obtain

$$||(P_\tau - I_\tau)\mathbf{f}(\mathbf{u}(t_j))|| \leq C\tau \, ||\mathbf{f}(\mathbf{u})|| + C \int_{t_j}^{t_{j+1}} ||\mathbf{f}'(\mathbf{u})|| \, ||\mathbf{u}'|| \, ds,$$

so that

$$||\mathbf{e}_k^2|| \leq C\tau \left(t_k ||\mathbf{f}|| + \int_0^{t_k} ||\mathbf{f}'|| \, ||\mathbf{u}'|| \, ds \right).$$

For $\mathbf{e}_k^3$, we have

$$\begin{aligned}
||P_\tau(\mathbf{f}(\mathbf{v}_j)) - \mathbf{f}(\mathbf{u}(t_j))|| &= \left|\left| \int_0^1 e^{-z(1-s)}(\mathbf{f}(\mathbf{v}_j)) - \mathbf{f}(\mathbf{u}(t_j)) \, ds + C\tau \right|\right| \\
&\leq C \left(||\mathbf{e}_j|| + \tau \right).
\end{aligned}$$

Thus,

$$||\mathbf{e}_k^3|| \leq C\tau \sum_{j=0}^{k-1} \left(||\mathbf{e}_j|| + \tau \right).$$

It is easy to show using mathematical induction that $||\mathbf{e}_k^3|| \leq Ct_k\tau$ since $\mathbf{e}_0 = 0$. Lastly, we estimate $\mathbf{e}_k^4$ using

$$\begin{aligned} I_\tau \mathbf{g}(t_j) &= \int_0^1 E(\tau(1-s))\mathbf{g}(t_j + s\tau)\, ds \\ &= \int_0^1 E(\tau(1-s))\mathbf{g}(t_j)\, ds + H_{1,2}\mathbf{g}(t_j) \end{aligned}$$

and

$$Q_\tau \mathbf{g}(t_j) = Q_1(\tau A)\mathbf{g}(t_j) + H_{1,3}\mathbf{g}(t_j),$$

where

$$H_{1,2}\mathbf{g}(t_j) = \int_0^1 E(\tau(1-s)) \left(\int_{t_j}^{t_{j+s\tau}} g'(w)\, dw \right) ds,$$

$$H_{1,3}\mathbf{g}(t_j) = Q_1(\tau A) \int_{t_j}^{t_{j+s\tau}} g'(w)\, dw.$$

Therefore,

$$(Q_\tau - I\tau)\mathbf{g}(t_j) = h_2(\tau A)\mathbf{g}(t_j) + H_1\mathbf{g}(t_j),$$

where $h_2(z) = Q_1(z) - \int_0^1 e^{-z(1-s)}\, ds$ and $H_1 = H_{1,2} + H_{1,3}$ satisfies

$$||H_1\mathbf{g}(t_j)|| \leq C \int_{t_j}^{t_{j+1}} ||\mathbf{g}'||\, ds.$$

Taking $m = 1$ in eqn. (3.20) of proposition (3.3.1), we have

$$h_2(z) = O(z) \ \text{ as } \ z \to 0 \Rightarrow |h_2(z)| \leq Cz \ \text{ on } \ \sigma(\tau A)$$

so that

$$||h_2(\tau A)v|| \leq \tau \sup_{z \in \sigma(\tau A)} \left| z^{-1} h_2(z) \right| \, ||Av|| \leq C\tau |v|_2.$$

Thus,

$$(Q_\tau - I_\tau)\mathbf{g}(t_j) \leq C \left(\tau |\mathbf{g}(t_j)|_2 + \int_{t_j}^{t_{j+1}} ||\mathbf{g}'||\, ds \right)$$

which implies

$$||\mathbf{e}_k^4|| \leq C\tau \left(t_k \sup_{s \leq t_k} |\mathbf{g}(s)|_2 + \int_0^{t_k} ||\mathbf{g}'||\, ds \right).$$

This completes the proof. □

Theorem 3.5.2. *Assume that the time discretization (3.27) is accurate of order two and that $|R(z)| < 1$ for $z > 0$. Then, if $\mathbf{g}^{(l)}(t) \in \dot{H}^{4-2l}$ for $l < 2$, when $t \geq 0$ and $\mathbf{f}(\mathbf{u})$ is Lipschitz continuous with respect to $\mathbf{u}$, then for the solution of eqns. (3.27) and (3.33), the error estimate*

$$||\mathbf{e}_k|| \leq C\tau^2 \left(\int_0^{t_k} \phi_1 \, ds + t_k \phi_2 + \max(t_k, 1) \right)$$

holds uniformly for $0 \leq t_k \leq T$, where $\phi_1 = |\mathbf{u}|_4 + |\mathbf{g}|_4 + |\mathbf{f}(\mathbf{0})|_4 + ||\boldsymbol{\psi}|| + ||\mathbf{g}^{(2)}||$, $\phi_2 = ||\mathbf{f}|| + \sup_{s \leq t_k} || \frac{d^2}{ds^2} \mathbf{f}(\mathbf{u}(s))|| + \sum_{l=0}^{1} \sup_{s \leq t_k} |\mathbf{g}^{(l)}(s)|_{4-2l}$ and $\mathbf{f}(\mathbf{u}(s)) = \int \boldsymbol{\psi}(\mathbf{u}(s)) \, ds$.

Proof. At first, we write

$$\begin{aligned}
\mathbf{v}_k^* &= \tau \sum_{j=0}^{k-1} R^{k-j-1}(\tau A) \left[\varphi(\tau A) \mathbf{f}(\mathbf{v}_j) + \sum_{i=1}^{2} Q_i(\tau A) \mathbf{g}(t_j + \xi_i \tau) \right] \\
&\quad + \tau \sum_{j=1}^{k-1} R^{k-j}(\tau A) P_2(\tau A) (\mathbf{f}(\mathbf{v}_j^*) - \mathbf{f}(\mathbf{v}_{j-1})),
\end{aligned}$$

$$\begin{aligned}
\mathbf{v}_k &= \mathbf{v}_k^* + \tau P_2(\tau A)(\mathbf{f}(\mathbf{v}_k^*) - \mathbf{f}(\mathbf{v}_{k-1})) \\
&= \tau \sum_{j=0}^{k-1} R^{k-j-1}(\tau A) \left[P_1(\tau A) \mathbf{f}(\mathbf{v}_j) + P_2(\tau A) \mathbf{f}(\mathbf{v}_{j+1}^*) + \sum_{i=1}^{2} Q_i(\tau A) \mathbf{g}(t_j + \xi_i \tau) \right].
\end{aligned}$$

Using the notations

$$\overline{P}_\tau \mathbf{f}(\mathbf{v}_j) = P_1(\tau A) \mathbf{f}(\mathbf{v}_j) + P_2(\tau A) \mathbf{f}(\mathbf{v}_{j+1}^*) \quad \text{and} \quad \overline{Q}_\tau \mathbf{g}(t_j) = \sum_{l=1}^{2} Q_i(\tau A) \mathbf{g}(t_j + \xi_i \tau),$$

we have

$$\begin{aligned}
\mathbf{e}_k &= \tau \sum_{j=0}^{k-1} \left[R^{k-j-1}(\tau A) \overline{P}_\tau \mathbf{f}(\mathbf{v}_j) - E(t_{k-j-1}) I_\tau \mathbf{f}(\mathbf{u}(t_j)) \right] \\
&\quad + \tau \sum_{j=0}^{k-1} \left[R^{k-j-1}(\tau A) \overline{Q}_\tau \mathbf{g}(t_j) - E(t_{k-j-1}) I_\tau \mathbf{g}(t_j) \right] \\
&= \tau \sum_{j=0}^{k-1} \left(R^{k-j-1}(\tau A) - E(t_{k-j-1}) \right) I_\tau (\mathbf{f}(\mathbf{u}(t_j)) + \mathbf{g}(t_j)) + \tau \sum_{j=0}^{k-1} R^{k-j-1}(\tau A) (\overline{P}_\tau - I_\tau) \mathbf{f}(\mathbf{u}(t_j)) \\
&\quad + \tau \sum_{j=0}^{k-1} R^{k-j-1}(\tau A) \overline{P}_\tau (\mathbf{f}(\mathbf{v}_j) - \mathbf{f}(\mathbf{u}(t_j))) + \tau \sum_{j=0}^{k-1} R^{k-j-1}(\tau A) (\overline{Q}_\tau - I_\tau) \mathbf{g}(t_j) \\
&= \mathbf{e}_k^1 + \mathbf{e}_k^2 + \mathbf{e}_k^3 + \mathbf{e}_k^4
\end{aligned}$$

Using eqn. (3.19) ($q = 2$) of proposition (3.3.1), the Lipschitz continuity of $\mathbf{f}(\mathbf{u})$ and observing that $E(\tau(1-s))$ commutes with $R^k(\tau A) - E(t_k)$, we obtain

$$\begin{aligned}
||\mathbf{e}_k^1|| &\leq \tau \sum_{j=0}^{k-1} \int_0^1 \left|\left|(R^{k-j-1}(\tau A) - E(t_{k-j-1}))(\mathbf{f}(\mathbf{u}(t_j)) + \mathbf{g}(t_j))\right|\right| \, ds \\
&\leq C\tau^3 \sum_{j=0}^{k+1} \int_0^1 |\mathbf{f}(\mathbf{u}(t_j + s\tau)) + \mathbf{g}(t_j + s\tau)|_4 \, ds \\
&\leq C\tau^2 \int_0^{t_k} (|\mathbf{u}|_4 + |\mathbf{g}|_4 + |\mathbf{f}(0)|_4) \, ds.
\end{aligned}$$

For the estimate of $\mathbf{e}_k^2$, we rewrite $\overline{P}_\tau \mathbf{f}(\mathbf{u}(t_j))$ as

$$\begin{aligned}
\overline{P}_\tau \mathbf{f}(\mathbf{u}(t_j)) &= P_1(\tau A)\mathbf{f}(\mathbf{u}(t_j)) + P_2(\tau A)\mathbf{f}(\mathbf{u}(t_{j+1})) \\
&= \varphi(\tau A)\mathbf{f}(\mathbf{u}(t_j)) + P_2(\tau A)(\mathbf{f}(\mathbf{u}(t_{j+1})) - \mathbf{f}(\mathbf{u}(t_j))), \\
I_\tau \mathbf{f}(\mathbf{u}(t_j)) &= \int_0^1 E(\tau(1-s))\mathbf{f}(\mathbf{u}(t_j + s\tau)) \, ds \\
&= \int_0^1 E(\tau(1-s)) \left(\mathbf{f}(\mathbf{u}(t_j)) + s\tau \frac{(\mathbf{f}(\mathbf{u}(t_{j+1})) - \mathbf{f}(\mathbf{u}(t_j)))}{\tau} \right) ds + H_{2,1}\mathbf{f}(\mathbf{u}(t_j)),
\end{aligned}$$

where

$$H_{2,1}\mathbf{f}(\mathbf{u}(t_j)) = \int_0^1 E(\tau(1-s)) \frac{s\tau(s\tau - \tau)}{2} \frac{d^2}{d\zeta^2}\mathbf{f}(\mathbf{u}(\zeta)), \qquad \zeta \in [t_j, \ t_{j+1}],$$

satisfies

$$||H_{2,1}\mathbf{f}(\mathbf{u}(t_j))|| \leq C\tau^2 \sup_{\zeta \in [t_j, t_{j+1}]} \left|\left| \frac{d^2}{d\zeta^2}\mathbf{f}(\mathbf{u}(\zeta)) \right|\right|.$$

Therefore,

$$(\overline{P}_\tau - I_\tau)\mathbf{f}(\mathbf{u}(t_j)) = \overline{h}_1(\tau A)\mathbf{f}(\mathbf{u}(t_j)) + \overline{h}_2(\tau A)\left[\mathbf{f}(\mathbf{u}(t_{j+1})) - \mathbf{f}(\mathbf{u}(t_j))\right] - H_{2,1}\mathbf{f}(\mathbf{u}(t_j)),$$

where $\overline{h}_1(z) = \varphi(z) - \int_0^1 e^{-z(1-s)} \, ds$ and $\overline{h}_2(z) = P_2(z) - \int_0^1 s e^{-z(1-s)} \, ds$. Taking $k = 1$ and $k = 2$ in eqns. (3.23) of proposition (3.3.1) with $\mathbf{f}(\mathbf{u}(s)) = \int \boldsymbol{\psi}(\mathbf{u}(s)) \, ds$, we have

$$||(\overline{P}_\tau - I_\tau)\mathbf{f}(\mathbf{u}(t_j))|| \leq C\tau^2 ||\mathbf{f}(\mathbf{u})|| + C\tau \int_{t_j}^{t_{j+1}} ||\boldsymbol{\psi}(\mathbf{u})|| \, ds + C\tau^2 \sup_{\zeta \in [t_j, t_{j+1}]} \left|\left| \frac{d^2}{d\zeta^2}\mathbf{f}(\mathbf{u}(\zeta)) \right|\right|$$

so that

$$||\mathbf{e}_k^2|| \leq C\tau^2 \left(t_k ||\mathbf{f}|| + \int_0^{t_k} ||\boldsymbol{\psi}(\mathbf{u})|| \, ds + t_k \sup_{s \leq t_k} \left|\left| \frac{d^2}{ds^2}\mathbf{f}(\mathbf{u}(s)) \right|\right| \right).$$

We estimate $\mathbf{e}_k^3$ using the Lipschitz continuity of $\mathbf{f}(\mathbf{u})$ which gives

$$\begin{aligned}||\overline{P}_\tau(\mathbf{f}(\mathbf{v}_j)-\mathbf{f}(\mathbf{u}(t_j)))|| &\le \left|\left|\int_0^1 e^{-z(1-s)}(\mathbf{f}(\mathbf{v}_j)-\mathbf{f}(\mathbf{u}(t_j)))\,ds + C\tau^2\right|\right| \\ &\quad + \left|\left|\int_0^1 se^{-z(1-s)}(\mathbf{f}(\mathbf{v}_{j+1}^*)-\mathbf{f}(\mathbf{u}(t_{j+1})))\,ds + C\tau\right|\right| \\ &\le C(||\mathbf{e}_j||+\tau^2)+C(||\mathbf{e}_{j+1}^*||+\tau).\end{aligned}$$

By construction $||\mathbf{e}_{j+1}^*|| \le ||\mathbf{e}_j||$ so that

$$||\mathbf{e}_k^3|| \le C\tau\sum_{j=0}^{k-1}(||\mathbf{e}_j||+\tau+\tau^2).$$

It is easy to show, using mathematical induction, that

$$\begin{aligned}||\mathbf{e}_k^3|| &\le C\tau^2(t_k+1) \\ &\le C\tau^2\max(t_k,1), \qquad \text{(since C is arbitrary).}\end{aligned}$$

Lastly, we estimate $\mathbf{e}_k^4$ as

$$\begin{aligned}\overline{Q}_\tau\mathbf{g}(t_j) &= \sum_{i=1}^{2} Q_i(\tau A)\mathbf{g}(t_j+\xi_i\tau) \\ &= \sum_{l=0}^{1}\frac{\tau^l}{l!}\left(\sum_1^2 \xi_i^l Q_i(\tau A)\right)\mathbf{g}^{(l)}(t_j)+H_{2,2}\mathbf{g}(t_j) \\ I_\tau\mathbf{g}(t_j) &= \int_0^1 E(\tau(1-s))\mathbf{g}(t_j+s\tau)\,ds \\ &= \sum_{l=0}^{1}\frac{\tau^l}{l!}\left(\int_0^1 s^l E(\tau(1-s))\,ds\right)\mathbf{g}^{(l)}(t_j)+H_{2,3}\mathbf{g}(t_j),\end{aligned}$$

where

$$\begin{aligned}H_{2,2}\mathbf{g}(t_j) &= \sum_{i=1}^{2} Q_i(\tau A)\left(\int_{t_j}^{t_j+\xi_i\tau}(t_j+\xi_i\tau-w)\mathbf{g}^{(2)}(w)\,dw\right), \\ H_{2,3}\mathbf{g}(t_j) &= \int_0^1 E(\tau(1-s))\left(\int_{t_j}^{t_j+s\tau}(t_j+s\tau-w)\mathbf{g}^{(2)}(w)\,dw\right)ds.\end{aligned}$$

We conclude that

$$(\overline{Q}_\tau - I_\tau)\mathbf{g}(t_j) = \sum_0^1 \frac{\tau^l}{l!}\overline{h}_l(\tau A)\mathbf{g}^{(l)}(t_j) + H_2\mathbf{g}(t_j),$$

where

$$\overline{h}_l(z) = \sum_{i=1}^{2} \xi_i^l Q_i(z) - \int_0^1 s^l e^{-z(1-s)}\, ds$$

and $H_2 = H_{2,2} + H_{2,3}$ satisfies

$$||H_2\mathbf{g}(t_j)|| \le C\tau \int_{t_j}^{t_{j+1}} ||\mathbf{g}'||\, ds.$$

Therefore,

$$||(\overline{Q}_\tau - I_\tau)\mathbf{g}(t_j)|| \le C\tau^2 \sum_{l=0}^{1} |\mathbf{g}^{(l)}(t_j)|_{4-2l} + C\tau \int_{t_j}^{t_{j+1}} ||\mathbf{g}^{(2)}||\, ds$$

so that

$$||\mathbf{e}_k^4|| \le C\tau^2 \left(t_k \sum_{l=0}^{1} \sup_{s\le t_k} |\mathbf{g}^{(l)}(s)|_{4-2l} + \int_0^{t_k} ||\mathbf{g}^{(2)}||\, ds \right).$$

This completes the proof. □

Corollary 3.5.1. *The R11-G, R02-G and RDP-G schemes are second-order accurate.*

3.5.2 Stability Analysis

Definition 3.5.1. *[129] A rational approximation $R(z)$ of e^{-z} is said to be A-acceptable if $|R(z)| < 1$ whenever $Re(z) < 0$, and L-acceptable if, in addition, $|R(z)| \to 0$ as $Re(z) \to \infty$.*

Lemma 3.5.1. *If $Re(z) > 0$, then the rational approximations $R_{11}(z)$, $R_{02}(z)$, $R_{RDP}(z)$ to e^{-z} satisfies*

$$|R_{11}(z)| = \left|\frac{2-z}{2+z}\right| < 1,$$

$$|R_{02}(z)| = \left|\frac{2}{2+2z+z^2}\right| < 1,$$

$$|R_{RDP}(z)| = \left|\frac{12-5z}{12+7z+z^2}\right| < 1.$$

In addition, $R_{02}(z) \to 0$ and $R_{RDP}(z) \to 0$ as $z \to \infty$.

Proof. For $R_{11}(z)$, we only need show that

$$|2+z|^2 - |2-z|^2 \geq 0.$$

Therefore

$$\begin{aligned} |2+z|^2 - |2-z|^2 &= (2+z)(2+\overline{z}) - (2-z)(2-\overline{z}) \\ &= 4 + 2z + 2\overline{z} + z\overline{z} - 4 + 2\overline{z} + 2z - z\overline{z} \\ &= 4(z+\overline{z}) \\ &= 8Re(z) \geq 0, \quad (\text{since } Re(z) > 0). \end{aligned}$$

In a similar manner, it is easy to show that $|2+2z+z^2|^2 - 4 \geq 0$ and $|12+7z+z^2|^2 - |12-5z|^2 \geq 0$. This completes the proof. □

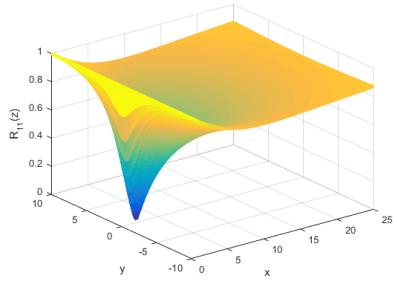

(a) R11-G scheme

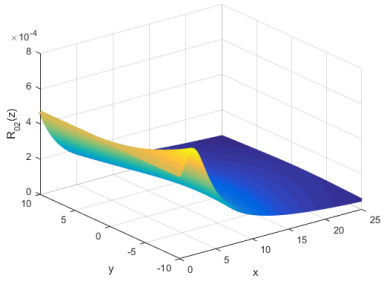

(b) R02-G scheme

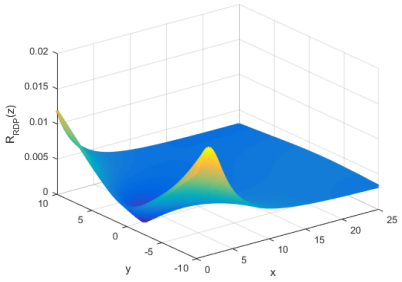

(c) RRDP-G scheme

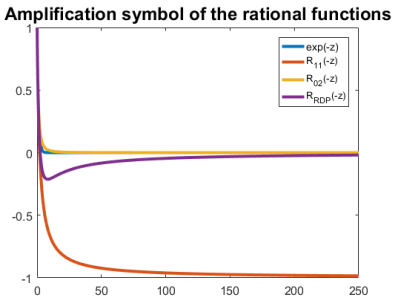

(d) Amplification symbols

Figure 1: Behavior of the rational functions for $z \in [0, 25] \times [-10, 10]$ and their amplification symbols.

Fig. 1(a) - (c) demonstrates the behavior of the $(1, 1)$- and $(0, 2)$-Padé approximations, and the real distinct pole approximation to the exponential function e^{-z}. In particular, we observe that the $(1, 1)$-Padé does not converge to zero for increasing values of z and does not satisfy the maximum modulus theorem for L-acceptability as defined in definition (3.5.1). Fig. 1(d) shows the amplification symbols of the rational functions compared to e^{-z}. As can be seen from the figure, the $(1, 1)$-Padé approximation does not approach zero. This also corroborates the fact that the R11-G scheme is not L-acceptable.

3.5.3 A Reliability Constraint on R11-G Scheme

Although the R11-G scheme is A-acceptable, unwanted finite oscillations may be introduced because the symbol $R_{1,1}(z) = (4(2+z)^{-1}-1),\ z = \tau\lambda^{\frac{\beta}{2}}$ approaches -1 as z becomes large. Lawson and Morris [94] explained that these oscillations will diminish provided the highest frequency component of the solution decays to zero faster than the lowest frequency component. The following proposition gives an estimate on the choice of τ for the R11-G scheme (3.28) on problems with homogeneous Dirichlet boundary conditions. This can be easily extended to problems with general boundary conditions if the eigenvalues of their matrix representation are known. However, the estimate given below could be used for the problems discussed in this dissertation since their matrix representations are obtained using homogeneous Dirichlet boundary conditions with some effects of the boundaries at the first and last rows of the matrix (it gives an upper bound on the choice of τ for these problems).

Proposition 3.5.1. *(**A priori reliability constraint**) Oscillations are guaranteed to dampen in the solution of the R11-G scheme for (3.6) with $d = 1$ provided*

$$\tau < \frac{2}{\kappa}\left(\frac{hX}{2\pi}\right)^{\frac{\beta}{2}}, \tag{3.34}$$

where $X = (b-a)$ if $\Omega = (a,b)$.

Proof. The highest component solution of the method decays to zero faster than the lowest components if $|(4(2+\tau\lambda_{N-1})^{-1}) - 1| < |(4(2+\tau\lambda_1)^{-1}) - 1|$ which implies

$$\left|\frac{2-\tau\lambda_{N-1}}{2+\tau\lambda_{N-1}}\right| < \left|\frac{2-\tau\lambda_1}{2+\tau\lambda_1}\right|,$$

that is,

$$\frac{-2+\tau\lambda_1}{2+\tau\lambda_1} < \frac{2-\tau\lambda_{N-1}}{2+\tau\lambda_{N-1}} < \frac{2-\tau\lambda_1}{2+\tau\lambda_1}.$$

The right hand inequality is satisfied automatically since $\lambda_i > 0$. The left hand inequality implies

$$\tau^2\lambda_1\lambda_{N-1} < 4 \Rightarrow \tau^2 < \frac{4}{\lambda_1\lambda_{N-1}}.$$

For large N, $\lambda_1 \approx \kappa\left(\frac{\pi}{X}\right)^{\beta}$ and $\lambda_{N-1} \approx \kappa\left(\frac{2}{h}\right)^{\beta}$ which implies that

$$\tau^2 < \frac{4}{\kappa^2\left(\frac{2\pi}{hX}\right)^{\beta}}$$

and the result follows. □

Corollary 3.5.2. *For d-dimensional problems, where*

$$\textit{smallest eigenvalue, say } \lambda_s \approx \kappa \left(\frac{d\pi^2}{X^2}\right)^{\frac{\beta}{2}}, \quad \textit{and}$$

$$\textit{largest eigenvalue, say } \lambda_l \approx \kappa \left(\frac{4d}{h^2}\right)^{\frac{\beta}{2}},$$

we generalize the constraint (3.34) to

$$\tau < \frac{2}{\kappa}\left(\frac{hX}{2\pi\sqrt{d}}\right)^{\frac{\beta}{2}}, \tag{3.35}$$

where $\Omega = (a,b)^d,\ d = 1,2,3.$

Remark 3.5.1. *We remark here that for* $d = 1$ *and* $\beta = 2.0$*, the estimate results to that given in Lawson and Morris [94]. For other combination of the parameters, these results are new for both integer and fractional order PDEs.*

Corollary 3.5.3. *Following Khaliq* et al. *[85], it is easy to show that the time constraint (3.35) can be extended to* (m,m)*-Padé approximants to the exponential function and is given as*

$$\tau < \min_{1\le k\le m} |c_k| \left(\frac{1}{\kappa}\left(\frac{hX}{2\pi\sqrt{d}}\right)^{\frac{\beta}{2}}\right), \tag{3.36}$$

where c_k *are the roots of the Padé approximants.*

Remark 3.5.2. *A large diffusive coefficient* κ *will make the system highly stiff and ill-conditioned, therefore a smaller time step will be required to avoid any oscillations. We also remark here that the estimates (3.34), (3.35) and (3.36) depend on the eigenvalues of the matrix representation of the fractional Laplacian based on central difference approximations and will differ if other difference approximations are used.*

3.6 Numerical Examples

In this section, we consider several numerical examples to illustrate the simplicity, efficiency, reliability and robustness of the schemes discussed in the previous sections. In particular, we discuss the problems with sharp variations in solution profile or non-smooth initial data or mismatched initial and boundary conditions, linear problems ($\mathbf{f}(\mathbf{u}) = 0$), homogeneous Dirichlet boundary conditions ($\mathbf{g}(t) = 0$), nonlinear

problems with mixed Dirichlet boundary conditions and multidimensional problems. For the linear problems, the accuracy of the scheme is computed using the L_2 error norms and the rate of convergence is calculated as

$$\text{ROC} = \log_2 \frac{||U_{h,\tau} - u_{h,\tau}||}{||U_{\frac{h}{2},\frac{\tau}{2}} - u_{\frac{h}{2},\frac{\tau}{2}}||},$$

where U is the exact solution of the problem. For nonlinear problems, the L_2 error norm is also used and the ROC is given as

$$\text{ROC} = \log_2 \frac{||u_{h,\tau} - u_{\frac{h}{2},\frac{\tau}{2}}||}{||u_{\frac{h}{2},\frac{\tau}{2}} - u_{\frac{h}{4},\frac{\tau}{4}}||}.$$

3.6.1 Problem with Non-smooth Initial Data (PNID)

We consider the problem

$$\frac{\partial u}{\partial t} = -\left(-\Delta\right)^{\frac{\beta}{2}} u + f(u), \qquad (x,t) \in [0,1] \times (0,1]$$

subject to the step function initial condition and homogeneous Dirichlet boundary conditions

$$u(x,0) = \begin{cases} 0, & 0 < x < \frac{1}{4}, \\ 1, & \frac{1}{4} \leq x < \frac{3}{4}, \\ 0, & \frac{3}{4} \leq x < 1. \end{cases} \qquad u(0,t) = u(1,t) = 0.$$

The exact solution[1] of this problem with $f(u) = 0$ is given by

$$u(x,t) = \sum_{n=1}^{\infty} \frac{4}{n\pi} \sin\left(\frac{n\pi}{2}\right) \sin\left(\frac{n\pi}{4}\right) \sin\left(n\pi x\right) \exp\left(-\kappa(n\pi)^{\beta} t\right).$$

[1]The analytical solution $u(x,t)$ was obtained using the approach discussed in Yang *et al.* [177]

$h = \tau$	R01-G	ROC	R11-G	ROC	R02-G	ROC	RDP-G	ROC
0.2500	1.121e-02		1.520e-02		1.603e-03		5.307e-04	
0.1250	3.703e-03	1.5984	1.313e-02	0.2114	4.107e-04	1.9645	9.837e-05	2.4316
0.0625	1.353e-03	1.4523	5.272e-03	1.3165	1.123e-04	1.8705	2.144e-05	2.0268
0.0313	5.567e-04	1.2813	1.850e-03	1.5108	3.057e-05	1.8774	5.927e-06	2.0260
0.0156	2.496e-04	1.1570	5.563e-04	1.7338	8.091e-06	1.9175	1.466e-06	2.0158
0.0078	1.179e-04	1.0829	1.387e-04	2.0040	2.091e-06	1.9522	3.642e-07	2.0086

Table 1: Rate of convergence for PNID with $\beta = 1.7$ and $f(u) = 0$.

$h = \tau$	R01-G	ROC	R11-G	ROC	R02-G	ROC	RDP-G	ROC
0.2500	2.538e-02		2.567e-03		4.766e-03		1.104e-03	
0.1250	1.137e-02	1.1589	6.664e-04	1.9455	1.480e-03	1.7389	2.638e-04	2.0648
0.0625	5.219e-03	1.1232	1.682e-04	1.9857	4.041e-04	1.8213	6.390e-05	2.0455
0.0313	2.475e-03	1.0766	4.219e-05	1.9956	1.089e-04	1.8913	1.570e-05	2.0246
0.0156	1.201e-03	1.0427	1.056e-05	1.9982	2.840e-05	1.9394	3.905e-06	2.0079
0.0078	5.913e-04	1.0225	2.647e-06	1.9966	7.261e-06	1.9676	9.872e-07	1.9838

Table 2: Rate of convergence for PNID $\beta = 1.3$ and $f(u) = 0$.

$h = \tau$	R01-G	ROC	R11-G	ROC	R02-G	ROC	RDP-G	ROC
0.2500	1.127e-03		3.0151e-03		1.249e-04		6.461e-05	
0.1250	2.759e-04	2.0303	1.293e-03	1.2210	2.703e-05	2.2074	5.098e-06	3.6637
0.0625	7.873e-05	1.8095	6.120e-04	1.0796	7.024e-06	1.9444	1.193e-06	2.0958
0.0313	2.718e-05	1.5343	4.824e-04	0.3435	1.919e-06	1.8717	2.726e-07	2.1295
0.0156	1.094e-05	1.3130	3.607e-04	0.4195	5.183e-07	1.8887	6.114e-08	2.1565
0.0078	4.860e-06	1.1705	2.547e-04	0.5021	1.371e-07	1.9182	1.321e-08	2.2102

Table 3: Rate of convergence for PNID $\beta = 1.8$ and $f(u) = u^2$.

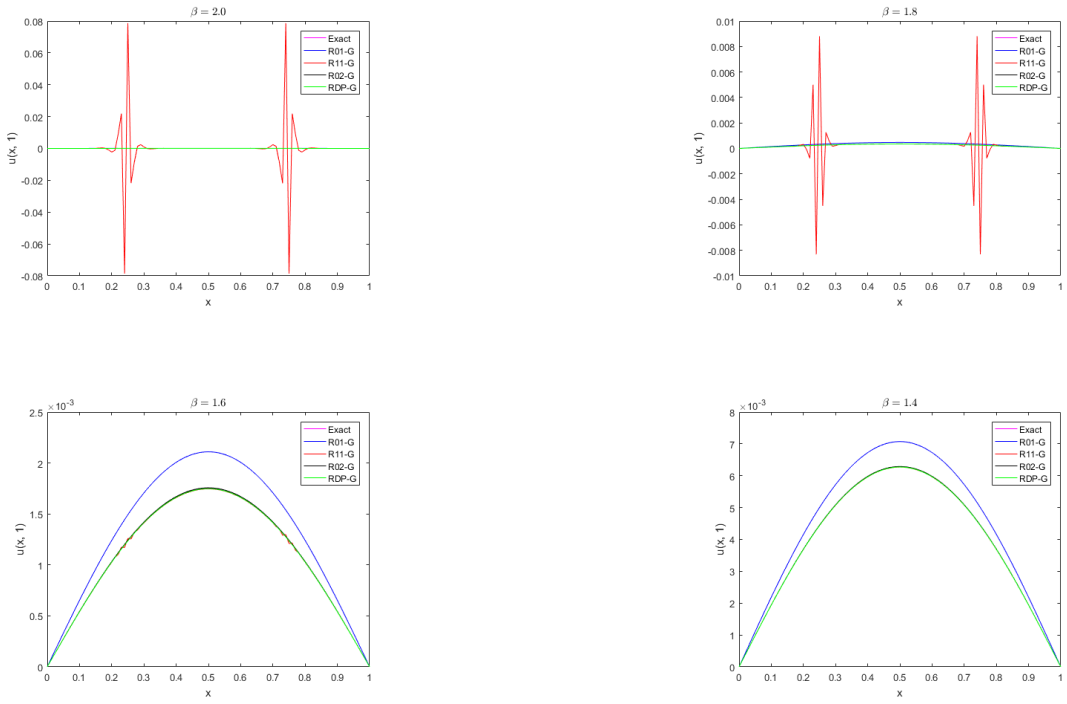

Figure 2: Solution profiles at $T = 1$ for PNID.

Tables 1 to 3 show the L_2 error norms for the problem at the final time $T = 1$. Fig. 2 shows the comparison of the solution profiles at time $T = 1$ (with $\tau = h = 0.01$) between the exact solution, R01-G, R02-G, R11-G and RDP-G schemes. Observe the oscillations in the solution produced by the R11-G scheme near the points of discontinuity which decreases as the space-fractional order decreases. With $\beta = 1.4$, the reliability constraint (3.34) is satisfied, and no oscillation is present in the solution as seen in Fig. 2. These observations are also corroborated by the results given in tables 1 to 3 where the first few entries in the ROC column (table 1) corresponding to the R11-G scheme does not give the accurate order of convergence (2.0) whereas the same columns in table 2 gives the correct order of convergence. In table 3, we observe the same phenomenon due to the use of a higher fractional order, that is, $\beta = 1.8$. These observations show that the oscillations are due to high frequency components present in the solution of the R11-G scheme and decreases as the space-fractional order is decreased. We also observe that the solution profile of R01-G scheme in Fig. 2 is quite different from the other schemes, this is simply because it is a first-order accurate scheme and thus less accurate than the other second-order accurate schemes.

3.6.2 Linear Problem with Dirichlet Time-dependent Boundary Condition (LPDTBC)

We consider

$$\frac{\partial u(x,t)}{\partial t} = -\kappa(-\Delta)^{\frac{\beta}{2}} u(x,t), \qquad (x,t) \in [0,1] \times (0,1]$$

with $\kappa = 1$ and $u(x,0) = -(x^2 - x - 1)$ subject to the non-homogeneous time-dependent boundary conditions

$$u(0,t) = u(1,t) = e^{-t}.$$

The exact solution[1] is given as:

$$\begin{aligned} u(x,t) = e^{-t} &- 2\sum_{n=1}^{\infty} \frac{[(-1)^n - 1]}{n\pi} \frac{\sin(n\pi x)}{(n\pi)^\beta - 1} e^{-t} \\ &- 2\sum_{n=1}^{\infty} \left[\frac{2}{(n\pi)^3} + \frac{1}{n\pi}\right] [(-1)^n - 1] e^{-(n\pi)^\beta t} \sin(n\pi x) \\ &+ 2\sum_{n=1}^{\infty} \frac{[(-1)^n - 1](n\pi)^{\beta-1}}{(n\pi)^\beta - 1} e^{-(n\pi)^\beta t} \sin(n\pi x). \end{aligned}$$

Tables 4–6 show the result for the schemes for different values of β. We observe that the RDP-G scheme is more accurate than the other second-order schemes. This is because it has the smallest error constant of $\frac{1}{24}$. Fig. 3 shows a log-log plot of the L_2-error norms against the time and space stepsize showing the order of convergence of the different schemes. We note that this is a linear problem with smooth initial data, so the solution for any time step do not depend on the constraint (3.34).

$h = \tau$	R01-G	ROC	R11-G	ROC	R02-G	ROC	RDP-G	ROC
0.2500	5.737e-02		2.252e-03		1.673e-03		1.284e-03	
0.1250	2.971e-02	0.9493	6.158e-04	1.8705	6.739e-04	1.3116	3.405e-04	1.9153
0.0625	1.497e-02	0.9889	1.600e-04	1.9442	2.207e-04	1.6107	8.740e-05	1.9621
0.0313	7.498e-03	0.9975	4.083e-05	1.9704	6.410e-05	1.7834	2.223e-05	1.9750
0.0156	3.751e-03	0.9994	1.035e-05	1.9796	1.742e-05	1.8796	5.649e-06	1.9765

Table 4: Rate of convergence for LPDTBC with $\beta = 1.7$.

[1]The exact solution was gotten from Ilić *et al.* [73]

$h = \tau$	R01-G	ROC	R11-G	ROC	R02-G	ROC	RDP-G	ROC
0.2500	5.950e-02		2.636e-03		1.824e-03		1.550e-03	
0.1250	3.1331e-02	0.9255	7.219e-04	1.8682	7.057e-04	1.3699	4.289e-04	1.8541
0.0625	1.590e-02	0.9781	1.901e-04	1.9248	2.244e-04	1.6528	1.144e-04	1.9062
0.0313	7.991e-03	0.9928	4.950e-05	1.9417	6.411e-05	1.8077	3.042e-05	1.9112
0.0156	4.003e-03	0.9972	1.287e-05	1.9435	1.728e-05	1.8914	8.150e-06	1.9002

Table 5: Rate of convergence for LPDTBC with $\beta = 1.5$.

$h = \tau$	R01-G	ROC	R11-G	ROC	R02-G	ROC	RDP-G	ROC
0.2500	6.037e-02		2.952e-03		1.547e-03		1.891e-03	
0.1250	3.246e-02	0.8950	8.411e-04	1.8114	6.039e-04	1.3569	5.600e-04	1.7558
0.0625	1.666e-02	0.9623	2.307e-04	1.8661	1.914e-04	1.6579	1.592e-04	1.8143
0.0313	8.419e-03	0.9848	2.307e-04	1.8553	5.591e-05	1.7753	4.646e-05	1.7773
0.0156	4.229e-03	0.9932	1.803e-05	1.8223	1.597e-05	1.8079	1.402e-05	1.7286

Table 6: Rate of convergence for LPDTBC with $\beta = 1.3$.

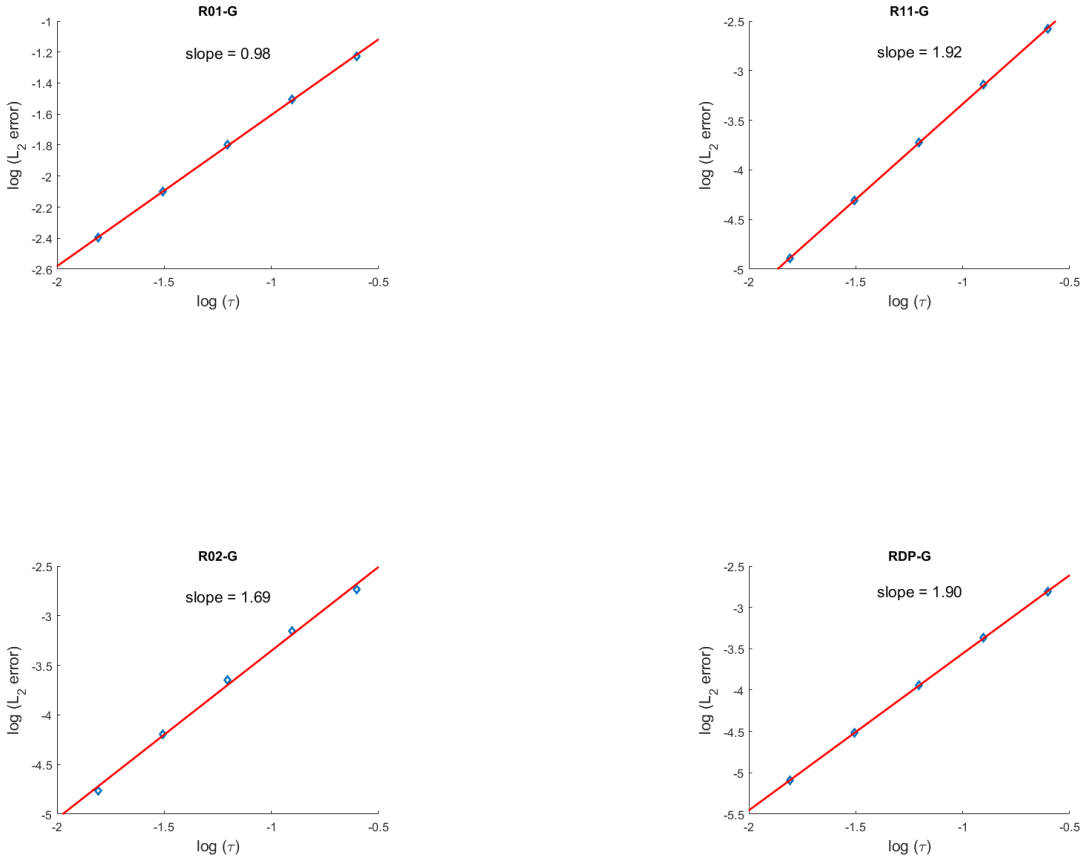

Figure 3: Log-log plots for LPDTBC with $h = \tau$ showing the convergence schemes for $\beta = 1.5$ at $T = 1.0$..

3.6.3 Nonlinear Problem with Robin Boundary Condition (NPRBC)

In this subsection, we consider

$$\frac{\partial u(x,t)}{\partial t} = -\kappa(-\Delta)^{\frac{\beta}{2}}u(x,t) + u(1-u), \qquad (x,t) \in [0,1] \times (0,1] \tag{3.37}$$

with $\kappa = 1$ and $u(x,0) = x^2(1-x)^2$ subject to the non-homogeneous Robin boundary conditions

$$u_x(0,t) - u(0,t) = e^{-t} \quad \text{and} \quad u_x(1,t) + u(1,t) = t.$$

This problem demonstrates the efficiency of the schemes on time-dependent Robin-type boundary conditions. Tables 7–9 show the result for different values of β. Fig. 4 shows the surface plots of the solutions obtained for each of the schemes. We observe

that the solution produced by each of the schemes are similar showing the accuracy and efficiency of the developed schemes.

$h = \tau$	R01-G	ROC	R11-G	ROC	R02-G	ROC	RDP-G	ROC
0.2500	1.125e-03		7.444e-04		1.697e-03		1.420e-04	
0.1250	5.346e-04	1.0728	1.263e-04	2,5589	4.940e-04	1.7805	3.725-05	1.9303
0.0625	2.721e-04	0.9743	3.558e-05	1.8280	1.334e-04	1.8893	9.782e-06	1.9292
0.0313	1.396e-04	0.9633	8.571e-06	2.0535	3.472e-05	1.9416	2.550e-06	1.9398
0.0156	7.102e-05	0.9746	2.042e-06	2.0695	8.870e-06	1.9686	6.560e-07	1.9584
0.0078	3.587e-05	0.9853	5.041e-07	2.0182	2.244e-06	1.9828	1.670e-07	1.9736

Table 7: Rate of convergence for NPRBC with $\beta = 1.7$.

$h = \tau$	R01-G	ROC	R11-G	ROC	R02-G	ROC	RDP-G	ROC
0.2500	1.357e-03		5.517e-04		1.636e-03		1.819e-04	
0.1250	6.632e-04	1.0326	1.273e-04	2.1152	4.714e-04	1.7954	4.827e-05	1.9141
0.0625	3.417e-04	0.9566	3.533e-05	1.8495	1.262e-04	1.9010	1.307e-05	1.8851
0.0313	1.761e-04	0.9560	9.253e-06	1.9330	3.265e-05	1.9508	3.498e-06	1.9015
0.0156	8.984e-05	0.9712	2.361e-06	1.9704	8.303e-06	1.9754	9.199e-07	1.9269
0.0078	4.543e-05	0.9837	5.973e-07	1.9831	2.093e-06	1.9878	2.384e-07	1.9483

Table 8: Rate of convergence for NPRBC with $\beta = 1.5$.

$h = \tau$	R01-G	ROC	R11-G	ROC	R02-G	ROC	RDP-G	ROC
0.2500	1.655e-03		5.519e-04		1.572e-03		2.528e-04	
0.1250	8.373e-04	0.9833	1.442e-04	1.9362	4.466e-04	1.8153	6.906e-05	1.8718
0.0625	4.367e-04	0.9390	3.822e-05	1.9157	1.183e-04	1.9164	1.956e-05	1.8200
0.0313	2.258e-04	0.9518	1.008e-05	1.9228	3.034e-05	1.9633	5.470e-06	1.8383
0.0156	1.152e-04	0.9705	2.639e-06	1.9336	7.662e-06	1.9853	1.497e-06	1.8692
0.0078	5.827e-05	0.9837	6.853e-07	1.9453	1.921e-06	1.9957	4.019e-07	1.8974

Table 9: Rate of convergence for NPRBC with $\beta = 1.3$.

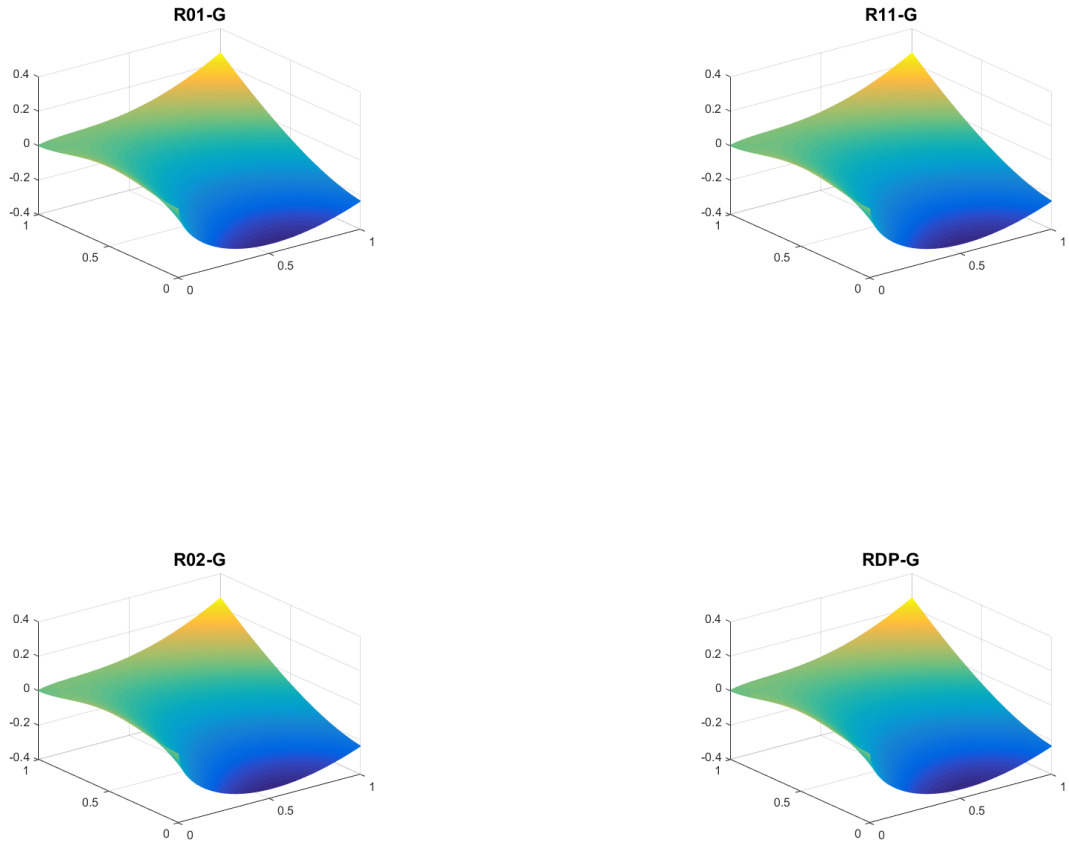

Figure 4: Surface plot of solutions for NPRBC with $\beta = 1.5$.

3.6.4 Two Dimensional Nonlinear Problem with Mismatched Initial and Time-dependent Boundary Condition (2D-NPBC)

We consider the two dimensional problem

$$\frac{\partial u(x,y,t)}{\partial t} = -\kappa(-\Delta)^{\frac{\beta}{2}}u(x,y,t) + u(1-u), \qquad (x,y,t) \in \Omega \times (0,1] \tag{3.38}$$

with $\kappa = \frac{1}{6}$, $\Omega = [0,2]^2$ and the mismatched initial and time-dependent boundary conditions

$$u(x,y,0) = \sin(\frac{\pi y}{2}),$$

$$u(x,y,t) = e^{-t}, \quad (x,y) \in \delta\Omega$$

This example shows the simplicity with which the schemes handle higher dimensional problems. Tables 10–12 show the numerical results. We observe that the R11-G scheme do not actually attain the second-order accuracy in this example. This is due to the use of the mismatched initial and boundary conditions which produces initial oscillations in the first few steps of the solutions. To avoid these oscillations, we either have to constrain the time step size such that the constraint (3.35) is satisfied or use an initial damping scheme, such as R01-G, as discussed in Khaliq *et al.* [84], [86]. Fig. 5(a) - (d) shows the plots of the numerical results produced by the schemes. Fig. 5(a) shows the plot of the R11-G without any initial damping scheme. The choice of the time and space step size (τ and h) are chosen so that (3.35) is not satisfied. We observe oscillations in the first few steps of the simulation which are then propagated to the final time. Fig. 5(b) is a plot of the R11-G with R01-G scheme used as a smoothing (initial damping) scheme. Fig. 5(c) - (d) show the plots of the R02-G and RDP-G schemes respectively.

$h = \tau$	R01-G	ROC	R11-G	ROC	R02-G	ROC	RDP-G	ROC
0.5000	4.397e-03		6.474e-03		8.477e-03		6.216e-03	
0.2500	3.782e-03	0.2173	3.502e-03	0.8865	3.488e-03	1.2811	2.406e-03	1.3694
0.1250	1.977e-03	0.9359	1.209e-04	1.5340	1.067e-03	1.7084	6.686e-04	1.8473
0.0625	9.161e-04	1.1098	3.604e-04	1.7466	2.842e-04	1.9090	1.714e-04	1.9641

Table 10: Rate of convergence for 2D-NPBC with $\beta = 1.7$.

$h = \tau$	R01-G	ROC	R11-G	ROC	R02-G	ROC	RDP-G	ROC
0.5000	3.523e-03		5.105e-03		6.407e-03		4.383e-03	
0.2500	2.758e-03	0.3535	2.635e-03	0.9281	2.471e-03	1.3747	1.7500e-03	1.3246
0.1250	1.560e-03	0.8218	1.003e-03	1.3937	7.597e-04	1.7013	5.247e-04	1.7378
0.0625	7.883e-04	0.9847	3.049e-04	1.7180	2.004e-04	1.9229	1.364e-04	1.9433

Table 11: Rate of convergence for 2D-NPBC with $\beta = 1.5$.

$h = \tau$	R01-G	ROC	R11-G	ROC	R02-G	ROC	RDP-G	ROC
0.5000	2.900e-03		3.654e-03		3.982e-03		2.697e-03	
0.2500	1.464e-03	0.9858	1.208e-03	1.5964	1.108e-03	1.8455	8.474e-04	1.6704
0.1250	7.469e-04	0.9713	4.369e-04	1.4676	2.670e-04	2.0533	2.254e-04	1.9106
0.0625	3.777e-04	0.9838	1.349e-04	1.6951	6.190e-05	2.1086	5.641e-05	1.9985

Table 12: Rate of convergence for 2D-NPBC with $\beta = 1.3$.

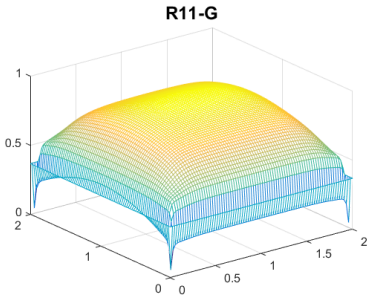

(a) R11-G without initial damping

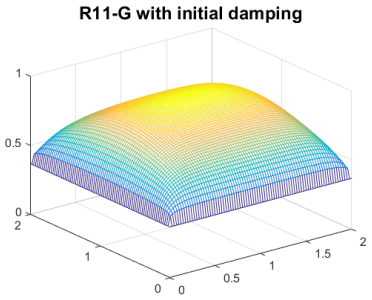

(b) R11-G with R01-G as initial damping scheme

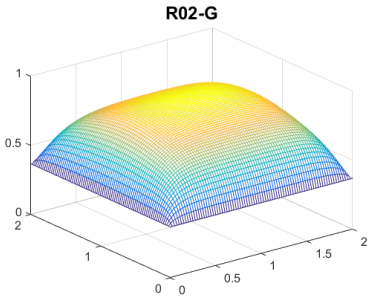

(c) R02-G Scheme

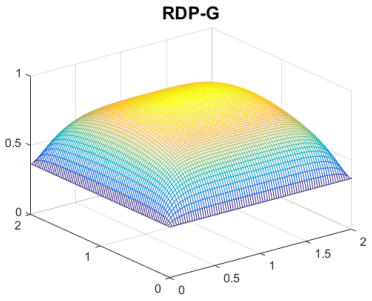

(d) RDP-G Scheme

Figure 5: Surface plots of solution for 2D-NPBC with $\beta = 1.5$.

CHAPTER 4

Numerical Methods for Time-Space Fractional PDEs

4.1 Introduction

In this chapter, we discuss a novel numerical scheme for the time-space fractional PDEs (1.1) with time-dependent boundary conditions. This has been achieved via a spatial discretization using matrix transfer technique (MTT) and a numerical approximation of the integral representation of the resulting (after spatial discretization) system of time-fractional differential equations. The scheme developed is similar to the Crank-Nicholson scheme for integer-order PDEs and is shown to be of order $1+\alpha$, where α is the order of the time-derivative. After spatial discretization of eqn. (1.1) with any suitable boundary condition by the MTT, we obtain the system of time-fractional differential equations

$$\begin{aligned} {}_cD^{\alpha}_{0,t}\mathbf{u} + A^{\frac{\beta}{2}}\mathbf{u} &= \mathbf{f}(t,\mathbf{u}), \\ \mathbf{u}(0) &= \mathbf{u}_0, \end{aligned} \tag{4.39}$$

where $\mathbf{u}$ and $\mathbf{f}(t,\mathbf{u})$ denote the vectors of the node values of u and f, respectively.

Some of the simulations in this chapter were written in Matlab on an Intel(R) Core(TM) i7-4870HQ CPU running at 2.50GHz. The parallel algorithms were written in C on an Intel(R) Xeon(R) CPU E5-2650 v3 with 20 physical cores running at 2.30GHz clock speed (MTSU Computational Science COMS Babbage).

4.2 Time Discretization

In this subsection, we discuss the development of a time-stepping scheme for the numerical solution of the semi-discretized problem (4.39). Let $t_n = n\tau,\ n = 0,\ldots,M$, where $\tau = T/M$ is the time step size, $\mathbf{u}(t_n) := \mathbf{u}_n$ and $\mathbf{f}(t_n,\mathbf{u}(t_n)) := \mathbf{f}_n$, eqn. (4.39) is equivalent to the Volterra integral equation

$$\begin{aligned} \mathbf{u}(t) - \mathbf{u}_0 &= \frac{1}{\Gamma(\alpha)}\int_0^t (t-s)^{\alpha-1}\left(-A^{\frac{\beta}{2}}\mathbf{u}(s) + \mathbf{f}(s,\mathbf{u}(s))\right)\,ds \\ &= -A^{\frac{\beta}{2}}\,{}_0\mathfrak{I}_t\,\mathbf{u}(t) + {}_0\mathfrak{I}_t\,\mathbf{f}(t,\mathbf{u}(t)), \end{aligned} \tag{4.40}$$

where ${}_0\mathfrak{I}_t$ is an integral operator given as

$$ {}_0\mathfrak{I}_t\, y(t) = \frac{1}{\Gamma(\alpha)} \int_0^t (t-s)^{\alpha-1} y(s)\, ds. $$

4.2.1 Derivation of Numerical Scheme

At $t = t_n$ and t_{n+1}, eqn. (4.40) becomes

$$ \begin{aligned} \mathbf{u}(t_{n+1}) - \mathbf{u}_0 &= -A^{\frac{\beta}{2}}\, {}_0\mathfrak{I}_{t_{n+1}}\, \mathbf{u}(t_{n+1}) + {}_0\mathfrak{I}_{t_{n+1}}\, \mathbf{f}(t_{n+1}, \mathbf{u}_{n+1}), \\ \mathbf{u}(t_n) - \mathbf{u}_0 &= -A^{\frac{\beta}{2}}\, {}_0\mathfrak{I}_{t_n}\, \mathbf{u}(t_n) + {}_0\mathfrak{I}_{t_n}\, \mathbf{f}(t_n, u_n), \end{aligned} \tag{4.41} $$

from which we obtain

$$ \begin{aligned} \mathbf{u}(t_{n+1}) - \mathbf{u}(t_n) &= -A^{\frac{\beta}{2}} \left({}_0\mathfrak{I}_{t_{n+1}}\, \mathbf{u}(t_{n+1}) - {}_0\mathfrak{I}_{t_n}\, \mathbf{u}(t_n) \right) + \left({}_0\mathfrak{I}_{t_{n+1}}\, \mathbf{f}(t_{n+1}, \mathbf{u}_{n+1}) - {}_0\mathfrak{I}_{t_n}\, \mathbf{f}(t_n, \mathbf{u}_n) \right) \\ &= -A^{\frac{\beta}{2}}\, {}_{t_n}\mathfrak{I}_{t_{n+1}}\, \mathbf{u}(t_{n+1}) + {}_{t_n}\mathfrak{I}_{t_{n+1}}\, \mathbf{f}(t_{n+1}, \mathbf{u}_{n+1}) + \mathbb{H}_n^e, \end{aligned} $$

where

$$ \mathbb{H}_n^e = -A^{\frac{\beta}{2}}\, {}_0\mathfrak{I}_{t_n} \left(\mathbf{u}(t_{n+1}) - \mathbf{u}(t_n) \right) + {}_0\mathfrak{I}_{t_n} \left(\mathbf{f}(t_{n+1}, \mathbf{u}_{n+1}) - \mathbf{f}(t_n, \mathbf{u}_n) \right). $$

Therefore,

$$ \mathbf{u}(t_{n+1}) - \mathbf{u}(t_n) = -\frac{1}{\Gamma(\alpha)} A^{\frac{\beta}{2}} \int_{t_n}^{t_{n+1}} (t_{n+1}-s)^{\alpha-1} \mathbf{u}(s)\, ds + \frac{1}{\Gamma(\alpha)} \int_{t_n}^{t_{n+1}} (t_{n+1}-s)^{\alpha-1} \mathbf{f}(s, \mathbf{u}(s))\, ds + \mathbb{H}_n^e. \tag{4.42} $$

Suppose $\mathbf{u}(s)$ and $\mathbf{f}(s, \mathbf{u}(s))$ are approximated by a linear interpolation in the interval $[t_n, t_{n+1}]$, that is

$$ \mathbf{u}(s) = \mathbf{u}_n + (s - t_n) \frac{\mathbf{u}_{n+1} - \mathbf{u}_n}{\tau}, \quad s \in [t_n, t_{n+1}], $$

and

$$ \mathbf{f}(s, \mathbf{u}) = \mathbf{f}(t_n, \mathbf{u}_n) + (s - t_n) \frac{\mathbf{f}(t_{n+1}, \mathbf{u}_{n+1}) - \mathbf{f}(t_n, \mathbf{u}_n)}{\tau}, \quad s \in [t_n, t_{n+1}], $$

we obtain

$$ \mathbf{u}_{n+1} - \mathbf{u}_n = \frac{-\alpha\, \tau^\alpha}{\Gamma(\alpha+2)} A^{\frac{\beta}{2}} \mathbf{u}_n - \frac{\tau^\alpha}{\Gamma(\alpha+2)} A^{\frac{\beta}{2}} \mathbf{u}_{n+1} + \frac{\alpha\, \tau^\alpha}{\Gamma(\alpha+2)} \mathbf{f}_n + \frac{\tau^\alpha}{\Gamma(\alpha+2)} \mathbf{f}_{n+1} + \mathbb{H}_n^e. \tag{4.43} $$

To be able to use (4.43), we either need to solve a nonlinear equation at each time step since it involves the term $\mathbf{f}_{n+1} := \mathbf{f}(t_{n+1}, \mathbf{u}_{n+1})$ on the right hand side or we provide an initial approximation for $\mathbf{u}_{n+1}$. We shall prefer the latter option since the cost of solving a nonlinear equation can be very expensive. To achieve this, we use the constant approximation $\mathbf{f}(s, u(s)) = \mathbf{f}(t_n, \mathbf{u}(t_n))$ and the linear approximation for $\mathbf{u}(s)$ given above to obtain the predictor scheme

$$\mathbf{u}_{n+1}^p - \mathbf{u}_n = \frac{-\alpha\,\tau^\alpha}{\Gamma(\alpha+2)} A^{\frac{\beta}{2}}\mathbf{u}_n - \frac{\tau^\alpha}{\Gamma(\alpha+2)} A^{\frac{\beta}{2}}\mathbf{u}_{n+1} + \frac{\tau^\alpha}{\Gamma(\alpha+1)}\mathbf{f}_n + \mathbb{H}_n^e.$$

After some simplification, the predictor-corrector scheme is obtained as

$$\begin{cases} \mathbf{u}_{n+1}^p = \Big(\Gamma(\alpha+2)\mathbb{I} + \tau^\alpha A^{\frac{\beta}{2}}\Big)^{-1}\Big[\Big(\Gamma(\alpha+2)\mathbb{I} - \alpha\,\tau^\alpha A^{\frac{\beta}{2}}\Big)\mathbf{u}_n + \tau^\alpha(\alpha+1)\mathbf{f}(t_n,\mathbf{u}_n) + \Gamma(\alpha+2)\mathbb{H}_n^e\Big], \\ \mathbf{u}_{n+1} = \Big(\Gamma(\alpha+2)\mathbb{I} + \tau^\alpha A^{\frac{\beta}{2}}\Big)^{-1}\Big[\Big(\Gamma(\alpha+2)\mathbb{I} - \alpha\,\tau^\alpha A^{\frac{\beta}{2}}\Big)\mathbf{u}_n + \tau^\alpha\Big(\alpha\,\mathbf{f}(t_n,\mathbf{u}_n) + \mathbf{f}(t_{n+1},\mathbf{u}_{n+1}^p)\Big) \\ \qquad\qquad + \Gamma(\alpha+2)\mathbb{H}_n^e\Big], \end{cases} \tag{4.44}$$

where $\mathbb{H}_n^e$ is the history term and $\mathbb{I}$ is the identity matrix.

4.2.2 Approximation of the history term $\mathbb{H}_n^e$

Suppose $\mathbf{g}(s) = -A^{\frac{\beta}{2}}\mathbf{u}(s) + \mathbf{f}(s, u(s))$, the history term $\mathbb{H}_n^e$ of the predictor-corrector scheme may be written as

$$\begin{aligned} \mathbb{H}_n^e &= \frac{1}{\Gamma(\alpha)}\int_0^{t_n}\big[(t_{n+1}-s)^{\alpha-1} - (t_n-s)^{\alpha-1}\big]\,\mathbf{g}(s)\,ds, \\ &\approx \frac{1}{\Gamma(\alpha)}\sum_{j=0}^{n-1}\int_{t_j}^{t_{j+1}}\big[(t_{n+1}-s)^{\alpha-1} - (t_n-s)^{\alpha-1}\big]\left(\mathbf{g}_j + (s-t_j)\frac{\mathbf{g}_{j+1}-\mathbf{g}_j}{\tau}\right)ds, \quad s\in[t_j,t_{j+1}], \\ &= \frac{1}{\Gamma(\alpha)}\left\{\sum_{j=0}^{n-1}\int_{t_j}^{t_{j+1}}\big[(t_{n+1}-s)^{\alpha-1} - (t_n-s)^{\alpha-1}\big]\,\mathbf{g}_j\,ds\right. \\ &\left. + \sum_{j=0}^{n-1}\int_{t_j}^{t_{j+1}}\big[(t_{n+1}-s)^{\alpha-1} - (t_n-s)^{\alpha-1}\big]\,(s-t_j)\frac{\mathbf{g}_{j+1}-\mathbf{g}_j}{\tau}\,ds\right\}. \end{aligned}$$

After some simplification, we obtain the approximation

$$\mathbb{H}_n^e \approx \mathbb{H}_n^a = \sum_{j=0}^{n} a_{j,n}\Big(-A^{\frac{\beta}{2}}\mathbf{u}_j + \mathbf{f}(t_j,\mathbf{u}_j)\Big), \tag{4.45}$$

where

$$a_{j,n} = \frac{\tau^\alpha}{\Gamma(\alpha+2)} \begin{cases} -(n-\alpha)(n+1)^\alpha + n^\alpha(2n-\alpha-1) - (n-1)^{\alpha+1}, & j=0, \\ (n-j+2)^{\alpha+1} - 3(n-j+1)^{\alpha+1} + 3(n-j)^{\alpha+1} & \\ -(n-j-1)^{\alpha+1}, & 1 \le j \le n-1, \\ 2^{\alpha+1} - \alpha - 3, & j = n. \end{cases}$$

We note that $\mathbb{H}_0^a = 0$ as no history term is required to advance from the initial solution to the next solution value.

4.3 Convergence Analysis

In this subsection, we shall discuss the stability and error analysis of the derived scheme. For simplicity, we shall let $A^{\frac{\beta}{2}}$ be the matrix representation resulting from the spatial discretization of a homogeneous Dirichlet boundary problem. The analysis in this section holds for other matrix representations with some slight modification. For a scheme to be useful in practice, it need be stable and consistent with the PDE. Thus, we discuss the stability and convergence properties of the scheme. Moreover, we provide an error estimate on the order of convergence of the scheme.

4.3.1 Stability Analysis

The stability analysis carried out in this section refers to perturbations in the initial data, that is, the numerical solutions are not sensitive to small perturbations in the initial data. We assume that the nonlinear function $\mathbf{f}(t, \mathbf{u})$ is Lipschitz continuous in a region $\Omega \times (0, T]$ with respect to $\mathbf{u}$. In the various upper bounds below, K is used to denote some generic positive constant and $||\cdot||$ is the ℓ_2-norm.

Definition 4.3.1. *Let $\mathbf{u}_n$ and $\overline{\mathbf{u}}_n$ be two solutions of the predictor-corrector scheme (4.44) with initial values $\mathbf{u}_0$ and $\overline{\mathbf{u}}_0$, respectively. The predictor-corrector scheme is stable if there exists a positive constant C independent of τ and n, such that*

$$||\mathbf{u}_n - \overline{\mathbf{u}}_n|| \le C||\mathbf{u}_0 - \overline{\mathbf{u}}_0||, \; n = 1, 2, \cdots, M.$$

Lemma 4.3.1. *If* $0 < \alpha \leq 1$, *then*

$$a_{0,n} \leq \frac{\tau^\alpha}{\Gamma(\alpha+2)} \left[(n+1)^\alpha - n^\alpha + n^{\alpha+1} - (n-1)^{\alpha+1}\right].$$

Proof. From the coefficients of $\mathbb{H}_n^a$, we have

$$\begin{aligned}
a_{0,n} &= \frac{\tau^\alpha}{\Gamma(\alpha+2)} \left[-n(n+1)^\alpha + \alpha(n+1)^\alpha + 2n^{\alpha+1} - (\alpha+1)n^\alpha - (n-1)^{\alpha+1}\right] \\
&= \frac{\tau^\alpha}{\Gamma(\alpha+2)} \left[n(2n^\alpha - (n+1)^\alpha) + \alpha\,(n+1)^\alpha - (\alpha+1)n^\alpha - (n-1)^{\alpha+1}\right] \\
&= \frac{\tau^\alpha}{\Gamma(\alpha+2)} \left[n(n^\alpha + (n^\alpha - (n+1)^\alpha)) + \alpha\,(n+1)^\alpha - (\alpha+1)n^\alpha - (n-1)^{\alpha+1}\right] \\
&\leq \frac{\tau^\alpha}{\Gamma(\alpha+2)} \left[n^{\alpha+1} + (n+1)^\alpha - n^\alpha - (n-1)^{\alpha+1}\right] \qquad \text{since} \quad 0 < \alpha \leq 1.
\end{aligned}$$

□

Lemma 4.3.2. *If* $0 < \alpha \leq 1$, *and* $t_j = j\tau,\ j = 0, 1, \cdots, n$, *then the following estimate holds*

$$a_{j,n} \leq C_\alpha \begin{cases} \tau t_{n+1}^{\alpha-1} + t_n^\alpha, & j = 0, \\ t_{n-j+2}^\alpha - t_{n-j}^\alpha, & 1 \leq j \leq n-1, \\ \tau^\alpha, & j = n, \end{cases}$$

where C_α *is a generic positive constant which does not depend on* τ *but depends on* α *and* T.

Proof. For $j = 0$ and from Lemma 4.3.1, we have

$$a_{0,n} \leq \frac{1}{\Gamma(\alpha+2)} \left[t_{n+1}^\alpha - t_n^\alpha + \tau^{-1}(t_n^{\alpha+1} - t_{n-1}^{\alpha+1})\right].$$

By the mean value theorem with $\eta_i \in (t_{n-i+1}, t_{n-i+2}),\ i = 1, 2,$

$$\begin{aligned}
a_{0,n} &\leq \frac{1}{\Gamma(\alpha+2)} \Big[\alpha\tau\eta_1^{\alpha-1} + (\alpha+1)\eta_2^\alpha\Big] \\
&\leq \frac{1}{\Gamma(\alpha+1)} \Big[\tau t_{n+1}^{\alpha-1} + t_n^\alpha\Big].
\end{aligned}$$

For $1 \le j \le n-1$,

$$\begin{aligned} a_{j,n} &= \frac{\tau^{-1}}{\Gamma(\alpha+2)}\Big[t_{n-j+2}^{\alpha+1} - 3t_{n-j+1}^{\alpha+1} + 3t_{n-j}^{\alpha+1} - t_{n-j-1}^{\alpha+1}\Big] \\ &= \frac{\tau^{-1}}{\Gamma(\alpha+2)}\Big[t_{n-j+2}^{\alpha+1} - t_{n-j+1}^{\alpha+1} - 2\Big(t_{n-j+1}^{\alpha+1} - t_{n-j}^{\alpha+1}\Big) + t_{n-j}^{\alpha+1} - t_{n-j-1}^{\alpha+1}\Big]. \end{aligned}$$

Applying the mean value theorem with $\eta_i \in (t_{n-j+i-4}, t_{n-j+i-3}),\ i = 3, 4, 5,$

$$\begin{aligned} a_{j,n} &\le \frac{\tau^{-1}}{\Gamma(\alpha+2)}\Big[(\alpha+1)\tau\Big(\eta_3^{\alpha} - 2\eta_4^{\alpha} + \eta_5^{\alpha}\Big)\Big] \\ &\le \frac{1}{\Gamma(\alpha+1)}\Big(t_{n-j+2}^{\alpha} - 2t_{n-j}^{\alpha} + t_{n-j}^{\alpha}\Big). \end{aligned}$$

For $j = n$, $a_{n,n} = C_\alpha \tau^\alpha$ where $C_\alpha = \dfrac{2^{\alpha+1} - \alpha - 3}{\Gamma(\alpha+2)}$. □

Next, we propose a modified Gronwall inequality which is useful to prove the stability and error estimates in the sequel.

Lemma 4.3.3. *Assume that $0 < \alpha \le 1$, and $a_{j,n}$ is as defined in eqn. (4.45) for $0 = t_0 < t_1 < \cdots < t_M = T,\ n = 1, 2, \cdots, M$, where M is a positive integer. Let g_0 be positive and the sequence $\{\psi_n\}$ satisfies*

$$\begin{cases} \psi_0 \le g_0, \\ \psi_n \le \sum\limits_{j=0}^{n-1} a_{j,n}\psi_j + C_0 g_0, \end{cases} \tag{4.46}$$

then

$$\psi_n \le C_0 g_0, \quad n = 1, 2, \cdots, M,$$

where C_0 is a positive constant.

Proof. Applying the inequality (4.46) recursively and noting the $\psi_0 \leq g_0$, we have

$$
\begin{aligned}
\psi_n &\leq g_0 + \sum_{j_1=0}^{n-1} a_{j_1,n}\,\psi_{j_1} \\
&\leq g_0 + \sum_{j_1=0}^{n-1} a_{j_1,n} \left(g_0 + \sum_{j_2=0}^{j_1-1} a_{j_2,j_1}\psi_{j_2} \right) \\
&= g_0 + g_0 \sum_{j_1=0}^{n-1} a_{j_1,n} + \sum_{j_1=0}^{n-1} a_{j_1,n} \sum_{j_2=0}^{j_1-1} a_{j_2,j_1}\psi_{j_2} \\
&\leq g_0 + g_0 \sum_{j_1=0}^{n-1} a_{j_1,n} + \sum_{j_1=0}^{n-1} a_{j_1,n} \sum_{j_2=0}^{j_1-1} a_{j_2,j_1} \left(g_0 + \sum_{j_3=0}^{j_2-1} a_{j_3,j_2}\psi_{j_3} \right) \\
&= g_0 + g_0 \sum_{j_1=0}^{n-1} a_{j_1,n} + g_0 \sum_{j_1=0}^{n-1} a_{j_1,n} \sum_{j_2=0}^{j_1-1} a_{j_2,j_1} + \sum_{j_1=0}^{n-1} a_{j_1,n} \sum_{j_2=0}^{j_1-1} a_{j_2,j_1} \sum_{j_3=0}^{j_2-1} a_{j_3,j_2}\psi_{j_3} \\
&\quad \vdots \\
&\leq g_0 + g_0 \sum_{j_1=0}^{n-1} a_{j_1,n} + g_0 \sum_{j_1=0}^{n-1} a_{j_1,n} \sum_{j_2=0}^{j_1-1} a_{j_2,j_1} + g_0 \sum_{j_1=0}^{n-1} a_{j_1,n} \sum_{j_2=0}^{j_1-1} a_{j_2,j_1} \sum_{j_3=0}^{j_2-1} a_{j_3,j_2} \\
&\quad + g_0 \sum_{j_1=0}^{n-1} a_{j_1,n} \sum_{j_2=0}^{j_1-1} a_{j_2,j_1} \cdots \sum_{j_n=0}^{j_{n-1}-1} a_{j_n,j_{n-1}} \\
&= g_0 + g_0 \sum_{j_1=0}^{n-1} a_{j_1,n} + g_0 \sum_{j_2=0}^{n-1} a_{j_2,n} \sum_{j_1=0}^{j_2-1} a_{j_1,j_2} + g_0 \sum_{j_3=0}^{n-1} a_{j_3,n} \sum_{j_2=0}^{j_3-1} a_{j_2,j_3} \sum_{j_1=0}^{j_2-1} a_{j_1,j_2} \\
&\quad + g_0 \sum_{j_n=0}^{n-1} a_{j_n,n} \sum_{j_{n-1}=0}^{j_n-1} a_{j_{n-1},j_n} \cdots \sum_{j_1=0}^{j_2-1} a_{j_1,j_2}.
\end{aligned}
\tag{4.47}
$$

Now, for $\mu \geq 0$ and $0 < \alpha \leq 1$, we have

$$\begin{aligned}
\sum_{j_r=0}^{j_s-1} a_{j_r,j_s} t_{j_r}^{\mu} &\leq C_0 \left[\sum_{j_r=1}^{j_s-1} \left(t_{j_s-j_r+2}^{\alpha} - t_{j_s-j_r}^{\alpha} \right) t_{j_r}^{\mu} + \left(\tau\, t_{j_s+1}^{\alpha-1} + t_{j_s}^{\alpha} \right) t_0^{\mu} \right] \\
&\leq C_0 \left[\sum_{j_r=1}^{j_s-1} \left(t_{j_s-j_r+2} - t_{j_s-j_r} \right)^{\alpha} t_{j_r}^{\mu} + 2 t_{j_s}^{\alpha} t_0^{\mu} \right] \\
&= C_0 \left[\sum_{j_r=1}^{j_s-1} (2\tau)^{\alpha} t_{j_r}^{\mu} + 2 t_{j_s}^{\alpha} t_0^{\mu} \right] \\
&\leq C_0 t_{j_s}^{\alpha} \sum_{j_r=0}^{j_s-1} t_{j_r}^{\mu} \\
&\leq C_0 \tau^{-1} t_{j_s}^{\alpha} \int_0^{t_{j_s}} t^{\mu}\, dt \\
&= \frac{C_0 \tau^{-1} t_{j_s}^{\alpha+\mu+1}}{(\mu+1)}.
\end{aligned}$$

Hence, we have

$$\begin{aligned}
E_{r,n} &= g_0 \sum_{j_r=0}^{n-1} a_{j_r,n} \sum_{j_{r-1}=0}^{j_r-1} a_{j_{r-1},j_r} \cdots \sum_{j_1=0}^{j_2-1} a_{j_1,j_2} \\
&\leq C_0 \tau^{-1} g_0 \sum_{j_r=0}^{n-1} a_{j_r,n} \sum_{j_{r-1}=0}^{j_r-1} a_{j_{r-1},j_r} \cdots \sum_{j_2=0}^{j_3-1} a_{j_2,j_3} t_{j_2}^{\alpha+1} \\
&\leq g_0 \frac{C_0^2 \tau^{-2}}{(\alpha+2)} \sum_{j_r=0}^{n-1} a_{j_r,n} \sum_{j_{r-1}=0}^{j_r-1} a_{j_{r-1},j_r} \cdots \sum_{j_3=0}^{j_4-1} a_{j_3,j_4} t_{j_3}^{2\alpha+2} \\
&\leq g_0 \frac{C_0^3 \tau^{-3}}{(\alpha+2)(2\alpha+3)} \sum_{j_r=0}^{n-1} a_{j_r,n} \sum_{j_{r-1}=0}^{j_r-1} a_{j_{r-1},j_r} \cdots \sum_{j_4=0}^{j_5-1} a_{j_4,j_5} t_{j_4}^{3\alpha+3} \\
&\leq g_0\, C_0^r\, \tau^{-r} t_n^{r(\alpha+1)} \prod_{j=0}^{r-1} \frac{1}{(j\alpha+j+1)} \\
&\leq g_0\, C_0^r\, \tau^{-r} T^{r(\alpha+1)} \prod_{j=0}^{r-1} \frac{1}{(j\alpha+j+1)}, \qquad r = 1, 2, \cdots, n.
\end{aligned}$$

Let $b_r = g_0\, C_0^r\, \tau^{-r} T^{r(\alpha+1)} \prod_{j=0}^{r-1} \frac{1}{(j\alpha+j+1)}$, then $\frac{b_{r+1}}{b_r} = C_0\, \tau^{-1} T^{\alpha+1} (r\alpha + r + 1)^{-1}$. Thus, $\lim_{r\to\infty} \frac{b_{r+1}}{b_r} = 0$ which implies that $\sum_{r=1}^{\infty} b_r$ is convergent, thus the right hand side

of (4.47) is bounded, that is,

$$\psi_n \leq g_0 + g_0 \sum_{r=1}^{k} b_r \leq C_0 g_0$$

which completes the proof. □

Theorem 4.3.1. *Suppose that* $\mathbf{u}_j$ $(j = 1, 2, \cdots, n)$ *are the solutions of (4.39) produced by the predictor-corrector scheme (4.44) and* $\mathbf{f}(t, \mathbf{u})$ *satisfies the Lipschitz condition with respect to* $\mathbf{u}$ *in a region* $\Omega \times (0, T]$ *of its unique solution, then the predictor-corrector scheme (4.44) is stable.*

Proof. Let $\widetilde{\mathbf{u}}_j$, $(j = 0, 1, \cdots, n-1)$ and $\widetilde{\mathbf{u}}_n^p$, $(n = 0, 1, \cdots, M-1)$ be perturbations of $\mathbf{u}_j$ and $\mathbf{u}_n^p$, respectively. We first consider the following perturbation equation for the history term

$$\widetilde{\mathbb{H}}_n^a = a_{0,n}\Big(- A^{\frac{\beta}{2}}\widetilde{\mathbf{u}}_0 + \mathbf{f}(t_0, \mathbf{u}_0 + \widetilde{\mathbf{u}}_0) - \mathbf{f}(t_0, \mathbf{u}_0)\Big) + \sum_{j=1}^{n-1} a_{j,n}\Big(- A^{\frac{\beta}{2}}\widetilde{\mathbf{u}}_j + \mathbf{f}(t_j, \mathbf{u}_j + \widetilde{\mathbf{u}}_j) - \mathbf{f}(t_j, \mathbf{u}_j)\Big)$$

$$+ a_{n,n}\Big(- A^{\frac{\beta}{2}}\widetilde{\mathbf{u}}_n + \mathbf{f}(t_n, \mathbf{u}_n + \widetilde{\mathbf{u}}_n) - \mathbf{f}(t_n, \mathbf{u}_n)\Big).$$

Using the Lipschitz continuity of $\mathbf{f}(\mathbf{u})$ and Lemma 4.3.2, we obtain

$$||\widetilde{\mathbb{H}}_n^a|| \leq K\left(\sum_{j=0}^{n-1} a_{j,n}||\widetilde{\mathbf{u}}_j|| + \tau^\alpha||\widetilde{u}_n||\right).$$

where K is a generic positive constant. The perturbation equation for eqn. (4.44) is

$$\begin{cases} \widetilde{\mathbf{u}}_{n+1}^p &= \left(\Gamma(\alpha+2)\mathbb{I} + \tau^\alpha A^{\frac{\beta}{2}}\right)^{-1}\left[\left(\Gamma(\alpha+2)\mathbb{I} - \alpha\tau^\alpha A^{\frac{\beta}{2}}\right)\widetilde{\mathbf{u}}_n + \tau^\alpha(\alpha+1)(\mathbf{f}(t_n, \mathbf{u}_n + \widetilde{\mathbf{u}}_n) - \mathbf{f}(t_n, \mathbf{u}_n))\right] \\ \qquad &+ \left(\Gamma(\alpha+2)\mathbb{I} + \tau^\alpha A^{\frac{\beta}{2}}\right)^{-1}\left[\Gamma(\alpha+2)\widetilde{\mathbb{H}}_n^a\right], \\ \widetilde{\mathbf{u}}_{n+1} &= \left(\Gamma(\alpha+2)\mathbb{I} + \tau^\alpha A^{\frac{\beta}{2}}\right)^{-1}\left[\left(\Gamma(\alpha+2)\mathbb{I} - \alpha\tau^\alpha A^{\frac{\beta}{2}}\right)\widetilde{\mathbf{u}}_n + \tau^\alpha\alpha(\mathbf{f}(t_n, \mathbf{u}_n + \widetilde{\mathbf{u}}_n) - \mathbf{f}(t_n, \mathbf{u}_n))\right], \\ \qquad &+ \left(\Gamma(\alpha+2)\mathbb{I} + \tau^\alpha A^{\frac{\beta}{2}}\right)^{-1}\left[(\mathbf{f}(t_{n+1}, \mathbf{u}_{n+1}^p + \widetilde{\mathbf{u}}_{n+1}^p) - \mathbf{f}(t_{n+1}, \mathbf{u}_{n+1}^p)) + \Gamma(\alpha+2)\widetilde{\mathbb{H}}_n^a\right]. \end{cases}$$

Due to the positive definiteness of $A^{\frac{\beta}{2}}$, it holds that $0 < c < 1$, where

$$c = \left\| \left(\Gamma(\alpha+2)\mathbb{I} + \tau^\alpha A^{\frac{\beta}{2}}\right)^{-1}\left(\Gamma(\alpha+2)\mathbb{I} - \alpha\tau^\alpha A^{\frac{\beta}{2}}\right)\right\|.$$

Thus, we have

$$\begin{cases} ||\widetilde{\mathbf{u}}_{n+1}^{p}|| \leq c\,||\widetilde{\mathbf{u}}_n|| + C\tau^{\alpha}||\widetilde{\mathbf{u}}_n|| + K\tau^{\alpha}||\widetilde{\mathbf{u}}_n|| + K\sum_{j=0}^{n-1} a_{j,n}||\widetilde{\mathbf{u}}_j||, \\ ||\widetilde{\mathbf{u}}_{n+1}|| \leq c\,||\widetilde{\mathbf{u}}_n|| + C\tau^{\alpha}(||\widetilde{\mathbf{u}}_n|| + ||\widetilde{\mathbf{u}}_{n+1}^{p}||) + K\tau^{\alpha}||\widetilde{\mathbf{u}}_n|| + K\sum_{j=0}^{n-1} a_{j,n}||\widetilde{\mathbf{u}}_j||, \end{cases}$$

where C is a positive constant. We show the rest of the proof using mathematical induction. For $n = 0$ and for sufficiently small τ, it can be easily deduced that

$$||\widetilde{\mathbf{u}}_{n+1}^{p}|| \leq ||\widetilde{\mathbf{u}}_0|| \quad \text{and} \quad ||\widetilde{\mathbf{u}}_{n+1}|| \leq ||\widetilde{\mathbf{u}}_0||.$$

Suppose that

$$||\widetilde{\mathbf{u}}_j|| \leq ||\widetilde{\mathbf{u}}_0||, \quad j = 1, 2, \cdots, n.$$

We consider $j = n+1$, for $\widetilde{\mathbf{u}}_{n+1}^{p}$, that is,

$$\begin{aligned} ||\widetilde{\mathbf{u}}_{n+1}^{p}|| &\leq c\,||\widetilde{\mathbf{u}}_n|| + C\tau^{\alpha}||\widetilde{\mathbf{u}}_n|| + K\tau^{\alpha}||\widetilde{\mathbf{u}}_n|| + K\sum_{j=0}^{n-1} a_{j,n}||\widetilde{\mathbf{u}}_j|| \\ &\leq c_1\,||\widetilde{\mathbf{u}}_n|| + K\sum_{j=0}^{n-1} a_{j,n}||\widetilde{\mathbf{u}}_j|| \\ &\leq ||\widetilde{\mathbf{u}}_0||, \end{aligned}$$

where $0 < c_1 = c + C\tau^{\alpha} + K\tau^{\alpha} < 1$ for sufficiently small τ and Lemma 4.3.3 has been used. Then, for sufficiently small τ, we have

$$\begin{aligned} ||\widetilde{\mathbf{u}}_{n+1}|| &\leq c\,||\widetilde{\mathbf{u}}_n|| + C\tau^{\alpha}(||\widetilde{\mathbf{u}}_n|| + ||\widetilde{\mathbf{u}}_{n+1}^{p}||) + K\tau^{\alpha}||\widetilde{\mathbf{u}}_n|| + K\sum_{j=0}^{n-1} a_{j,n}||\widetilde{\mathbf{u}}_j|| \\ &\leq c_2\,||\widetilde{\mathbf{u}}_n|| + K\sum_{j=0}^{n-1} a_{j,n}||\widetilde{\mathbf{u}}_j|| \\ &\leq ||\widetilde{\mathbf{u}}_0||, \end{aligned}$$

where $0 < c_2 = c + 2C\tau^{\alpha} + K\tau^{\alpha} < 1$. This completes the proof. □

4.3.2 Error Analysis

In this section, we give the error analysis of the predictor-corrector scheme (4.44). We use the notation $\mathbf{g}(s) = -A^{\frac{\beta}{2}}\mathbf{u}(s) + \mathbf{f}(s, u(s))$ and present some lemmas which are useful in the sequel.

Lemma 4.3.4. *Let* $\mathbf{g}(t) \in C^2[0,T]$, *then*

$$||\mathbb{H}_n^e - \mathbb{H}_n^a|| \leq \frac{||\mathbf{g}''||}{2\Gamma(\alpha+1)}\tau^2 T^\alpha.$$

Proof. From the expression of $\mathbb{H}_n^e$ and $\mathbb{H}_n^a$, we have

$$\begin{aligned}
&\left|\left|\frac{1}{\Gamma(\alpha)}\int_0^{t_n}\left[(t_{n+1}-s)^{\alpha-1}-(t_n-s)^{\alpha-1}\right]\mathbf{g}(s)\,ds - \frac{\tau^\alpha}{\Gamma(\alpha+2)}\sum_{j=0}^{n} a_{j,n}\mathbf{g}(t_j)\right|\right| \\
&= \frac{1}{\Gamma(\alpha)}\left|\left|\sum_{j=0}^{n-1}\int_{t_j}^{t_{j+1}}\left[(t_{n+1}-s)^{\alpha-1}-(t_n-s)^{\alpha-1}\right]\left(\mathbf{g}(s) - \frac{s-t_{j+1}}{\tau}\mathbf{g}(t_j) - \frac{s-t_j}{\tau}\mathbf{g}(t_{j+1})\right)ds\right|\right| \\
&\leq \frac{1}{\Gamma(\alpha)}\sum_{j=0}^{n-1}\int_{t_j}^{t_{j+1}}\left|(t_{n+1}-s)^{\alpha-1}-(t_n-s)^{\alpha-1}\right|\left|\left|\frac{1}{2}(s-t_j)(s-t_{j+1})\mathbf{g}''(\xi_j)\right|\right|ds, \quad \xi_j \in (t_j,\, t_{j+1}) \\
&\leq \frac{\|\mathbf{g}''\|\tau^2}{2\Gamma(\alpha)}\int_0^{t_n}\left|(t_{n+1}-s)^{\alpha-1}-(t_n-s)^{\alpha-1}\right|ds \\
&\leq \frac{\|\mathbf{g}''\|\tau^2}{2\Gamma(\alpha+1)}T^\alpha.
\end{aligned}$$

□

Lemma 4.3.5. *Let* $\mathbf{g}(t) \in C^2[0,T]$, *then*

$$\left|\left|\frac{1}{\Gamma(\alpha)}\int_{t_n}^{t_{n+1}}(t_{n+1}-s)^{\alpha-1}\,\mathbf{g}(s)\,ds - \sum_{j=0}^{1} b_j\mathbf{g}(t_{n+j})\right|\right| \leq \frac{||\mathbf{g}''||\tau^2}{2\Gamma(\alpha+1)}T^\alpha,$$

where $b_0 = \dfrac{\alpha\tau^\alpha}{\Gamma(\alpha+2)}$ *and* $b_1 = \dfrac{\tau^\alpha}{\Gamma(\alpha+2)}$.

Proof.

$$\begin{aligned}
&\left|\left|\frac{1}{\Gamma(\alpha)}\int_{t_n}^{t_{n+1}}(t_{n+1}-s)^{\alpha-1}\,\mathbf{g}(s)\,ds \;-\sum_{j=0}^{1} b_j\mathbf{g}(t_{n+j})\right|\right| \\
&\qquad\leq \frac{1}{\Gamma(\alpha)}\int_{t_n}^{t_{n+1}}(t_{n+1}-s)^{\alpha-1}\left|\left|\mathbf{g}(s) + \frac{s-t_{n+1}}{\tau}\mathbf{g}(t_n)\right.\right. \\
&\qquad\quad \left.\left. -\frac{s-t_n}{\tau}\mathbf{g}(t_{n+1})\right|\right| ds \\
&\qquad\leq \frac{\|\mathbf{g}''(\xi)\|\tau^2}{2\Gamma(\alpha)}\int_{t_n}^{t_{n+1}}(t_{n+1}-s)^{\alpha-1}\,ds, \quad \xi \in (t_n, t_{n+1}) \\
&\qquad\leq \frac{\|\mathbf{g}''\|\tau^2}{2\Gamma(\alpha+1)}T^\alpha.
\end{aligned}$$

□

Lemma 4.3.6. *Let* $\mathbf{g}(t) \in C^1[0,T]$, *then*

$$\left|\left|\frac{1}{\Gamma(\alpha)}\int_{t_n}^{t_{n+1}}(t_{n+1}-s)^{\alpha-1}\,\mathbf{g}(s)\,ds-\frac{\tau^\alpha}{\Gamma(\alpha+1)}\mathbf{g}(t_n)\right|\right| \le \frac{||\mathbf{g}'||\tau}{\Gamma(\alpha+1)}T^\alpha.$$

Proof. The proof is similar to those given in Lemmas 4.3.4 and 4.3.5. □

Lemma 4.3.7. *Suppose* $\mathbf{f}(\mathbf{u})$ *is Lipschitz continuous and* $\mathbf{f}'(t,\mathbf{u})$ *is continuous with respect to* t, *then there exists a positive constant* c_0 *such that the error estimate*

$$\left|\left|\mathbf{e}_{n+1}^p\right|\right| \le c_0\tau$$

holds uniformly on $0 \le t_k \le T$, *where* $\mathbf{e}_{n+1}^p = \mathbf{u}(t_{n+1}) - \mathbf{u}_{n+1}^p$ *and* $c_0 = \dfrac{||\mathbf{f}'||}{\Gamma(\alpha+1)}T^\alpha$.

Proof. Let $\mathbf{e}_n = \mathbf{u}(t_n) - \mathbf{u}_n$, and $\mathbf{e}_n^p = \mathbf{u}(t_n) - \mathbf{u}_n^p$, $n = 0, 1\cdots, M$ be the error of the predictor and corrector schemes, respectively, at t_n. Then from equations (4.42) and the first of (4.44), we have

$$\mathbf{u}(t_{n+1}) = \mathbf{u}(t_n) - \frac{1}{\Gamma(\alpha)}A^{\frac{\beta}{2}}\int_{t_n}^{t_{n+1}}(t_{n+1}-s)^{\alpha-1}\mathbf{u}(s)\,ds + \frac{1}{\Gamma(\alpha)}\int_{t_n}^{t_{n+1}}(t_{n+1}-s)^{\alpha-1}\mathbf{f}(s,\mathbf{u}(s))\,ds + \mathbb{H}_n^e,$$

$$\mathbf{u}_{n+1}^p = \mathbf{u}_n - A^{\frac{\beta}{2}}\sum_{j=0}^{1} b_j\mathbf{u}_{n+j} + \frac{\tau^\alpha}{\Gamma(\alpha+1)}\mathbf{f}(t_n,\mathbf{u}_n) + \mathbb{H}_n^a.$$

Therefore,

$$\begin{aligned}\left|\left|\mathbf{u}_{n+1}^p - \mathbf{u}(t_{n+1})\right|\right| \le\ & ||\mathbf{e}_n|| + K\left|\left|\frac{1}{\Gamma(\alpha)}\int_{t_n}^{t_{n+1}}(t_{n+1}-s)^{\alpha-1}\mathbf{u}(s)\,ds - \sum_{j=0}^{1}b_j\mathbf{u}(t_{n+j})\right|\right| \\ & + K\left|\left|\sum_{j=0}^{1}b_j\left(\mathbf{u}(t_{n+j}) - \mathbf{u}_{n+j}\right)\right|\right| \\ & + \left|\left|\frac{1}{\Gamma(\alpha)}\int_{t_n}^{t_{n+1}}(t_{n+1}-s)^{\alpha-1}\mathbf{f}(s,\mathbf{u}(s))\,ds - \frac{\tau^\alpha}{\Gamma(\alpha+1)}\mathbf{f}(t_n,\mathbf{u}(t_n))\right|\right| \\ & + \frac{\tau^\alpha}{\Gamma(\alpha+1)}\left|\left|\mathbf{f}(t_n,\mathbf{u}(t_n)) - \mathbf{f}(t_n,\mathbf{u}_n)\right|\right| + \left|\left|\mathbb{H}_n^e - \mathbb{H}_n^a\right|\right|.\end{aligned}$$

where $K = \left|\left|A^{\frac{\beta}{2}}\right|\right|$. Using Lemmas 4.3.4, 4.3.5, 4.3.6 and the Lipschitz continuity of $\mathbf{f}(t,\mathbf{u})$, we obtain

$$\left|\left|\mathbf{e}_{n+1}^p\right|\right| \le \left(1 + Kb_0 + \frac{L\tau^\alpha}{\Gamma(\alpha+1)}\right)||\mathbf{e}_n|| + Kb_1\,||\mathbf{e}_{n+1}|| + c_0\tau + c_1\tau^2,$$

where L is a Lipschitz constant, $c_0 = \dfrac{||\mathbf{f}'||}{\Gamma(\alpha+1)}T^\alpha$ and $c_1 = \dfrac{K||\mathbf{u}''|| + ||\mathbf{f}''||}{2\Gamma(\alpha+1)}T^\alpha$. By construction $||\mathbf{e}_{n+1}|| \leq \left|\left|\mathbf{e}^p_{n+1}\right|\right|$ so that

$$\left|\left|\mathbf{e}^p_{n+1}\right|\right| \leq \frac{1}{1-Kb_1}\left[\left(1 + Kb_0 + \frac{L\tau^\alpha}{\Gamma(\alpha+1)}\right)||\mathbf{e}_n|| + c_0\tau + c_1\tau^2\right].$$

It is easy to show using mathematical induction that

$$\left|\left|\mathbf{e}^p_{n+1}\right|\right| \leq c_0\tau.$$

□

Theorem 4.3.2. *Suppose $\mathbf{f}(u)$ is Lipschitz continuous and $\mathbf{f}''(t,\mathbf{u})$ is continuous with respect to t, then the error estimate*

$$||\mathbf{e}_{n+1}|| \leq k_1\tau^{\alpha+1}$$

holds uniformly on $0 \leq t_k \leq T$, where $k_1 = \dfrac{\alpha c_1 L}{(1-Kb_1)\Gamma(\alpha+2)}$.

Proof. From equations (4.42) and the second of (4.44), we have

$$\mathbf{e}_{n+1} = \mathbf{e}_n + \frac{1}{\Gamma(\alpha)}A^{\frac{\beta}{2}}\left[\int_{t_n}^{t_{n+1}}(t_{n+1}-s)^{\alpha-1}\mathbf{u}(s)\,ds - \sum_{j=0}^{1} b_j\mathbf{u}_{n+j}\right]$$
$$+ \frac{1}{\Gamma(\alpha)}\int_{t_n}^{t_{n+1}}(t_{n+1}-s)^{\alpha-1}\mathbf{f}(s,\mathbf{u}(s))\,ds - \left(b_0\mathbf{f}(t_n,\mathbf{u}_n) + b_1\mathbf{f}(t_{n+1},\mathbf{u}^p_{n+1})\right) + \mathbb{H}^e_n - \mathbb{H}^a_n.$$

$$||\mathbf{e}_{n+1}|| \leq ||\mathbf{e}_n|| + K\left|\left|\frac{1}{\Gamma(\alpha)}\int_{t_n}^{t_{n+1}}(t_{n+1}-s)^{\alpha-1}\mathbf{u}(s)\,ds - \sum_{j=0}^{1} b_j\mathbf{u}(t_{n+j})\right|\right|$$
$$+ K\left|\left|\sum_{j=0}^{1} b_j\left(\mathbf{u}(t_{n+j}) - \mathbf{u}_{n+j}\right)\right|\right| + \left|\left|\frac{1}{\Gamma(\alpha)}\int_{t_n}^{t_{n+1}}(t_{n+1}-s)^{\alpha-1}\mathbf{f}(s,\mathbf{u}(s))\,ds - \sum_{j=0}^{1} b_j\mathbf{f}(t_{n+j},\mathbf{u}(t_{n+}\right.\right.$$
$$+ b_0\,||\mathbf{f}(t_n,\mathbf{u}(t_n)) - \mathbf{f}(t_n,\mathbf{u}_n)|| + b_1\left|\left|\mathbf{f}(t_{n+1},\mathbf{u}(t_{n+1})) - \mathbf{f}(t_{n+1},\mathbf{u}^p_{n+1})\right|\right| + ||\mathbb{H}^e_n - \mathbb{H}^a_n||$$
$$\leq \left(1 + Kb_0 + \frac{L\tau^\alpha}{\Gamma(\alpha+2)}\right)||\mathbf{e}_n|| + \frac{\alpha c_1 L\tau^{\alpha+1}}{\Gamma(\alpha+2)}\left|\left|\mathbf{e}^p_{n+1}\right|\right| + Kb_1\,||\mathbf{e}_{n+1}|| + c_1\tau^2$$
$$+ \frac{K||\mathbf{u}''|| + ||\mathbf{f}''||}{\Gamma(\alpha+1)}T^\alpha\,\tau^2.$$

$$||\mathbf{e}_{n+1}|| \leq k_0\,||\mathbf{e}_n|| + k_1\tau^{\alpha+1} + k_2\tau^2,$$

where $k_0 = \dfrac{1 + Kb_0 + \frac{L\tau^\alpha}{\Gamma(\alpha+2)}}{1-Kb_1}$, $k_1 = \dfrac{\alpha c_1 L}{(1-Kb_1)\Gamma(\alpha+2)}$, $k_2 = \dfrac{K||\mathbf{u}''|| + ||\mathbf{f}''||}{(1-Kb_1)\Gamma(\alpha+1)}T^\alpha$. The result is easily obtained using mathematical induction. □

4.4 An Improved Scheme Based on Time-Graded Meshes

In section (4.2), we derive a Crank-Nicholson-type scheme for time-space fractional-order PDEs and show that the order (in time) is $1+\alpha$ which differs from the order two (in time) of the Crank-Nicholson scheme for integer-order PDEs. This is due to the singularity of the kernel $(t-s)^{\alpha-1}$ which produces continuous solutions with singularity near $t=0$. Thus, the use of uniform meshes reduces the accuracy of the derived scheme. To alleviate this drawback, we introduce the idea of non-uniform meshes (time-graded meshes) which were originally proposed and used in the context of Volterra integral equations with singular kernels [22], [23], [32]. The idea was later succesfully implemented to improve the convergence order and accuracy of fractional differential equations [81], [107], [108], [116], [117], [123]. The basic idea of time-graded meshes is the construction of non-uniform meshes in such a way that the time step-size is smaller near the potential singularity of the equation so as to compensate for the inccuracies near this singularity point. Now, we consider the time-fractional differential equation (4.39) and divide the $(0,T]$ into M subintrevals $[t_{k-1},t_k]$ for $k=0,1,\cdots,N$ with $0=t_0<t_1<\cdots,<t_{M-1}<t_M=T$ such that $t_k=T(k/M)^{2-\alpha}$. We denote $\tau_k=t_k-t_{k-1}$. As in the previous section, the solution to (4.39) at time t_{k+1} may be written as

$$\begin{aligned}\mathbf{u}(t_{k+1})-\mathbf{u}(t_k) &= -A^{\frac{\beta}{2}}\left({}_0\mathfrak{I}_{t_{k+1}}\,\mathbf{u}(t_{k+1})-{}_0\mathfrak{I}_{t_k}\,\mathbf{u}(t_k)\right)+\left({}_0\mathfrak{I}_{t_{k+1}}\,\mathbf{f}(t_{k+1},\mathbf{u}_{k+1})-{}_0\mathfrak{I}_{t_k}\,\mathbf{f}(t_k,\mathbf{u}_k)\right)\\ &= -A^{\frac{\beta}{2}}\,{}_{t_k}\mathfrak{I}_{t_{k+1}}\,\mathbf{u}(t_{k+1})\;+\;{}_{t_k}\mathfrak{I}_{t_{k+1}}\,\mathbf{f}(t_{k+1},\mathbf{u}_{k+1})\;+\mathbb{H}_k^e,\end{aligned}$$

from which we obtain the Time-Graded scheme (TGS)

$$\begin{aligned}\left(\Gamma(\alpha+2)\mathbb{I}+\tau_{k+1}^{\alpha}A^{\frac{\beta}{2}}\right)\mathbf{u}_{k+1}^{p} &= \left(\Gamma(\alpha+2)\mathbb{I}-\alpha\,\tau_{k+1}^{\alpha}A^{\frac{\beta}{2}}\right)\mathbf{u}_k+(\alpha+1)\,\tau_{k+1}^{\alpha}\mathbf{f}(\mathbf{u}_k)+\Gamma(\alpha+2)\mathbb{H}_k^e\\ \left(\Gamma(\alpha+2)\mathbb{I}+\tau_{k+1}^{\alpha}A^{\frac{\beta}{2}}\right)\mathbf{u}_{k+1} &= \left(\Gamma(\alpha+2)\mathbb{I}-\alpha\,\tau_{k+1}^{\alpha}A^{\frac{\beta}{2}}\right)\mathbf{u}_k+\alpha\,\tau_{k+1}^{\alpha}\mathbf{f}(\mathbf{u}_k)+\tau_{k+1}^{\alpha}\mathbf{f}(\mathbf{u}_{k+1}^{p})\\ &\quad+\;\Gamma(\alpha+2)\mathbb{H}_k^e,\end{aligned}\tag{4.48}$$

where

$$\mathbb{H}_k^e\approx\mathbb{H}_k^a=\sum_{j=0}^{k}a_{j,k}\Big(-A^{\frac{\beta}{2}}\mathbf{u}_j+\mathbf{f}(t_j,\mathbf{u}_j)\Big),$$

and by letting $\tau_{k,j} = (t_k - t_j)$, we have

$$a_{j,k} = \begin{cases} -\tau_{k+1}^{\alpha}(\tau_{k+1,1} - \alpha\,\tau_1) + (\tau_{k+1,1}^{1+\alpha} + \tau_{k,1}\tau_{k,0}^{\alpha} - \alpha\tau_1\tau_k^{\alpha}) - \tau_{k,1}^{1+\alpha}, & j = 0, \\ \tau_{k+1,j-1}^{1+\alpha} - \tau_{k,j-1}^{1+\alpha} + \tau_{k+1,j+1}^{1+\alpha} - \tau_{k,j+1}^{1+\alpha} + \alpha\,(t_{j+1} - 2t_j + t_{j-1})\left(\tau_{k+1,j}^{\alpha} - \tau_{k,j}^{\alpha}\right) & \\ +\tau_{k,j}^{\alpha}\,(\tau_{k,j+1} + \tau_{k,j-1}) - \tau_{k+1,j}^{\alpha}\,(\tau_{k+1,j+1} + \tau_{k+1,j-1})\,, & 1 \le j \le k-1, \\ \tau_{k+1,k-1}^{\alpha+1} - \tau_{k+1,k-1}\tau_{k+1}^{\alpha} - \tau_k^{1+\alpha} - \alpha\,\tau_k\tau_{k+1}^{\alpha}, & j = k. \end{cases}$$

4.5 Parallel Algorithms for Time-Space Fractional PDEs

In this subsection, we focus on the implementation of the predictor-corrector scheme (4.44). In particular, we discuss sequential and parallel algorithms for (4.44). Efficient parallelism of the sequential algorithm is possible by exploiting the structure of the history term $\mathbb{H}_n^a$ as discussed in the sequel. As discussed in the previous sections, we efficiently precompute and store the LU decomposition of the matrix $\left(\Gamma(\alpha+2)\mathbb{I} + \tau^{\alpha}A^{\frac{\beta}{2}}\right)$ or its inverse. For simplicity of notation, we refer to the solution $L\mathbf{y} = \mathbf{b}$, $U\mathbf{x} = \mathbf{y}$ as $P\mathbf{b}$ where L and U are lower and upper triangular matrices. Also, we compute and store the matrix $Q = \left(\Gamma(\alpha+2)\mathbb{I} - \alpha\tau^{\alpha}A^{\frac{\beta}{2}}\right)$.

4.5.1 Sequential Algorithm

Given a stencil $0 = t_0 < t_1 < \cdots < t_M = T$ in the t-direction with (M+1) grid points, we seek solutions at time t_i which are dependent on all solutions at the previous time steps (history term). For the first iteration, only the initial values are needed to advance to the next step as there are no known history of the solutions. Each other iteration performs the following step:

1. Compute the history term

$$\mathbb{H}_n^a = \sum_{j=0}^{n} a_{j,n}\Big(- A^{\frac{\beta}{2}}\mathbf{u}_j + \mathbf{f}(t_j, \mathbf{u}_j)\Big)$$

2. Compute and store

$$\mathbf{w}_1 = Q\mathbf{u}_n + \mathbb{H}_n^a \quad \text{and} \quad \mathbf{w}_2 = \mathbf{f}(t_n, \mathbf{u}_n)$$

   It is more efficient to store these values since they would be used twice in each step.

3. Compute the right hand side vector for the predictor: $\mathbf{z} = \mathbf{w}_1 + \tau^\alpha(\alpha+1)\mathbf{w}_2$

4. Compute the predicted value: $\mathbf{v} = P\mathbf{z}$

5. Compute the right hand side vector for the corrector: $\mathbf{v} = \mathbf{w}_1 + \tau^\alpha\left(\alpha\,\mathbf{w}_2 + \mathbf{f}(t_{n+1}, \mathbf{v})\right)$

6. Compute the final solution: $\mathbf{u}_{n+1} = P\mathbf{v}$

Next, we present the algorithm.

Algorithm 4 Sequential algorithm

1: **procedure** SEQUENTIAL VERSION

2: $\mathbf{w}_1 \leftarrow Q\mathbf{u}_0$

3: $\mathbf{w}_2 \leftarrow \mathbf{f}(\mathbf{u}_0)$

4: $\mathbf{v} \leftarrow P\Big(\mathbf{w}_1 + \tau^\alpha(\alpha+1)\mathbf{w}_2\Big)$

5: $\mathbf{u}_1 \leftarrow P\Big(\mathbf{w}_1 + \tau^\alpha\left(\alpha\,\mathbf{w}_2 + \mathbf{f}(t_1, \mathbf{v})\right)\Big)$

6: **for** $n = 1$ *to* $M-1$ **do**

7: Compute $\mathbb{H}_n^a \leftarrow \sum_{j=0}^{n} a_{j,n}\Big(-A^{\frac{\beta}{2}}\mathbf{u}_j + \mathbf{f}(t_j, \mathbf{u}_j)\Big)$

8: $\mathbf{w}_1 \leftarrow Q\mathbf{u}_n + \mathbb{H}_n^a$

9: $\mathbf{w}_2 \leftarrow \mathbf{f}(t_n, \mathbf{u}_n)$

10: $\mathbf{v} \leftarrow P\left(\mathbf{w}_1 + \tau^\alpha(\alpha+1)\mathbf{w}_2\right)$

11: $\mathbf{u}_{n+1} \leftarrow P\left(\mathbf{w}_1 + \tau^\alpha\Big(\alpha\,\mathbf{w}_2 + \mathbf{f}(t_{n+1}, \mathbf{v})\Big)\right)$

12: **end for**

13: **end procedure**

The major workhorse of the algorithm is the matrix-vector multiplication. There are 3 matrix-vector multiplications at the first step (outside the loop) and $(n+4)$ matrix-vector multiplications at each step within the for-loop. Thus, the total number of matrix-vector multiplications is

$$T(M) = 3 + \sum_{i=1}^{M-1}(i+4) = \frac{(M+8)(M-1)}{2} + 3 \in O(M^2).$$

Each matrix-vector multiplication is $O(N^2)$ operations, so that the algorithm requires $O(M^2N^2)$ number of scalar multiplications. In a similar manner, the algorithm requires $O(M^2N^2)$ number of scalar additions.

4.5.2 Parallel Algorithms

In this subsection, we discuss parallel versions of the algorithm using the shared memory systems (OpenMP) and the distributed memory systems (MPI). We also briefly discuss a hybrid version where both the shared and memory distributed systems are used in implementing the algorithm.

4.5.2.1 MPI Version

At first, we rewrite eqn. (4.44) as

$$\mathbf{u}_{n+1}^p = P\Big(\mathbf{I}_1 + \mathbf{I}_2^p + \mathbf{I}_3 + \mathbf{I}_4\Big),$$

$$\mathbf{u}_{n+1} = P\Big(\mathbf{I}_1 + \mathbf{I}_2^c + \mathbf{I}_3 + \mathbf{I}_4\Big),$$

where

$$P = \Big(\Gamma(\alpha+2)\mathbb{I} + \tau^\alpha A^{\frac{\beta}{2}}\Big)^{-1},$$

$$\mathbf{I}_1 = Q\mathbf{u}_n,$$

$$\mathbf{I}_2^p = (\alpha+1)\tau^\alpha \mathbf{f}(\mathbf{u}_n),$$

$$\mathbf{I}_2^c = \tau^\alpha\Big(\alpha\,\mathbf{f}(t_n,\mathbf{u}_n) + \mathbf{f}(t_{n+1},\mathbf{u}_{n+1}^p\Big),$$

$$\mathbf{I}_3 = \tau^\alpha \sum_{j=0}^{(k-1)p} a_{j,n}\Big(-A^{\frac{\beta}{2}}\mathbf{u}_j + \mathbf{f}(t_j,\mathbf{u}_j)\Big),$$

$$\mathbf{I}_4 = \tau^\alpha \sum_{j=(k-1)p+1}^{n} a_{j,n}\Big(-A^{\frac{\beta}{2}}\mathbf{u}_j + \mathbf{f}(t_j,\mathbf{u}_j)\Big).$$

Suppose we have p cores or processes available and given M the number of time steps, we divide the work (computation of each time step $t_j,\ j = 1(1)M$) among the p processors in a certain number of blocks. For instance, if $M = 500$ and $p = 3$, then the work is done in 167 blocks (or iterates) with two processors working on the last block while others remain idle. In essence, each processor is given the task of computing $\mathbf{u}_{n+1}^p$ and $\mathbf{u}_{n+1}$ for one and only one value of n in each iteration of the block. The following steps show the implementation procedure.

1. For the computation of $\mathbf{I}_3$, the only required values are the initial value and the precomputed values $\mathbf{u}_n$ already obtained from previous blocks so that at the start of the kth block all required data (solution values) are available. In this step, each process performs the computation of $\mathbf{I}_3$ since it is totally independent of the data/computations of the other processes. Therefore, no communication is required between the processes and thus, this step scales linearly with k.

2. After the computation of $\mathbf{I}_3$ which is independent of the data available to each process, we are left with the task of computing $\mathbf{I}_1,\ \mathbf{I}_2^p,\ \mathbf{I}_2^c$ and $\mathbf{I}_4$. This section is sequential as each process requires some data from at least one of the other processes. For $n = kp,\ k \in \mathbb{N},\ \mathbf{I}_4 = 0$ and process p_1 immediately computes $\mathbf{I}_2^p,\ \mathbf{I}_1$ and $\mathbf{u}_{n+1}^p$ followed by the evaluation of $\mathbf{I}_2^c$ so that $\mathbf{u}_{n+1}$ is readily obtained. p_1 sends the result of the vector $\mathbf{u}_{n+1}$ to the next process p_2 and then becomes idle until the next block. On receiving the required data for the computation of $\mathbf{u}_{n+2}$, p_2 computes $\mathbf{I}_4 = a_{n+1,n+1}\Big(- A^{\frac{\beta}{2}}\mathbf{u}_{n+1} + \mathbf{f}(t_{n+1}, \mathbf{u}_{n+1})\Big)$ followed by the evaluation of $\mathbf{I}_1 = Q\mathbf{u}_{n+1}$, $\mathbf{I}_2^p = (\alpha+1)\tau^\alpha \mathbf{f}(t_{n+1}, \mathbf{u}_{n+1})$ and $\mathbf{u}_{n+2}^p$. With all these available data, p_2 finally computes $\mathbf{u}_{n+2}$. p_2 sends $\mathbf{u}_{n+1}$ and $\mathbf{u}_{n+2}$ to process p_3 and then becomes idle until the next block. This process is continued until the last process computes $\mathbf{u}_{n+p}$. At the end of each block, the last process p_p broadcasts all solutions (computed in each block) to all the other processes for update to the array of solutions.The work load in this step increases from process p_1 to p_p as the first process p_1 has no summand in $\mathbf{I}_4$ while the last process p_p has $(p-1)$ summands to compute. There are p ($(p-1)$ sends/receive and 1 broadcast) communications between the processes so that the amount of time spent in this step depends more on the number of available processes than on k. As k increases, there is a nice trade-off between the computation and communication time and the workload imbalance becomes less severe.

3. An iterative continuation of Step 2 is carried out for $k = 1, 2, \cdots, \left\lfloor \frac{M}{p} \right\rfloor$.

4. If M is exactly divisible by p, then the algorithm is terminated. Otherwise, the remaining solutions $\mathbf{u}_{\lfloor \frac{M}{p} \rfloor + 1},\ \cdots, \mathbf{u}_M$ are computed the same manner as in Step 3. The only difference here is that we have less work than the number of processes. So we need choose $(M - p\lfloor \frac{M}{p} \rfloor)$ processes to perform the remaining work while the remaining $(p - (M - \lfloor \frac{M}{p} \rfloor))$ processes remain idle.

Algorithm 5 MPI Version

procedure MPI VERSION
  Compute num_blocks = $\lfloor \frac{M}{p} \rfloor$ ▷ p is the number of processes.
  Each process creates new data types as follows:
    MPI__Datatype send_type, broadcast_type
    *MPI__Type__Contiguous((my_rank+1)*N, MPI__DOUBLE, &send_type)*
    *MPI__Type__Contiguous(p*N, MPI__DOUBLE, &broadcast_type)*
    MPI__Type__commit(&send_type) ▷ my_rank is the process ID (0 to $(p-1)$).
    MPI__Type__commit(&broadcast_type)
  for $k = 0$ *to* num_blocks-1 **do**
    $n = kp$
    Each process computes its own $\mathbf{I}_3$ given as
    $\mathbf{I}_3 \leftarrow \tau^\alpha \sum_{j=0}^{n} a_{j,n+my\_rank}\Big(- A^{\frac{\beta}{2}}\mathbf{u}_j + \mathbf{f}(t_j, \mathbf{u}_j)\Big)$
    Set $\mathbf{I}_3 = \mathbf{O}$ if n is 0. ▷ $\mathbf{O}$ is the zero vector
    if my_rank is 0 **then**
      $\mathbf{I}_1 \leftarrow Q\mathbf{u}_n$ and $\mathbf{w}_1 \leftarrow \mathbf{f}(t_n, \mathbf{u}_n)$
      $\mathbf{w}_2 \leftarrow \mathbf{I}_1 + \mathbf{I}_3$ and $\mathbf{I}_2^p \leftarrow (\alpha+1)\tau^\alpha \mathbf{w}_1$
      $\mathbf{v} \leftarrow P\Big(\mathbf{I}_2^p + \mathbf{w}_2\Big)$ ▷ predicted value
      $\mathbf{I}_2^c \leftarrow \tau^\alpha\Big(\alpha\,\mathbf{w}_1 + \mathbf{f}(t_{n+1}, \mathbf{v})\Big)$
      $\mathbf{u}_{n+1} \leftarrow P\Big(\mathbf{I}_2^c + \mathbf{w}_2\Big)$ ▷ corrected value
      if $p > 1$ **then** ▷ Send data only when $p > 1$.
        Send $\mathbf{u}_{n+1}$ to process $my\_rank + 1$ using send_type.
      end if
    else
      Receive $\mathbf{u}_{n+1}, \cdots, \mathbf{u}_{n+my\_rank}$ from process $my\_rank - 1$ using send_type.
      $\mathbf{I}_4 \leftarrow \tau^\alpha \sum_{j=n+1}^{n+my\_rank} a_{j,n+my\_rank}\Big(- A^{\frac{\beta}{2}}\mathbf{u}_j + \mathbf{f}(t_j, u_j)\Big)$
      $\mathbf{I}_1 \leftarrow Q\mathbf{u}_{n+my\_rank}$ and $\mathbf{w}_1 \leftarrow \mathbf{f}(t_{n+my\_rank}, \mathbf{u}_{n+my\_rank})$
      $\mathbf{w}_2 \leftarrow \mathbf{I}_1 + \mathbf{I}_3 + \mathbf{I}_4$ and $\mathbf{I}_2^p \leftarrow (\alpha+1)\tau^\alpha \mathbf{w}_1$
      $\mathbf{v} \leftarrow P\Big(\mathbf{I}_2^p + \mathbf{w}_2\Big)$ ▷ predicted value
      $\mathbf{I}_2^c \leftarrow \tau^\alpha\Big(\alpha\,\mathbf{w}_1 + \mathbf{f}(t_{n+my\_rank+1}, \mathbf{v})\Big)$
      $\mathbf{u}_{n+my\_rank+1} \leftarrow P\Big(\mathbf{I}_2^c + \mathbf{w}_2\Big)$ ▷ corrected value
      if my_rank is not $(p-1)$ **then**
        Send $\mathbf{u}_{n+1}, \cdots, \mathbf{u}_{n+my\_rank+1}$ to process $my\_rank + 1$ using send_type
      else ▷ Last process sends the most updated data to all processes
        Broadcast computed solutions in this block using broadcast_type.
      end if
    end if
  end for
  if M is not divisible by p **then**
    Select $(M \ mod \ p)$ processes to participate in one iteration of the for-loop.
  end if
end procedure

4.5.2.2 OpenMP Version

The OpenMP version of the algorithm is straightforward. The history term $\mathbb{H}_n^a$ is easily parallelizable by adding the ***#pragma omp parallel*** construct. In the parallel region, each thread or rank locally creates a vector to hold its partial sum of the history which is later updated using the ***#pragma omp critical*** construct. Also each matrix addition/subtraction, vector addition/subtraction, matrix-vector multiplication, matrix/vector-scalar multiplication, constructing the zero vector/matrix or constructing the identity matrix are all straightforwardly implemented in parallel by adding ***#pragma omp parallel*** (with appropriate declaration of private or shared variables) construct. In our implementation, the OpenMP version seems more efficient than the MPI version. This may be attributed to the communication time between each processes in the MPI version as there are $p-1$ *MPI_Send* and *MPI_Recv*, and one *MPI_Bcast* in each iteration of the for-loop. Next, we present the algorithm as follows.

Algorithm 6 OpenMP Version

procedure OpenMP version
  $\mathbf{w}_1 \leftarrow Q\mathbf{u}_0$
  $\mathbf{w}_2 \leftarrow \mathbf{f}(t_0, \mathbf{u}_0)$
  $\mathbf{v} \leftarrow P\Big(\mathbf{w}_1 + \tau^\alpha(\alpha+1)\mathbf{w}_2\Big)$
  $\mathbf{u}_1 \leftarrow P\Big(\mathbf{w}_1 + \tau^\alpha\left(\alpha\,\mathbf{w}_2 + \mathbf{f}(t_1, \mathbf{v})\right)\Big)$
  for $n = 1$ *to* $M-1$ **do**
    Set $\mathbb{H}_n^a$ to $\mathbf{O}$.
    #pragma omp parallel num_threads(num_thrds)
    { ▷ num_thrds is the number of threads used.
      Locally create a vector *temp*.
      Set *temp* to $\mathbf{O}$.
      #pragma omp for schedule(dynamic)
      for $j = 0$ *to* n **do**
        $temp \leftarrow temp + a_{j,n}\Big(-A^{\frac{\beta}{2}}\mathbf{u}_j + \mathbf{f}(t_j, \mathbf{u}_j)\Big)$
      end for
      #pragma omp critical
      $\mathbb{H}_n^a \leftarrow \mathbb{H}_n^a + temp$
    }
    $\mathbf{w}_1 \leftarrow Q\mathbf{u}_n + \mathbb{H}_n^a$
    $\mathbf{w}_2 \leftarrow \mathbf{f}(t_n, \mathbf{u}_n)$
    $\mathbf{v} \leftarrow P\left(\mathbf{w}_1 + \tau^\alpha(\alpha+1)\mathbf{w}_2\right)$
    $\mathbf{u}_{n+1} \leftarrow P\left(\mathbf{w}_1 + \tau^\alpha\Big(\alpha\mathbf{w}_2 + \mathbf{f}(t_{n+1}, \mathbf{v})\Big)\right)$
  end for
end procedure

4.5.2.3 Hybrid version

The hybrid version makes use of the OpenMP and MPI. The algorithm descrip-

tion is similar to the MPI version. The only difference is that the matrix addition/subtraction, vector addition/subtraction, matrix-vector multiplication, matrix/vector-scalar multiplication, constructing zero vector/matrix or constructing the identity matrix are performed using OpenMP constructs with some number of threads. We show the advantages of the hybrid version over the other two parallel versions in the implementation section.

4.6 Numerical Examples

In this subsection, we implement the sequential and the parallel algorithms. The programs were written in C language and compiled using the ***gcc -fopenmp*** and ***mpicc*** commands in Linux for the OpenMP and MPI programs, respectively, without any level of optimization. For practical purposes, optimization flags will greatly increase the efficiency of the algorithms. The codes were implemented on an Intel(R) Xeon(R) CPU E5-2640 v3 with 32 physical cores running at 2.60GHz clock speed. At first, we corroborate our theoretical analysis by obtaining the order of convergence of the scheme using some test examples. Furthermore, we test the problem using the sequential and parallel algorithms, and discuss the merits and demerits of each of the parallel version of the algorithms over one another. For all the programs, we use a time function for timing results. Although we could have used ***omp_get_wtime()*** and ***MPI_wtime()***, we deem it fit, for comparison purposes, to use same timing function for both the sequential and all versions of the parallel algorithms.
We remark that there are $(n+3)$ function evaluations in each step of the for-loop (Algorithm 4) so that the computation for $f(u) \neq 0$ is more computationally demanding than for $f(u) = 0$. In fact, for $f(u) = 0$, only the computation

$$\mathbf{u}_{n+1} = PQ\mathbf{u}_n + \mathbb{H}_n^a,$$

$$\mathbb{H}_n^a = -\sum_{j=0}^{n} a_{j,n} \left(A^{\frac{\beta}{2}} \mathbf{u}_j \right)$$

is required with $\mathbb{H}_n^a = \mathbf{O}$ for $n = 0$. For nonlinear problems, the rate of convergence (ROC), is obtained as $ROC = \dfrac{\log\left(\text{Error}_\tau / \text{Error}_{\frac{\tau}{2}}\right)}{\log 2}$, where $\text{Error}_\tau = \left|\left|\mathbf{u}_{\frac{\tau}{2}} - \mathbf{u}_\tau\right|\right|_2$ and $\mathbf{u}_\tau$ is the solution vector with time step-size τ.

4.6.1 One-Dimensional Time-Space Fractional Problem (1D-TSFP)

We consider

$${}_cD_{0,t}^{\alpha} u = -\kappa(-\Delta)^{\frac{\beta}{2}} u(x,t) + f(t,u), \quad \text{in} \quad [0,1] \times (0,1]$$

subject to homogeneous Dirichlet boundary conditions and the initial condition $u(x,0) = x^2(1-x)^2$ with $\kappa = 1$. At first, we solve the problem with $f(t,u) = 0$ whose solution is given by

$$u(x,t) = \sum_{n=1}^{\infty} \frac{4\left(-12 + n^2\pi^2\right)\left(-1 + (-1)^n\right)}{n^5\pi^5} \mathbb{E}_\alpha(-(n\pi)^\beta t^\alpha) \sin(n\pi x),$$

where $\mathbb{E}_\alpha(x)$ is the Mittag-Leffler function of x. Tables 13–14 and 15–16 show the L_2 error norm using $f(t,u) = 0$ and $f(t,u) = u^2$, respectively with the convergence rates. We observe that the experimental rate of convergence corroborate our theoretical order of the schemes. We used $h = 0.001$ in the tables 13–20. This choice of h is to ensure that the errors are solely due to time so that we can obtain a computational order of convergence in time.

	$\alpha = 0.2$		$\alpha = 0.4$		$\alpha = 0.6$		$\alpha = 0.8$	
τ	Error	ROC	Error	ROC	Error	ROC	Error	ROC
$\frac{1}{4}$	4.029e-04		3.979e-04		2.852e-04		3.421e-04	
$\frac{1}{8}$	1.684e-04	1.2586	1.481e-04	1.4255	9.319e-05	1.6135	5.311e-05	2.6872
$\frac{1}{16}$	7.164e-05	1.2330	5.468e-05	1.4379	2.975e-05	1.6474	1.457e-05	1.8663
$\frac{1}{32}$	3.080e-05	1.2177	2.038e-05	1.4235	9.565e-06	1.6370	4.025e-06	1.8557
$\frac{1}{64}$	1.332e-05	1.2095	7.647e-06	1.4144	3.096e-06	1.6275	1.115e-06	1.8519
$\frac{1}{128}$	5.776e-06	1.2054	2.879e-06	1.4094	1.006e-06	1.6216	3.092e-07	1.8503

Table 13: Results for 1D-TSFP with $f(t,u) = 0,\ \beta = 1.4$.

	$\alpha = 0.2$		$\alpha = 0.4$		$\alpha = 0.6$		$\alpha = 0.8$	
τ	Error	ROC	Error	ROC	Error	ROC	Error	ROC
$\frac{1}{4}$	4.256e-04		4.037e-04		2.729e-04		5.407e-04	
$\frac{1}{8}$	1.781e-04	1.2566	1.528e-04	1.4015	9.109e-05	1.5831	4.866e-04	3.4741
$\frac{1}{16}$	7.582e-05	1.2322	5.650e-05	1.4354	2.923e-05	1.6398	1.247e-05	1.9638
$\frac{1}{32}$	3.261e-05	1.2172	2.109e-05	1.4219	9.427e-06	1.6326	3.467e-06	1.8471
$\frac{1}{64}$	1.410e-05	1.2092	7.917e-06	1.4133	3.058e-06	1.6240	9.655e-07	1.8443
$\frac{1}{128}$	6.118e-06	1.2051	2.982e-06	1.4085	9.959e-07	1.6187	2.691e-07	1.8431

Table 14: Results for 1D-TSFP with $f(t,u) = 0,\ \beta = 1.6$.

	$\alpha = 0.2$		$\alpha = 0.4$		$\alpha = 0.6$		$\alpha = 0.8$	
τ	Error	ROC	Error	ROC	Error	ROC	Error	ROC
$\frac{1}{4}$	3.716e-04		3.820e-04		2.135e-04		5.891e-04	
$\frac{1}{8}$	1.533e-04	1.2760	1.462e-04	1.3861	9.703e-05	1.1375	5.728e-05	3.3623
$\frac{1}{16}$	6.470e-05	1.2443	5.363e-05	1.4466	3.086e-05	1.6525	1.556e-05	1.8803
$\frac{1}{32}$	2.769e-05	1.2242	1.988e-05	1.4314	9.876e-06	1.6439	4.295e-06	1.8570
$\frac{1}{64}$	1.194e-05	1.2143	7.412e-06	1.4236	3.181e-06	1.6345	1.190e-06	1.8523
$\frac{1}{128}$	5.154e-06	1.2115	2.763e-06	1.4236	1.029e-06	1.6282	3.308e-07	1.8464

Table 15: Results for 1D-TSFP with $f(t,u) = u^2,\ \beta = 1.4$.

	$\alpha = 0.2$		$\alpha = 0.4$		$\alpha = 0.6$		$\alpha = 0.8$	
τ	Error	ROC	Error	ROC	Error	ROC	Error	ROC
$\frac{1}{4}$	3.914e-04		3.811e-04		2.729e-04		9.204e-04	
$\frac{1}{8}$	1.628e-04	1.2729	1.507e-04	1.3382	9.444e-05	1.5014	5.712e-05	4.0100
$\frac{1}{16}$	6.842e-05	1.2431	5.440e-05	1.4429	3.039e-05	1.6359	1.338e-05	2.0946
$\frac{1}{32}$	2.931e-05	1.2231	2.060e-05	1.4280	9.764e-06	1.6380	3.718e-06	1.8471
$\frac{1}{64}$	1.265e-05	1.2124	7.704e-06	1.4193	3.156e-06	1.6293	1.035e-06	1.8444
$\frac{1}{128}$	5.477e-06	1.2076	2.885e-06	1.4171	1.024e-06	1.6235	2.893e-07	1.8392

Table 16: Results for 1D-TSFP with $f(t,u) = u^2,\ \beta = 1.6$.

4.6.2 Two-Dimensional Time-Space Fractional Problem (2D-TSFP)

We consider the two-dimensional time-space fractional reaction-diffusion equation

$$ {}_cD^{\alpha}_{0,t}u = -(-\Delta)^{\frac{\beta}{2}}u + f(t,u), \quad t > 0, \quad (x,y) \in [0,1]^2 $$

$$ u(x,y,0) = xy(1-x)(1-y) $$

with homogeneous Dirichlet boundary conditions. At first, we solve the problem with $f(t,u) = 0$ whose solution, given in Yang *et al.* [178], is

$$ u(x,y,t) = \sum_{n=1}^{\infty}\sum_{m=1}^{\infty} \mathbb{E}_{\alpha}\left(-\lambda_{n,m}^{\frac{\beta}{2}} t^{\alpha}\right) c_{n,m}\phi_{n,m}(x,y). $$

$$ \lambda = (n^2 + m^2)\pi^2, $$

$$ \phi_{n,m}(x,y) = 2\sin(n\pi x)\sin(n\pi y), $$

$$ c_{n,m} = \int_0^1 \int_0^1 xy(1-x)(1-y)\,\phi_{n,m}(x,y)\,dx\,dy. $$

This simulation shows the effectiveness of the scheme for high-dimensional problem. We have used $h = 0.01$ in all the simulations of this problem. Tables 17–20 shows the numerical results and rate of convergence of the scheme.

	$\alpha = 0.2$		$\alpha = 0.4$		$\alpha = 0.6$		$\alpha = 0.8$	
τ	Error	ROC	Error	ROC	Error	ROC	Error	ROC
$\frac{1}{4}$	3.724e-02		3.392e-02		1.732e-02		1.158e-02	
$\frac{1}{8}$	1.559e-02	1.2556	1.308e-02	1.3749	7.436e-03	1.2195	3.180-03	1.8650
$\frac{1}{16}$	6.631e-03	1.2337	4.834e-03	1.4358	2.384e-03	1.6412	8.876e-04	1.8411
$\frac{1}{32}$	2.843e-03	1.2217	1.797e-03	1.4276	7.634e-04	1.6428	2.432e-04	1.8679
$\frac{1}{64}$	1.220e-03	1.2202	6.663e-04	1.4316	2.406e-04	1.6659	6.298e-05	1.9491
$\frac{1}{128}$	5.199e-04	1.2311	2.421e-04	1.4603	7.084e-05	1.7639	1.252e-05	2.3307

Table 17: Results for 2D-TSFP with $f(t, u) = 0,\ \beta = 1.4$.

	$\alpha = 0.2$		$\alpha = 0.4$		$\alpha = 0.6$		$\alpha = 0.8$	
τ	Error	ROC	Error	ROC	Error	ROC	Error	ROC
$\frac{1}{4}$	3.893e-02		3.340e-02		9.626e-03		1.821e-02	
$\frac{1}{8}$	1.633e-02	1.2531	1.336e-02	1.3223	7.215e-03	0.4160	2.774e-03	2.7151
$\frac{1}{16}$	6.949e-03	1.2326	4.948e-03	1.4329	2.325e-03	1.6338	7.651e-04	1.8580
$\frac{1}{32}$	2.982e-03	1.2205	1.843e-03	1.4249	7.479e-04	1.6362	2.114e-04	1.8555
$\frac{1}{64}$	1.282e-03	1.2181	6.851e-04	1.4274	2.374e-04	1.6555	5.561e-05	1.9268
$\frac{1}{128}$	5.477e-04	1.2268	2.506e-04	1.4511	7.121e-05	1.7372	1.170e-05	2.2489

Table 18: Results for 2D-TSFP with $f(t, u) = 0,\ \beta = 1.6$.

	$\alpha = 0.2$		$\alpha = 0.4$		$\alpha = 0.6$		$\alpha = 0.8$	
τ	Error	ROC	Error	ROC	Error	ROC	Error	ROC
$\frac{1}{4}$	2.163e-02		2.081e-02		9.999e-03		9.984e-03	
$\frac{1}{8}$	8.957e-03	1.2719	8.226e-03	1.3893	5.035e-03	0.9899	2.288e-03	2.1258
$\frac{1}{16}$	3.789e-03	1.2414	3.027e-03	1.4421	1.613e-03	1.6419	6.425e-04	1.8321
$\frac{1}{32}$	1.634e-03	1.2131	1.130e-03	1.4213	5.234e-04	1.6239	1.809e-04	1.8282
$\frac{1}{64}$	7.290e-04	1.1647	4.344e-04	1.3798	1.762e-04	1.5707	5.233e-05	1.7897

Table 19: Results for 2D-TSFP with $f(t, u) = u^3,\ \beta = 1.4$.

	$\alpha = 0.2$		$\alpha = 0.4$		$\alpha = 0.6$		$\alpha = 0.8$	
τ	Error	ROC	Error	ROC	Error	ROC	Error	ROC
$\frac{1}{4}$	2.259e-02		2.002e-02		9.943e-03		1.923e-02	
$\frac{1}{8}$	9.375e-03	1.2686	8.395e-03	1.2542	4.876e-03	1.0280	2.027e-03	3.2459
$\frac{1}{16}$	3.963e-03	1.2421	3.095e-03	1.4397	1.569e-03	1.6355	5.513e-04	1.8787
$\frac{1}{32}$	1.700e-03	1.2207	1.152e-03	1.4253	5.079e-04	1.6274	1.556e-04	1.8249
$\frac{1}{64}$	7.407e-04	1.1991	4.344e-04	1.4073	1.675e-04	1.6003	4.462e-05	1.8020

Table 20: Results for 2D-TSFP with $f(t,u) = u^3,\ \beta = 1.6$.

4.6.3 Examples with Time-Graded Scheme (TGS)

Here, we solve the examples in subsections (4.6.1) and (4.6.2) using the time-graded scheme. The rate of convergence is given as $ROC = \dfrac{\log\left(\text{Error}_M/\text{Error}_{2M}\right)}{\log 2}$, where $\text{Error}_M = ||\mathbf{u}_M - U||_2$ for linear problems (U is exact solution and $\mathbf{u}_M$ is the TGS solution with M grid points) and $\text{Error}_M = ||\mathbf{u}_{2M} - \mathbf{u}_M||_2$ for nonlinear problems. As seen in Tables 21–24, the scheme is second-order accurate for different time-fractional order derivatives. This shows a great improvement in accuracy and performance over the other results given in Table 13–20.

	$\alpha = 0.2$		$\alpha = 0.4$		$\alpha = 0.6$		$\alpha = 0.8$	
M	Error	ROC	Error	ROC	Error	ROC	Error	ROC
10	4.587e-04		5.974e-04		6.575e-04		6.423e-04	
20	1.106e-04	2.0519	1.492e-04	2.0014	1.691e-04	1.9589	1.604e-04	2.0013
40	2.673e-05	2.0490	3.737e-05	1.9973	4.332e-05	1.9651	4.121e-05	1.9608
80	6.444e-06	2.0528	9.356e-06	1.9980	1.104e-05	1.9718	1.053e-05	1.9692
160	3.034e-06	2.0938	2.304e-06	2.0217	2.774e-06	1.9929	2.657e-06	1.9859

Table 21: Results for 1D-TSFP using TGS with $f(t,u) = 0,\ h = 0.001,\ \beta = 1.6$.

	$\alpha = 0.2$		$\alpha = 0.4$		$\alpha = 0.6$		$\alpha = 0.8$	
M	Error	ROC	Error	ROC	Error	ROC	Error	ROC
10	3.468e-04		4.188e-04		4.288e-04		5.357e-04	
20	8.288e-05	2.0649	1.033e-04	2.0194	1.102e-04	1.9599	9.407e-05	2.5095
40	1.967e-05	2.0754	2.543e-05	2.0223	2.819e-05	1.9670	2.427e-05	1.9543
80	4.428e-06	2.1509	6.188e-06	2.0389	7.193e-06	1.9782	6.239e-06	1.9641
160	7.291e-07	2.6026	1.445e-06	2.0983	1.826e-06	1.9914	1.599e-06	1.9678

Table 22: Results for 1D-TSFP using TGS with $f(t,u) = u^2,\ h = 0.001,\ \beta = 1.8$.

	$\alpha = 0.2$		$\alpha = 0.4$		$\alpha = 0.6$		$\alpha = 0.8$	
M	Error	ROC	Error	ROC	Error	ROC	Error	ROC
10	2.417e-03		2.954e-03		3.054e-03		2.548e-03	
20	5.722e-04	2.0790	7.268e-04	2.0229	7.804e-04	1.9685	6.607e-04	1.9475
40	1.311e-04	2.1262	1.758e-04	2.0474	1.959e-04	1.9940	1.678e-04	1.9774
80	2.546e-05	2.3636	3.877e-05	2.1811	4.599e-05	2.0908	4.046e-05	2.0523
160	3.617e-06	2.8158	5.148e-06	2.9128	7.729e-06	2.5731	7.733e-06	2.3872

Table 23: Results for 2D-TSFP using TGS with $f(t,u) = 0,\ h = 0.005,\ \beta = 1.4$.

	$\alpha = 0.2$		$\alpha = 0.4$		$\alpha = 0.6$		$\alpha = 0.8$	
M	Error	ROC	Error	ROC	Error	ROC	Error	ROC
10	1.825e-03		2.385e-03		2.636e-03		2.531e-03	
20	4.370e-04	2.0620	5.907e-04	2.0132	6.771e-04	1.9611	6.582e-04	1.9433
40	1.005e-04	2.1201	1.444e-04	2.0322	1.727e-04	1.9709	1.691e-04	1.9604
80	1.865e-05	2.4303	3.404e-05	2.0849	4.379e-05	1.9799	4.328e-05	1.9663
160	1.001e-06	4.2204	7.178e-06	2.2457	1.099e-05	1.9943	1.105e-05	1.9701

Table 24: Results for 2D-TSFP using TGS with $f(t,u) = u^2,\ h = 0.005,\ \beta = 1.2$.

4.7 Discussion of Parallel algorithms

In this subsection, we implement the scheme on 1D-TSFP with $\beta = 1.6,\ \alpha = 0.4,\ dx = 0.05,\ \tau = 0.1$ and $f(u) = u^2$ using all versions of the parallel algorithm discussed in previous sections. p in the hybrid version denotes the number of distributed processes used in the simulation. Each process uses only two threads in the simulation for the hybrid version of the parallel algorithms. The simulation is done for large T and the timing results are reported here. It is evident from tables 25 – 27 and figures 6 and 7 that the hybrid version takes less running time than the MPI and OpenMP versions. The hybrid version reported here only uses p distributed memories that spawns two threads each (for the OpenMP constructs). For practical purposes, more threads may be spawned, however, as the number of threads and processes increases, so does the communication time, synchronization procedures, and waiting time to receive data increases. As there are no message passing in the OpenMP versions, it is expected to be more efficient than the MPI version due to synchronization procedures and communication time in Step 2 of the MPI pseudocode. This assertion is corroborated by the experimental results in tables 25 – 27. It can be seen from fig. 7 that the OpenMP version gives almost linear speedups as T becomes large. The MPI version uses the most execution time and it is seen from the tables that the number of processes used is related to the time T. For example, while we expect around 1.524 and 3.162 seconds for $T = 400$ and 800 (with $p = 16$, MPI version), the results are slightly different due to the use of more processes on an input T of relatively small size. In fact, if too many processes are used on an input of relatively small size, then

the communication time between processes, waiting time for data from other processes and time for synchronizing the processes will exceed the actual computation time of the simulation and thus dominate the overall execution time of the program. The speedup given in the tables is calculated as the ratio of the run-time for the sequential version to the run-time for p processes and the efficiency = speedup/p.

	$T = 400$			$T = 800$		
p	Run time (secs)	Speedup	Efficiency (%)	Run time (secs)	Speedup	Efficiency (%)
1	19.294			74.686		
2	7.826	2.465	123.3	30.401	2.456	122.8
4	4.028	4.789	119.7	15.789	4.730	118.3
8	2.384	8.093	101.1	8.899	8.393	104.9
16	1.628	11.851	74.1	5.540	13.481	84.3

Table 25: OpenMP version with $T = 400$ and 800

	$T = 400$			$T = 800$		
p	Run time (secs)	Speedup	Efficiency (%)	Run time (secs)	Speedup	Efficiency (%)
1	19.294			74.686		
2	9.281	2.079	103.9	37.295	2.003	100.1
4	5.169	3.733	93.3	19.328	3.864	96.6
8	3.054	6.318	78.9	11.116	6.719	83.9
16	2.561	7.534	47.1	9.650	7.739	48.4

Table 26: MPI version with $T = 400$ and 800

	$T = 400$			$T = 800$		
p	Run time (secs)	Speedup	Efficiency (%)	Run time (secs)	Speedup	Efficiency (%)
1	19.294			74.686		
2	4.587	4.206	210.3	17.855	4.183	209.1
4	2.699	7.149	178.7	10.075	7.413	185.3
8	1.832	10.532	131.6	6.842	10.916	136.5
16	1.526	12.643	79.0	7.112	10.501	65.6

Table 27: Hybrid version with $T = 400$ and 800

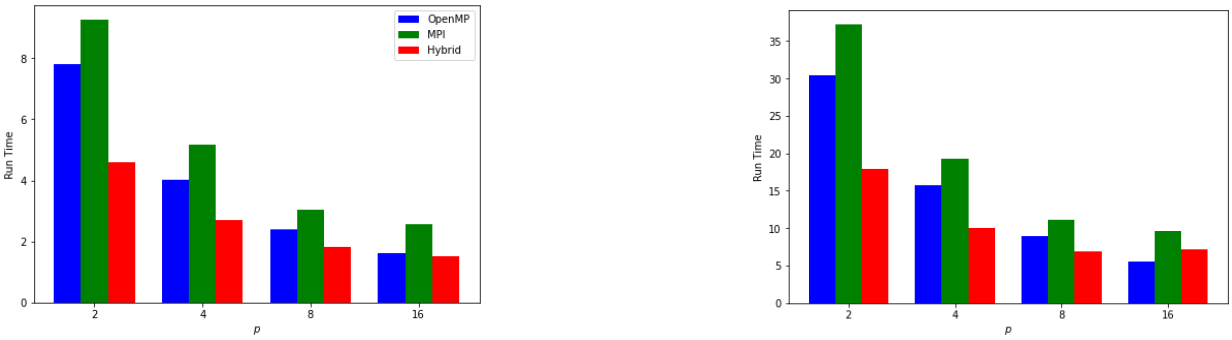

Figure 6: Bar chart showing the performance of the three parallel algorithms

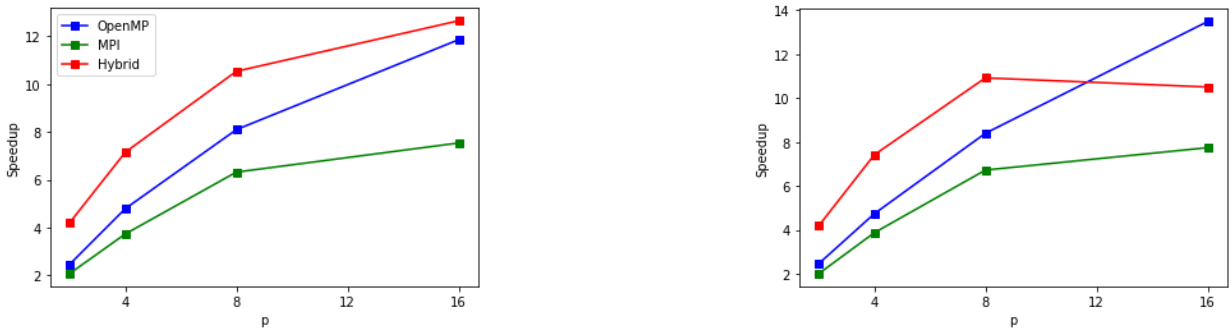

Figure 7: Speedup vs p showing the linear scalability of the parallel algorithms

CHAPTER 5
A Fractional-Order Compartmental Model for COVID-19

5.1 Introduction

Fractional differential equations (FDEs) are used to model complex phenomena such as the modeling of memory-dependent phenomena (DiGuiseppe *et al.* [41], Baleanu *et al.* [12], Podlubny [133]), mechanical properties of materials (Caputo and Mainardi [26]), anomalous diffusion in porous media (Fomin *et al.* [55], Metzler and Klafter[120]), groundwater flow problems (Cloot and Botha [36], Iaffaldano *et al.* [71]), and control theory (Podlubny [132]), among others. They serve as a generalization of the integer-order differential equations and give more degree of freedom for modeling of biological and physical processes. FDEs have been applied in biological tissues [112], DNA sequencing [110], Pine Wilt disease [148], lung tissue mechanics and models [74] , harmonic oscillators [14], Dengue fever [44], measles **Islam2014**, human liver [13], diffusion processes [152], SEIR models [3]. Infectious disease outbreaks are one of the main causes of deaths in human. Their dynamics and spread are modeled and studied before the introduction of vaccines. The novel coronavirus began in December 2019 in China and has spread rapidly leading to over 2 million deaths worldwide. The first occurrence in the United States was seen around mid January in Washington [126] and has spread across America with over 390,000 deaths and 24 million infected cases. The epidemic has disrupted the day-to-day activities of the human life with over six million jobs lost in the United States. Several actions and measures have been taken by the federal, state and local governments to mitigate the spread of the epidemic. The most prominent measures taken include social distancing, testing, use of face-masks and contact tracing. It is important to model this epidemic in order to better understand the spread and dynamics as well as address the challenges of the epidemic. In short, mathematical models are important to guide the decisions of health and government officials.

This study aims to examine and analyze the epidemic's spread using a modification of the Susceptible-Exposed-Infected-Recovered (SEIR) model with a time-fractional derivative. The use of fractional derivatives in the model stems from the fact that the spread of infectious diseases depends not only on the current state but also on its past states (history or memory dependency). In particular, it is used to capture any possible nonlocal impact or any apparent delay in the outbreak. Additionally, time-fractional order models reduce errors resulting from neglect of parameters in models. We shall focus on some selected states in the US. We note that models that consider the US as a whole may be misleading and have limited applicability as different states have different economical and political perspectives which determines the different control strategies used for each state. For example, while some states such as Maryland, New Jersey, New York, Connecticut, among others, enforced the use of masks in public places and longer stay-at-home order [37], other

states do not enforce these measures thereby allowing for a possibility of increase of infected individuals in such states. There have been several models for the study of the epidemic. Lu *et al.* [106] considered a fractional-order SEIHDR model which incorporates intercity movements. Liu *et al.* [105] studied the dynamics of the pandemic by considering asymptomatic and symptomatic infected populations separately. Giordano *et al.* [62] studied the COVID-19 epidemic with intervention strategies in Italy. They proposed a model consisting of different stages: susceptible, infected, diagnosed, ailing, recognized, threatened, healed and extinct. They further discuss the long time behavior of the populations in which the susceptible, healed and extinct population remains. Stella *et al.* [160] studied the role of asymptomatic individuals via complex networks. In particular, they formulated a model that aims to study the interactions in the population through complex networks. They further extended the model to a structured nonhomogenous version using the Watts-Strogatz complex network. Wu *et al.* [171] studied domestic and international spread of the epidemic by using different data sets. Zhao and Chen [189] discussed the dynamics of the pandemic by considering the Susceptible, unquarantined infected, quarantined infected and Confirmed infected (SUQC) model and parametrize the intervention effect of control measures. Zhang *et al.* [188] considered a fractional-order SEIR model with different order of the time-fractional derivative for each of the different population being studied. Tuan *et al.* [165] proposed a fractional-order model using the Caputo derivative for studying the transmission of COVID-19. They discussed the existence and uniqueness of solutions to the proposed model. They further used the generalized Adams-Bashforth-Moulton method for simulating the model. Bahloul *et al.* [10] proposed a fractional-order Susceptible-Exposed-Infected-Quarantined- Recovered-Death-Insusceptible (SEIQRDP) model for predicting the spread of COVID-19. Furati *et al.* [56] proposed a time-fractional order compartmental model with government intervention and public perception incorporated into their model. Gumel *et al.* [64] presented a primer for formulating, analysing and simulating mathematical models for understanding the dynamics of COVID-19.
The simulations in this chapter were written in Python with Anaconda on an Intel(R) Core(TM) i7-4870HQ CPU running at 2.50GHz. Next, We give some preliminary definitions which will be used in the sequel.

Definition 5.1.1. *[133] The Mittag-Leffler function which generalizes the exponential function for fractional calculus is defined as*

$$E_\alpha(z) = \sum_{k=0}^{\infty} \frac{z^k}{\Gamma(\alpha k + 1)}, \quad \alpha \in \mathbb{R}^+, \ z \in \mathbb{C}.$$

Remark 5.1.1.

More generally, the two parameter Mittag-Leffler function is defined as

$$E_{\alpha,\beta}(z) = \sum_{k=0}^{\infty} \frac{z^k}{\Gamma(\alpha k + \beta)}, \quad \alpha, \beta \in \mathbb{R}^+, \ z \in \mathbb{C}.$$

It has the following properties:

1. $E_{\alpha,\beta}(z) = zE_{\alpha,\alpha+\beta}(z) + \dfrac{1}{\Gamma(\beta)}$.
2. ${}_0\mathcal{D}_t^{\alpha} e^{\lambda t} = t^{-\alpha} E_{1,1-\alpha}(\lambda t)$.
3. ${}_0\mathcal{D}_t^{\alpha} E_{\alpha,1}(\lambda t^{\alpha}) = \lambda E_{\alpha,1}(\lambda t^{\alpha})$.

Definition 5.1.2. *[98] A point x^* is said to be an equilibrium point of the system ${}_{t_0}\mathcal{D}_t^{\alpha} = f(t, x(t)), \ x(t_0) > 0$ if and only if $f(t, x^*(t)) = 0$.*

Definition 5.1.3. *[106] An equilibrium point x^* of the system ${}_{t_0}\mathcal{D}_t^{\alpha} x(t) = f(t, x(t)), \ x(t_0) > 0$ is said to be asymptotically stable if all the eigenvalues of the Jacobian matrix $J = \partial f/\partial x$, evaluated at the equilibrium point, satisfies $|arg(\lambda_i)| > \dfrac{\alpha\pi}{2}$, where λ_i are the eigenvalues of J.*

5.2 Model Formulation

5.2.1 Initial Model

We begin with a basic time-fractional SEIR model consisting of four compartments that represents the susceptible (S), exposed (E), infected (I), recovered (R). We assumed that all the infected individuals are unreported and thus not hospitalized. The following system of differential equations models the transmission dynamics of the population:

$$
\begin{aligned}
{}_0\mathcal{D}_t^{\alpha} S(t) &= -\beta_0 \frac{SI}{N} \\
{}_0\mathcal{D}_t^{\alpha} E(t) &= \beta_0 \frac{SI}{N} - \sigma E \\
{}_0\mathcal{D}_t^{\alpha} I(t) &= \sigma E - \gamma I \\
{}_0\mathcal{D}_t^{\alpha} R(t) &= \gamma I
\end{aligned}
$$

where β_0 is the disease transmission rate, σ ($1/\sigma$) is the transition rate (disease incubation period) from the exposed class to the infectious class, γ ($1/\gamma$) is the recovery rate (time from infectiousness until recovery) of an infected individual. We note that the parameters of the model are non-negative and have dimensions given by $1/\text{time}^{\alpha}$. This observation was originally noted in Diethelm [44]. To alleviate this difference in dimensions, we replace the parameters with a power α of new parameters to obtain the new system of equations:

$$\begin{aligned} {}_0\mathcal{D}_t^{\alpha} S(t) &= -\beta_0^{\alpha} \frac{SI}{N} \\ {}_0\mathcal{D}_t^{\alpha} E(t) &= \beta_0^{\alpha} \frac{SI}{N} - \sigma^{\alpha} E \\ {}_0\mathcal{D}_t^{\alpha} I(t) &= \sigma^{\alpha} E - \gamma^{\alpha} I \\ {}_0\mathcal{D}_t^{\alpha} R(t) &= \gamma^{\alpha} I. \end{aligned} \tag{5.49}$$

5.2.2 Final Model

The next step in the development of our model is the incorporation of hospitalized compartments (H) and splitting of the infected cases into reported (R) and unreported cases (U). This step is necessary as published studies [34], [52], [105] have shown that a considerable number of infected cases go unreported either due to unawareness or early recovery or just perceptions of the infected individuals. We note that only the reported cases are being hospitalized during the infectious period and neglect the possibility of transmission of an hospitalized individual since they are not exposed to the general population. Furthermore, we introduce a time-dependent transmission rate which is a function of the number of deaths (the severity of the epidemic). The schema given in fig. 8 below shows the transmission flow of the model.

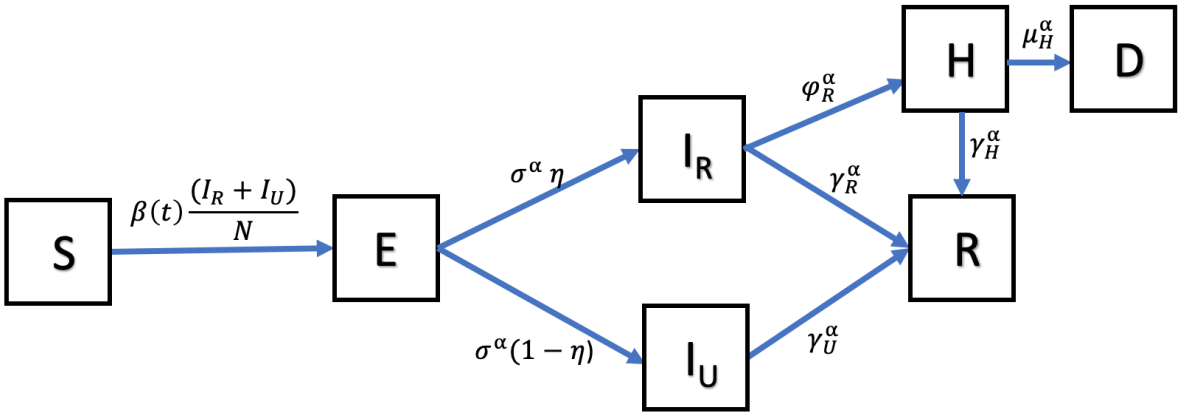

Figure 8: Schematic diagram of the proposed $\mathrm{SEI}_R\mathrm{I}_U\mathrm{HRD}$ model

Thus, we obtain the following system of time-fractional differential equations:

$$
\begin{aligned}
{}_0\mathcal{D}_t^\alpha S(t) &= -\beta(t)\frac{S}{N}(I_R+I_U)\\
{}_0\mathcal{D}_t^\alpha E(t) &= \beta(t)\frac{S}{N}(I_R+I_U)-\sigma^\alpha E\\
{}_0\mathcal{D}_t^\alpha I_R(t) &= \eta\sigma^\alpha E-(\gamma_{_R}^\alpha+\varphi_{_R}^\alpha)I_R\\
{}_0\mathcal{D}_t^\alpha I_U(t) &= (1-\eta)\sigma^\alpha E-\gamma_{_U}^\alpha I_U\\
{}_0\mathcal{D}_t^\alpha H(t) &= \varphi_{_R}^\alpha I_R-(\gamma_{_H}^\alpha+\mu_{_H}^\alpha)H\\
{}_0\mathcal{D}_t^\alpha R(t) &= \gamma_{_R}^\alpha I_R+\gamma_{_U}^\alpha I_U+\gamma_{_H}^\alpha H\\
{}_0\mathcal{D}_t^\alpha C(t) &= \sigma^\alpha E\\
{}_0\mathcal{D}_t^\alpha D(t) &= \mu_{_H}^\alpha H,
\end{aligned}
\tag{5.50}
$$

where $C(t)$ and $D(t)$ represents the number of cumulative infected (both reported and unreported) and the disease-induced deaths, respectively. These numbers can be

explicitly calculated as

$$C(t) = C(0) + \frac{\sigma^\alpha}{\Gamma(\alpha)} \int_0^t (t-s)^{\alpha-1} E(s)\, ds,$$
$$D(t) = \frac{\mu_{_H}^\alpha}{\Gamma(\alpha)} \int_0^t (t-s)^{\alpha-1} H(s)\, ds.$$

$\beta(t) = \beta_0^\alpha(1-\kappa_1)\left(1 - \frac{D(t)}{N}\right)^{\kappa_2}$ is the disease transmission rate which takes into account effects of governmental actions with $\kappa_1 \in [0,1)$ being the strength of the governmental intervention and κ_2 the intensity of individual reaction which quantifies how the population adheres to the public health measures. This is modelled as a step function that links the contacts among individuals as a proportion of death, that is, the severity of the epidemic. $\gamma_{_R}$, $\gamma_{_U}$, and $\gamma_{_H}$ are the recovery rates of a symptomatic, asymptomatic and hospitalized individuals, respectively. $\varphi_{_R}$ is the hospitalization rate of symptomatic infected person, $\mu_{_H}$ is the disease-induced death rate and η is the fraction of exposed individuals that becomes symptomatic.

5.3 Model Analysis

In this section, we discuss the properties of the model beginning with the existence, uniqueness, non-negativity and boundedness of solutions of the model (5.50). For simplicity in analysis, we reduce the system (5.50) to

$$\begin{aligned}
{}_0\mathcal{D}_t^\alpha S(t) &= -\beta(t)\frac{S}{N}(I_R + I_U) \\
{}_0\mathcal{D}_t^\alpha E(t) &= \beta(t)\frac{S}{N}(I_R + I_U) - \sigma^\alpha E \\
{}_0\mathcal{D}_t^\alpha I_R(t) &= \eta\sigma^\alpha E - (\gamma_{_R}^\alpha + \varphi_{_R}^\alpha) I_R \\
{}_0\mathcal{D}_t^\alpha I_U(t) &= (1-\eta)\sigma^\alpha E - \gamma_{_U}^\alpha I_U \\
{}_0\mathcal{D}_t^\alpha H(t) &= \varphi_{_R}^\alpha I_R - (\gamma_{_H}^\alpha + \mu_{_H}^\alpha) H
\end{aligned} \tag{5.51}$$

since R, D and C are linear combinations of populations in some other compartments. Clearly, $\beta(t)$ is a bounded function with $|\beta(t)| \leq \beta_0$.

Theorem 5.3.1. *There exist a unique solution to the system (5.51) and the solution is non-negative and bounded for any given initial data* $(S_0, E_0, I_{R0}, I_{U0}, H_0) \geq \mathbf{0} \in \mathbb{R}_+^5$.

Proof. By applying [101, Theorem 3.1], we obtain the existence of the solutions. To show the uniqueness and boundedness of solutions, it suffices to show by [101, Remark 3.2] that $F = (f_1, f_2, f_3, f_4, f_5)$ is locally Lipschitz continuous where

$$\begin{aligned}
f_1 &= -\beta(t)\frac{S}{N}\left(I_R + I_U\right), \\
f_2 &= \beta(t)\frac{S}{N}\left(I_R + I_U\right) - \sigma^\alpha E, \\
f_3 &= \eta\sigma^\alpha E - (\gamma_{_R}^\alpha + \varphi_{_R}^\alpha) I_R, \\
f_4 &= (1-\eta)\sigma^\alpha E - \gamma_{_U}^\alpha I_U, \\
f_5 &= \varphi_{_R}^\alpha I_R - (\gamma_{_H}^\alpha + \mu_{_H}^\alpha) H.
\end{aligned}$$

Let $X = (S, E, I_R, I_U, H)$, $\tilde{X} = (\tilde{S}, \tilde{E}, \tilde{I}_R, \tilde{I}_U, \tilde{H})$ and $||\cdot||$ denote the L_2 norm, then

$$\begin{aligned}
||F(X) - F(\tilde{X})|| &\leq ||f_1(X) - f_1(\tilde{X})|| + ||f_2(X) - f_2(\tilde{X})|| \\
&\quad + ||f_3(X) - f_3(\tilde{X})|| + ||f_4(X) - f_4(\tilde{X})|| \\
&\quad + ||f_5(X) - f_5(\tilde{X})|| \\
&\leq L||X - \tilde{X}||,
\end{aligned}$$

where $\mathrm{L} = \max_{1\leq i\leq 5} L_i$ and $L_1 = \beta_0$, $L_2 = \beta_0 + \sigma^\alpha$, $L_3 = \eta\sigma^\alpha + \gamma_{_R}^\alpha + \varphi_{_R}^\alpha$, $L_4 = (1-\eta)\sigma^\alpha + \gamma_{_U}^\alpha$ and $L_5 = \varphi_{_R}^\alpha + \gamma_{_H}^\alpha + \mu_{_H}^\alpha$. Thus, F satisfies the local Lipschitz conditions with respect to X which proves the uniqueness and boundedness of solution to (5.51). Next we show the non-negativity of solutions. At first, we consider moving along the S-axis, that is $E(0) = I_R(0) = I_U(0) = H(0) = 0$ and $0 < S(0) = S_0 \leq N$, then ${}_0\mathcal{D}_t^\alpha S(t) = 0$ whose solution is given as $S(t) = S_0 > 0$. In a similar manner, moving along each of the other respective axis (that is all initial conditions are zeros except for the axis being considered), it is easy to show that

$$\begin{aligned}
E(t) &= E_{\alpha,1}\left(-\sigma^\alpha t^\alpha\right) E_0 \geq 0, \\
I_R(t) &= E_{\alpha,1}\left(-(\gamma_{_R}^\alpha + \varphi_{_R}^\alpha) t^\alpha\right) I_{R0} \geq 0, \\
I_U(t) &= E_{\alpha,1}\left(-\gamma_{_U}^\alpha t^\alpha\right) I_{U0} \geq 0, \\
H(t) &= E_{\alpha,1}\left(-(\gamma_{_H}^\alpha + \mu_{_H}^\alpha) t^\alpha\right) H_0 \geq 0.
\end{aligned}$$

Therefore, all axis are non-negative invariant. Now, if the solution of the system is non-negative in the $S - E - I_U - I_R$ plane, then let $S(t^*) \geq 0$, $E(t^*) \geq 0$, $I_R(t^*) \geq 0$,

$I_U(t^*) \geq 0$ and $H(t^*) = 0$ for some t^* such that $H(t) < H(t^*)$. But

$$ {}_0\mathcal{D}_t^{\alpha} H \mid_{t=t^*} = \varphi_{R}^{\alpha} I_R \geq 0$$

in this plane. Using the mean value theorem for Caputo-fractional derivative

$$H(t) - H(t^*) = \frac{1}{\Gamma(\alpha)} \mathcal{D}_t^{\alpha}(\tau)(t - t^*)^{\alpha}$$

for some $\tau \in [t^*, t)$, we see that $H(t) \geq H(t^*)$. This contradicts our previous statement that $H(t) < H(t^*)$. Thus, $H(t) \geq 0$. Similar argument can be used for each of the remaining population variables. □

5.3.1 Computation of the basic reproduction number $\mathcal{R}_0$

We shall use the next generation matrix originally proposed by Diekmann *et al.* [43] and further elaborated on by van den Driesche and Watmough [51] and Diekmann *et al.* [42] to determine $\mathcal{R}_0$. Consider the three compartments $Y = (Y_1, Y_2, Y_3) = (E, I_R, I_U)$ containing the infected individuals and let Y^* be the disease free equilibrium (DFE) point. The linearized equation at the DFE is

$$ {}_0\mathcal{D}_t^{\alpha} Y_i = \mathcal{F}_i(Y) - \mathcal{V}_i(Y),\ i = 1(1)3,$$

where $\mathcal{F}_i(Y)$ is the rate of appearance of new infections in compartment i and $\mathcal{V}_i(Y)$ is the rate of transfer of infections to and from compartment i. We further define

$$\mathscr{F} = \frac{\partial \mathcal{F}_i(Y)}{\partial Y_j}\Big|_{Y=Y^*} \quad \text{and} \quad \mathscr{V} = \frac{\partial \mathcal{V}_i(Y)}{\partial Y_j}\Big|_{Y=Y^*}, \quad i,\ j = 1(1)3.$$

Then $\rho(\mathscr{F}\mathscr{V}^{-1})$ is the basic reproduction number $\mathcal{R}_0$, where $\rho(x)$ is the spectral radius of x and FV^{-1} is the next generation matrix. Thus, we obtain

$$\mathscr{F} = \begin{bmatrix} 0 & \beta(t) & \beta(t) \\ 0 & 0 & 0 \\ 0 & 0 & 0 \end{bmatrix}, \quad \mathscr{V} = \begin{bmatrix} \sigma^{\alpha} & 0 & 0 \\ -\eta\sigma^{\alpha} & \gamma_{R}^{\alpha} + \varphi_{R}^{\alpha} & 0 \\ -(1-\eta)\sigma^{\alpha} & 0 & \gamma_{U}^{\alpha} \end{bmatrix}.$$

The basic reproduction number of the model, denoted by $\mathcal{R}_0$, is given by

$$\mathcal{R}_0 = \beta(t) \left(\frac{\eta}{\gamma_{R}^{\alpha} + \varphi_{R}^{\alpha}} + \frac{1-\eta}{\gamma_{U}^{\alpha}} \right).$$

5.3.1.1 $\mathcal{R}_0$-Sensitivity Here, we check the sensitivity of $\mathcal{R}_0$ by obtaining its derivative with respect to each parameter. We replace $\beta(t)$ by its maximum value β_0^α and obtain the following:

$$\begin{aligned}
\frac{\partial \mathcal{R}_0}{\partial \beta_0} &= \alpha \beta_0^{\alpha-1}\left(\frac{\eta}{\gamma_{_R}^\alpha + \varphi_{_R}^\alpha} + \frac{1-\eta}{\gamma_{_U}^\alpha}\right),\\
\frac{\partial \mathcal{R}_0}{\partial \eta} &= \beta_0^\alpha\left(\frac{1}{\gamma_{_R}^\alpha + \varphi_{_R}^\alpha} - \frac{1}{\gamma_{_U}^\alpha}\right),\\
\frac{\partial \mathcal{R}_0}{\partial \gamma_{_R}} &= -\frac{\eta\alpha\beta_0^\alpha \gamma_{_R}^{\alpha-1}}{(\gamma_{_R}^\alpha + \varphi_{_R}^\alpha)^2},\\
\frac{\partial \mathcal{R}_0}{\partial \varphi_{_R}} &= -\frac{\eta\alpha\beta_0^\alpha \varphi_{_R}^{\alpha-1}}{(\gamma_{_R}^\alpha + \varphi_{_R}^\alpha)^2},\\
\frac{\partial \mathcal{R}_0}{\partial \gamma_{_U}} &= -\frac{\eta\alpha\beta_0^\alpha}{\gamma_{_U}^{\alpha+1}}.
\end{aligned}$$

Since all parameters are positive and $0 < \eta < 1$, then $\dfrac{\partial \mathcal{R}_0}{\partial \beta_0} > 0$, $\dfrac{\partial \mathcal{R}_0}{\partial \gamma_{_R}} < 0$, $\dfrac{\partial \mathcal{R}_0}{\partial \gamma_{_U}} < 0$ and $\dfrac{\partial \mathcal{R}_0}{\partial \varphi_{_R}} < 0$. This shows that $\mathcal{R}_0$ is increasing with β_0 and decreasing with $\gamma_{_U}$, $\gamma_{_R}$, $\varphi_{_R}$, but we cannot conclude on the monotonicity of $\mathcal{R}_0$ with respect to the other parameters of the model.

5.3.2 Linear Analysis of the Fractional-Order Dynamical Equations

A linearization of the fracional-order system (5.51) informs us about the early time growth of the epidemic and the trajectory of its solution vector. At the beginning of the epidemic, $S \approx N$ and $E, I_R, I_U, H << N$. We define new variables $x_1 = N - S$, $x_2 = E$, $x_3 = I_R$, $x_4 = I_U$, $x_5 = H$ and noting that $x_i << N$, we obtain the linear equations:

$$_0\mathcal{D}_t^\alpha X = AX, \quad \text{with} \quad X = (x_1, x_2, x_3, x_4, x_5)^T,$$

where

$$A = \begin{bmatrix}
0 & 0 & -\beta(t) & -\beta(t) & 0\\
0 & -\sigma^\alpha & \beta(t) & \beta(t) & 0\\
0 & \eta\sigma^\alpha & -(\gamma_{_R}^\alpha + \varphi_{_R}^\alpha) & 0 & 0\\
0 & (1-\eta)\sigma^\alpha & 0 & -\gamma_{_U}^\alpha & 0\\
0 & 0 & -\varphi_{_R}^\alpha & 0 & -(\gamma_{_H}^\alpha + \mu_{_H}^\alpha)
\end{bmatrix}.$$

The matrix has two obvious eigenvalues $\lambda_1 = 0$ and $\lambda_2 = -(\gamma_{_H}^{\alpha} + \mu_{_H}^{\alpha})$. The remaining eigenvalues are the roots of the cubic equation: $\lambda^3 + a_2\lambda^2 + a_1\lambda + a_0$, where

$$a_2 = (\sigma^{\alpha} + \gamma_{_R}^{\alpha} + \gamma_{_U}^{\alpha} + \varphi_{_R}^{\alpha}),$$

$$a_1 = \sigma^{\alpha}(-\beta(t) + \gamma_{_U}^{\alpha}) + (\sigma^{\alpha} + \gamma_{_U}^{\alpha})(\varphi_{_R}^{\alpha} + \gamma_{_R}^{\alpha}),$$

$$a_0 = \sigma^{\alpha}\gamma_{_U}^{\alpha}(\gamma_{_R}^{\alpha} + \varphi_{_R}^{\alpha})(1 - \mathcal{R}_0).$$

Next, we need find the conditions under which the roots of the equation are negative. We use the Routh-Hurwitz criterion which gives $a_0 > 0$, $a_2 > 0$ and $a_2a_1 > a_0$. Clearly $a_2 > 0$ and $a_0 > 0$ if $\mathcal{R}_0 < 1$. Let λ_L be the largest eigenvalue for A, then the total number of infected (both reported and unreported) cases would grow as $\sim \mathbb{E}_{\alpha,1}(\lambda_L t^{\alpha})$. If $\mathcal{R}_0 \approx 1$, then we would expect λ_L to be close to zero and thus

$$\lambda_L \approx \max\left(\frac{\gamma_{_U}^{\alpha}\sigma^{\alpha}(\mathcal{R}_0 - 1)}{(\sigma^{\alpha} + \gamma_{_U}^{\alpha}) + \sigma^{\alpha}(\gamma_{_R}^{\alpha} + \varphi_{_R}^{\alpha})^{-1}(-\beta(t) + \gamma_{_U}^{\alpha})}, -(\gamma_{_H}^{\alpha} + \mu_{_H}^{\alpha})\right).$$

Considering that $\beta(t)$ is time dependent, we use its maximum value β_0 to estimate $\mathcal{R}_0$ and λ_L so that β_0 represents the worst case scenario for the fastest eradication of the virus.

5.3.3 Choice of Initial Conditions

Here, we discuss the choice of the initial conditions for the fractional-order system (5.51). At first, we note that the initial conditions $X_0 = (x_1(0), x_2(0), x_3(0), x_4(0), x_5(0))$ (with $S_0 \approx N$ which implies $x_1(0) \approx 0$) quickly moves along the dominant eigenvalue and should provide an indication of the correct choice of the initial conditions. Let $\mathbb{L}_L$ and $\mathbb{R}_L$ be the left and right eigenvectors corresponding to the largest eigenvalue λ_L, then the time evolution of X is given as

$$\begin{aligned} X(t) &= \sum_k (\mathbb{L}_k \cdot X_0)\, \mathbb{R}_k \mathbb{E}_{\alpha,1}(\lambda_k t^{\alpha}) \\ &\approx \sum_k (\mathbb{L}_k \cdot X_0)\, \mathbb{R}_L \mathbb{E}_{\alpha,1}(\lambda_L t^{\alpha}), \quad \text{for sufficiently large times,} \\ &\approx c\, \mathbb{R}_L \mathbb{E}_{\alpha,1}(\lambda_L t^{\alpha}), \end{aligned}$$

where $c = \sum_k (\mathbb{L}_k \cdot X_0)$, $\mathbb{L}_k = (L_k^{(1)}, L_k^{(2)}, L_k^{(3)}, L_k^{(4)}, L_k^{(5)})$ and $\mathbb{R}_k = (R_k^{(1)}, R_k^{(2)}, R_k^{(3)}, R_k^{(4)}, R_k^{(5)})$. The explicit form of the dominant eigenvalue gives the relation:

$$\frac{x_3(t)}{x_4(t)} = \frac{R_L^{(3)}}{R_L^{(4)}} = \frac{\eta(\lambda_L + \gamma_{_U}^{\alpha})}{(1-\eta)(\lambda_L + \gamma_{_R}^{\alpha} + \varphi_{_R}^{\alpha})}.$$

This shows that the direction of the solution vector X is determined by the dominant eigenvector and is independent of the initial conditions.

Now, let us consider the initial condition $X_0 = (\epsilon, 0, \epsilon, 0, 0, 0)$ and noting that $R_L^{(1)} = 0$, we obtain the solution

$$x_i(t) \approx \epsilon\, R_L^{(i)} L_L^{(3)} \mathbb{E}_{\alpha,1}(\lambda_L t^\alpha). \tag{5.52}$$

Let $C(t_l)$ be the number of infected (both reported and unreported) at a sufficiently large time t_l, then $x_3(t_l) + x_4(t_l) = C(t_l)$ which implies that

$$\epsilon\, \mathbb{E}_{\alpha,1}(\lambda_L t_l^\alpha) = \frac{C(t_l)}{R_L^{(3)} L_L^{(3)} + R_L^{(4)} L_L^{(3)}}$$

from which we obtain

$$x_i(0) = \frac{R_L^{(i)}}{R_L^{(3)} + R_L^{(4)}} C_0.$$

This shows that the direction of the solution vector for different initial conditions is a mere time translation of one another and does not have any effect on the trajectory of the growth of the vector. Thus, the leading eigenvector is responsible for these trajectories.

5.3.4 Peak Infections and Time of Peak

Of particular importance in the study of epidemic outbreaks is detecting the peak of infections and the time at which this peak occurs. The peak of the infected population is given by setting ${}_0\mathcal{D}_t^\alpha I_T = 0$ at the time $t = t^{(m)}$, where $I_T = I_R + I_U$ is the total number of infected population. However, before the onset of this peak point, there exists a point, see [4], where the incidence rate starts to decrease. This point is attained when ${}_0\mathcal{D}_t^\alpha E(t) = 0$ which implies that

$$S = \frac{\sigma^\alpha E}{\beta(t) I_T} N := \Phi(E, I_R, I_U). \tag{5.53}$$

We note that Φ is not defined at the equilibrium point $\mathbb{E}_0$ in the phase space and in particular is not defined at the point $(E_0, 0, 0)$. Equation (5.53) gives a description of the epidemic just before the equilirbium point $\mathbb{E}_0$ is reached. If $S > \Phi(E, I_R, I_U)$, then the epidemic is not close to reaching this point and naturally propagates over time. If on the other hand, $S < \Phi(E, I_R, I_U)$, sufficient susceptible population have been infected such that the epidemic cannot sustain itself anymore. As such, the point $\mathbb{E}_0$ is eventually reached. From data, only the terms I_R and I_U are observable quantities and as such it may be impossible to show that (5.53) holds in the phase field.

Due to the restriction on (5.53), we turn our focus to the observable quantities I_R

and I_U. The peak point is thus the point where I_T is maximum, that is, the point where ${}_0\mathcal{D}_t^\alpha(I_R + I_U) = 0$ which implies that

$$\sigma^\alpha E = (\gamma_{_R}^\alpha + \varphi_{_R}^\alpha)I_R + \gamma_{_U}^\alpha I_U. \tag{5.54}$$

The occurrence of the conditions necessary for the peak to occur can be inferred from data using (5.54) since $\sigma^\alpha E$ is the rate at which new infections occur, $(\gamma_{_R}^\alpha + \varphi_{_R}^\alpha)I_R$ and $\gamma_{_U}^\alpha I_U$ are the rates at which the reported and unreported infected are resolved. Based on the discussion in subsection 5.3.3, an estimate of the time to reach this peak value can be obtained using the linearized dynamics till the time $I_R(t)$ and $I_U(t)$ reaches their peak values $I_R^{(m)}$ and $I_U^{(m)}$, respectively. Hence, we write $I_R^{(m)} \sim I_R(0)\mathbb{E}(\lambda_L t^\alpha)$ and $I_U^{(m)} \sim I_U(0)\mathbb{E}(\lambda_L t^\alpha)$ so that

$$t^{(m)} \sim \left(\frac{\mathbb{E}_\alpha^{-1}\left[\left(I_R^{(m)} + I_U^{(m)}\right) / \left(I_R(0) + I_U(0)\right)\right]}{\lambda_L} \right)^{1/\alpha},$$

where $\mathbb{E}_\alpha^{-1}(x)$ is the inverse Mittag Leffler function.

5.3.5 Asymptotic Population in Each Compartment

Let $\tilde{S}, \tilde{E}, \tilde{I}_R, \tilde{I}_U, \tilde{H}, \tilde{R}$ and $\tilde{D}$ denote the asymptotic population (that is at very long times) in the different compartments. Given the initial conditions with $S(0)+E(0)+I_R(0)+I_U(0)+H(0)+R(0)+D(0) = N$, the variables converge to the equilibrium

$$\mathbb{E}_0 = \left(\tilde{S} > 0, \tilde{E} = 0, \tilde{I}_R = 0, \tilde{I}_U = 0, \tilde{H} = 0, \tilde{R} > 0, \tilde{D} > 0\right).$$

This implies that the epidemic is over and only the susceptible, recovered and dead population are eventually present. To understand the asymptotic behavior of the variables, we consider, following Giordano *et al.* [62], the EI_RI_UH subsystem

$${}_0\mathcal{D}_t^\alpha Y(t) = FY(t) + bU(t), \tag{5.55}$$

where

$$F = \begin{bmatrix} -\sigma^\alpha & 0 & 0 & 0 \\ \eta\sigma^\alpha & -(\gamma_{_R}^\alpha + \varphi_{_R}^\alpha) & 0 & 0 \\ (1-\eta)\sigma^\alpha & 0 & -\gamma_{_U}^\alpha & 0 \\ 0 & -\varphi_{_R}^\alpha & 0 & -(\gamma_{_H}^\alpha + \mu_{_H}^\alpha) \end{bmatrix}, \qquad b = \begin{bmatrix} 1 \\ 0 \\ 0 \\ 0 \end{bmatrix},$$

$$
\begin{aligned}
Y(t) &= [E \;\; I_R \;\; I_U \;\; H]^T, \\
X_S(t) &= c^T Y(t) = [0 \;\; \beta(t) \;\; \beta(t) \;\; 0]\, Y(t), \\
X_R(t) &= d^T Y(t) = [0 \;\; \gamma_R^\alpha \;\; \gamma_U^\alpha \;\; \gamma_H^\alpha]\, Y(t), \\
X_D(t) &= e^T Y(t) = [0 \;\; 0 \;\; 0 \;\; \mu_H^\alpha]\, Y(t), \\
U(t) &= \frac{S(t)}{N} X_S(t).
\end{aligned}
$$

The remaining variables satisfy the time-fractional differential equations

$$
\begin{aligned}
{}_0\mathcal{D}_t^\alpha S(t) &= -\frac{S(t)}{N} X_S(t), \\
{}_0\mathcal{D}_t^\alpha R(t) &= X_R(t), \\
{}_0\mathcal{D}_t^\alpha D(t) &= X_D(t).
\end{aligned}
\tag{5.56}
$$

Proposition 5.3.1. *The EI_RI_UH subsystem is asymptotically stable if and only if*

$$
\tilde{S} < \tilde{S}^* = \frac{N}{\mathcal{R}_0}.
$$

Proof. The Jacobian matrix of the dynamical system (5.50) around the equilibrium $(\tilde{S}, 0, 0, 0, 0, \tilde{R}, \tilde{D})$ is

$$
A = \begin{bmatrix}
0 & 0 & -\beta(t)\frac{\tilde{S}}{N} & -\beta(t)\frac{\tilde{S}}{N} & 0 & 0 & 0 \\
0 & -\sigma^\alpha & \beta(t)\frac{\tilde{S}}{N} & \beta(t)\frac{\tilde{S}}{N} & 0 & 0 & 0 \\
0 & \eta\sigma^\alpha & -(\gamma_R^\alpha + \varphi_R^\alpha) & 0 & 0 & 0 & \\
0 & (1-\eta)\sigma^\alpha & 0 & -\gamma_U^\alpha & 0 & 0 & 0 \\
0 & 0 & -\varphi_R^\alpha & 0 & -(\gamma_H^\alpha + \mu_H^\alpha) & 0 & 0 \\
0 & 0 & \gamma_R^\alpha & \gamma_U^\alpha & \gamma_H^\alpha & 0 & 0 \\
0 & 0 & 0 & 0 & \mu_H^\alpha & 0 & 0
\end{bmatrix}.
$$

The matrix has three zero eigenvalues and $-(\gamma_{_H}^{\alpha}+\mu_{_H}^{\alpha})$ as a negative eigenvalue. The other three eigenvalues are given as the roots of the equation $\lambda^3+a_2\lambda^2+a_1\lambda+a_0=0$, where

$$\begin{aligned}
a_2 &= N(\sigma^{\alpha}+\gamma_{_R}^{\alpha}+\gamma_{_U}^{\alpha}+\varphi_{_R}^{\alpha}),\\
a_1 &= N^2[\sigma^{\alpha}(-\beta(t)+\gamma_{_U}^{\alpha})+(\sigma^{\alpha}+\gamma_{_U}^{\alpha})(\varphi^{\alpha}+\gamma_{_R}^{\alpha})],\\
a_0 &= N^3\sigma^{\alpha}\gamma_{_U}^{\alpha}(\gamma_{_R}^{\alpha}+\varphi_{_R}^{\alpha})(1-\mathcal{R}_0).
\end{aligned}$$

The polynomial is Hurwitz if and only if $a_2>0,\ a_0>0$ and $a_2a_1>a_0$. Clearly, $a_2>0$ and $a_0>0\Rightarrow \tilde{S}<\dfrac{N}{\mathcal{R}_0}$. This concludes the proof. □

Corollary 5.3.1. *For positive initial conditions, the limiting value of S,*

$$\tilde{S}=\lim_{t\to\infty}S(t)<\tilde{S}^{*}.$$

Lemma 5.3.1. *Suppose $x(t)\in C^{\infty}(\mathbb{R}_0^{+})$ with $|x^{(r)}(t)|\le M|x^{(r-1)}(t)|,\ r\in\mathbb{N}$, where $x^{(r)}(t)$ is the r-th derivative of $x(t)$, then $\lim\limits_{t\to\infty}{}_0\mathfrak{I}_t^{\alpha}x(t)$ exists and is finite, where ${}_0\mathfrak{I}_t^{\alpha}\,y(t)=\dfrac{1}{\Gamma(\alpha)}\int_0^t(t-s)^{\alpha-1}y(s)\,ds$.*

Proof. We proceed with the proof as follows:

$$\begin{aligned}
{}_0\mathfrak{I}_t^{\alpha}x(t) &= \frac{1}{\Gamma(\alpha)}\int_0^t(t-s)^{\alpha-1}x(s)\,ds\\
&= \frac{1}{\Gamma(\alpha)}\int_0^t(t-s)^{\alpha-1}\left[x(t)+(s-t)x'(t)+\frac{(s-t)^2}{2!}x''(t)+\cdots\right]ds\\
&= \frac{1}{\Gamma(\alpha)}\int_0^t(t-s)^{\alpha-1}\sum_{r=0}^{\infty}\frac{(-1)^r(t-s)^r}{r!}x^{(r)}(t)\,ds\\
&= \frac{1}{\Gamma(\alpha)}\sum_{r=0}^{\infty}\frac{(-1)^r}{r!}x^{(r)}(t)\int_0^t(t-s)^{r+\alpha-1}\,ds\\
&= \frac{1}{\Gamma(\alpha)}\sum_{r=0}^{\infty}\frac{(-1)^r t^{r+\alpha}}{r!(r+\alpha)}x^{(r)}(t).
\end{aligned}$$

Next, we show that the series is convergent. Given $a_r=\dfrac{(-1)^r t^{r+\alpha}}{r!(r+\alpha)}x^{(r)}(t)$, then

$$\lim_{r\to\infty}\left|\frac{a_{r+1}}{a_r}\right|=\lim_{r\to\infty}\frac{t(r+\alpha)}{(r+1)(r+\alpha+1)}\left|\frac{x^{(r+1)}(t)}{x^{(r)}(t)}\right|=0.$$

The series converges and thus the integral ${}_0\mathfrak{I}_t^{\alpha}x(t)$ exists and is finite. □

Proposition 5.3.2. *For positive initial conditions, the limit values* $\tilde{S} = \lim_{t\to\infty} S(t)$, $\tilde{R} = \lim_{t\to\infty} R(t)$ *and* $\tilde{D} = \lim_{t\to\infty} D(t)$ *are given as*

$$\begin{aligned} f_S \ &+ \mathcal{R}_0(S_0 - \tilde{S}) = K, \\ \tilde{R} &= f_R + R_0 + R_R(S_0 - \tilde{S}), \\ \tilde{D} &= f_D + D_0 + R_D(S_0 - \tilde{S}), \end{aligned}$$

where $f_S = -c^T F^{-1} Y(0)$, $f_R = -d^T F^{-1} Y(0)$, $f_D = -e^T F^{-1} Y(0)$, $R_R = -d^T F^{-1} b$, $R_D = -e^T F^{-1} b$ *and* $K = \lim_{t\to\infty} {}_0\mathfrak{I}_t^\alpha \, X_S(t)$.

Proof. Taking the limits of the solution of the equations in (5.56), we have

$$\begin{aligned} \tilde{S} - S_0 &= -\lim_{t\to\infty} {}_0\mathfrak{I}_t^\alpha \left(\frac{S(t)}{N} X_S(t) \right), \\ \tilde{R} - R_0 &= \lim_{t\to\infty} {}_0\mathfrak{I}_t^\alpha \left(d^T Y(t) \right), \\ \tilde{D} - D_0 &= \lim_{t\to\infty} {}_0\mathfrak{I}_t^\alpha \left(e^T Y(t) \right). \end{aligned}$$

Now, consider taking the limits of the Riemann-Liouville integral of (5.55),we obtain

$$\begin{aligned} \lim_{t\to\infty} Y(t) - Y(0) &= \lim_{t\to\infty} {}_0\mathfrak{I}_t^\alpha \, [FY(t) + bU(t)] \\ -Y(0) &= \lim_{t\to\infty} [F \, {}_0\mathfrak{I}_t^\alpha Y(t) + b \, {}_0\mathfrak{I}_t^\alpha \, U(t)] \\ &= \lim_{t\to\infty} \left[F \, {}_0\mathfrak{I}_t^\alpha Y(t) + b \, {}_0\mathfrak{I}_t^\alpha \left(\frac{S(t)}{N} X_S(t) \right) \right], \end{aligned}$$

$$-Y(0) = -b(\tilde{S} - S_0) + \lim_{t\to\infty} [F \, {}_0\mathfrak{I}_t^\alpha Y(t)]. \tag{5.57}$$

Premultiplying (5.57) by $c^T F^{-1}$ and taking into account that $X_S(t) = c^T Y(t)$, we obtain

$$-c^T F^{-1} Y(0) = -c^T F^{-1} b[\tilde{S} - S_0] + \lim_{t\to\infty} {}_0\mathfrak{I}_t^\alpha X_S(t).$$

Noting that $-c^T F^{-1} b = \mathcal{R}_0$, we obtain the desired result. The equations for $\tilde{R}$ and $\tilde{D}$ can be easily obtained by premultiplying (5.57) by $d^T F^{-1}$ and $e^T F^{-1}$, respectively. □

Corollary 5.3.2. *The total population that would eventually be affected by the disease and either recovered or dead is given by*

$$T_I = \tilde{R} + \tilde{D} = f_R + f_D + R_0 + D_0 + (R_R + R_D)(S_0 - \tilde{S}). \tag{5.58}$$

5.4 Parameter Sensitivity and Identifiability Analysis

We shall discuss, in this section, the sensitivity and identifiability of the parameters with respect to the proposed model. This analyis informs us about the significance of the parameters of the model and their interactions with the other parameters.

5.4.1 Sensitivity analysis

The sensitivity analysis (SA) deals with the significance or importance of the parameters in the model. In particular, it finds the most influential parameters that drives the dynamics of the model. It also describes the extent to which parameter changes affects the result of the methods or models with the goal of identifying the best set of parameters that describes the process or phenomena in question. There are several SA methods which are broadly classified as local and global methods. In this dissertation, we shall focus on the Morris screening method (local method) and Sobol analysis method (global method).

5.4.1.1 Morris Screening Method

The Morris screening method is a local sensitivity measure that makes use of the first order derivative of an output function $y = f(\theta) = f(\theta_1, \cdots, \theta_p)$ with respect to the input parameter θ. It measures the effect of the output when the input variable is perturbed one at a time around a nominal value. It serves as a first check, in most analysis, in screening parameters for identifiability. The method evaluates elementary effects [145], [146], [179] with the ith parameter through the forward perturbation

$$g_i(\theta) = \frac{f(\theta_1, \theta_2, \cdots, \theta_i + \Delta\theta_i, \cdots, \theta_p) - f(\theta_i, \cdots, \theta_p)}{\Delta\theta_i}, \quad i = 1(1)p.$$

Morris [122] proposed two sensitivity measures, the mean (μ) and the standard deviation ($\tilde{\sigma}$) of the elementary effects. For non-monotonic models, μ may lead to a very small value due to cancellation effects. For this reason, Campolongo *et al.* [25] proposed the use of absolute values for evaluating the mean. In order to obtain a dimension-free sensitivity, we prefer the use of the sensitivity measure δ given in Brun *et al.* [21] as

$$\delta_i = \sqrt{\frac{1}{N}\sum_{j=1}^{N} \tilde{g}_{ij}^2}, \qquad i = 1(1)p, \text{ and } j = 1(1)N,$$

where N is the number of sample points and

$$\tilde{g}_i(\theta) = \frac{f(\theta_1, \theta_2, \cdots, \theta_i + \Delta\theta_i, \cdots, \theta_p) - f(\theta_1, \cdots, \theta_p)}{\Delta\theta_i} \frac{\theta_i}{f(\theta_1, \cdots, \theta_p)}.$$

A common practice in the literature [134], [179], [180] is to plot the indices δ against $\tilde{\sigma}$, the standard deviation. We observe that the fractional order α has the highest

influence on the model output over time. Fig. 9(a) shows that the strength of the governmental action κ_1, transmission rate β_0, and the recovery rate γ_U are the next most influential parameters in the model. This is further corroborated by fig. 9(b). The parameter α was excluded from this figure because of its high δ and $\tilde{\sigma}$ index. The parameters ($\gamma_H, \varphi_R, \mu_H$ and κ_2) represented by the blue squares have the least influence on the model output and can be considered unimportant. The other parameters represented by the green squares have more influence than the parameters represented by the blue squares.

One major setback of the Morris screening test for sensitivity analysis is the consideration of each parameter individually and independently of the other parameters. In real applications, this is not true as parameters have collinearity and dependencies on one another.

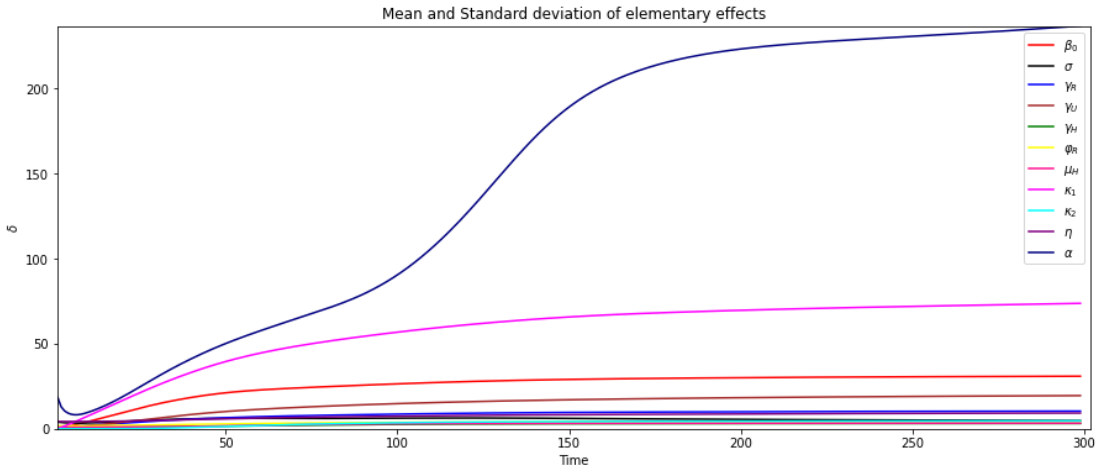

(a) Sensitivity of the parameters over time

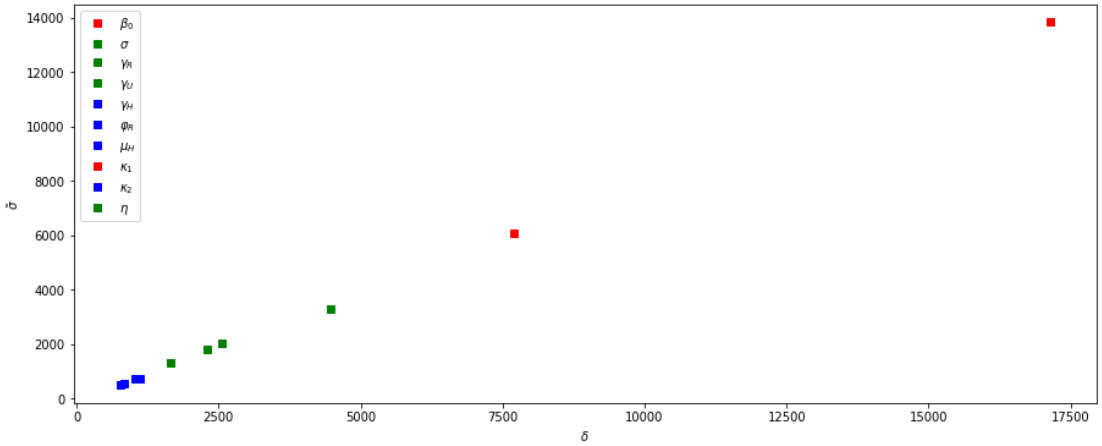

(b) Parameter Importance

Figure 9: Morris screening test

5.4.1.2 Sobol Analysis

The Sobol method is a variance-based sensitivity analysis method which unlike the Morris screening method takes into account the effect of the relationship between each parameters of the model. It uses the decomposition of variance to calculate Sobol's sensitivity indices: first and total order sensitivity measures. The basic idea of the Sobol's method is the decomposition of the model output function $y = f(\theta_1, \cdots, \theta_p)$ into summands of increasing dimensionality, that is

$$V(y) = V_{1,\cdots,p} + \sum_{i=1}^{p} V_i + \sum_{i=1}^{p} \sum_{j>1}^{p} V_{i,j} + \cdots,$$

where V_i is the partial variance of the contribution of the parameter θ_i and $V_{i,\cdots,s}$ is the partial variances caused by the interaction of the parameters $(\theta_1, \cdots, \theta_s)$ for $s \leq p$.
The first order sensitivity index measures the main effect of parameter θ_i on the model output; that is the partial contribution of θ_i to the variance $V(y)$.The index [154], [155] is defined as

$$S_i = \frac{V_i}{V(y)}.$$

The larger this index, the more sensitive the parameter is to the model output [154], [155]. Using the law of total variances [155], [179], the index can also be expressed as

$$V(y) = V_{\theta_i}(E_{\theta_{\sim i}}(y|\theta_i)) + E_{\theta_i}(V_{\theta_{\sim i}}(y|\theta_i))$$

and

$$S_i = \frac{V_{\theta_i}(E_{\theta_{\sim i}}(y|\theta_i))}{V(y)}$$

where $V_{\theta_i}(E_{\theta_{\sim i}}(y|\theta_i))$ is the partial variance caused by θ_i and $E_{\theta_{\sim i}}(y|\theta_i)$ is the mean of the model output calculated by using all the values of the other parameters $\theta_{\sim i}$ (except θ_i) and $V(y)$ is the total variance.
The total sensitivity indices [68] measures the effects of parameter θ_i and the interaction with the other parameters. It is defined as

$$S_{T_i} = \frac{V_i + V_{i,j} + \cdots + V_{i,j,\cdots,p}}{V(y)}.$$

The total variance, $V(y)$, for this index is given as

$$V(y) = V_{\theta_{\sim i}}(E_{\theta_i}(y|\theta_{\sim i})) + E_{\theta_{\sim i}}(V_{\theta_i}(y|\theta_{\sim i}))$$

and

$$\begin{aligned} S_{T_i} &= \frac{E_{\theta_{\sim i}}(V_{\theta_i}(y|\theta_{\sim i}))}{V(y)} \\ &= \frac{V(y) - V_{\theta_{\sim i}}(E_{\theta_i}(y|\theta_{\sim i}))}{V(y)}. \end{aligned}$$

The mean and the variance can be evaluated using quasirandom sampling method [144], [179] and are given as

$$V_{\theta_i}(E_{\theta_{\sim i}}(y|\theta_i)) = \frac{1}{N}\sum_{j=1}^{N} f(\mathbf{B}_j)\left(f(\mathbf{A}^i_{\mathbf{B},j}) - f(\mathbf{A}_j)\right),$$

and

$$E_{\theta_{\sim i}}(V_{\theta_i}(y|\theta_{\sim i})) = \frac{1}{2N}\sum_{j=1}^{N}\left(f(\mathbf{A}_j) - f(\mathbf{A}^i_{\mathbf{B},j})\right)^2,$$

where $\mathbf{A}$ and $\mathbf{B}$ are two independent parameter sample matrices of dimensions $N \times p$. We used the python SALib package [67] to compute the first and total order variance indices. Fig. 10 shows that the fractional order α, the governmental action strength κ_1, the transmission coefficient β_0 and the disease-induced death-rate $\mu_{_H}$ have the highest interaction with the other parameters. The parameters $(\kappa_2, \gamma_{_R}, \gamma_{_H})$ have the least interaction with the other parameters of the model. These results are consistent with the results in the Morris screening test as important parameters of the test show high interaction with the other parameters.

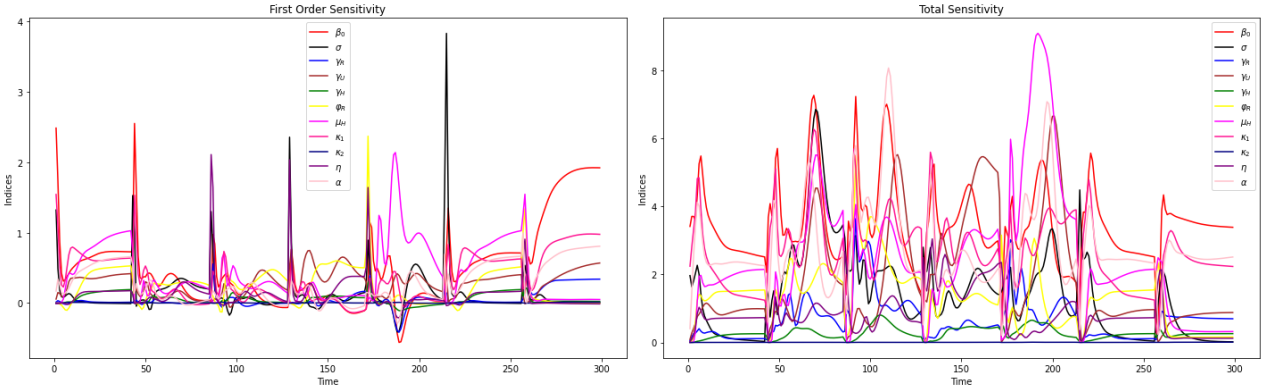

(a) First order sensitivity over time

(b) Total sensitivity over time

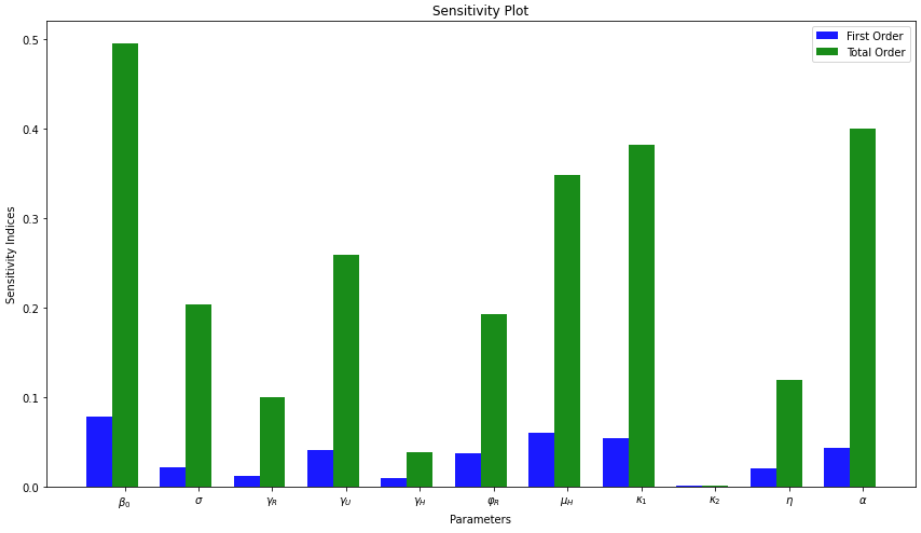

(c) Sobol Sensitivity Indices

Figure 10: Sobol Indices

5.4.2 Parameter Identifiability

The concept of identifiability is dependent on sensitivity. It entails the selection of the subset of parameters of a model having little or no collinearity and uncertainty, and which can be identified uniquely from a given set of observed data or measurements. In other words, it answers the question "Can the available data be described by the model and the selected subset of parameters?". There are several techniques or tests for parameter identifiability. Most of the tests are based on the Fisher information matrix (FIM) $F = \chi^T\chi$ where $\chi = \partial y/\partial\theta$ for a model output function y. Cobelli and Di Stefano [38] showed that a sufficient condition for identifiability is the non-singularity of FIM. Burth *et al.* [24] proposed an iterative estimation process which implements a reduced-order estimation by finding parameters whose axis lie closest to the direction of FIM. The associated parameter values are then fixed at prior estimates during the iterated process. Brun *et al.* [21] studied parameter identifiability using two indices; a parameter importance ranking index δ and a collinearity index $\gamma_{_K}$ which depends on the smallest eigenvalues of submatrices of $\chi^T\chi$ corresponding to the parameter subset K. Cintrón-Arias *et al.* [35] explained the need for a good parameter subset for identifiability to satisfy the full rank test. They further introduced two indices; the selection score and the condition number of $\chi^T\chi$. The smaller these indices the lesser the collinearity and uncertainty in the parameter values of the subset. Finally, they used the coefficient of variation index to examine the effect of parameters in the parameter subset. In this dissertation, we shall use the test proposed by Cintrón-Arias *et al.* [35] in identifying the parameters. The algorithm can be summarized in the following steps.

Algorithm 7 Algorithm for Parameter subset Selection [35]

1: Perform a combinatorial search for all possible parameter subsets. Let

$$S_p = \{\theta = (\lambda_1, \lambda_2, \cdots, \lambda_p) \in \mathbb{R}^p \big| \lambda_k \in \mathcal{I} \text{ and } \lambda_k \neq \lambda_m \ \forall\ k, m = 1, \cdots, p\},$$

where $\mathcal{I} = \{\beta_0, \sigma, \gamma_{_R}, \gamma_{_U}, \gamma_{_H}, \varphi_{_R}, \mu_{_H}, \eta, \alpha\}$.

2: Select parameter subsets that pass the full rank test; that is

$$\Theta_p = \{\theta \big| \theta \in S_p \subset \mathbb{R}^p,\ \text{Rank}(\chi(\theta)) = p\}.$$

3: For each $\theta \in \Theta_p$, calculate the parameter selection score $\zeta(\theta) = |\vartheta(\theta)|$ where

$$\vartheta = \frac{\sqrt{\Sigma(\theta)_{ii}}}{\theta_i}, \quad i = 1, \cdots, p,$$

and $\Sigma(\theta) = \sigma_0^2 \left[\chi^T(\theta)\chi(\theta)\right]^{-1} \in \mathbb{R}^p$.

4: Calculate the condition number $\kappa(\chi(\theta))$ for each parameter subset $\theta \in \Theta_p$. The smaller the values of $\kappa(\chi(\theta))$ and $\vartheta(\theta)$, the lower the uncertainty possibilities in the estimate.

To discuss the results in this section, we shall use the state of Tennessee as a case study to understand parameter identifiability. Furthermore, we used the following values as the nominal parameter set θ_0 for the model:

$$\beta_0 = 0.5000, \quad \sigma = 1/5.1, \quad \gamma_{_R} = \gamma_{_U} = 1/7, \quad \gamma_{_H} = 1/14, \quad \varphi_{_R} = 0.0500,$$

$$\mu_{_H} = 0.0010, \quad \kappa_1 = 0.6000, \quad \kappa_2 = 1117.3, \quad \eta = 0.3500, \quad \alpha = 0.9900$$

and the nominal error variance $\sigma_0 = 50$. We further divide the parameters into three groups according to their importance rankings discussed in the section 5.4.1.1:

$$S_1 = (\beta_0, \kappa_1, \alpha),$$

$$S_2 = (\sigma, \gamma_{_R}, \gamma_{_U}, \eta),$$

$$S_3 = (\gamma_{_H}, \varphi_{_R}, \mu_{_H}, \kappa_2),$$

where S_1 and S_3 are the most and least influential parameter sets, respectively, while S_2 contains more influential parameters than S_3. We display some selections of the

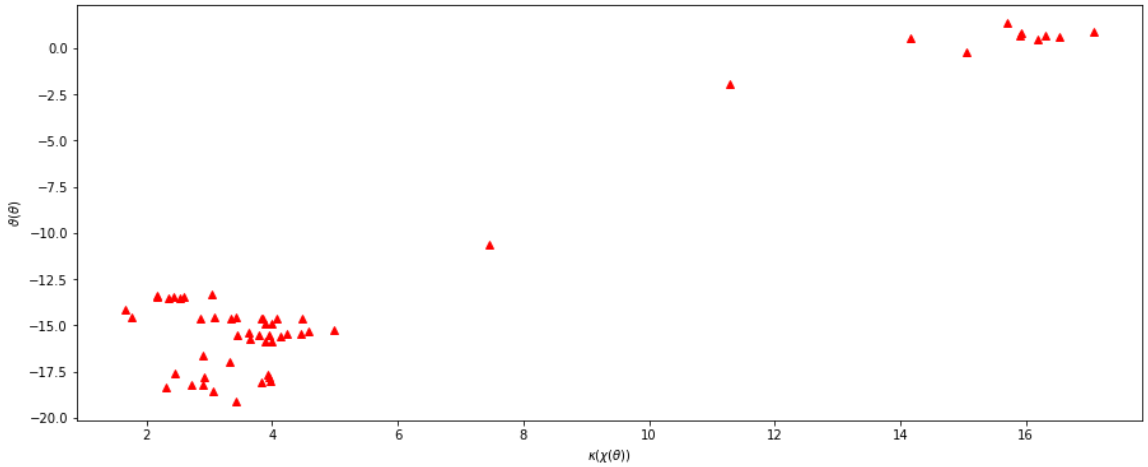

Figure 11: The condition number $\kappa(\chi(\theta))$ against the parameter selection scores $\vartheta(\theta)$ of the $N \times p$ sensitivity matrices for all parameter subsets $\theta = \Theta_p$ with $p = 2$. Logarithmic scales are used on both axis.

parameter subsets of size p in Table 28 where we have chosen the subsets with the smallest score values. The entries in Table 28 are ordered with respect to the selection score $\vartheta(\theta)$ for each subset of same cardinality. A high selection score and condition number for a parameter subset indicates substantial collinearity and linear dependence, and thus is poorly identifiable even if the parameter subsets contains S_1, that is contains the set of most influential parameters. We observe that most of the selections in Table 28 contains at least one element in each of the groups listed above. This shows that while parameter importance ranking is crucial in recognizing parameters that drives the dynamics of a model, it does not have substantial effect in identifiability. Identifiability depends on proper selection of subsets including parameters in each of the three groups above that describes the measurement or data. To have an idea of the variations of the condition number and the selection score, we give a plot of these values for $p = 2$ in fig. 11 (with logarithmic scales). Good parameter combination in fig. 11 corresponds to values in the lower left corner of the figure where the values, $\vartheta(\theta)$ and $\kappa(\chi(\theta))$, are relatively small. To further analyze

p	Parameter Subsets	$\kappa(\chi(\theta))$	$\vartheta(\theta)$
11	$(\beta_0, \sigma, \gamma_R, \gamma_U, \gamma_H, \varphi_R, \mu_H, \kappa_1, \kappa_2, \eta, \alpha)$	5.394e+08	4.616e+02
10	$(\beta_0, \sigma, \gamma_R, \gamma_U, \gamma_H, \varphi_R, \mu_H, \kappa_1, \eta, \alpha)$	1.383e+04	4.709e-04
9	$(\beta_0, \sigma, \gamma_R, \gamma_U, \gamma_H, \varphi_R, \mu_H, \eta, \alpha)$	2.779e+03	1.387e-04
	$(\sigma, \gamma_R, \gamma_U, \gamma_H, \varphi_R, \mu_H, \kappa_1, \eta, \alpha)$	3.001e+03	1.396-04
7	$(\beta_0, \sigma, \gamma_R, \varphi_R, \mu_H, \eta, \alpha)$	2.669e+02	2.483e-06
	$(\beta_0, \sigma, \gamma_R, \gamma_U, \varphi_R, \mu_H, \alpha)$	2.946e+02	2.514e-06
	$(\sigma, \gamma_R, \gamma_U, \varphi_R, \mu_H, \kappa_1, \alpha)$	2.661e+02	2.559e-06
5	$(\sigma, \gamma_U, \kappa_1, \eta, \alpha)$	2.306e+02	3.209e-07
	$(\sigma, \gamma_R, \gamma_U, \kappa_1, \alpha)$	2.260e+02	3.384e-07
	$(\beta_0, \sigma, \gamma_U, \eta, \alpha)$	2.422e+02	3.556e-07
4	$(\sigma, \gamma_U, \kappa_1, \alpha)$	1.927e+02	1.044e-07
	$(\beta_0, \sigma, \gamma_U, \alpha)$	2.151e+02	1.698e-07
	$(\sigma, \gamma_R, \eta, \alpha)$	8.341e+01	2.067e-07
3	$(\sigma, \gamma_U, \kappa_1)$	8.597e+01	4.311e-08
	$(\sigma, \gamma_U, \alpha)$	8.292e+01	4.703e-08
	$(\beta_0, \sigma, \gamma_U)$	9.536e+01	5.565e-08
	$(\sigma, \kappa_1, \alpha)$	1.037e+02	6.312e-08

Table 28: Selection scores and condition numbers for some selected parameter subsets

the parameter identifiability of the model, we consider the parameter subsets:

$$\theta_1 = (\beta_0, \sigma, \gamma_R, \gamma_U, \gamma_H, \varphi_R, \mu_H, \kappa_1, \kappa_2, \eta, \alpha),$$

$$\theta_2 = (\sigma, \gamma_R, \gamma_U, \gamma_H, \varphi_R, \mu_H, \kappa_1, \eta, \alpha),$$

$$\theta_3 = (\sigma, \gamma_R, \gamma_U, \varphi_R, \mu_H, \kappa_1, \alpha),$$

$$\theta_4 = (\sigma, \gamma_R, \gamma_U, \kappa_1, \alpha),$$

$$\theta_5 = (\sigma, \gamma_U, \alpha),$$

such that $\theta_{i+1} \subset \theta_i,\ i = 1, \cdots, 4$. The choice of these parameter subsets are due to their relative small condition numbers and selection scores. In other to create synthetic data, we assume the nominal parameter subsets and error variance (given at the beginning of this section) to be the true parameter vectors and true variance. Furthermore, we add random noise to the model output as follows:

$$Y_j = z(t_j, \theta_0) + \sigma_0 \mathcal{N}(0, 1), \quad j = 1, \cdots, N.$$

We solve five inverse problems for each of the parameter subsets $\theta_i,\ i = 1, \cdots, 5$. We

$\tilde{\theta}$	AIC	BIC
θ_1	414.79	443.45
θ_2	408.59	432.04
θ_3	403.52	421.76
θ_4	400.34	413.36
θ_5	394.69	402.50

Table 29: AIC and BIC metrics to estimate the quality of the model with different parameter sets.

analyze the result using the coefficient of variation and standard error [35] given as

$$SE_j(\tilde{\theta}) = \sqrt{\tilde{\Sigma}_{j,j}}, \quad j = 1. \cdots, p$$

and

$$v_j(\tilde{\theta}) = \frac{SE_j(\tilde{\theta})}{\theta_j}, \quad j = 1. \cdots, p,$$

where $\tilde{\Sigma}_{j,j} = \tilde{\sigma_0}^2 \left[\chi(\tilde{\theta})^T \chi(\tilde{\theta})\right]^{-1}$ and $\tilde{\sigma_0}^2 = \frac{1}{n-p}|Y - z(\tilde{\theta})|$.

It is seen from table A.1 that the standard errors of $\beta_0, \kappa_1, \gamma_U, \eta, \alpha$ in θ_2 show improvements and implies lower linear dependence and collinearity than in θ_1. Thus, a substantial improvement in uncertainty quantification is seen from θ_1 to θ_2. Further improvements are observed for each of the other parameter subsets as more parameters are removed. For instance, with the removal of γ_H and η in θ_2, it seen that the standard error for γ_U dropped from 4.76% to approximately 0.56% of their estimates. Other improvements in θ_3 include σ and φ_R. We note that there is no substantial gain in the removal of φ_R and μ_H from θ_3 as seen in Table A.1.

Parameter identifiability might be misleading without the investigation of the residual of the model [35]. The Akaike Information Criterion (AIC) and Bayesian Information Criterion (BIC) indices make use of residuals to determine the quality of models in the presence of a given set of data. Table 29 shows the AIC and BIC estimates for each parameter set $\theta_i,\ i = 1, \cdots, 5$. It is seen that the best improvements occur from θ_i to θ_{i+1} for $i = 1, 2$. Thus, the best case scenario of uncertainty quantification obtained, for the analysis discussed in this section, is that of θ_3.

5.4.3 Epidemiological parameters of the model

For simplicity, we shall use prior studies to fix several parameters and fit the other parameters of the model. In particular, we shall fit some parameters based on the discussions in section 5.4.2 and the default values in table 30 using the COVID-19 data obtained from John Hopkins University [50]. Prior modeling studies suggest that the effective transmission rate β_0 ranges between 0.5-1.5 day^{-1} [52], [97], [138],

[150] and the incubation period lies in the range between 2–9 days [19], [57], [100], [171]. The average of 5.1 days was estimated by Lauer *et al.* [93]. The infectious duration seems to have agreeing values of around 7 days for several modeling studies [52], [54], [97], [105], [127], [162]. The fraction of cases that are symptomatic varies with Fergusson *et al.* [54] using the value $\eta = 2/3$ in their work. Lachmann *et al.* [92] and Li *et al.* [143] estimated that around 88% and 86%, respectively, of all infections are undocumented with a 95% credible interval. Maugeri *et al.* [115] estimated that the proportion of unreported new infections by day ranged from 52.1% to 100% with a total of 91.8% of infections going unreported. Table 30 gives a summary of these values and the default values used in our model simulation. The other parameters of the model are fixed using the values in table 30.

Parameters	Not.	Ranges	References	Default
Effective transmission rate	β_0	0.2–1.5 day^{-1}	[52], [54], [97], [150]	Fitted
Governmental action strength	κ_1	0.4239–0.8478	[66]	Fitted
Intensity of responds	κ_2	1117.3	[66]	1117.3
Incubation Period	σ^{-1}	2–14 days	[52], [93], [100], [143]	5.1
Proportion of reported new infections	η	0.10–0.48	[92], [115], [143]	0.35
Recovery rate (Reported)	$\gamma_{_R}$	1/14–1/3 day^{-1}	[54], [97], [171]	1/7
Recovery rate (Unreported)	$\gamma_{_U}$	1/14–1/3 day^{-1}	[54], [97], [171]	1/7
Recovery rate (Hospitalized)	$\gamma_{_H}$	1/30–1/3 day^{-1}	[162], [191]	1/14
Hospitalization rate	$\varphi_{_R}$	0.002–0.1 day^{-1}	[54], [191]	0.05
Disease-induced death rate	$\mu_{_H}$	0.0001–0.1 day^{-1}	[54]	Fitted
Time-fractional order	α	0.5–1.0	[19]	Fitted

Table 30: Summary of parameter ranges and default values used in our simulation. "Not" denotes Notations.

5.5 Methods and Model Fitting

We use the infected and cumulative mortality data compiled by the Center for Systems and Science Engineering at John Hopkins University (2020) [50] starting from the day of the first record of infection with two intermediate days for the first 200 days (the parameters are adjusted accordingly) in a given state to calibrate the parameter set $(\beta_0, \kappa_1, \mu, \alpha)$ and the initial condition E_0. The other initial conditions are fixed, for example, I_{R0} is matched with the first recorded case, $I_{U0} = (0.65/0.35)I_{R0}$ since 65% of the cases are taken to be unreported and the rest are set to zero. The remaining parameters in the model are fixed at default values given in Table 30. Parameter fittings were performed using a nonlinear least squares algorithm in python with the limited memory Broyden-Fletcher-Goldfarb-Shannon (L-BFGS) method. One main benefit of the routine is the use of bounds for fit parameters. This allows faster convergence of the algorithm and ensures obtaining meaningful fit parameters. The

fitted parameters and their standard errors are given in Table 31. A comparison of the fractional-order model with its corresponding integer-order model is given in table 32 for California and Washington. We have excluded the states of Tennessee and Texas because their models are simply integer-order models as shown in table 31 where $\alpha \approx 1$. All numerical simulations were done with our numerical scheme [18] from which we obtain the solution of the proposed model at each time step as

1. Predictor:

$$S_p = S_j + \frac{\tau^\alpha}{\Gamma(1+\alpha)} F_1(t_j, S_j, E_j, I_{R,j}, I_{U,j}, H_j, R_j, D_j) + \tilde{H}_{1,j}$$

$$E_p = E_j + \frac{\tau^\alpha}{\Gamma(1+\alpha)} F_2(t_j, S_j, E_j, I_{R,j}, I_{U,j}, H_j, R_j, D_j) + \tilde{H}_{2,j}$$

$$I_{R,p} = I_{R,j} + \frac{\tau^\alpha}{\Gamma(1+\alpha)} F_3(t_j, S_j, E_j, I_{R,j}, I_{U,j}, H_j, R_j, D_j) + \tilde{H}_{3,j}$$

$$I_{U,p} = I_{U,j} + \frac{\tau^\alpha}{\Gamma(1+\alpha)} F_4(t_j, S_j, E_j, I_{R,j}, I_{U,j}, H_j, R_j, D_j) + \tilde{H}_{4,j}$$

$$H_p = H_j + \frac{\tau^\alpha}{\Gamma(1+\alpha)} F_5(t_j, S_j, E_j, I_{R,j}, I_{U,j}, H_j, R_j, D_j) + \tilde{H}_{5,j}$$

$$R_p = R_j + \frac{\tau^\alpha}{\Gamma(1+\alpha)} F_6(t_j, S_j, E_j, I_{R,j}, I_{R,j}, H_j, R_j, D_j) + \tilde{H}_{6,j}$$

$$D_p = D_j + \frac{\tau^\alpha}{\Gamma(1+\alpha)} F_7(t_j, S_j, E_j, I_{R,j}, I_{R,j}, H_j, R_j, D_j) + \tilde{H}_{7,j}$$

2. Corrector:

$$
\begin{aligned}
S_{j+1} &= S_j + \frac{\tau^\alpha}{\Gamma(2+\alpha)}\Big(\alpha\, F_1(t_j, S_j, E_j, I_{R,j}, I_{U,j}, H_j, R_j, D_j) \\
&\quad + \; F_1(t_{j+1}, S_p, E_p, I_{R,p}, I_{U,p}, H_p, R_p, D_p)\Big) + \tilde{H}_{1,j}, \\
E_{j+1} &= E_j + \frac{\tau^\alpha}{\Gamma(2+\alpha)}\Big(\alpha\, F_2(t_j, S_j, E_j, I_{R,j}, I_{U,j}, H_j, R_j, D_j) \\
&\quad + \; F_2(t_{j+1}, S_p, E_p, I_{R,p}, I_{U,p}, H_p, R_p, D_p)\Big) + \tilde{H}_{2,j}, \\
I_{R,j+1} &= I_{R,j} + \frac{\tau^\alpha}{\Gamma(2+\alpha)}\Big(\alpha\, F_3(t_j, S_j, E_j, I_{R,j}, I_{U,j}, H_j, R_j, D_j) \\
&\quad + \; F_3(t_{j+1}, S_p, E_p, I_{R,p}, I_{U,p}, H_p, R_p, D_p)\Big) + \tilde{H}_{3,j}, \\
I_{U,j+1} &= I_{U,j} + \frac{\tau^\alpha}{\Gamma(2+\alpha)}\Big(\alpha\, F_4(t_j, S_j, E_j, I_{R,j}, I_{U,j}, H_j, R_j, D_j) \\
&\quad + \; F_4(t_{j+1}, S_p, E_p, I_{R,p}, I_{U,p}, H_p, R_p, D_p)\Big) + \tilde{H}_{4,j}, \\
H_{j+1} &= H_j + \frac{\tau^\alpha}{\Gamma(2+\alpha)}\Big(\alpha\, F_5(t_j, S_j, E_j, I_{R,j}, I_{U,j}, H_j, R_j, D_j) \\
&\quad + \; F_5(t_{j+1}, S_p, E_p, I_{R,p}, I_{U,p}, H_p, R_p, D_p)\Big) + \tilde{H}_{5,j}, \\
R_{j+1} &= R_j + \frac{\tau^\alpha}{\Gamma(2+\alpha)}\Big(\alpha\, F_6(t_j, S_j, E_j, I_{R,j}, I_{U,j}, H_j, R_j, D_j) \\
&\quad + \; F_6(t_{j+1}, S_p, E_p, I_{R,p}, I_{U,p}, H_p, R_p, D_p)\Big) + \tilde{H}_{6,j}, \\
D_{j+1} &= D_j + \frac{\tau^\alpha}{\Gamma(2+\alpha)}\Big(\alpha\, F_7(t_j, S_j, E_j, I_{R,j}, I_{U,j}, H_j, R_j, D_j) \\
&\quad + \; F_7(t_{j+1}, S_p, E_p, I_{R,p}, I_{U,p}, H_p, R_p, D_p)\Big) + \tilde{H}_{7,j},
\end{aligned}
$$

where

$$F_1(t_j, S_j, E_j, I_{R,j}, I_{U,j}, H_j, R_j, D_j) = -\beta(t)\frac{S_j}{N}\left(I_{R,j} + I_{U,j}\right),$$

$$F_2(t_j, S_j, E_j, I_{R,j}, I_{U,j}, H_j, R_j, D_j) = \beta(t)\frac{S_j}{N}\left(I_{R,j} + I_{U,j}\right) - \sigma^\alpha E_j,$$

$$F_3(t_j, S_j, E_j, I_{R,j}, I_{U,j}, H_j, R_j, D_j) = \eta\sigma^\alpha E_j - (\gamma_R^\alpha + \varphi_R^\alpha) I_{R,j},$$

$$F_4(t_j, S_j, E_j, I_{R,j}, I_{U,j}, H_j, R_j, D_j) = (1-\eta)\sigma^\alpha E_j - \gamma_U^\alpha I_{U,j},$$

$$F_5(t_j, S_j, E_j, I_{R,j}, I_{U,j}, H_j, R_j, D_j) = \varphi_R^\alpha I_{R,j} - (\gamma_H^\alpha + \mu_H^\alpha) H_j,$$

$$F_6(t_j, S_j, E_j, I_{R,j}, I_{U,j}, H_j, R_j, D_j) = \gamma_R^\alpha I_{R,j} + \gamma_U^\alpha I_{U,j} + \gamma_H^\alpha H_j,$$

$$F_7(t_j, S_j, E_j, I_{R,j}, I_{U,j}, H_j, R_j, D_j) = \mu_H^\alpha H_j,$$

and

$$\tilde{H}_{1,j} = \frac{\tau^\alpha}{\Gamma(2+\alpha)} \sum_{l=0}^{j} a_{l,j}\, F_1(t_l, S_l, E_l, I_{R,l}, I_{U,l}, H_l, R_l, D_l),$$

$$\tilde{H}_{2,j} = \frac{\tau^\alpha}{\Gamma(2+\alpha)} \sum_{l=0}^{j} a_{l,j}\, F_2(t_l, S_l, E_l, I_{R,l}, I_{U,l}, H_l, R_l, D_l),$$

$$\tilde{H}_{3,j} = \frac{\tau^\alpha}{\Gamma(2+\alpha)} \sum_{l=0}^{j} a_{l,j}\, F_3(t_l, S_l, E_l, I_{R,l}, I_{U,l}, H_l, R_l, D_l),$$

$$\tilde{H}_{4,j} = \frac{\tau^\alpha}{\Gamma(2+\alpha)} \sum_{l=0}^{j} a_{l,j}\, F_4(t_l, S_l, E_l, I_{R,l}, I_{U,l}, H_l, R_l, D_l),$$

$$\tilde{H}_{5,j} = \frac{\tau^\alpha}{\Gamma(2+\alpha)} \sum_{l=0}^{j} a_{l,j}\, F_5(t_l, S_l, E_l, I_{R,l}, I_{U,l}, H_l, R_l, D_l),$$

$$\tilde{H}_{6,j} = \frac{\tau^\alpha}{\Gamma(2+\alpha)} \sum_{l=0}^{j} a_{l,j}\, F_6(t_l, S_l, E_l, I_{R,l}, I_{U,l}, H_l, R_l, D_l),$$

$$\tilde{H}_{7,j} = \frac{\tau^\alpha}{\Gamma(2+\alpha)} \sum_{l=0}^{j} a_{l,j}\, F_7(t_l, S_l, E_l, I_{R,l}, I_{U,l}, H_l, R_l, D_l)$$

are the memory terms of the respective population variables and

$$a_{l,j} = \frac{\tau^{\alpha}}{\Gamma(\alpha+2)} \begin{cases} -(j-\alpha)(j+1)^{\alpha} + j^{\alpha}(2j-\alpha-1) - (j-1)^{\alpha+1}, & l = 0, \\ (j-l+2)^{\alpha+1} - 3(j-l+1)^{\alpha+1} + 3(j-l)^{\alpha+1} & \\ -(j-l-1)^{\alpha+1}, & 1 \leq l \leq j-1, \\ 2^{\alpha+1} - \alpha - 3, & l = j. \end{cases}$$

States	E_0		κ_1		β_0		μ_H		α		$\mathcal{R}_0$
	Value	SE	Value	SE	Value	SE	Value	SE	Value	SE	
CA	2356	159	0.343	0.359	0.874	0.607	0.0002	1.1e-9	0.787	0.020	2.16
TN	1867	59	0.400	1.6e-6	0.799	2.0e-7	0.003	8.7e-5	0.999	1.8e-5	2.54
TX	1000	46	0.404	0.054	0.869	0.267	0.006	7.2e-5	0.999	1.7e-5	2.76
WA	4999	34	0.514	0.216	0.980	0.127	5.4e-5	2.8e-5	0.790	0.016	2.70

Table 31: Fitted Parameters to some selected States in the US, where SE denotes the standard error and CA, TN, TX and WA are acronyms for California, Tennessee, Texas and Washington, respectively.

States	Integer-order model			Fractional-order model		
	MSE	AIC	BIC	MSE	AIC	BIC
CA	1.112e+09	1573.08	1583.50	7.006e+08	1130.84	1143.86
WA	4.588e+10	1545.99	1556.42	3.203e+10	1513.11	1526.14

Table 32: Computational Comparison of the Fractional-order model with its corresponding integer-order model. MSE denotes mean squared error, AIC and BIC denotes Akaike and Bayesian Information criterion.

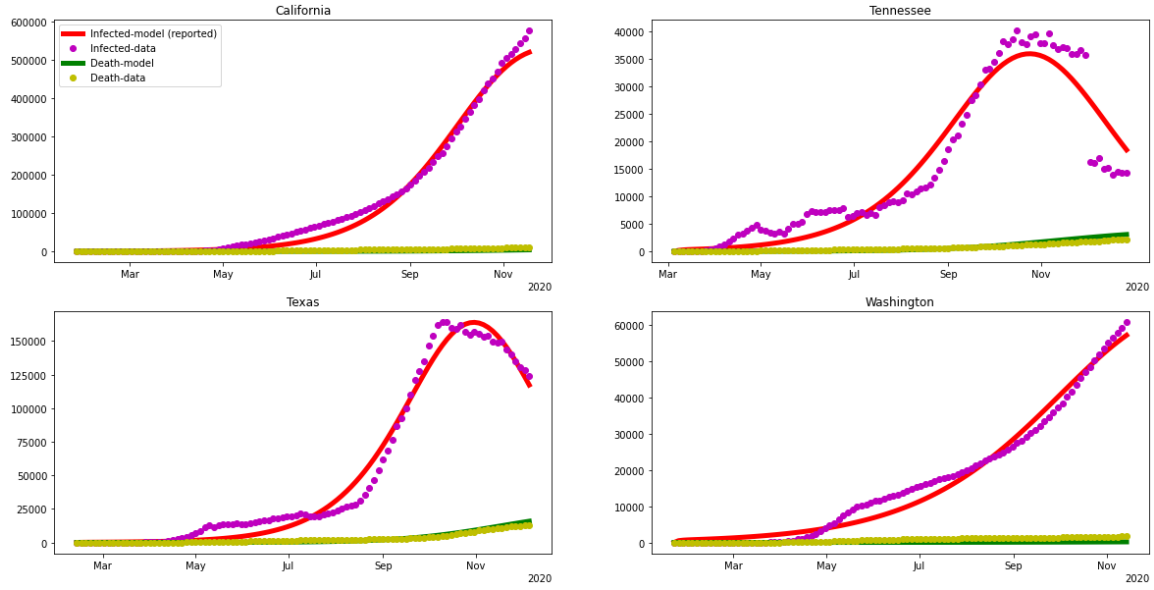

Figure 12: Data and model fits for some selected states in the US.

5.6 Conclusions

Four inverse problems for California, Tennessee, Texas and Washington were solved to estimate some parameters of the model. As seen in fig. 12, the fits are reasonably good even for a state like Tennessee and Texas whose current infected population begins to flatten. Tables 31 show the fit parameter sets for each of the states and table 32 shows the comparison between the fractional-order model and its corresponding integer-order model. We see that the transmission rate β_0^α for the infected population lies within 0.15–1.5 day^{-1}, a range suggested by Li *et al.* [97], Read *et al.* [138], Shen *et al.* [150], Eikenberry *et al.* [52]. The last column of table 31 shows the reproduction number computed for the model. The epidemic is expected to continue indefinitely if $\mathcal{R}_0 > 1$ as predicted for all states considered. This suggests that stricter measures such as the use of masks in public places, social distancing, contact tracing and vaccination need to be enforced in order to eradicate the epidemic.

CHAPTER 6

The Compartmental Model with Contact Tracing Observables

6.1 Introduction

Infectious diseases are often spread via direct and indirect contacts such as person-to-person contact, droplets spread, airborne transmissions, and so on. Several studies [6], [58], [78], [128], [136], [156], [159], [187] have shown that the novel coronavirus infection spread through these means. Some measures that include social distancing, lockdowns, self-isolation/quarantine, use of face-masks, contact tracing, amongst others, have been enforced by authorities to reduce the spread of the virus. Therefore, in any disease outbreak, contact tracing is an important tool for combating the outbreak's spread. Contact tracing (CT) is when persons who have come in contact with a reported/isolated infected case are traced, tracked, and monitored. If they become symptomatic, they are efficiently isolated to reduce transmissions. Previous outbreaks of infectious diseases have been rapidly controlled with CT and isolation, for example, the Ebola outbreak in West Africa in 2014, see [170]. Furthermore, it is important to evaluate the efficacy of intervention strategies such as CT in any disease control. Thus, the need to explicitly measure how CT can help mitigate the transmission of coronavirus cannot be over-emphasized. A lot of studies have been conducted on the efficacy of contact tracing in relation to some diseases in the past, see [20], [65], [70], [89], [91], [149], [166].

Several mathematical models have been proposed for the dynamics of the novel coronavirus, see for example [19], [52], [105], [127], [171], [188], [189], and several models have incorporated CT using stochastic modeling approach [90] and networks [82]. However, these studies did not include the CT's effect on the reproduction number of COVID-19 and the expression of this reproduction number in terms of observable quantities, a quick and efficient way of estimating the reproduction number. In 2015, Browne et al. [20] developed a deterministic CT model for Ebola epidemics which links tracing back to transmissions and incorporates disease traits and control together with monitoring protocols. Eikenberry *et al.* [52] examined the potential of face masks use by the general public to curtail the COVID-19 epidemic. Their findings suggest that face mask should be adopted nation-wide and be implemented without delay, even if most masks are homemade and of relatively low quality. Motivated essentially by the works of [20] and [52], we develop a deterministic model to measure CT's efficacy in mitigating the spread of COVID-19. As noted in [20], explicitly incorporating CT with disease dynamics presents challenges, and CT's population-level effects are difficult to determine. Here, we propose a compartmental model which incorporates the disease traits and monitoring protocols. We describe the impact on the reproduction number $\mathcal{R}_0$ of COVID-19 and discuss the importance and relevance of model's parameters. We use the model given in the previous chapter, where we

have divided the total infected population into reported and unreported infected. This logic is necessary as reporting of cases is crucial in determining the efficacy of CT.

6.2 Model Incorporating Contact Tracing

We incorporate CT into the model discussed in the previous chapter by linking the disease model's dynamics with actions of contact tracers such as monitoring and tracking. This general modeling framework is similar to a variety of CT models employed in [20], [65], [70]. At first, we describe CT's four step for COVID-19 as described by the Center for Disease Control (CDC) [31]. The Public health officer tries to identify contacts (contact investigation) by working with infected patients to help recall people they've been in contact with while being infectious. The second step (contact tracing) involves notifying and tracing of recorded contacts of the patient. Next (contact support), the officer informs and educates the contacts on the risk and dangers of being exposed. They also provide support on the next line of action for the contacts. If a contact is already showing symptoms, the tracers will call an ambulance to remove/isolate the contact. Lastly (contact self-quarantine), contacts are encouraged to quarantine for a minimum of 14 days in case they also become ill. To model the described process, we further make the following assumptions:

(a) Contact tracing can only be triggered by a reported or hospitalized case;

(b) If a traced contact is tracked being infectious, they are immediately isolated; otherwise they are monitored for symptoms and possible isolation if symptoms develop;

(c) We introduce parameters ρ_1 and ρ_2 that determine the probability or fraction of first or higher-order traced contacts who will be incubating and infectious, respectively, when tracked. We simplify the model by assuming that $\rho_1 = \rho_2 = \rho$.

Furthermore, we introduce a parameter β_M such that $0 \leq \beta_M \leq \beta_0$ to control the efficacy of the monitoring policy of contact tracers and health officers and ϵ to denote the fraction of reported cases that will be traced. With these new parameters and assumptions, we have the following system of differential equations and whose schema

is given in fig. 13:

$$
\begin{aligned}
{}_0\mathcal{D}_t^\alpha S(t) &= -\beta(t)\frac{S}{N}\left(I_R + I_U\right) - \beta(t)\frac{SI_T}{N} - \beta_M^\alpha \frac{SI_M}{N} \\
{}_0\mathcal{D}_t^\alpha E(t) &= \beta(t)\frac{S}{N}I_U + (1-\epsilon)\beta(t)\frac{S}{N}I_R + (1-\epsilon)\beta(t)\frac{SI_T}{N} \\
&\quad + (1-\epsilon)\beta_M^\alpha \frac{SI_M}{N} - \sigma^\alpha E \\
{}_0\mathcal{D}_t^\alpha E_{IC}(t) &= \rho\,\epsilon\left(\beta(t)\frac{S}{N}I_R + \beta(t)\frac{SI_T}{N} + \beta_M^\alpha \frac{SI_M}{N}\right) - \sigma^\alpha E_{IC} \\
{}_0\mathcal{D}_t^\alpha E_{IF}(t) &= (1-\rho)\epsilon\left(\beta(t)\frac{S}{N}I_R + \beta(t)\frac{SI_T}{N} + \beta_M^\alpha \frac{SI_M}{N}\right) - \sigma^\alpha E_{IF} \\
{}_0\mathcal{D}_t^\alpha I_R(t) &= \eta\sigma^\alpha E - (\gamma_R^\alpha + \varphi_R^\alpha) I_R \\
{}_0\mathcal{D}_t^\alpha I_U(t) &= (1-\eta)\sigma^\alpha E - \gamma_U^\alpha I_U \\
{}_0\mathcal{D}_t^\alpha I_M(t) &= \sigma^\alpha E_{IC} - \gamma_M^\alpha I_M \\
{}_0\mathcal{D}_t^\alpha I_T(t) &= \sigma^\alpha E_{IF} - (\gamma_T^\alpha + \varphi_T^\alpha) I_T \\
{}_0\mathcal{D}_t^\alpha H(t) &= \varphi_R^\alpha I_R + \varphi_T^\alpha I_T - (\gamma_H^\alpha + \mu_H^\alpha) H \\
{}_0\mathcal{D}_t^\alpha R(t) &= \gamma_R^\alpha I_R + \gamma_U^\alpha I_U + \gamma_M^\alpha I_M + \gamma_T^\alpha I_T + \gamma_H^\alpha H \\
{}_0\mathcal{D}_t^\alpha C_1(t) &= \sigma^\alpha E \\
{}_0\mathcal{D}_t^\alpha C_2(t) &= \sigma^\alpha E_{IC} \\
{}_0\mathcal{D}_t^\alpha C_3(t) &= \sigma^\alpha E_{IF} \\
{}_0\mathcal{D}_t^\alpha D(t) &= \mu_H^\alpha H,
\end{aligned}
\tag{6.59}
$$

where I_R and I_U are the number of reported and unreported individuals, respectively. E_{IC} and E_{IF} are exposed individuals who will be traced and tracked during the incubation and infectious stage, respectively. I_M are infectious individuals who have been tracked while incubating and are being monitored. I_T are infectious individuals who are symptomatic when tracked and will be removed or isolated. The last four

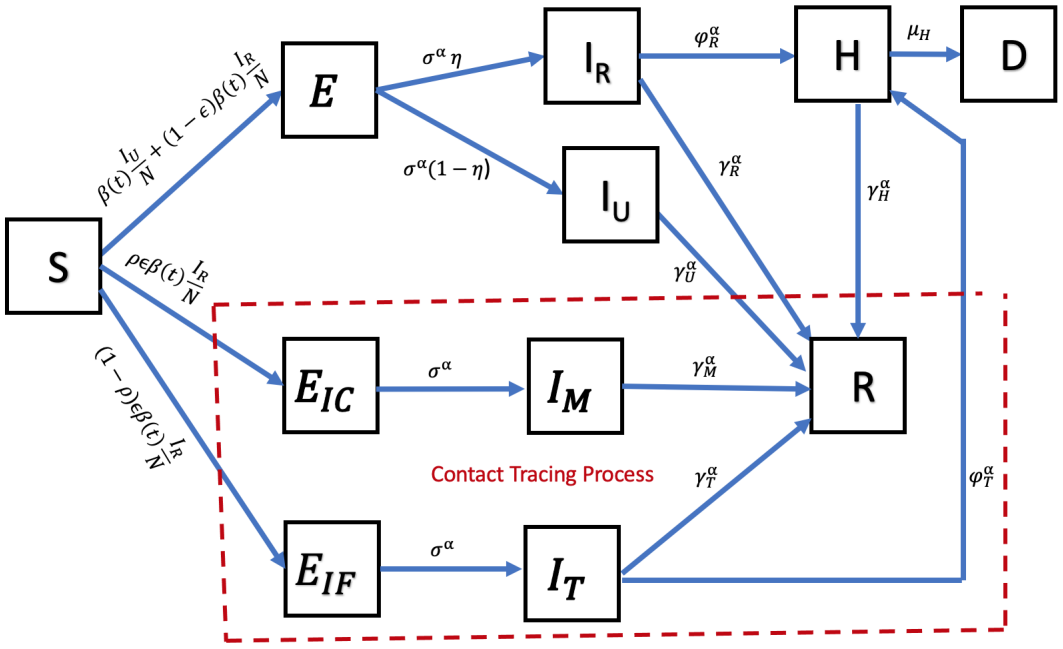

Figure 13: Mechanistic Model of Contact Tracing: Compartments dividing transmissions into untraced (who will either be reported or unreported) and traced who will either be incubating or infectious when tracked.

equations in (6.59) are used to estimate the cumulative total cases (both unreported and reported cases whose contacts are not being traced), cumulative cases of traced persons who will be tracked while incubating, cumulative cases of traced persons who are infectious when tracked and the resulting cumulative deaths from the impact of CT.

6.2.1 Effective Reproduction Number of Model with CT

In a similar manner to the discussions in Section 5.3.1, the matrix $\mathscr{F}$ of new infections and $\mathscr{V}$ of transfer terms are given by

$$\mathscr{F} = \begin{bmatrix} 0 & 0 & 0 & (1-\epsilon)\beta(t) & \beta(t) & (1-\epsilon)\beta_M^\alpha & \epsilon\,\beta(t) \\ 0 & 0 & 0 & \rho\,\epsilon\,\beta(t) & 0 & \rho\,\epsilon\,\beta_M^\alpha & \rho\,\epsilon\,\beta(t) \\ 0 & 0 & 0 & (1-\rho)\epsilon\,\beta(t) & 0 & (1-\rho)\epsilon\,\beta_M^\alpha & (1-\rho)\epsilon\,\beta(t) \\ 0 & 0 & 0 & 0 & 0 & 0 & 0 \\ 0 & 0 & 0 & 0 & 0 & 0 & 0 \\ 0 & 0 & 0 & 0 & 0 & 0 & 0 \\ 0 & 0 & 0 & 0 & 0 & 0 & 0 \end{bmatrix},$$

$$\mathscr{V} = \begin{bmatrix} \sigma^\alpha & 0 & 0 & 0 & 0 & 0 & 0 \\ 0 & \sigma^\alpha & 0 & 0 & 0 & 0 & 0 \\ 0 & 0 & \sigma^\alpha & 0 & 0 & 0 & 0 \\ -\eta\sigma^\alpha & 0 & 0 & \gamma_{_R}^\alpha + \varphi_{_R}^\alpha & 0 & 0 & 0 \\ -(1-\eta)\sigma^\alpha & 0 & 0 & 0 & \gamma_{_U}^\alpha & 0 & 0 \\ 0 & -\sigma^\alpha & 0 & 0 & 0 & \gamma_{_M}^\alpha & 0 \\ 0 & 0 & -\sigma^\alpha & 0 & 0 & 0 & (\gamma_{_T}^\alpha + \varphi_{_T}^\alpha) \end{bmatrix}.$$

The effective reproduction number cannot be written explicitly here. However, the given matrices are used to obtain the reproduction numbers for each of the special cases considered in the following sections.

6.2.2 Perfect Monitoring and Tracking (Imperfect Reporting)

In this case, we assume that the tracked and monitored contacts do not cause secondary infections, in which case $\beta_M = 0$ and that all traced contacts will be tracked while incubating, that is, $\rho = 1$. Thus, we obtain the system of time-fractional differential equations

$$\begin{aligned}
{}_0\mathcal{D}_t^\alpha S(t) &= -\beta(t)\frac{S}{N}\left(I_R + I_U\right) \\
{}_0\mathcal{D}_t^\alpha E(t) &= \beta(t)\frac{S}{N}I_U + (1-\epsilon)\beta(t)\frac{S}{N}I_R - \sigma^\alpha E \\
{}_0\mathcal{D}_t^\alpha E_{IC}(t) &= \epsilon\beta(t)\frac{S}{N}I_R - \sigma^\alpha E_{IC} \\
{}_0\mathcal{D}_t^\alpha I_R(t) &= \eta\sigma^\alpha E - (\gamma_{_R}^\alpha + \varphi_{_R}^\alpha)I_R \\
{}_0\mathcal{D}_t^\alpha I_U(t) &= (1-\eta)\sigma^\alpha E - \gamma_{_U}^\alpha I_U \\
{}_0\mathcal{D}_t^\alpha I_M(t) &= \sigma^\alpha E_{IC} - \gamma_{_M}^\alpha I_M \\
{}_0\mathcal{D}_t^\alpha H(t) &= \varphi_{_R}^\alpha I_R - (\gamma_{_H}^\alpha + \mu_{_H}^\alpha)H \\
{}_0\mathcal{D}_t^\alpha R(t) &= \gamma_{_R}^\alpha I_R + \gamma_{_U}^\alpha I_U + \gamma_{_M}^\alpha I_M + \gamma_{_H}^\alpha H \\
{}_0\mathcal{D}_t^\alpha D(t) &= \mu_{_H}^\alpha H.
\end{aligned} \tag{6.60}$$

The effective reproduction number (where we have used the maximum value for

$\beta(t))$ $\mathcal{R}_c$ is given as

$$\mathcal{R}_c = \tilde{\mathcal{R}}_0 \left[\eta \frac{\gamma_U^\alpha}{\gamma_R^\alpha + \varphi_R^\alpha}(1-\epsilon) + (1-\eta) \right],$$

where $\tilde{\mathcal{R}}_0 = \beta_0^\alpha / \gamma_U^\alpha$ is the basic reproduction number of the initial model (5.49) (no contact tracing or hospitalization of cases). Thus, the contact tracing effort required to ensure that the effective reproduction number is below one is:

$$\mathcal{R}_c < 1 \Leftrightarrow \eta \left[1 - \frac{\gamma_U^\alpha}{\gamma_R^\alpha + \varphi_R^\alpha}(1-\epsilon) \right] > 1 - \frac{1}{\tilde{\mathcal{R}}_0}.$$

In the special case where we have high hospitalization rate and low recovery rates (see Table 30) such that $\gamma_U^\alpha = \gamma_R^\alpha = \varphi_R^\alpha$, then

$$0.5\eta\,(1+\epsilon) > \left(1 - \frac{1}{\tilde{\mathcal{R}}_0} \right),$$

where $0.5\eta\,(1+\epsilon)$ is the critical proportion of the total cases which must be traced in order for $\mathcal{R}_c < 1$. Another special case is when we have low hospitalization rate and high recovery rates such that $\gamma_U^\alpha = \gamma_R^\alpha + \varphi_R^\alpha$, then

$$\eta\,\epsilon > \left(1 - \frac{1}{\tilde{\mathcal{R}}_0} \right).$$

This indicates that a larger proportion of reported cases will be traced in the former (special) case with high hospitalization and low recovery rates than the latter one with low hospitalization and high recovery rates. Now, let's rewrite ϵ as

$$\epsilon = \frac{\text{Number of traced contacts per reported cases}}{\text{Total number of contacts reported}} = \frac{\ell}{n},$$

and let $\beta(t) = p\,c(t)$, where p is the probability of transmission per contact and $c(t)$ is the contact rate. For an untraced reported case,

$$n = c(t) \left(\frac{1}{\gamma_R^\alpha} + \frac{1}{\varphi_R^\alpha} \right) = \beta(t) \frac{(\gamma_R^\alpha + \varphi_R^\alpha)}{p\,\gamma_R^\alpha\,\varphi_R^\alpha}.$$

Let κ be the average number of secondary infected traced contacts identified per untraced reported case, then

$$\kappa := p\ell = \epsilon\,\beta(t) \frac{\gamma_R^\alpha + \varphi_R^\alpha}{\gamma_R^\alpha\,\varphi_R^\alpha}. \tag{6.61}$$

Also, we define the parameter s as the fraction of reported cases which are traced, that is

$$\begin{aligned} s &= \frac{\epsilon\left(\frac{1}{\gamma_R^\alpha}+\frac{1}{\varphi_R^\alpha}\right)}{\epsilon\left(\frac{1}{\gamma_R^\alpha}+\frac{1}{\varphi_R^\alpha}\right)+\eta(1-\epsilon)\left(\frac{1}{\gamma_R^\alpha}+\frac{1}{\varphi_R^\alpha}\right)+(1-\eta)/\gamma_U^\alpha} \\ &= \frac{\epsilon}{\epsilon+\eta(1-\epsilon)+(1-\eta)\frac{\gamma_R^\alpha\varphi_R^\alpha}{\gamma_U^\alpha(\gamma_R^\alpha+\varphi_R^\alpha)}}. \end{aligned} \tag{6.62}$$

Noting the formulas (6.61) and (6.62) for κ and s, respectively, we have

$$\begin{aligned} \mathcal{R}_c &= \tilde{\mathcal{R}}_0\left[\eta\frac{\gamma_U^\alpha}{\gamma_R^\alpha+\varphi_R^\alpha}(1-\epsilon)+(1-\eta)\right] \\ &< \tilde{\mathcal{R}}_0\left[\eta(1-\epsilon)\gamma_U^\alpha\left(\frac{1}{\gamma_R^\alpha}+\frac{1}{\varphi_R^\alpha}\right)+(1-\eta)\right] \\ &= \tilde{\mathcal{R}}_0\frac{\gamma_U^\alpha\left(\gamma_R^\alpha+\varphi_R^\alpha\right)}{\gamma_R^\alpha\varphi_R^\alpha}\left[\eta(1-\epsilon)+(1-\eta)\frac{\gamma_R^\alpha\varphi_R^\alpha}{\gamma_U^\alpha\left(\gamma_R^\alpha+\varphi_R^\alpha\right)}\right]. \\ \mathcal{R}_c &< \kappa\left(\frac{1-s}{s}\right) = \mathcal{R}_c^*, \end{aligned}$$

where $\mathcal{R}_c^*$ is the product of the average number of secondary infected traced contacts per untraced reported case and the odds that a reported case is not a traced contact. For 100% reporting, $s = \kappa/(\kappa+m)$ which implies that a reported case causes $\kappa+m$ secondary infections where κ (or m) of these cases are traced (or untraced). Thus, $\mathcal{R}_c^* = m$ which is the fraction of secondary infected contacts to be traced that are not yet tracked.

6.2.3 Perfect Reporting and Tracking (Imperfect Monitoring)

Here, we consider the case where each traced contact is tracked during the incubation stage and all infected individuals are reported. This implies that $\eta = \rho = 1$. Thus,

we have the system of time-fractional differential equations

$$\begin{aligned}
{}_0\mathcal{D}_t^\alpha S(t) &= -\beta(t)\frac{SI_R}{N} - \beta_M^\alpha \frac{SI_M}{N} \\
{}_0\mathcal{D}_t^\alpha E(t) &= (1-\epsilon)\beta(t)\frac{SI_R}{N} + (1-\epsilon)\beta_M^\alpha \frac{SI_M}{N} - \sigma^\alpha E \\
{}_0\mathcal{D}_t^\alpha E_{IC}(t) &= \epsilon\left(\beta(t)\frac{SI_R}{N} + \beta_M^\alpha \frac{SI_M}{N}\right) - \sigma^\alpha E_{IC} \\
{}_0\mathcal{D}_t^\alpha I_R(t) &= \sigma^\alpha E - (\gamma_{_R}^\alpha + \varphi_{_R}^\alpha) I_R \\
{}_0\mathcal{D}_t^\alpha I_M(t) &= \sigma^\alpha E_{IC} - \gamma_{_M}^\alpha I_M \\
{}_0\mathcal{D}_t^\alpha H(t) &= \varphi_{_R}^\alpha I_R - (\gamma_{_H}^\alpha + \mu_{_H}^\alpha) H \\
{}_0\mathcal{D}_t^\alpha R(t) &= \gamma_{_R}^\alpha I_R + \gamma_{_M}^\alpha I_M + \gamma_{_H}^\alpha H \\
{}_0\mathcal{D}_t^\alpha D(t) &= \mu_{_H}^\alpha H.
\end{aligned} \tag{6.63}$$

The reproduction number in the absence of CT is given as $\tilde{\mathcal{R}}_0 = \beta_0^\alpha/(\gamma_{_R}^\alpha + \varphi_{_R}^\alpha)$. In a similar manner, the reproduction number of contact traced (monitored) person is $\mathcal{R}_M = \beta_{_M}^\alpha/\gamma_{_M}^\alpha$. Then $\theta_1 = \mathcal{R}_M/\tilde{\mathcal{R}}_0$ is the reduction in secondary cases of a traced (monitored) person compared to an untraced person. Thus $\mathcal{R}_c = (1-\epsilon)\tilde{\mathcal{R}}_0 + \epsilon\,\mathcal{R}_M$ and the proportion of cases to be traced so that $\mathcal{R}_c$ is below one is

$$\epsilon > (1-\theta_1)^{-1}\left(1 - \frac{1}{\tilde{\mathcal{R}}_0}\right).$$

Using CT observables, we describe $\mathcal{R}_c$ by defining $\kappa = \epsilon\,\tilde{\mathcal{R}}_0$ and $\kappa_{_M} = \epsilon\,\mathcal{R}_M$ as the average number of traced infected secondary cases per primary reported untraced and traced infected, respectively, with s given as $s = \epsilon$, then

$$\mathcal{R}_c = \kappa\left(\frac{1-s}{s}\right) + \kappa_{_M}.$$

6.2.4 Perfect Reporting and Monitoring (Imperfect Tracking)

Lastly, we consider perfect reporting and monitoring with secondary traced individual during the incubation stage (or infectious stage) with probability ρ (or $(1-\rho)$). This implies that $\beta_M = 0$ and $\eta = 1$. Thus, we obtain the system of time-fractional

differential equations

$$
\begin{aligned}
{}_0\mathcal{D}_t^\alpha S(t) &= -\beta(t)\frac{SI_R}{N} - \beta(t)\frac{SI_T}{N} \\
{}_0\mathcal{D}_t^\alpha E(t) &= (1-\epsilon)\beta(t)\frac{SI_R}{N} + (1-\epsilon)\beta(t)\frac{SI_T}{N} - \sigma^\alpha E \\
{}_0\mathcal{D}_t^\alpha E_{IC}(t) &= \rho\,\epsilon\left(\beta(t)\frac{S}{N}I_R + \beta(t)\frac{SI_T}{N}\right) - \sigma^\alpha E_{IC} \\
{}_0\mathcal{D}_t^\alpha E_{IF}(t) &= (1-\rho)\epsilon\left(\beta(t)\frac{S}{N}I_R + \beta(t)\frac{SI_T}{N}\right) - \sigma^\alpha E_{IF} \\
{}_0\mathcal{D}_t^\alpha I_R(t) &= \sigma^\alpha E - (\gamma_{_R}^\alpha + \varphi_{_R}^\alpha)I_R \\
{}_0\mathcal{D}_t^\alpha I_M(t) &= \sigma^\alpha E_{IC} - \gamma_{_M}^\alpha I_M \\
{}_0\mathcal{D}_t^\alpha I_T(t) &= \sigma^\alpha E_{IF} - (\gamma_{_T}^\alpha + \varphi_{_T}^\alpha)I_T \\
{}_0\mathcal{D}_t^\alpha H(t) &= \varphi_{_R}^\alpha I_R + \varphi_{_T}^\alpha I_T - (\gamma_{_H}^\alpha + \mu_{_H}^\alpha)H \\
{}_0\mathcal{D}_t^\alpha R(t) &= \gamma_{_R}^\alpha I_R + \gamma_{_M}^\alpha I_M + \gamma_{_T}^\alpha I_T + \gamma_{_H}^\alpha H \\
{}_0\mathcal{D}_t^\alpha D(t) &= \mu_{_H}^\alpha H.
\end{aligned}
\tag{6.64}
$$

The reproduction number in the absence of CT is $\tilde{\mathcal{R}}_0 = \beta(t)/(\gamma_{_R}^\alpha + \varphi_R^\alpha)$ and the reproduction number of contact traced individual who are incubating or infectious when tracked is $\mathcal{R}_T = \beta(t)(1-\rho)/(\gamma_{_T}^\alpha + \varphi_{_T}^\alpha)$. Thus, $\theta_2 = \mathcal{R}_T/\tilde{\mathcal{R}}_0$ is the reduction in secondary cases of a traced individual (who will be infectious or incubating when tracked) compared to an untraced reported case. Thus, the reproduction number $\mathcal{R}_c$ reduces to $\mathcal{R}_c = (1-\epsilon)\tilde{\mathcal{R}}_0 + \epsilon\,\mathcal{R}_T$. As in the previous cases, the critical proportion of total cases which is to be traced for $\mathcal{R}_c < 1$ is

$$\epsilon > (1-\theta_2)^{-1}\left(1 - \frac{1}{\tilde{\mathcal{R}}_0}\right).$$

To describe the reproduction number in terms of CT observables, we let $\kappa_{_T} = \epsilon\,\mathcal{R}_T$ be the average number of traced infected secondary cases per primary reported traced infected with $s = \epsilon$, then

$$\mathcal{R}_c = \kappa\left(\frac{1-s}{s}\right) + \kappa_{_T}.$$

6.3 Simulation Experiments and Results

Here, we perform some simulation experiments to show the efficacy of CT. In particular, we compare the effects of the different scenarios such as reporting, tracking and monitoring.

6.3.1 CT in Simulated Model with Perfect Tracking and Monitoring

We note that CT will have approximately same effect on the dynamics of the model for the different states. Thus, we consider results for Texas as a case study in the following sections.

6.3.1.1 Immediate CT Adoption with Perfect Tracking and Monitoring

We run the simulated model with $\beta_M = 0$ and $\rho = 1$ for around 20 months under stable conditions while studying the effect of the number of traced reported cases on the number of infected, hospitalized and dead. Fig. 14 shows that the total mortality (and infected and hospitalized) increases with no contact traced individual ($\epsilon = 0$) and decreases with increased number of traced reported cases. Furthermore, we simulate the model with several values in $\epsilon \times \eta,\ \eta, \epsilon \in [0, 1]$ to observe the effect of reporting and tracing on the model. The outcome of interest is total mortality, peak hospitalization and peak infected which are normalized against their respective maximum and the results are presented in Fig. 15. The results in this figure show that while high reporting rate is crucial for mitigating the spread of the epidemic, the percentage of traced reported cases have a more substantial effect on the spread. Using the formula given in eqn. 6.62, we estimate the number of reported cases which will be traced. The results are presented in fig. 16. A contour plot of the reproduction number $\mathcal{R}_c$ as a function of fraction of the infected population reported, and proportion of exposed individuals that is traced is shown in fig. 17. The figure shows that if at least 60% contacts of reported cases (with perfect reporting) are traced or at least 70% of total cases are reported where all their contacts are traced; then disease elimination is feasible.

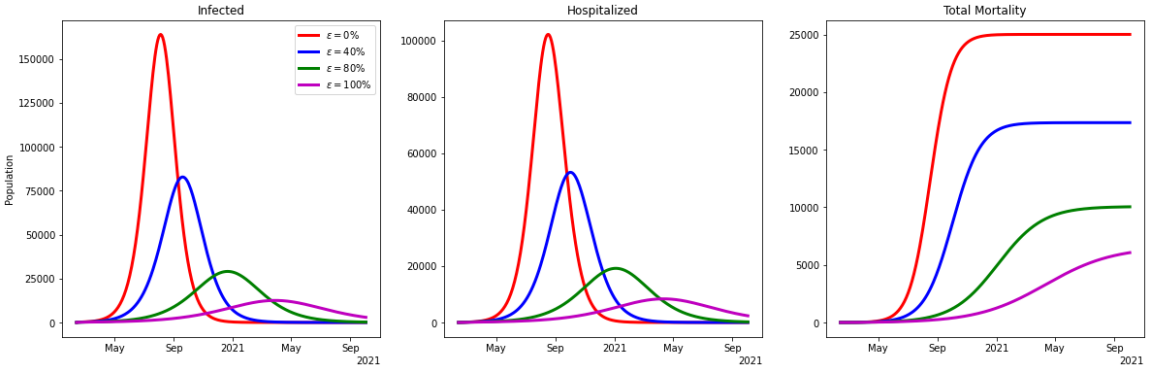

Figure 14: Current infected, hospitalized and total mortality with varying fraction of traced reported cases in a perfect tracking and monitoring case.

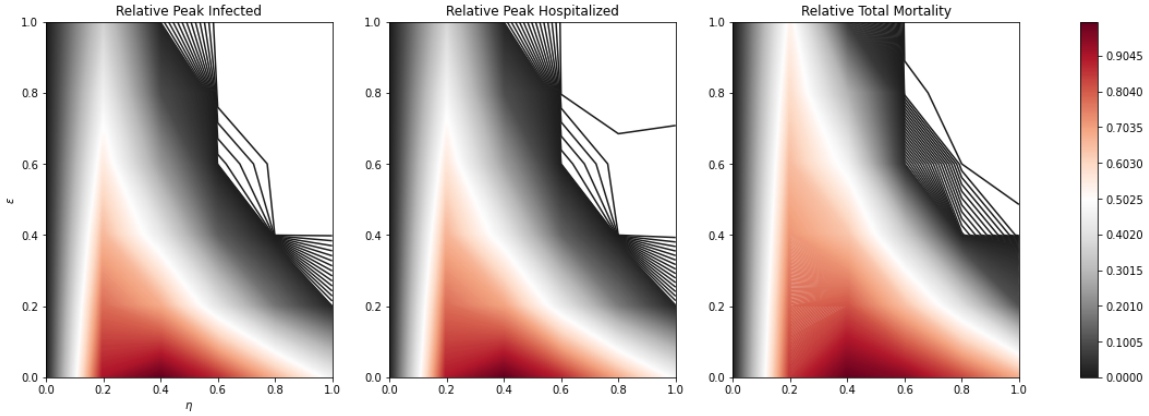

Figure 15: Relative peak infected, hospitalizations and total mortality simulated epidemics under different reporting and tracing levels.

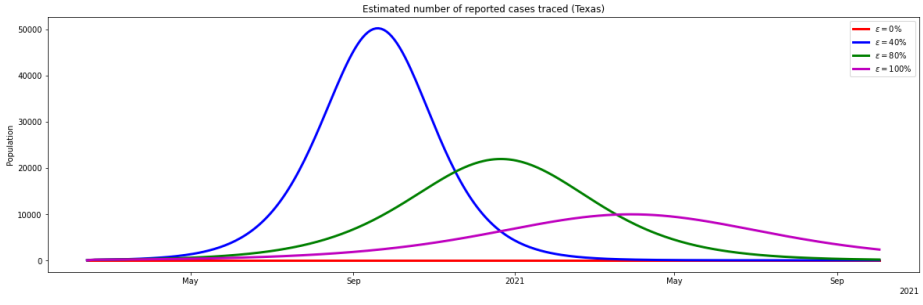

Figure 16: Estimated number of reported cases traced.

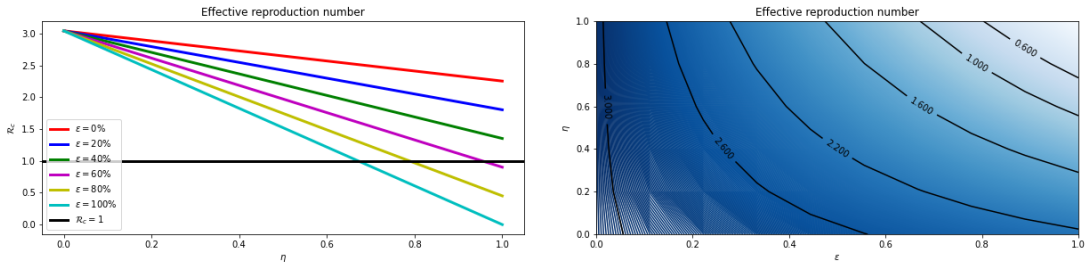

Figure 17: Effect of CT. The first column shows profiles of the control reproduction number as a function of proportion of reported cases (η). The second column shows contour plots of the control of reproduction number as a function of proportion of reported cases (η) and traced individuals (ϵ).

6.3.1.2 CT Intervention after delay We run the simulated CT epidemics by assuming that CT was only introduced after some discrete time delay (50, 100, 150 days). The fraction of reported cases traced was fixed at 50%. We observe, in fig. 18, that the intervention of CT reduces the number of infected, hospitalization and mortality even with a late intervention time (150 days).

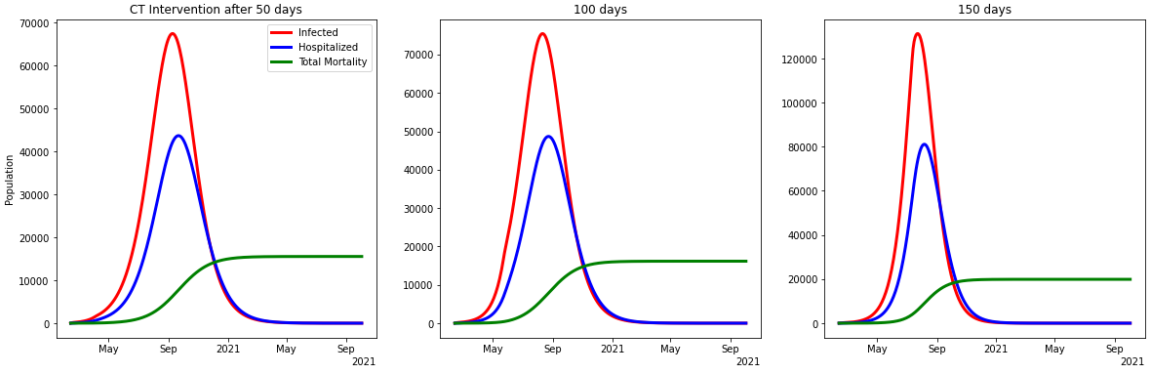

Figure 18: CT Intervention after some discrete time delay.

6.3.1.3 Perfect Reporting and Tracking We run the simulated CT model with $\rho = \eta = 1$ where CT was immediately introduced. The fraction of reported cases traced was fixed at 50%. We examine the effect of monitoring policy on the number of infected, hospitalizations, and mortality. Fig. 19 shows that a 50% effective monitoring policy reduces hospitalizations and total mortality to less than a quarter of its value. Furthermore, we run several simulations with values in $\epsilon \times \beta_M,\ \epsilon,\ \beta_M \in [0, 1]$, and the results are shown in fig. 20. Similar to previous contour plots, the outcome

of interests are relative peak hospitalization and total mortality. We observe that the results are quite surprising. The peak hospitalizations and cumulative mortality occur when $\beta_M \approx \beta_0$ and the fraction of traced reported cases is around 20-80%, where we would have expected this to be around 0-20%. This shows that the monitoring policy has a more significant effect in reducing the peak values than the fraction of traced reported cases. A contour plot of the reproduction number $\mathcal{R}_c$ as a function of the monitoring efficacy and proportion of exposed individuals that is traced is shown in fig. 21. The figure shows that the disease will die out if traced individuals are being monitored so that they are at least one-third as infectious as an unmonitored or untraced infected case with all contacts of reported cases being traced or with at least 60% of reported cases being traced with a perfect monitoring policy.

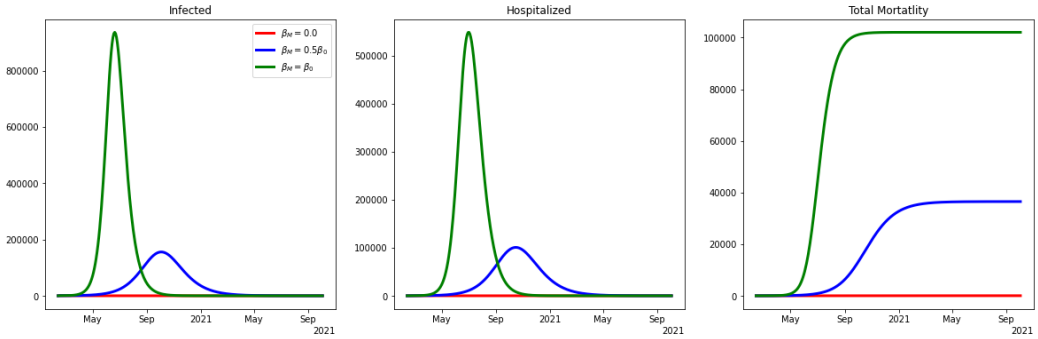

Figure 19: Efficiency of monitoring policy in CT. The β_M are selected to indicate 0%, 50% and 100% (corresponding to $\beta_M = \beta_0,\ \beta_0/2$ and 0, respectively) effective monitoring policy.

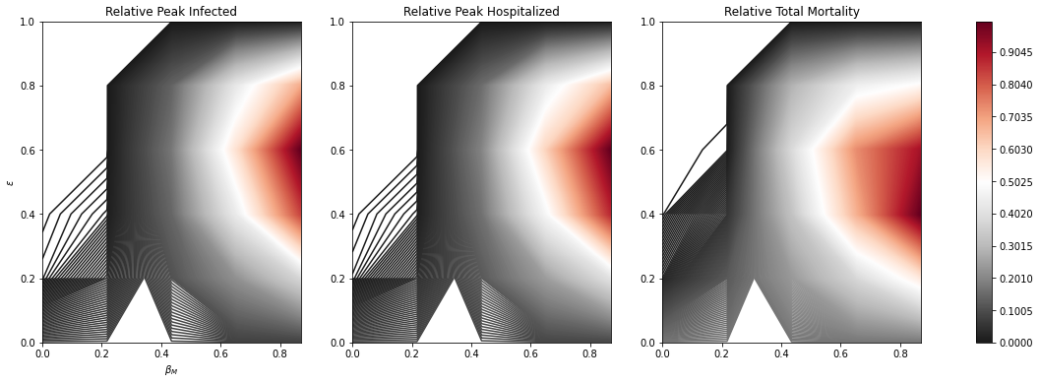

Figure 20: Relative peak infected, hospitalizations and total mortality of simulated epidemics under different monitoring conditions and fraction of traced reported cases.

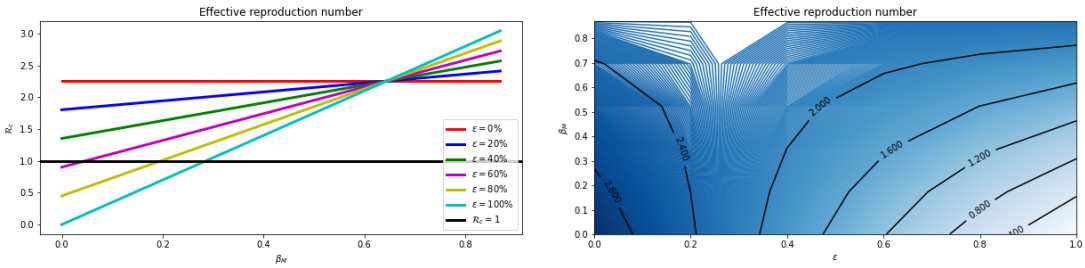

Figure 21: Effect of CT. The first column shows profiles of the reproduction number as a function of monitoring efficacy (β_M). The second column shows contour plots of reproduction number as a function of monitoring efficacy (β_M) and proportion of traced individuals (ϵ).

6.3.1.4 Perfect Reporting and Monitoring In this case, we consider the numerical experiment where we assume that every infected case is reported ($\eta = 1$) and tracked contacts of reported cases are effectively monitored ($\beta_M = 0$) so that they do not cause secondary infections. We run the simulated CT model under constant conditions to explore the effect of ρ (the fraction or probability that a traced reported case is incubating when tracked) on peak hospitalization and mortality. Unsurprisingly, we see that the higher the fraction of tracked contacts who are incubating the lower the number of hospitalizations and deaths. These results are evident in figures 22–24.

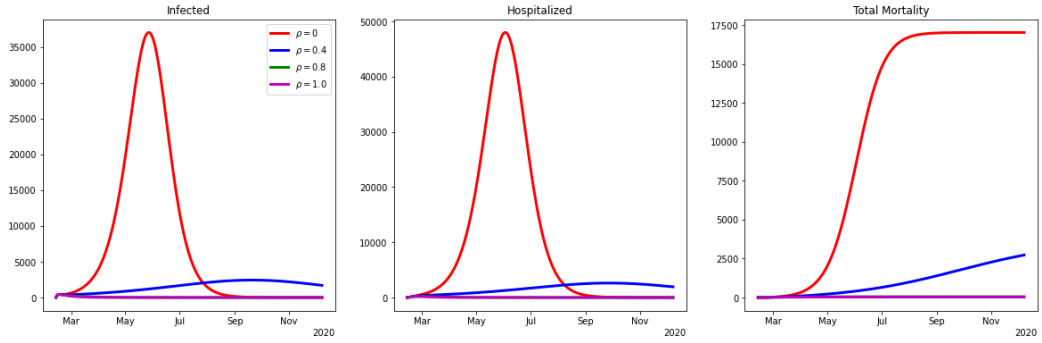

Figure 22: Effects of tracking contacts of reported cases when incubating or being infectious. The ρ values are selected to show 0%, 40%, 80% and 100% of traced reported cases are incubating when tracked. Perfect tracking implies $\rho = 1$.

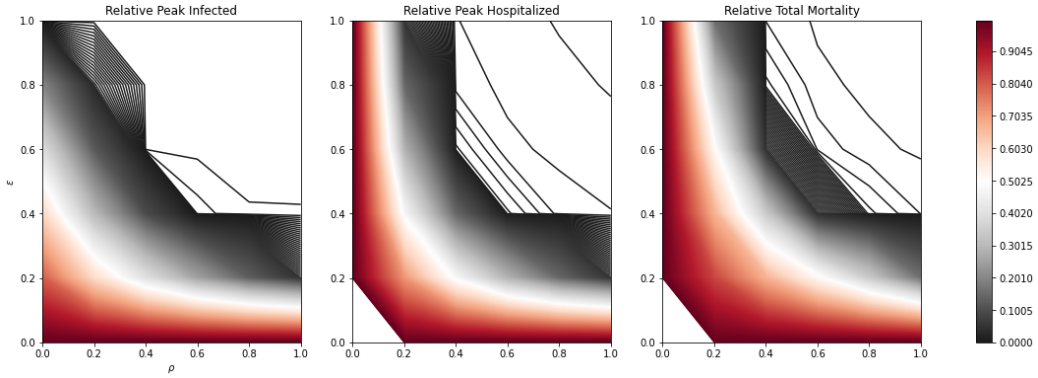

Figure 23: Relative peak infected, hospitalizations and total mortality of simulated epidemics under different monitoring conditions and fraction of traced reported cases.

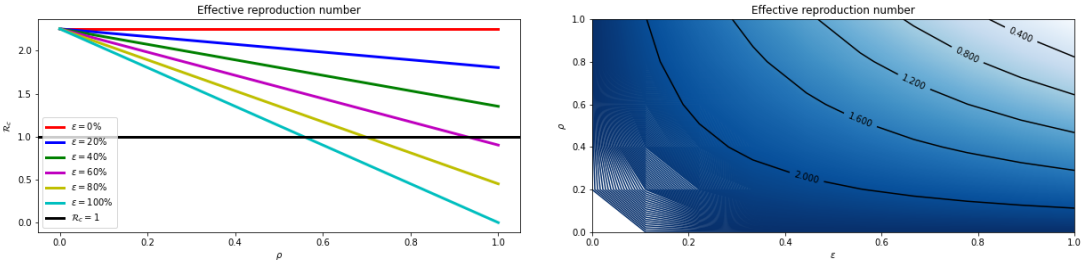

Figure 24: Effect of CT. The first column shows profiles of the control reproduction number as a function of tracking efficacy (ρ). The second column shows contour plots of the control of reproduction number as a function of tracking efficacy (ρ) and proportion of traced individuals (ϵ).

6.4 Discussions and Conclusions

We study the efficacy of contact tracing on the spread of COVID-19. We particularly consider exceptional cases where we have perfect tracking and monitoring, perfect reporting and tracking, and perfect reporting and monitoring. We developed a time-fractional order differential equation model of the contact tracing process in the COVID-19 outbreak. Our deterministic model links contact tracers' actions such as monitoring and tracking to the number of reported cases traced. Our framework separates the infected population into unreported and reported, and further splitting

the reported cases into fractions whose contacts will be traced. Additionally, we incorporate the effect of tracking by considering the probability that a traced contact will be incubating (or infectious) when tracked. This inherent structure in the model captures the dynamics of contact tracing and enables us to express the reproduction number in terms of observable quantities. In particular, under the assumption that there are perfect tracking and monitoring, we gave an upper bound for the effective reproduction number as $\mathcal{R}_c < \kappa(1-s)/s$. κ is the average number of secondary infected individuals traced per reported untraced case, and $(1-s)/s$ is the odds that a reported case is not a traced contact. In the case of perfect tracking with either perfect monitoring or perfect reporting, we obtain the result $\mathcal{R}_c = \kappa(1-s)/s + \kappa_{_M}$, where $\kappa_{_M}$ is the average number of secondary infected individuals per reported traced case. With these observable quantities, these formulas can provide a quick and straightforward estimate of the reproduction number in the population. Furthermore, we estimated the proportion of contacts that need be traced to ensure that the reproduction number is below one. We would have loved to provide daily or weekly estimates of $\mathcal{R}_c$ from the formulas (above) involving observable quantities, but we were unable to find CT data for the COVID-19 epidemic. However, we relied on model simulations to gain insights on CT's impact with different special cases during different stages of the epidemic. The decline of peak hospitalizations and total deaths in CT model simulations compared to the preliminary model shows its efficacy.

With the simulated CT model, the efficiency of CT in mitigating the spread of the virus and altering the epidemiological outcomes of peak hospitalizations and total deaths is a nonlinear function of η, $\beta_{_M}$, ρ and ϵ (see fig. 15, 20 and 23). In the first case ("perfect tracking and monitoring") and considering that 35% of infected cases are reported with 40%, 80%, and 100% of reported cases being traced, the peak hospitalizations are reduced by 47.9%, 81.2%, and 91.8%, respectively. The total mortality is also seen to decline by 30.6%, 59.8%, and 75.7%. Furthermore, we investigated the intervention of CT after some discrete-time delay. We observe that early intervention of CT may significantly reduce peak hospitalizations and total mortality. Even with a late intervention (after 150 days), we see that the total mortality is reduced by at least 20.5%.

In the second case, we assumed a perfect reporting of infected cases and perfect tracking of contacts of reported cases. With 50% of these cases traced and the monitoring policies being implemented at 50% and 100% efficiency, we observe the reduction in total mortality (peak hospitalizations) by 64.2% and 99%. Furthermore, the contour plots (see fig. 20) show that while both fraction of traced reported cases and the monitoring strategy are crucial in mitigating the spread, the monitoring strategy or policy is of substantial importance so that tracked reported individuals do not cause secondary infections while being monitored. Similar results are observed in the case of perfect reporting and monitoring. Finally, we showed the effects of the proportion of traced cases (ϵ), monitoring efficacy (β_M), and tracking efficacy (ρ) in lowering the reproduction number so that the disease eventually dies out after some

time.

In conclusion, our findings suggest that almost all US states should adopt (if not yet) CT programs. In particular, our findings show that tracking a larger proportion of traced contacts while incubating and perfect monitoring of tracked contacts so that they do not cause secondary infections are very crucial for the impact of CT to be seen.

CHAPTER 7
Conclusions

This dissertation entails the numerical solution of fractional partial differential equations with time-dependent boundary conditions. We employ the Matrix Transfer Technique (MTT) to discretize the space derivative. With the MTT, the fractional PDEs with time-dependent boundary conditions results in a system of nonlinear equations with a source term that constitutes the effects at the boundaries of the problem. For the resulting nonlinear equations system, the discretization schemes developed depend on whether the time-derivative order is an integer or non-integer and are implemented in a predictor-corrector manner. We develop schemes based on rational approximations to the exponential function with Gaussian quadrature points for integer-order time-derivative. In particular, we develop schemes based on $(1,1)$-, $(0,2)$- Padé and real distinct pole approximation to the exponential function. The theoretical analysis of the derived schemes shows that the schemes are stable and second-order convergent.

For non-integer or fractional-order time-derivative, we develop a scheme similar to the Crank-Nicholson scheme for integer-order PDEs. The scheme developed consists of a history term or memory term due to the nonlocality of fractional operators. Error analysis of the scheme showed that the scheme's order is $1+\alpha \leq 2$, where α is the order of the time-derivative. This is in contrast with the Crank-Nicholson scheme which is of order two. This contrast is due to the singular kernel in the definition of the time-derivative. To increase the accuracy and order of convergence, we used a time-graded mesh with more mesh points around the kernel's singularity point. For long time intervals, the implementation of the derived scheme can be time-consuming due to the computation and re-computation of the history term at each time step. We lessen this computational time by implementing three parallel versions of the algorithms. We used the shared (OpenMP) and distributed (MPI) memory systems are used to implement the schemes. A third version that uses both the shared and distributed parallel versions is also discussed. We discuss the advantages of the parallel algorithms over the sequential ones. In particular, our experimentation shows a lot more gain in execution time when the hybrid version of the algorithm is used. While this version may be the best in terms of execution time, its speedup is not close to linear, unlike the MPI and OpenMP versions. For practical purposes, we will recommend the hybrid version with some level of optimization.

Lastly, we applied the numerical scheme on a compartmental model of COVID-19. The model comprises a susceptible-exposed, infected, hospitalized, recovered, and dead population. The model's analysis is discussed, and numerical simulations show that the model fits the dynamics of the epidemic quite well. Furthermore, we incorporate the contact tracing observables in the model. We discuss actions of contact tracers such as reporting, tracking, and monitoring policies.

BIBLIOGRAPHY

[1] N. H. Abel, Solution de quelques problemes a l'aide d'integrales definies, *Oeuvres*, vol. 1, pp. 11–27, 1881.

[2] L. Aceto and P. Novati, Rational approximation to the fractional Laplacian operator in reaction-diffusion problems, *SIAM Journal on Scientific Computing*, vol. 39, no. 1, A214–A228, 2017.

[3] R. Almeida, Analysis of a fractional SEIR model with treatment, *Applied Mathematics Letters*, vol. 84, pp. 56 –62, 2018.

[4] J. Arino and S. Portet, A simple model for COVID-19, *Infectious Disease Modelling*, vol. 5, pp. 309 –315, 2020.

[5] S. Arshad, J. Huang, A. Q. M. Khaliq, and Y. Tang, Trapezoidal scheme for time–space fractional diffusion equation with riesz derivative, *Journal of Computational Physics*, vol. 350, pp. 1 –15, 2017, ISSN: 0021-9991.

[6] S. Asadi, N. Bouvier, A. S. Wexler, and W. D. Ristenpart, The coronavirus pandemic and aerosols: Does COVID-19 transmit via expiratory particles? *Aerosol Sci Technol.*, vol. 0, no. 1-4, 2020.

[7] E. O. Asante-Asamani, A. Q. M. Khaliq, and B. A. Wade, A real distinct poles exponential time differencing scheme for reaction-diffusion systems, *Journal of Comput. Appl. Math.*, vol. 299, pp. 24–34, 2016.

[8] T. M. Atanacković, S. Pilipović, B. Stanković, and D. Zorica, *Fractional Calculus with Applications in Mechanics: Wave Propagation, Impact and variational Principles*. John Wiley & Sons, Inc., 2014.

[9] A. Atangana and N. Bildik, The use of fractional order derivative to predict the groundwater flow, *Mathematical Problems in Engineering*, vol. 2013, Article ID 543026, pp. 1–9, 2013.

[10] M. Bahloul, A. Chahid, and T.-M. Laleg-Kirati, Fractional-order SEIQRDP Model for Simulating the Dynamics of COVID-19 Epidemic, *IEEE Open Journal of Engineering in Medicine and Biology*, vol. 1, pp. 249–256, 2020.

[11] Baleanu, *Fractional Dynamics and Control, edited by D. Baleanu, J. T. Machado and A. C. J. Luo*. Springer, New York, 2012.

[12] D. Baleanu, K. Diethelm, E. Scalas, and J. Trujillo, *Fractional calculus: models and numerical methods*. World Scientific, 2016, vol. 5.

[13] D. Baleanu, A. Jajarmi, H. Mohammadi, and S. Rezapour, A new study on the mathematical modelling of human liver with Caputo–Fabrizio fractional derivative, *Chaos, Solitons & Fractals*, vol. 134, p. 109 705, 2020.

[14] D. Baleanu, A. Jajarmi, S. S. Sajjadi, and J. H. Asad, The fractional features of a harmonic oscillator with position-dependent mass, *Communications in Theoretical Physics*, vol. 72, no. 5, p. 055 002, 2020.

[15] H. P. Bhatt, A. Q. M. Khaliq, and K. M. Furati, Efficient high-order compact exponential time differencing method for space-fractional reaction-diffusion systems with non-homogeneous boundary conditions, *Numerical Algorithms*, vol. 83, 1373–1397, 2020.

[16] H. P. Bhatt and A. Q. M Khaliq, The locally extrapolated exponential time differencing LOD scheme for multidimensional reaction–diffusion systems, *Journal of Computational and Applied Mathematics*, vol. 285, pp. 256–278, 2015.

[17] T. A. Biala and S. N. Jator, Block implicit adams methods for fractional differential equations, *Chaos, Solitons and Fractals*, vol. 81, pp. 365–367, 2015.

[18] T. A. Biala and A. Q. M. Khaliq, Parallel algorithms for nonlinear time–space fractional parabolic PDEs, *Journal of Computational Physics*, vol. 375, pp. 135 –154, 2018, ISSN: 0021-9991.

[19] T. A. Biala and A. Q. M. Khaliq, A fractional-order compartmental model for the spread of the COVID-19 pandemic, *Communications in Nonlinear Science and Numerical Simulation*, vol. 98, pp. 105–764, 2021.

[20] C. Browne, H. Gulbudak, and G. Webb, Modeling contact tracing in outbreaks with application to Ebola, *Journal of Theoretical Biology*, vol. 384, pp. 33 –49, 2015.

[21] R. Brun, P. Reichert, and H. R. Künsch, Practical identifiability analysis of large environmental simulation models, *Water Resources Research*, vol. 37, no. 4, pp. 1015–1030, 2001.

[22] H. Brunner, *Collocation Methods for Volterra Integral and Related Functional Equations Methods*. Cambridge University Press, Cambridge, 2004.

[23] H. Brunner, A. Pedas, and G. Vainikko, The piecewise polynomial collocation method for weakly singular volterra integral equations. *Mathematics of Computation*, vol. 68, no. 227, pp. 1079–1095, 1999.

[24] M. Burth, G. C. Verghese, and M. Velez-Reyes, Subset selection for improved parameter estimation in on-line identification of a synchronous generator, *IEEE Transactions on Power Systems*, vol. 14, no. 1, pp. 218–225, 1999.

[25] F. Campolongo, J. Cariboni, and A. Saltelli, An effective screening design for sensitivity analysis of large models, *Environmental Modelling & Software*, vol. 22, no. 10, pp. 1509 –1518, 2007.

[26] M Caputo and F Mainardi, A new dissipation model based on memory mechanism, *Pure and Applied Geophysics*, vol. 91, no. 1, pp. 134–147, 1971.

[27] M. Caputo and F. Mainardi, Linear models of dissipation in elastic solids, *La Rivista del Nuovo Cimento (1971-1977)*, vol. 1, no. 2, pp. 161–198, 1971.

[28] M. Caputo, Diffusion with space memory modelled with distributed order space fractional differential equations, *Annals of Geophysics*, vol. 46, no. 2, pp. 223–234, 2003.

[29] M. Caputo, Linear models of dissipation whose Q is almost frequency independent-II, *Geophysical Journal of the Royal Astronomical Society*, vol. 13, 529–539, 1967.

[30] C. Çelik and M. Duman, Crank–Nicolson method for the fractional diffusion equation with the Riesz fractional derivative, *Journal of Computational Physics*, vol. 231, no. 4, pp. 1743 –1750, 2012.

[31] *Center for Disease Control and Prevention:* https://www.cdc.gov/coronavirus/2019-ncov/daily-life-coping/contact-tracing.html.

[32] G. A. Chandler and I. G. Graham, Product integration-collocation methods for noncompact integral operator equations, *Mathematics of Computation*, vol. 50, no. 181, 125–138, 1988.

[33] S. Chen, X. Jiang, F. Liu, and I. Turner, High order unconditionally stable difference schemes for the Riesz space-fractional telegraph equation, *Journal of Computational and Applied Mathematics*, vol. 278, pp. 119 –129, 2015.

[34] C. C. Chow, J. C. Chang, R. C. Gerkin, and S. Vattikuti, Global prediction of unreported SARS-CoV2 infection from observed COVID-19 cases, *medRxiv*, 2020. DOI: 10.1101/2020.04.29.20083485.

[35] A. Cintrón-Arias, H. T. Banks, A. Capaldi, and A. L. Lloyd, A sensitivity matrix based methodology for inverse problem formulation, *Journal of Inverse and Ill-posed Problems*, vol. 17, no. 6, pp. 545 –564, 2009.

[36] A Cloot and J. Botha, A generalised groundwater flow equation using the concept of non-integer order derivatives, *Water SA*, vol. 32, no. 1, pp. 1–7, 2006.

[37] *CNN News,* https://www.cnn.com/2020/04/20/us/states-that-require-masks-trnd/index.html.

[38] C. Cobelli and J. J. DiStefano, Parameter and structural identifiability concepts and ambiguities: A critical review and analysis, *American Journal of Physiology-Regulatory, Integrative and Comparative Physiology*, vol. 239, no. 1, R7–R24, 1980.

[39] S. M. Cox and P. C. Matthews, Exponential time differencing for stiff systems, *Journal of Computational Physics*, vol. 176, no. 2, pp. 430–455, 2002.

[40] W. Deng, Finite element method for the space and time fractional Fokker–Planck equation, *SIAM Journal on Numerical Analysis*, vol. 47, no. 1, pp. 204–226, 2009.

[41] E. Di Giuseppe, M. Moroni, and M. Caputo, Flux in porous media with memory: Models and experiments, *Transport in Porous Media*, vol. 83, no. 3, pp. 479–500, 2010.

[42] O. Diekmann, J. A. P. Heesterbeek, and M. G. Roberts, The construction of next-generation matrices for compartmental epidemic models, *Journal of Royal Society Interface*, vol. 7, 873–885, 2010.

[43] O. Diekmann, J. Heesterbeek, and J. Metz, On the definition and the computation of the basic reproduction ratio R_0 in models for infectious diseases in heterogeneous populations, *Journal of Mathematical Biology*, vol. 28, 365–382, 1990.

[44] K. Diethelm, A fractional calculus based model for the simulation of an outbreak of Dengue fever, *Nonlinear Dynamics*, vol. 71, no. 613–619, 2013.

[45] K. Diethelm, An algorithm for the numerical solution of differential equations of fractional order, *Electronic transactions on numerical analysis*, vol. 5, no. 1, pp. 1–6, 1997.

[46] K. Diethelm and N. J. Ford, Analysis of fractional differential equations, *Journal of Mathematical Analysis and Applications*, vol. 265, no. 2, pp. 229–248, 2002.

[47] K. Diethelm, N. J. Ford, and A. D. Freed, A predictor-corrector approach for the numerical solution of fractional differential equations, *Nonlinear Dynamics*, vol. 29, no. 1, pp. 3–22, 2002.

[48] K. Diethelm and N. Ford, Numerical solution of the Bagley-Torvik equation, *BIT Numerical Mathematics*, vol. 42, no. 3, pp. 490–507, 2002.

[49] H. Ding and Y. Zhang, New numerical methods for the Riesz space fractional partial differential equations, *Computers & Mathematics with Applications*, vol. 63, no. 7, pp. 1135 –1146, 2012.

[50] E. Dong, H. Du, and L. Gardner, An interactive web-based dashboard to track covid-19 in real time, *The Lancet Infectious Diseases*, vol. 20, no. 5, pp. 533–534, 2020.

[51] P. van den Driessche and J. Watmough, Reproduction numbers and subthreshold endemic equilibria for compartmental models of disease transmission, *Mathematical Biosciences*, vol. 180, no. 1, pp. 29 –48, 2002.

[52] S. E. Eikenberry, M. Mancuso, E. Iboi, T. Phan, K. Eikenberry, Y. Kuang, E. Kostelich, and A. B. Gumel, To mask or not to mask: Modeling the potential for face mask use by the general public to curtail the COVID-19 pandemic, *Infectious Disease Modelling*, vol. 5, pp. 293 –308, 2020.

[53] H. A. Fallahgoul, S. M. Focardi, and F. J. Fabozzi, *Fractional calculus and Fractional Processes with Applications to Financial economics: Theory and Applications*. Academic Press, 2017.

[54] N. Ferguson, D. Laydon, N. Gilani, N. Imai, K. Ainslie, M. Baguelin, and *et al.*, Impact of non-pharmaceutical interventions (npis) to reduce covid19 mortality and healthcare demand, *Report 9*, 2020.

[55] S. Fomin, V. Chugunov, and T. Hashida, Mathematical modeling of anomalous diffusion in porous media, *Fractional Differential Calculus*, vol. 1, no. 1, pp. 1–28, 2011.

[56] K. M. Furati, I. O. Sarumi, and A. Q. M. Khaliq, Fractional model for the spread of COVID-19 subject to government intervention and public perception, *Applied Mathematical Modelling*, vol. 95, pp. 89 –105, 2021.

[57] N. W. Furukawa, J. T. Brooks, and J. Sobel, Evidence supporting transmission of severe acute respiratory syndrome coronavirus 2 while presymptomatic or asymptomatic, *Emerging Infectious Diseases*, vol. 26, no. 7, e1–e6, 2020.

[58] T. Galbadage, B. M. Peterson, and R. S. Gunasekera, Does COVID-19 spread through droplets alone? *Frontiers in Public Health*, vol. 8, p. 163, 2020.

[59] E. Gallopoulos and Y. Saad, "On the parallel solution of parabolic equations," in *Proceedings of the 3rd International Conference on Supercomputing*, ser. ICS '89, Crete, Greece: ACM, 1989, pp. 17–28.

[60] R. Garrappa, Exponential integrators for time-fractional partila differential equations, *The European Journal of Physical Journal, Special Topics*, vol. 222, pp. 1915–1927, 2013.

[61] R. Garrappa and M. Popolizio, Generalized exponential time differencing methods for fractional order problems, *Computers & Mathematics with Applications*, vol. 62, no. 3, pp. 876 –890, 2011.

[62] G. Giordano, F. Blanchini, R. Bruno, P. Colaneri, A. D. Filippo, A. D. Matteo, and M. Colaneri, Modelling the COVID-19 epidemic and implementation of population-wide interventions in Italy, *Nature Medicine*, vol. 26, 855–860, 2020.

[63] A. K. Grünwald, Úber "begrenzte" derivation en und deren anwendung, *Zeitschrift fur Mathematik und Physik*, vol. 12, 441–480, 1867.

[64] A. B. Gumel, E. A. Iboi, C. N. Ngonghala, and E. H. Elbasha, A primer on using mathematics to understand COVID-19 dynamics: Modeling, analysis and simulations, *Infectious Disease Modelling*, vol. 6, pp. 148–168, 2021.

[65] G. Guzzetta, M. Ajelli, Z. Yang, L. N. Mukasa, N. Patil, J. H. Bates, D. E. Kirschner, and S. Merler, Effectiveness of Contact Investigations for Tuberculosis Control in Arkansas, *Journal of Theoretical Biology*, vol. 380, pp. 238–246, 2015.

[66] D. He, J. Dushoff, T. Day, J. Ma, and D. J. D. Earn, Inferring the causes of the three waves of the 1918 Influenza pandemic in England and Wales, *Proceedings of the Royal Society B: Biological Sciences*, vol. 280, no. 1766, p. 20 131 345, 2013.

[67] J. Herman and W. Usher, SALib: An open-source python library for sensitivity analysis, *The Journal of Open Source Software*, vol. 2, no. 9, 2017.

[68] T. Homma and A. Saltelli, Importance measures in global sensitivity analysis of nonlinear models, *Reliability Engineering & System Safety*, vol. 52, no. 1, pp. 1 –17, 1996.

[69] Y. Hu, C. Li, and H. Li, The finite difference method for caputo-type parabolic equation with fractional laplacian: More than one space dimension, *International Journal of Computer Mathematics*, vol. 95, no. 6-7, pp. 1114–1130, 2018.

[70] J. M. Hyman, J. Li, and E. A. Stanley, Modeling the impact of random screening and contact tracing in reducing the spread of HIV, *Mathematical Biosciences*, vol. 181, no. 1, pp. 17–54, 2003.

[71] G. Iaffaldano, M Caputo, and S. Martino, Experimental and theoretical memory diffusion of water in sand, *Hydrology and Earth System Sciences Discussions*, vol. 2, no. 4, pp. 1329–1357, 2005.

[72] M. Ilic, F. Liu, I. Turner, and V. Anh, Numerical Approximation of a Fractional-In-Space Diffusion Equation, I, *Fractional Calculus and Applied Analysis*, vol. 8, no. 3, pp. 323–341, 2005.

[73] M Ilic, F. Liu, I. Turner, and V. Anh, Numerical approximation of a fractional-in-space diffusion equation (II)- with nonhomogenous boundary conditions, *Fractional Calculus and Applied Analysis*, vol. 9, no. 2, pp. 333–349, 2006.

[74] C. Ionescu, A. Lopes, D. Copot, J. Machado, and J. Bates, The role of fractional calculus in modeling biological phenomena: A review, *Communications in Nonlinear Science and Numerical Simulation*, vol. 51, pp. 141 –159, 2017.

[75] O. S. Iyiola, E. O. Asante-Asamani, K. M. Furati, A. Q. M. Khaliq, and B. A. Wade, Efficient time discretization scheme for nonlinear space fractional reaction-diffusion equations, *International Journal of Computer Mathematics*, vol. 95, no. 6-7, pp. 1274–1291, 2018.

[76] O. Iyiola, E. Asante-Asamani, and B. Wade, A real distinct poles rational approximation of generalized mittag-leffler functions and their inverses: Applications to fractional calculus, *Journal of Computational and Applied Mathematics*, vol. 330, pp. 307 –317, 2018.

[77] O. Iyiola and B. Wade, Exponential integrator methods for systems of nonlinear space-fractional models with super-diffusion processes in pattern formation, *Computers & Mathematics with Applications*, vol. 75, no. 10, pp. 3719 –3736, 2018.

[78] M. Jayaweera, H. Perera, Gunawardana, and J. Manatunge, Transmission of COVID-19 virus by droplets and aerosols: A critical review on the unresolved dichotomy, *Environ Res.*, vol. 188, pp. 1–18, 2020.

[79] K. Diethelm, An efficient parallel algorithm for the numerical solution of fractional differential equations, *Fractional Calculus and Applied Analysis*, vol. 14, pp. 475–490, 2011.

[80] Kai Diethelm, *The analysis of fractional differential equations: An application-oriented exposition using differential operators of Caputo type*. Springer, 2010.

[81] Kassem Mustapha, An L1-Approximation for a Fractional Reaction-Diffusion Equation, a Second-Order Error Analysis over Time-Graded Meshes, *SIAM Journal on Numerical Analysis*, vol. 58, no. 2, pp. 1319–1338, 2020.

[82] M. J. Keeling, T. D. Hollingsworth, and J. M. Read, Efficacy of contact tracing for the containment of the 2019 novel coronavirus (COVID-19), *J. Epidemiol Community Health*, vol. 74, no. 10, 861–866, 2020.

[83] A. Q. M. Khaliq, X Liang, and K. M. Furati, A fourth-order implicit-explicit scheme for the space-fractional nonlinear Schrödinger equations, *Numerical Algorithms*, vol. 75, pp. 147–172, 1 2017.

[84] A. Q. M Khaliq, J. Martin-Vaquero, B. Wade, and M Yousuf, Smoothing schemes for reaction-diffusion systems with nonsmooth data, *Journal of Computational and Applied Mathematics*, vol. 223, no. 1, pp. 374–386, 2009.

[85] A. Q. M. Khaliq, E. H. Twizell, and D. A. Voss, On parallel algorithms for semidiscretized parabolic partial differential equations based on subdiagonal Padé approximations, *Numerical Methods for Partial Differential Equations*, vol. 9, no. 2, pp. 107–116, 1993.

[86] A. Q. M. Khaliq, B. A. Wade, M. Yousuf, and J. Vigo-Aguiar, High order smoothing schemes for inhomogeneous parabolic problems with applications in option pricing, *Numer Methods Partial Differential Eq.*, vol. 23, pp. 1249 –1276, 2007.

[87] A Kilbas, H. Srivastava, and J. Trujillo, *Theory and Applications of Fractional Differential Equations*. Elsevier, North-Holland Mathematics Studies, 2006, vol. 204.

[88] B Kleefeld, A. Q. M. Khaliq, and B. A. Wade, An ETD Crank-Nicolson method for reaction-diffusion systems, *Numerical Methods for Partial Differential Equations*, vol. 28, no. 4, pp. 1309–1335, 2012.

[89] D. Klinkenberg, C. Fraser, and H. Heesterbeek, The effectiveness of contact tracing in emerging epidemics, *PLoS One*, vol. 1, no. e12, pp. 1–7, 1 2006.

[90] M. E. Kretzschmar, G. Rozhnova, M. C. J. Bootsma, M. V. Boven, J. V. de Wijgert, and M. J. M. Bonten, Impact of delays on effectiveness of contact tracing strategies for COVID-19: A modeling study, *The Lancet Public Health*, vol. 5, e452–e459, 2020.

[91] K. O. Kwok, A. Tang, V. Wei, W. H. Park, E. K. Yeoh, and S. Riley, Epidemic models of contact tracing: Systematic review of transmission studies of severe acute respiratory syndrome and middle east respiratory syndrome, *Comput Struct Biotechnol J.*, vol. 17, pp. 186–194, 2019.

[92] A. Lachmann, K. M. Jagodnik, F. M. Giorgi, and F. Ray, Correcting underreported COVID-19 case numbers: Estimating the true scale of the pandemic, *medRxiv*, 2020.

[93] S. L. Lauer, K. H. Grantz, Q. Bi, F. K. Jones, Q. Zheng, H. R. Meredith, A. S. Azman, N. G. Reich, and J. Lessler, The Incubation Period of Coronavirus Disease 2019 (COVID-19) From Publicly Reported Confirmed Cases: Estimation and Application, *Annals of Internal Medicine*, vol. 172, no. 9, pp. 577–582, 2020.

[94] J. D. Lawson and J. L. Morris, The extrapolation of first order methods for parabolic partial differential equations. *SIAM Journal on Numerical Analysis*, vol. 15, no. 6, pp. 1212–1224, 1978.

[95] A. V. Letnikov, Theory of differentiation with an arbitraryindex, (in russian), *Sbornik: Mathematics*, vol. 3, 1–66, 1868.

[96] C. Li, Z. Zhao, and Y. Chen, Numerical approximation of nonlinear fractional differential equations with subdiffusion and superdiffusion, *Computers & Mathematics with Applications*, vol. 62, no. 3, pp. 855 –875, 2011.

[97] R. Li, S. Pei, B. Chen, Y. Song, T. Zhang, W. Yang, and J. Shaman, Substantial undocumented infection facilitates the rapid dissemination of novel coronavirus (SARS-COV-2), *Science*, vol. 368, no. 6490, pp. 489–493, 2020.

[98] Y. Li, Y. Chen, and I. Podlubny, Mittag–leffler stability of fractional order nonlinear dynamic systems, *Automatica*, vol. 45, no. 8, pp. 1965 –1969, 2009.

[99] Z. Li, H. Wang, and D. Yang, A space–time fractional phase-field model with tunable sharpness and decay behavior and its efficient numerical simulation, *Journal of Computational Physics*, vol. 347, pp. 20 –38, 2017.

[100] Q. Lin, S. Zhao, D. Gao, Y. Lou, S. Yang, S. S. Musa, M. H. Wang, Y. Cai, W. Wang, L. Yang, and D. He, A conceptual model for the coronavirus disease 2019 (COVID-19) outbreak in wuhan, china with individual reaction and governmental action, *International Journal of Infectious Diseases*, vol. 93, pp. 211 –216, 2020.

[101] W. Lin, Global existence theory and chaos control of fractional differential equations, *Journal of Mathematical Analysis and Applications*, vol. 332, no. 1, pp. 709 –726, 2007.

[102] J. Liouville, Memoire sur quelques queśtions de geómetrie et de mećanique, et sur un nouveau genre de calcul pour reśoudre queśtions, *J. Ećole Polytech.*, vol. 13, 1–69, 1832.

[103] A. Lischke, G. Pang, M. Gulian, F. Song, C. Glusa, X. Zheng, Z. Mao, W. Cai, M. M. Meerschaert, M. Ainsworth, and G. E. Karniadakis, What is the fractional Laplacian? A comparative review with new results, *Journal of Computational Physics*, vol. 404, pp. 1–62, 2020.

[104] F. Liu, V. Anh, and I. Turner, Numerical solution of the space fractional Fokker–Planck equation, *Journal of Computational and Applied Mathematics*, vol. 166, no. 1, pp. 209 –219, 2004.

[105] Z. Liu, P. Magal, O. Seydi, and G. Webb, Understanding Unreported Cases in the COVID-19 Epidemic Outbreak in Wuhan, China, and the Importance of Major Public Health Interventions, *Biology*, vol. 9, no. 50, pp. 1–12, 2020.

[106] Z. Lu, Y. Yu, Y. Chen, G. Ren, C. Xu, S. Wang, and Z. Yin, A fractional-order SEIHDR model for COVID-19 with inter-city networked coupling effects, *Nonlinear dynamics*, vol. 2020, pp. 1–14, 2020.

[107] P. Lyu and S. Vong, A graded scheme with bounded grading for a time-fractional boussinesq type equation, *Applied Mathematics Letters*, vol. 92, pp. 35 –40, 2019.

[108] J. Ma and Y. Jiang, On a graded mesh method for a class of weakly singular volterra integral equations, *Journal of Computational and Applied Mathematics*, vol. 231, no. 2, pp. 807 –814, 2009.

[109] J. T. Machado, V. Kiryakova, and F. Mainardi, Recent history of fractional calculus, *Communications in Nonlinear Science and Numerical Simulation*, vol. 16, no. 3, pp. 1140–1153, 2011.

[110] J. T. Machado, A. C. Costa, and M. D. Quelhas, Fractional dynamics in DNA, *Communications in Nonlinear Science and Numerical Simulation*, vol. 16, no. 8, pp. 2963 –2969, 2011.

[111] J. T. Machado and M. E. Mata, Pseudo phase plane and fractional calculus modeling of western global economic downturn, *Communications in Nonlinear Science and Numerical Simulation*, vol. 22, no. 1, pp. 396 –406, 2015.

[112] R. L. Magin, Fractional calculus models of complex dynamics in biological tissues, *Computers & Mathematics with Applications*, vol. 59, no. 5, pp. 1586 –1593, 2010.

[113] F. Mainardi, *Fractional Calculus and Waves in Linear Viscoelastivity: An introduction to Mathematical Models*. Imperial College Press, 2010.

[114] F. Mainardi, M. Raberto, R. Gorenflo, and E. Scalas, Fractional calculus and continuous-time finance ii: The waiting-time distribution, *Physica A: Statistical Mechanics and its Applications*, vol. 287, no. 3, pp. 468 –481, 2000.

[115] A. Maugeri, M. Barchitta, S. Battiato, and A. Agodi, Estimation of Unreported Novel Coronavirus (SARS-COV-2) Infections from Reported Deaths: A Susceptible–Exposed–Infectious–Recovered–Dead Model, *Journal of Clinical Medicine*, vol. 9, no. 5, pp. 1–9, 2020.

[116] W. McLean and K. Mustapha, A second-order accurate numerical method for a fractional wave equation, *Numer. Math.*, vol. 105, pp. 481–510, 2007.

[117] W. McLean, V. Thomée, and B. Wahlbin, Discretization with variable time steps of an evolution equation with a positive-type memory term, *J. Comput. Appl. Math.*, vol. 69, pp. 49–69, 1996.

[118] M. Meerschaert and C. Tadjeran, Finite difference approximations for fractional advection–dispersion flow equations, *Journal of Computational and Applied Mathematics*, vol. 172, no. 1, pp. 65 –77, 2004.

[119] M. M. Meerschaert and C. Tadjeran, Finite difference approximations for two-sided space-fractional partial differential equations, *Applied Numerical Mathematics*, vol. 56, no. 1, pp. 80–90, 2006.

[120] R. Metzler and J. Klafter, The random walk's guide to anomalous diffusion: A fractional dynamics approach, *Physics reports*, vol. 339, no. 1, pp. 1–77, 2000.

[121] K. S. Miller and B. Ross, *An introduction to the Fractional Calculus and Fractional Differential Equations*. John Wiley & Sons, New York, 1993.

[122] M. D. Morris, Factorial sampling plans for preliminary computational experiments, *Technometrics*, vol. 33, no. 2, pp. 161–174, 1991.

[123] K. Mustapha, A superconvergent discontinuous galerkin method for volterra integro-differential equations, smooth and non-smooth kernels, *Mathematics of Computations*, vol. 82, 1987–2005, 2013.

[124] K. Mustapha, B. Abdallah, and K. M. Furati, A discontinuous petrov–galerkin method for time-fractional diffusion equations, *SIAM Journal on Numerical Analysis*, vol. 52, no. 5, pp. 2512–2529, 2014.

[125] K. Mustapha, An implicit finite-difference time-stepping method for a sub-diffusion equation with spatial discretization by finite elements, *IMA Journal of Numerical Analysis*, vol. 31, no. 2, pp. 719–739, 2011.

[126] New York Times, `https://www.nytimes.com/2020/05/15/us/coronavirus-first-case-snohomish-antibodies.html`,,

[127] C. N. Ngonghala, E. Iboi, S. Eikenberry, M. Scotch, C. R. MacIntyre, M. H. Bonds, and A. B. Gumel, Mathematical assessment of the impact of non-pharmaceutical interventions on curtailing the 2019 novel coronavirus, *Mathematical Biosciences*, vol. 325, p. 108 364, 2020.

[128] R. Ningthoujam, COVID 19 can spread through breathing, talking, study estimates, *Curr Med Res Pract.*, vol. 10, no. 3, pp. 132–133, 2020.

[129] S. P. Nørsett and A. Wolfbrandt, Attainable order of rational approximations to the exponential function with only real poles, *BIT Numerical Mathematics*, vol. 17, no. 2, pp. 200–208, 1977.

[130] K. Oldham and J. Spanier, *The fractional calculus theory and applications of differentiation and integration to arbitrary order*. Elsevier, 1974, vol. 111.

[131] M. D. Ortigueira, Riesz potential operators and inverses via fractional centered derivatives, *International Journal of Mathematics and Mathematical Sciences*, vol. 2006, Article ID 048391, pp. 1–12, 2006.

[132] I. Podlubny, Fractional-order systems and fractional-order controllers, *Institute of Experimental Physics, Slovak Academy of Sciences, Kosice*, vol. 12, no. 3, pp. 1–18, 1994.

[133] I. Podlubny, Fractional differential equations, *Mathematics in Science and Engineering 198, Academic Press*, 1999.

[134] K. Pohlmann, M. Ye, D. Reeves, M. Zavarin, D. Decker, and J. Chapman, "Modeling of Groundwater Flow and Radionuclide Transport at the Climax Mine sub-CAU, Nevada Test Site (DOE/NV–26383-06) United States," 2007.

[135] C. Pozrikidis, *The Fractional Laplacian*. CRC Press, 2016.

[136] K. A. Prather, C. C. Wang, and R. T. Schooley, Reducing transmission of SARS-COV-2, *Science*, vol. 368, no. 6498, pp. 1422–1424, 2020.

[137] S. S. Ray, *Fractional Calculus with Applications for Nuclear Reactor Dynamics*. CRC Press, 2016.

[138] J. M. Read, J. R. Bridgen, D. A. Cummings, A. Ho, and C. P. Jewell, Novel coronavirus 2019-nCoV: early estimation of epidemiological parameters and epidemic predictions, *medRxiv*, 2020.

[139] G. F. B. Riemann, Ersuch einer allgemeinen auffassung der integration und differentiation, *Gesammelte Mathematische Werke, Leipzig*, 1876.

[140] M. Riesz, L'intégrale de Riemann-Liouville et le probléme de Cauchy, *Acta Mathematica*, vol. 81, 1–222, 1949.

[141] G. Roberto, Trapezoidal methods for fractional differential equations: Theoretical and computational aspects, *Mathematics and Computers in Simulation*, vol. 110, pp. 96–112, 2015.

[142] B. Ross, *Fractional Calculus and its Applications*. Springer, 1975, vol. 457.

[143] L. Ruiyun, P. Sen, C. Bin, S. Yimeng, Z. Tao, Y. Wan, and S. Jeffrey, Substantial undocumented infection facilitates the rapid dissemination of novel coronavirus (SARS-COV-2), *Science*, vol. 368, no. 6490, pp. 489–493, 2020.

[144] A. Saltelli, P. Annoni, I. Azzini, F. Campolongo, M. Ratto, and S. Tarantola, Variance based sensitivity analysis of model output. design and estimator for the total sensitivity index, *Computer Physics Communications*, vol. 181, no. 2, pp. 259–270, 2010.

[145] A. Saltelli, S. Tarantola, and F. Campolongo, Sensitivity analysis as an ingredient of modeling, *Statistical Science*, vol. 15, no. 4, pp. 377–395, Nov. 2000.

[146] A. Saltelli, S. Tarantola, F. Campolongo, and M. Ratto, *Sensitivity analysis in practice: a guide to assessing scientific models*. John Willy & Sons, Ltd, 2004.

[147] S. G. Samko, A. A. Kilbas, and O. I. Marichev, *Fractional integrals and derivatives*. Theory, Applications, Gordon, and Breach, Yverdon, 1993.

[148] K. Shah, M. A. Alqudah, F. Jarad, and T. Abdeljawad, Semi-analytical study of Pine Wilt disease model with convex rate under Caputo–Fabrizio fractional order derivative, *Chaos, Solitons & Fractals*, vol. 135, p. 109 754, 2020.

[149] A. G. Shankar, K. Janmohamed, B. Olowokure, G. E. Smith, A. H. Hogan, V. D. Souza, A. Wallensten, I. Oliver, O. Blatchford, P. Cleary, and S. Ibbotson, Contact tracing for influenza A(H1N1)pdm09 virus-infected passenger on international flight, *Emerging infectious diseases*, vol. 20, no. 1, 118–120, 2014.

[150] M. Shen, Z. Peng, Y. Xiao, and L. Zhang, Modelling the epidemic trend of the 2019 novel coronavirus outbreak in China, *bioRxiv*, 2020.

[151] S. Shen, F. Liu, and V. Anh, Numerical approximations and solution techniques for the space-time Riesz–Caputo fractional advection-diffusion equation, *Numerical Algorithms*, vol. 56, no. 3, pp. 383–403, 2011.

[152] D. Sierociuk, T. Skovranek, M. Macias, I. Podlubny, I. Petras, A. Dzielinski, and P. Ziubinski, Diffusion process modeling by using fractional-order models, *Applied Mathematics and Computation*, vol. 257, pp. 2 –11, 2015.

[153] D. P. Simpson, "Krylov subspace methods for approximating functions of symmetric positive definite matrices with applications to applied statistics and anomalous diffusion," Ph.D. dissertation, Queensland University of Technology, 2008.

[154] I. Sobol, Sensitivity analysis for nonlinear mathematical models, *Mathematical Models and Computer Experiment*, vol. 1, no. 4, pp. 407–414, 1993.

[155] I. M. Sobol, Global sensitivity indices for nonlinear mathematical models and their Monte Carlo estimates, *Mathematics and Computers in Simulation*, vol. 55, no. 1, pp. 271 –280, 2001.

[156] G. A. Somsen, C. V. Rijn, S. Kooil, R. A. Bem, and D. Bonn, Small droplets of aerosol in poorly ventilated spaces and SARS-COV-2 transmission, *The Lancet, Respiratory Medicine*, vol. 8, pp. 658–659, 7 2020.

[157] E. Sousa, Finite difference approximations for a fractional advection diffusion problem, *Journal of Computational Physics*, vol. 228, no. 11, pp. 4038–4054, 2009.

[158] E. Sousa and C. Li, A weighted finite difference method for the fractional diffusion equation based on the Riemann–Liouville derivative, *Applied Numerical Mathematics*, vol. 90, pp. 22 –37, 2015.

[159] V. Stadnytskyi, C. E. Bax, A. Bax, and P. Anfinrud, The airborne lifetime of small speech droplets and their potential importance in SARS-COV-2 transmission, *Proceedings of the National Academy of Sciences*, vol. 117, no. 22, pp. 11 875–11 877, 2020.

[160] L. Stella, A. P. Martínez, D. Bauso, and P. Colaneri, *The Role of Asymptomatic Individuals in the COVID-19 Pandemic via Complex Networks*, 2020. arXiv: 2009.03649.

[161] C. Tadjeran, M. M. Meerschaert, and H.-P. Scheffler, A second-order accurate numerical approximation for the fractional diffusion equation, *Journal of Computational Physics*, vol. 213, no. 1, pp. 205 –213, 2006.

[162] B. Tang, N. L. Bragazzi, Q. Li, S. Tang, Y. Xiao, and J. Wu, An updated estimation of the risk of transmission of the novel coronavirus (2019-ncov), *Infectious Disease Modelling*, vol. 5, pp. 248 –255, 2020.

[163] V. E. Tarasov, *Fractional dynamics: Applications of Fractional Calculus to Dynamics of Particles, Fields and Media*. Springer Heidelberg Dordrecht London New York, 2000.

[164] V. Thomée, Galerkin finite element methods for parabolic problems, *Series in Computational Mathematics, Springer-Verlag, Berlin*, vol. 25, 1997.

[165] N. H. Tuan, H. Mohammadi, and S. Rezapour, A mathematical model for COVID-19 transmission by using the caputo fractional derivative, *Chaos, Solitons & Fractals*, vol. 140, p. 110 107, 2020.

[166] G. M. Vazquez-Prokopec, B. L. Montgomery, P. Horne, J. A. Clennon, and S. A. Ritchie, Combining contact tracing with targeted indoor residual spraying significantly reduces dengue transmission, *Science Advances*, vol. 3, no. 2, 2017.

[167] D. A. Voss and A. Q. M. Khaliq, Parallel LOD methods for second order time dependent PDEs, *Computers Math. Appl.*, vol. 30, no. 10, pp. 25 –35, 1995.

[168] B. West, Fractal physiology and the fractional calculus: A perspective, *Frontiers in Physiology*, vol. 1, no. 12, pp. 1–17, 2010.

[169] H. Weyl, Bemerkungen zum begriff des differential quotienten gebrochenerordnung, *Vierteljschr. Naturforsch. Gesellsch.Zurich*, vol. 62, 296–302, 1917.

[170] *World Health Organization:* `https://www.who.int/csr/disease/ebola/training/contact-tracing/en/`.

[171] J. T. Wu, K. Leung, and G. M. Leung, Nowcasting and forecasting the potential domestic and international spread of the 2019-nCoV outbreak originating in Wuhan, China: a modelling study, *The Lancet*, vol. 395, no. 10225, pp. 689 –697, 2020.

[172] S. Wu and T. Zhou, Parareal algorithms with local time-integrators for time fractional differential equations, *Journal of Computational Physics*, vol. 358, pp. 135–149, 2018.

[173] S.-L. Wu and T. Zhou, Fast parareal iterations for fractional diffusion equations, *Journal of Computational Physics*, vol. 329, pp. 210–226, 2017.

[174] Q. Xu and J. Hesthaven, Stable multi-domain spectral penalty methods for fractional partial differential equations, *Journal of Computational Physics*, vol. 257, pp. 241–258, 2014.

[175] Q. Xu and J. S. Hesthaven, Discontinuous galerkin method for fractional convection-diffusion equations, *SIAM Journal on Numerical Analysis*, vol. 52, no. 1, pp. 405–423, 2014.

[176] Q. Xu, J. S. Hesthaven, and F. Chen, A parareal method for time-fractional differential equations, *Journal of Computational Physics*, vol. 293, pp. 173–183, 2015.

[177] Q. Yang, F. Liu, and I. Turner, Numerical methods for fractional partial differential equations with Riesz space fractional derivatives, *Applied Mathematical Modelling*, vol. 34, no. 1, pp. 200 –218, 2010.

[178] Q. Yang, I. Turner, F. Liu, and M. Ilić, Novel numerical methods for solving the time-space fractional diffusion equation in two dimensions, *SIAM Journal on Scientific Computing*, vol. 33, no. 3, pp. 1159–1180, 2011.

[179] M. Ye and M. Hill, "Chapter 10 - Global Sensitivity Analysis for Uncertain Parameters, Models, and Scenarios," in *Sensitivity Analysis in Earth Observation Modelling*, G. P. Petropoulos and P. K. Srivastava, Eds., Elsevier, 2017, pp. 177 –210.

[180] M. Ye, L. Wang, K. F. Pohlmann, and J. B. Chapman, Evaluating groundwater interbasin flow using multiple models and multiple types of data, *Groundwater*, vol. 54, no. 6, pp. 805–817, 2016.

[181] M. Zayernouri and G. Karniadakis, Fractional Sturm-Liouville eigen-problems: Theory and numerical approximation, *Journal of Computational Physics*, vol. 252, pp. 495 –517, 2013.

[182] M. Zayernouri and G. Karniadakis, Fractional spectral collocation methods for linear and nonlinear variable order fpdes, *Journal of Computational Physics*, vol. 293, pp. 312–338, 2015.

[183] M. Zayernouri and G. E. Karniadakis, Discontinuous spectral element methods for time-and space-fractional advection equations, *SIAM Journal on Scientific Computing*, vol. 36, no. 4, B684–B707, 2014.

[184] M. Zayernouri and A. Matzavinos, Fractional Adams—Bashforth/Moulton methods: An application to the fractional keller–segel chemotaxis system, *Journal of Computational Physics*, vol. 317, pp. 1 –14, 2016.

[185] F. Zeng, C. Li, F. Liu, and I. Turner, The use of finite difference/element approaches for solving the time-fractional subdiffusion equation, *SIAM Journal on Scientific Computing*, vol. 35, no. 6, A2976–A3000, 2013.

[186] F. Zeng, C. Li, F. Liu, and I. Turner, Numerical algorithms for time-fractional subdiffusion equation with second-order accuracy, *SIAM Journal on Scientific Computing*, vol. 37, no. 1, A55–A78, 2015.

[187] R. Zhang, Y. Li, A. L. Zhang, Y. Wang, and M. J. Molina, Identifying airborne transmission as the dominant route for the spread of COVID-19, *Proceedings of the National Academy of Sciences*, vol. 117, no. 26, pp. 14 857–14 863, 2020.

[188] Y. Zhang, X. Yu, H. Sun, G. R. Tick, W. Wei, and B. Jin, Applicability of time fractional derivative models for simulating the dynamics and mitigation scenarios of COVID-19, *Chaos, Solitons & Fractals*, vol. 138, p. 109 959, 2020.

[189] S. Zhao and H. Chen, Modeling the epidemic dynamics and control of COVID-19 outbreak in China, *Quantitative Biology*, vol. 8, no. 1, pp. 1–11, 2020.

[190] M. Zheng, F. Liu, I. Turner, and V. Anh, A novel high order space-time spectral method for the time fractional fokker–planck equation, *SIAM Journal on Scientific Computing*, vol. 37, no. 2, A701–A724, 2015.

[191] F. Zhou, T. Yu, R. Du, G. Fan, Y. Liu, Z. Liu, J. Xiang, Y. Wang, B. Song, X. Gu, L. Guan, and Y. Wei, Clinical course and risk factors for mortality of adult inpatients with COVID-19 in Wuhan, China: a retrospective cohort study, *The Lancet*, vol. 395, no. 10229, pp. 1054 –1062, 2020.

APPENDICES

APPENDIX A

STANDARD ERRORS AND COEFFICIENT OF VARIATION OF MODEL PARAMETERS

	β_0	σ	γ_R	γ_U	γ_H	φ_R	μ_H	κ_1	κ_2	η	α
$\tilde{\theta}$	4.32e-01	1.14e-01	1.27e-01	7.19e-02	3.08e-01	6.51e-03	1.00e-01	6.72e-01	1.11e+03	4.38e-01	9.65e-01
E	1.95e+00	1.50e-03	9.37e-02	7.98e-03	5.83e+00	8.69e-02	8.18e-02	1.43e+00	5.27e+03	4.53e-02	7.71e-03
V	4.52e+00	1.31e-02	7.38e-01	1.11e-01	1.89e+01	1.34e+01	8.18e-01	2.13e+00	4.74e+00	1.03e-01	7.99e-02
$\tilde{\theta}$		1.07e-01	1.31e-01	7.53e-02	3.07e-01	6.94e-03	1.00e-01	7.13e-01		4.61e-01	9.85e-01
E		1.03e-03	8.81e-02	3.59e-03	5.40e+00	8.67e-02	7.88e-02	5.22e-03		2.20e-02	5.72e-03
V		9.60e-03	6.74e-01	4.77e-02	1.76e+01	1.25e+01	7.89e-01	7.32e-03		4.78e-02	5.80e-03
$\tilde{\theta}$		1.47e-01	1.12e-01	7.14e-02		2.95e-03	1.00e-01	7.37e-01			9.52e-01
E		9.69e-04	1.91e-03	3.88e-04		1.04e-03	7.57e-02	2.34e-03			3.35e-03
V		6.59e-03	1.70e-02	5.43e-03		3.53e-01	7.57e-01	3.18e-03			3.63e-03
$\tilde{\theta}$		2.41e-01	1.30e-01	7.14e-02				4.21e-01			6.47e-01
E		1.83e-03	3.62e-03	4.72e-04				3.43e-03			2.03e-03
V		7.61e-03	2.78e-02	6.61e-03				8.15e-03			3.14e-03
$\tilde{\theta}$		3.38e-01		7.14e-02							7.87e-01
E		2.46e-03		2.42e-04							7.73e-04
V		7.27e-03		3.38e-03							9.83e-04

Table A.1: Parameter estimates for solving five inverse problems from a synthetic data generated using the given nominal parameters and variance. For each parameter subset, we display the estimate ($\tilde{\theta}$), the standard error, E and the coefficient of variation, $V = E/\tilde{\theta}$.